UK EPR	Title: PCSR – Sub-chapter 16.2 – Severe accident analysis (RRC-B)
	UKEPR-0002-162 Issue 05

Chapter Pilot: F. CERRU	
Name/Initials _(signature)_ *Date* *12-11-2012*	
Approved for EDF by: A. MARECHAL	Approved for AREVA by: G. CRAIG
Name/Initials A.Je-Maclal *Date* *12-11-2012*	*Name/Initials* _(signature)_ *Date* *12-11-2012*

REVISION HISTORY

Issue	Description	Date
00	First issue for INSA review	14/01/08
01	Integration of technical, co-applicant and INSA review comments	29/04/08
02	PCSR June 2009 update: – Clarification of text – Inclusion of references – Addition of French acronyms (section 1) – Section 1.3.2 completed. – Section 2.1.2.5 removed – Justification of the scenario selection improved (section 2.3) – MACE and OECD experiment descriptions improved (section 2.4)	28-06-09
03	Removal of RESTRICTED classification	10-06-10
04	Consolidated Step 4 PCSR update: - Minor editorial changes - Update and addition of references - Addition of information for higher enrichment and the more conservative layered configurations (§1.3.2.2) - Addition of further information on deposition rates of aerosol and gaseous iodine (§3.2.3) - Addition of information on the containment sump pH (§3.2.4)	30-03-2011

Text within this document that is enclosed within curly brackets "{…}" is AREVA or EDF Commercially Confidential Information and has been removed.

REVISION HISTORY (Cont'd)

Issue	Description	Date
05	Consolidated PCSR update: - References listed under each numbered section or sub-section heading numbered [Ref-1], [Ref-2], [Ref-3], etc - Minor editorial changes - Correction of number of fuel rods / guide tubes (Section 16.2.2.1 – Table 2) - Addition of general information regarding detailed performance of recombiners and addition of reference to recombiner sensitivity study and summary of analysis (§2.3.1) - Moving of one paragraph on recombiner qualification tests to a different position in the text (§2.3.1) - Inclusion of results of additional studies on the impact of PARs operation on iodine volatility in containment, and the dissociation ratio, and references added (§3.2.4) - Update of references	12-11-2012

Trade Mark

EPR™ is an AREVA Trade Mark.

For information address:

AREVA NP SAS
Tour AREVA
92084 Paris La Défense Cedex
France

EDF
Division Ingénierie Nucléaire
Centre National d'Equipement Nucléaire
165-173, avenue Pierre Brossolette
BP900
92542 Montrouge
France

TABLE OF CONTENTS

SUB-CHAPTER 16.2 – SEVERE ACCIDENT ANALYSIS (RRC-B)

0. SAFETY OBJECTIVES

0.1. GENERAL

A severe accident results in fuel rod failure, degradation of the structural integrity of the reactor core, and release of radioactive fission products into the reactor coolant system. Such an event can only occur as a result of a sustained loss of adequate core cooling, which leads to elevated core temperatures due to the sustained production of decay heat. Coupled with multiple failures of plant safety-grade emergency cooling systems, the resulting consequence of melting the reactor core (and internals) may lead to the breaching of the reactor vessel, and the transfer of molten core material in the containment may potentially compromise the ability of the containment to perform its function of radionuclide retention.

Given the potential consequences, the EPR is designed with multiple layers of defence mechanisms so that a severe accident is considered highly unlikely.

The plant's safety concept meets advanced regulatory requirements so that, on one hand, accident situations with core melt which would lead to large early releases are practically eliminated and, on the other hand, low pressure core melt sequences (RRC-B) necessitate protective measures for the public, which are very limited both in area and time. According to the Technical Guidelines [Ref-1], the radiological objectives associated with RRC-B accidents are expressed on the basis that only very limited countermeasures should be necessary in such situations i.e.

- limited sheltering duration for the public,

- no need for emergency evacuation beyond the immediate vicinity of the plant,

- no permanent relocation,

- no long-term restrictions on the consumption of foodstuffs.

Following the recommendations made by the International Commission on Radiological Protection (ICRP) [Ref-2], while at the same time considering their consistency with UK recommendations, the thresholds of 10 and 50 mSv (effective dose) have been adopted for sheltering and evacuation of the population, respectively, and a threshold of 100 mSv in equivalent thyroid dose for issuing iodine tablets. Detailed explanations are given in section 3.1 of this sub-chapter.

1. APPROACH TO SEVERE ACCIDENT CONTROL

1.1. BASIC STRATEGY

Severe accidents involve phenomena which pose an immediate threat to the integrity of the containment. An early failure of the containment in a severe accident situation would have major consequences (in terms of radiological dose) for the public. The main objective is therefore to avoid as far as possible any risk of early containment failure. A further, equally important objective for the EPR is the preservation of the containment integrity in the long-term.

In response, a two-staged approach is pursued. The first stage focuses on the *practical elimination* of highly energetic phenomena which have the potential to breach the containment early into the accident and thus result in large early releases. The second stage is then concerned with maintaining the containment integrity in the long-term. These tasks are achieved by influencing and controlling the accident progression with design measures such that well-determined states can be achieved and thus the safety objectives are fulfilled with traditional technologies. This approach has, therefore, a significant economic benefit and additionally allows the efficient conduct of supportive research and development.

Practical elimination is achieved by specific engineered safety features that concern the following phenomena:

- Core melt under high pressure and direct containment heating

High pressure failure of the reactor pressure vessel (RPV) following melting of the core can lead to direct containment heating (DCH) and to the formation of RPV missiles. Briefly, DCH denotes heating of the free containment volume by finely fragmented and dispersed melt, which results in a fast pressure build-up. The RPV missile denotes an RPV which detaches from its anchoring due to the thrust provided by failure of the RPV at high internal pressure. High pressure core melt is practically eliminated by deliberately depressurising the primary system, which transforms high pressure into low-pressure core melt sequences. In addition, the design of the reactor pit avoids any direct path for the core melt to escape into the containment.

- Large steam explosions which can threaten the containment

Steam explosions develop from the contact between molten reactor materials and water.

Regarding in-vessel steam explosion, analyses [Ref-1] have verified that the RPV would withstand the corresponding loads and thus no consequent effects on the containment would occur. Ex-vessel steam explosions are prevented by avoiding the presence of water in the reactor pit at the time of pressure-vessel failure and during the corium flow out of the RPV, as well as in the spreading compartment before the spreading phase. Specifically, water ingression into the reactor pit as a result of a loss-of coolant accident (LOCA) leading to core melt is prevented by the design of the pit, which isolates it from the rest of the containment. Therefore, there exist no direct pathways for water to enter the pit. The only possibility would be a break of one of the main coolant lines (MCL) directly at the connecting welds between the MCL and the RPV nozzles. Such a break is, however, highly unlikely due to the break preclusion concept applied in the UK EPR.

Regarding the spreading compartment, the only source of water would therefore be condensate arising from humidity increase in the containment atmosphere due to a LOCA. Since the spreading compartment is dead-ended, condensation in that compartment is highly limited and thus not of concern.

- Hydrogen combustion phenomena potentially critical to containment integrity

Hydrogen predominantly arises from the oxidation of Zr-cladding during in-vessel accident progression. It is also produced by molten core concrete interactions (MCCI) during the ex-vessel phase of a severe accident. After being released into the containment, hydrogen may form burnable and even more importantly, explosive mixtures with the containment atmosphere. The approach to the practical elimination of this hydrogen risk is based on good mixing of the containment atmosphere, which quickly and efficiently reduces local high concentrations and concentration gradients. Mixing is achieved by global convection in the atmosphere of both the accessible and inaccessible rooms of the containment. To achieve this, the two-zone containment consisting of accessible and inaccessible rooms has to be transformed into a one-room configuration. The corresponding system consists of rupture and convection foils as well as hydrogen mixing dampers, which under normal operating conditions separate the two zones of the containment. In combination with the convection induced by the direct discharge of the RCS coolant inventory into the containment, the inerting effect of steam and a containment volume of 80,000 m3, the convection system effectively prevents fast combustion which could be critical to the integrity of the containment.

Given the practical elimination of these phenomena, the second stage is concerned with preserving the containment integrity in the long-term. This task encompasses the prevention of

- hydrogen risks for the containment in the long-term,

- containment failure due to exposure of the concrete basemat to core melt,

- containment failure due to containment over-pressurisation.

The possibility of hydrogen combustion in the long-term is avoided by installing autocatalytic re-combiners at relevant locations in the containment, which reduce the hydrogen concentration below the flammability limit of 4% by volume even under steam-inerted conditions.

An ex-vessel core melt stabilisation system avoids the penetration of the liner and concrete basemat, and, subsequently, the interaction between molten core and subsoil, and long-term ground-water contamination. By maintaining the melt in a cooled configuration, the stabilisation system further prevents the heat-up of the concrete in the lower containment region. This eliminates the risk of thermal deformation and induced crack formation in the concrete slab.

The combined effect of decay heat and mass and energy release results in a continuous pressure and temperature increase, which would eventually challenge the containment integrity. The approach to pressure and temperature control takes advantage of available heat sinks inside the containment, which retard pressure and temperature increase and enable a grace period of 12 hours, during which no active measures for containment heat removal are necessary. For long-term decay heat removal, the EPR has a dedicated containment heat removal system (EVU [CHRS]) consisting of two trains, with each train sufficiently capable of limiting containment pressure below containment design pressure. One dedicated cooling chain per EVU [CHRS] train is employed to transport the heat removed from the containment to the ultimate heat sink.

It should be noted that the approach to decay heat removal from the containment in severe accidents only makes use of the EVU [CHRS]. This approach is adequate, as exposure of the concrete basemat to core melt is prevented by the core melt stabilisation system. The interaction between melt and concrete and resulting gas release into the containment is therefore limited to the ablation of the sacrificial concrete in the reactor pit and core catcher. Only if unlimited core concrete interactions take place a venting system needed for containment pressure relief. With regard to venting, a significant advantage of the EPR-solution is that heat removal in a severe accident is performed with a closed containment. In contrast, a venting system would require the opening of a valve for containment pressure relief.

In combination with the maximum containment leak rate of 0.3% by volume per day at containment design pressure of 5.5 bar, pressure and temperature control ensures that the radiological objectives as defined in section 0 of this sub-chapter are met.

The analysis of the EPR response in severe accidents employs representative and bounding scenarios. Representative scenarios are used for the design of severe accident mitigation systems and the analysis of their efficiency, while bounding scenarios involve pessimistic assumptions and are used to show that there is no sudden escalation of consequences just beyond the design basis.

The analyses employ best-estimate assumptions, codes and methods in order to exhibit the margins involved in the safety design of the plant. Corresponding codes and models have undergone validation against representative experiments. These validated codes then allow the extrapolation of experimental findings to reactor scale. In effect, the severe accident analyses are backed-up by representative experiments.

1.2. SPECIFIC DESIGN MEASURES

1.2.1. Primary System Depressurisation

A failure of the reactor vessel at high pressure is a significant potential contributor to early containment failure (missiles created by the pressure vessel movement, melt dispersal including direct containment heating). Even though such a failure is physically unlikely, given that the primary loop is assumed to fail prematurely, the Technical Guidelines clearly require a design objective of transforming high-pressure core melt scenarios into low-pressure core melt scenarios with high reliability, so that reactor vessel failure under high pressure can be practically eliminated.

For the EPR, this is achieved through two dedicated severe accident depressurisation valve trains that are part of the primary depressurisation system (PDS) but independent of the pressuriser safety valves. The 2 x 100% design philosophy is followed to provide performance margin. The valves are DC-powered and as such connected to the 12 hour batteries. Section 16.2.1 - Figure 1 shows the primary system depressurisation system.

Each depressurisation train has a discharge capacity of 900 t/h of saturated steam at design pressure. This capacity ensures that RCP [RCS] pressure at time of breach of the RPV is well below 20 bar for representative scenarios and does not exceed 20 bar for bounding scenarios. Depressurisation will eventually be activated by the operator when the core outlet temperature reaches 650°C. The coolant is discharged into the pressuriser relief tank (PRT), which itself is protected by rupture disks and connected to 2 of the 4 reactor coolant pump rooms. The rupture disks are designed to burst at a pressure difference of 20 bar.

Failure of the PRT rupture disks and consequent release of steam into the containment promotes global atmospheric mixing, which is highly advantageous for hydrogen control.

1.2.2. Hydrogen Control

The hydrogen control system of the EPR makes use of a staged approach consisting of

(i) the prevention of fast combustion that might challenge the containment integrity and

(ii) sustained reduction of hydrogen concentration below flammability limits.

In terms of fast combustion, the EPR incorporates a passive convection system, which transforms the two-zone containment to a single zone and thus quickly and efficiently reduces locally high concentrations and concentration gradients by enabling global convection. In combination with the direct discharge of the RCP [RCS] inventory into the containment and a free containment volume of 80,000 m^3, the convection system efficiently prevents fast combustion, which could be critical to the integrity of the containment. The technical solution for the transformation of the containment consists of

- rupture foils,

- convection foils combined with integrated rupture foils,

- hydrogen mixing dampers.

Rupture foils open passively at a nominal pressure difference of about 50 mbar. They are located above the steam generators and cover a surface area of about 32 m^2.

Convection foils open passively when the gas temperature directly below the foil reaches 85°C. They open also at a pressure difference of 50 mbar due to the integrated rupture foils. The convection foils are located above the SG compartment together with the rupture foils and cover a total surface area of ~40 m^2.

The hydrogen mixing dampers are fail-safe and open at a pressure difference of about 30 mbar, an absolute pressure of 1.2 bar or in case of power loss. The mixing dampers are installed at the wall separating the IRWST from the annular compartments and provide a total flow cross-section of about 5.5 m^2.

In terms of hydrogen reduction, the hydrogen control system uses 47 re-combiners, which are installed in the accessible part (main operation floor and annular rooms) as well as in the non-accessible part (SG-compartments) of the containment. The arrangement supports global convection, homogenises the atmosphere and reduces the average global hydrogen concentration as well as local peak hydrogen concentrations. The number of re-combiners has been derived from the requirement to reduce the integral hydrogen concentration below 4% by volume during the first 12 hours of a severe accident.

1.2.3. Core Melt Stabilisation

To prevent basemat exposure and melt-through by a core melt, the EPR is equipped with a core melt stabilisation system. The fundamental idea behind the melt stabilisation strategy is to spread the molten core into a core catcher located laterally to the reactor pit. This measure transforms the core melt to a configuration more easily coolable by significantly increasing the surface/volume ratio of the melt. The decay heat is removed from the melt upper surface by flooding and quenching the melt from the top and at the melt underside and lateral boundaries by the cooling structures of the core catcher. The coolant water needed for heat removal from the core catcher is stored in the IRWST and supplied to the core catcher completely passively. Water flows passively from the IRWST to the spreading compartment through water supply lines after the flooding valves open triggered by the arriving melt. The water fills up the cooling channels of the core catcher and ultimately spills over the core catcher upper edge and floods the melt free surface. Spill-over only starts well after melt spreading is completed. Passive overflow continues until equilibrium between the water columns in the spreading compartment and IRWST is achieved.

In order to render long-term melt stabilisation in the core catcher independent of the uncertainties involved in the late phases of in-vessel accident progression (notably the melt release sequence and melt properties), the overall approach includes a temporary melt retention in the reactor pit. This is achieved by a layer of sacrificial concrete on the inside of the pit which the corium has to penetrate. More specifically, the entire melt inventory, which may sequentially be released into the pit, is collected before it is spread into the core catcher in one shot. At the same time, a mixing of concrete decomposition products with the core melt results in properties which are favourable for melt spreading. Except for the bottom of the pit, the sacrificial concrete is backed-up by a refractory layer consisting of ZrO_2, which restricts the ablation depth in a radial direction to the depth of the sacrificial layer and which guides the melt to the melt gate.

Spreading of the melt from the reactor pit into the core catcher starts once the melt gate located underneath the sacrificial concrete at the bottom of the pit is contacted and destroyed by the melt. The gate is essentially a metal plate, consisting of an aluminium alloy, which ensures fast opening with sufficiently large cross-section so that the spreading process is swift and uniform.

Once released from the pit, the corium passes through the melt discharge channel and subsequently flows into the core catcher. Before the corium contacts the cooling structure of the core catcher, it has to penetrate through a layer of sacrificial concrete. The purpose of that layer, which covers the entire inner surface of the cooling structure, is to delay the contact between corium and cooling structure and at the same time to reduce the corium temperature at the time of initial contact. Furthermore, the density of the oxide portion of the corium relative to the density of metallic corium diminishes significantly until the end of the corium/concrete interaction, so that a stable configuration results in the corium pool, in which the molten oxides lie above the molten metals. Flooding the oxide pool during corium/concrete interaction is beneficial to cooling, given that the interaction encourages fragmentation and consequently solidification of the corium.

The cooling structure, whose purpose is to stabilise the corium without achieving loads critical to the integrity of the liner and basemat located underneath, consists of an array of cooling elements, which are fabricated from cast iron. For an efficient heat transfer to the coolant, the bottom and sidewall cooling elements have integrated fins at the interface to the water. The flow channels between these fins have an appropriate cross-section to allow the required flow of coolant water and steam in all flow regimes up to the maximum expected local heat flux.

In addition to passive cooling, the concept for heat removal from the core catcher includes an active cooling mode using the EVU [CHRS], which can be applied in the long-term. In this mode, either one or both EVU [CHRS] trains are used to feed water directly into the core catcher. While not essential for meeting the radiological objectives of the EPR, active cooling is advantageous in that it results in a sub-cooled water pool above the melt, thus terminating steam release into the containment and eventually leading to atmospheric pressure. In effect, radiological releases from the containment due to potential leakages are further reduced.

1.2.4. Control of Containment Pressure and Temperature

The EPR uses a dedicated containment heat removal system consisting of two trains to control containment environmental conditions in a severe accident and to avoid long-term over-pressure failure of the containment. Each train is equipped with a dedicated cooling chain to transfer decay heat to the ultimate heat sink.

Due to a system involving external circulation, the two trains are located in dedicated, radiologically-controlled rooms within two of the four plant safeguard buildings.

The essential components (per train) are a dedicated suction line from the IRWST, spray ring, recirculation pump, a heat exchanger and a flooding line to supply the core catcher with water. Strainers protect the intakes of both the EVU [CHRS] suction lines and flooding lines against debris potentially present in the IRWST as a result of the accident. To avoid clogging of the strainers, the EVU [CHRS] is provided with back-flushing. The system as a whole is designed in a highly robust manner, so that its operability after seismic events is ensured.

Following the lapse of the 12 hour grace period the EVU [CHRS] is designed to

- maintain the pressure in the containment below the containment design pressure of 5.5 bar (1 train),

- reduce the pressure below 2 bar in less than 24 hours, and then to keep the pressure at a value lower than 2 bar (2 trains).

Additionally, *one* train alone is sufficient to maintain the containment pressure below the containment design pressure at every stage of an accident and is capable of keeping the containment pressure below 2 bar after 10 days, if the core is a UO_2 core, and after 15 days if the core is MOX.

The principal system configuration is shown in Section 16.2.1 - Figure 2.

The basic operational scheme for the EVU [CHRS] is to switch on both spray systems after 12 hours into the severe accident at the latest to reduce containment pressure and temperature. A positive side-effect of spraying is the scrubbing of aerosols from the containment atmosphere. In this operational mode, the water is drawn by the EVU [CHRS] pumps from the IRWST, and routed through EVU [CHRS] heat exchangers to the spray nozzles, from where it is sprayed into the containment.

Due to the specific design of the floors of the reactor building compartments, this water flows back into the IRWST. At the same time, the core catcher is cooled with water flowing passively from the IRWST.

In addition to the spray mode, which alone is sufficient to fulfil the EPR safety objectives for severe accidents, the EVU [CHRS] provides for active core catcher cooling, which creates a sub-cooled water pool in the spreading compartment in the long-term, whereas passive cooling only allows for removal of heat from the melt by boiling and evaporation. Due to the high capacity of the EVU [CHRS] coolers, one train alone is sufficient to achieve this target. Therefore, the second EVU [CHRS] train can still be used for spraying and thus for removing decay heat produced by airborne and deposited fission products directly from the containment atmosphere.

Specifically, active cooling is achieved by closing the valve for water supply to the spray ring and opening the valves for water supply to the core catcher for the relevant EVU [CHRS] train. In order to prevent most of the coolant from flowing back into the IRWST through the open connection between IRWST and core catcher, a passive outflow reducer (POR) is placed between the IRWST and the connection to the flooding line. The POR has a high flow resistance in the IRWST direction and a low resistance in the opposite direction. Therefore, this element effectively limits direct backflow of water to the IRWST and ensures that most of the coolant will reach the core catcher.

As this is basically a traditional fluid system, no R&D is required for its implementation.

1.2.5. Limitation of Radiological Releases

A fundamental contributor to the limitation of radiological releases to the environment is the containment, which has a maximum leak rate of 0.3 vol%/day at containment design pressure. This leak tightness is secured by the containment steel liner, hatch and airlocks, penetrations and a containment isolation which are able to withstand ambient conditions prevailing inside the containment in severe accidents. Most leakage is collected in the annulus, which is kept at sub-atmospheric pressure by the annulus ventilation system (EDE [AVS]). This system is also used to route any leakage through HEPA and iodine filters in series to the stack, from which they are released to the environment in a controlled manner. Leakages which are not collected in the annulus enter the peripheral buildings and are filtered before being released.

The annulus ventilation system has two operation modes. If AC power is still available, two fans with a maximum exhaust rate of 1000 m^3/h each, keep sub-pressure in the annulus. Alternatively, the annulus ventilation in combination with the stack is designed to develop sufficient natural draught to maintain sub-pressure for the case that AC power is not available.

UK EPR

PRE-CONSTRUCTION SAFETY REPORT

CHAPTER 16: RISK REDUCTION AND SEVERE
ACCIDENT ANALYSES

SUB-CHAPTER : 16.2

PAGE   : 9 / 295

Document ID.No.
UKEPR-0002-162 Issue 05

SECTION 16.2.1 – FIGURE 1

Primary depressurisation system

Pressurizer safety valves

Dedicated severe accident depressurization valves (2 x 2 valves)
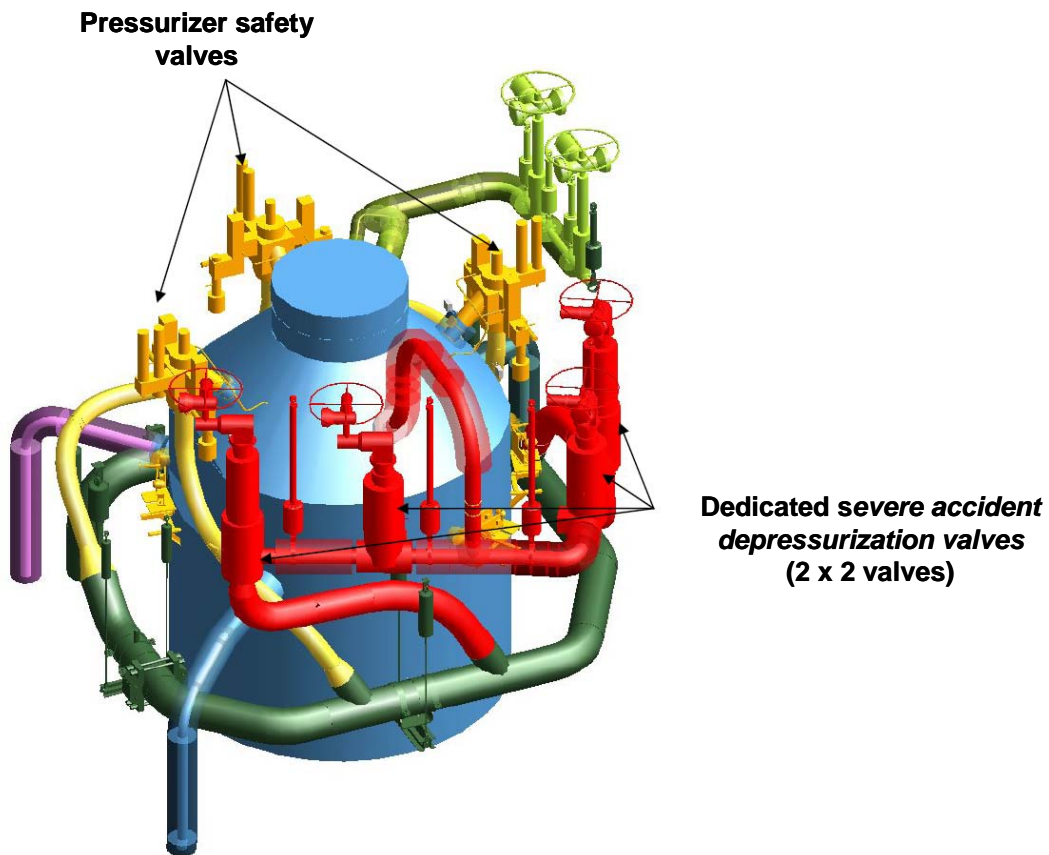
SECTION 16.2.1 – FIGURE 2

Schematic configuration of the EVU [CHRS] and components for active core catcher cooling (Passive outflow reducer, part of the yellow line closing the loop for core catcher cooling)

Dedicated Cooling Chain –
Containment Heat Removal System Overview

Containment Heat Removal System

Spray nozzles

Passive Flooding Valve

CHRS (2x)

Corium spreading area

IRWST

Melt flooding via cooling device and lateral gap

Ⓧ Water level in case of water injection into the spreading area

Ⓕⓛ Passive Outflow Reducer
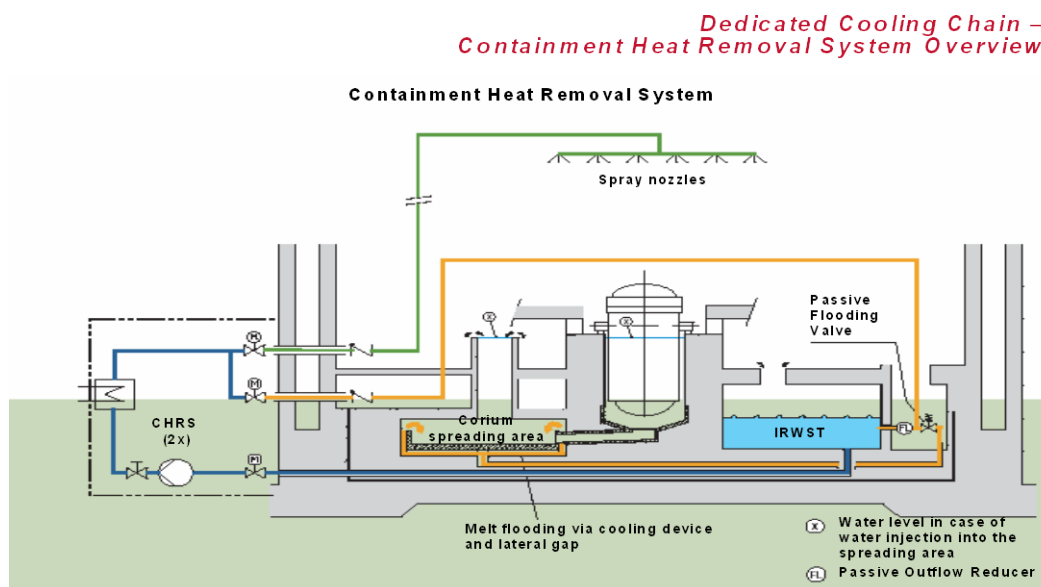
1.3. SPECIAL ISSUES

1.3.1. Steam explosion

1.3.1.1. In-vessel steam explosion

The term 'steam explosion' refers to a phenomenon in which molten fuel rapidly fragments and transfers its energy to the coolant resulting in steam generation, shock waves, and possible mechanical damage to surrounding structures. This phenomenon may occur during a PWR severe accident when a hot molten core relocates into the residual water filled lower head of the reactor vessel. The steam explosion is a fuel-coolant interaction process where the heat transfer from the melt to water is so intense and rapid that the timescale for heat transfer is shorter than the timescale for pressure relief [Ref-1]. These generated shock waves may lead to production of missiles that may endanger the containment vessel integrity during the expansion of the water vapour.

1.3.1.1.1. Involved Physical Phenomena

Steam explosions are a subclass of the so-called fuel coolant interactions (FCI) in safety studies of nuclear reactors. The steam explosion is a complex, highly nonlinear, coupled multi-component, multi-phase, multi-space-scale and multi-time-scale phenomenon. Consequently, modelling of steam explosions is a difficult task and the uncertainties of reactor simulations performed with steam explosion codes based on modelling fundamental steam explosion processes are still large [Ref-1]. Therefore, assessment of the reactor vessel and containment vulnerability to a steam explosion requires a parametric approach capturing the uncertainties of the phenomenon understanding and modelling.

Based on the phenomena occurring during a steam explosion, the event can be divided into four consecutive phases: the premixing phase, the triggering phase, the propagation phase and the expansion phase. A schematic presentation of the four phases of the steam explosion is shown below.

Premixing phase   Triggering phase   Propagation phase   Expansion phase

1.3.1.1.1.1.   *Premixing Phase*

In the premixing phase, the molten jet breaks up and a coarsely mixed region of molten corium and coolant water is formed. A vapour film separates the melt particles and the water, so the heat transfer between the melt and water is relatively low. The premixing phase is characterised by a relatively low steam production rate resulting in a slow pressurisation of the system or, if condensation is able to balance vaporisation, no pressurisation at all. The system can remain in this meta-stable state until the melt is quenched or, if the conditions are appropriate, until a steam explosion is triggered. The timescale of the premixing process is in the range of seconds, and the length of the melt particles is measured in centimetres.

1.3.1.1.1.2.   *Triggering Phase*

In the triggering phase, the steam explosion is triggered. The triggering event is a disturbance, which destabilises the vapour film around a melt particle allowing liquid-liquid contact and leads to locally enhanced heat transfer, pressurisation and local fine fragmentation. There are many reasons for vapour film destabilisation, including pressure pulses resulting from different impacts (in experiments interactions are often triggered when the melt reaches the bottom of the tank), transition from film boiling to nucleate boiling, and water entrapment at melt-structure contact.

1.3.1.1.1.3.   *Propagation Phase*

During the propagation phase, an escalation process takes place resulting from the coupling between pressure wave propagation, fine fragmentation, and heat transfer initiated by the triggering event. The pressurisation induced by the triggering event destabilises the vapour films of surrounding melt particles, leading to local liquid-liquid contacts between melt particles and coolant. Locally, some coolant is rapidly heated and pressurised and this causes some fine fragmentation of surrounding melt particles. This type of fragmentation is often called thermal fragmentation. Later, when the pressure is already high, the fine fragmentation is believed to be of a hydrodynamic nature owing to the relative motion between the melt and the coolant induced by their different densities and compressibilities.

The fine fragmentation propagates at a velocity which depends on the conditions in the premixing region. It can be governed by timescales corresponding to the propagation of disturbances in the premixing region, resulting in sequential "ignition" of the mixture. Typical velocities in this case are in the order of some tens of meters per second. In this case, the pressurisation of the system is relatively limited, slow and uniform, without generation of shock waves.

However, the fine fragmentation can escalate up to supersonic velocities in the pre-mixture and quasi steady state propagation. Depending on the conditions, the pre-mixture can "burn" more or less completely before the system can expand, thus creating a zone of high pressure. During the propagation phase, the thermal energy of the melt is converted into thermal energy of the coolant. The timescale of the explosion propagation process is in the range of milliseconds, and the length of the fine fragmented particles is measured in hundreds of micrometers.

1.3.1.1.1.4. *Expansion Phase*

During the expansion phase, the thermal energy of the coolant is converted into mechanical energy. The expansion of the high-pressure mixture against the inertial constraints imposed by the surroundings determines the damage potential of the steam explosion. The damage might be caused through pressure shock waves at the beginning of the process, and afterwards through the kinetic energy transmitted to the surrounding cavity structures. If the localised high pressures are quickly relieved, then they may not damage the surrounding structures, but the kinetic energy transmitted to the materials around the interaction zone may be the damaging agent.

A comprehensive description of the steam explosion phenomenon is provided in reference [Ref-1].

1.3.1.1.2. Insights from Previous Studies

To result in a significant safety concern the interaction must be very rapid and must involve a large fraction of the core mass. If such events were to take place within the reactor pressure vessel, missiles could be generated which might penetrate the containment and result in early release of radioactive material. In the Reactor Safety Study this mode of containment failure was denoted as the α-mode failure [Ref-1].

1.3.1.1.2.1. *Pressure Influence*

With the TMI-2 experience, it was clear that debris drainage into the RPV lower plenum must be considered even when the damaged core is completely submerged in water. It was also clear that no explosive interaction was created in the accident, which has been attributed to the elevated RCP [RCS] pressure. Substantial work has been reported on the influence of pressure to suppress explosive interactions. Recent experiments performed in the FARO facility and the ALPHA test in Japan [Ref-1] have further supported the influence of elevated pressure with the latter experiments showing that a pressure of 1.6 MPa is sufficient to suppress an explosive interaction. This result is consistent with that presented by the previous experimental programs.

1.3.1.1.2.2. *Mixing Behaviour*

Other experimental and analytical studies have focused on the potential for fine scale particulates and mixing of large quantities of high temperature melt and water. Both have concluded that it is extremely difficult to mix large quantities of high temperature melt with water and that substantial steam is formed during the premixing, which depletes the water in the interaction zone. This is a more refined assessment of the mechanism proposed by Henry and Fauske [Ref-1], which suggests that vapour formation during the premixing limits the molten material involved.

1.3.1.1.2.3. *Influence of Particulate Debris and Steam Generation*

Particulate Debris and in-vessel steam generation are also part of the understanding related to steam explosions. In particular, significant work has been performed with respect to the break-up of molten jets as they pour through water. Moreover, the FARO experiments [Ref-1] provide a substantial scale, real material demonstration of the steaming rate during this process. From the information accumulated to date, including the TMI-2 Vessel Inspection Project (VIP) [Ref-2], some particulates may occur, but the assessment of debris within the reactor vessel lower head must also consider that there is a substantial material layer which does not particulate. Particulate debris causes a net steam generation to the reactor coolant system with some potential for additional pressurisation as was observed in the TMI-2 accident. These integral system details are part of the lower plenum modelling in the MAAP4 code described in Appendix 16A. With the extensive information available on particulate debris and the net steaming rate from molten material draining into the lower plenum, the major issue is how much material does not particulate since this results in a potential threat to the RPV wall integrity.

1.3.1.1.3. US-NRC Studies

In 1985, the NRC formed the Steam Explosion Review Group (SERG) [Ref-1] and tasked this group to assess the likelihood of α-mode failure. The consensus was that explosive interactions sufficient to rupture the primary system and therefore the containment were very unlikely. During the 1993 CSNI-FCI Special Meeting in Santa Barbara [Ref-1], similar questions were asked, and again, the consensus was that the work performed since the NRC 1985 meeting supported the conclusions made by the SERG. In many instances, additional work had further refined key arguments related to the inability to establish the necessary initial conditions. In June of 1995, the NRC sponsored a workshop to update the understanding with respect to steam explosions. With the additional experiments provided in the FARO [Ref-2] and ALPHA facilities, as well as the additional analyses performed in 1999 [Ref-3] it would appear that there is a developing consensus on the α-mode failure issue.

In the thorough review of the probability of α-mode failure, the group of experts (SERG) performed independent analysis and examined available experimental data. The spectrum of opinions indicated that the probability of α-mode failure is considered to be much less likely than was estimated in WASH-1400 [Ref-4]. The SERG divided the fundamental processes of steam explosion into three general areas:

1) Initial conditions: this involves the geometrical configuration of the reactor vessel at the time of fuel–coolant contact and the amount of fuel and coolant available for the interaction.

2) Mixing and conversion ratio: this involves the basic physics of the vapour explosion such as the fuel–coolant mixing, triggering, propagation, and the resultant conversion of fuel thermal energy to the slug kinetic energy.

3) Slug–missile dynamics: this involves the expansion characteristics of the slug within the specific reactor geometry, and the coupling to solid missile generation and containment penetration.

The consensus reached by the SERG was that the occurrence of an in-vessel steam explosion of sufficient energy, which could lead to containment failure, was sufficiently low in probability to allow its elimination as a credible threat. The recent 1995 second SERG Workshop [Ref-1] concluded that the α-mode issue was resolved from a risk perspective.

1.3.1.1.4. Recent European Studies

The second steam explosion review group (SERG2) established in 1995 [Ref-1] deliberated on the phenomenology of steam explosions and provided expert estimates on the probability of containment failure because of an in-vessel steam explosion. Although there were some differences of opinion, the vast majority of the experts concluded that the conditional probability (i.e. if there is a core melt) is less than 0.001 [Ref-2], i.e. the containment failure is very unlikely. Recent European tests in the BERDA program at FZK [Ref-3] [Ref-4], also have shown that, for a scaled upper vessel head subjected to impact loads simulating those from a very strong steam explosion, the head and the bolts survived the impact energy of a corium slug above 0.8 GJ.

Much experimental and analysis-development work is in progress presently on in-vessel steam explosions. Experiments have been performed with several kilogram quantities of heated particles and molten materials. Elaborate three-field analysis codes: MC3D [Ref-5], IVA [Ref-6], ESPROSE.m [Ref-7] and PM-ALPHA [Ref-8] have been developed. Some of the insights gained are:

1) steam explosion probability is much reduced due to the extensive water-depletion that occurs around the fragmented particles of a jet in the pre-mixture;

2) super-critical steam explosions, however, cannot be excluded.

The most remarkable observations derived from the experimental program employing prototypic corium melt (UO_2–ZrO_2) in the FARO and (UO_2–ZrO_2) and A1203 in the KROTOS [Ref-9] facilities at Ispra, Italy are:

- UO_2–ZrO_2 melt jets dropped in sub-cooled and saturated water at low pressure do not generate spontaneous steam explosions;

- Strongly-triggered UO_2–ZrO_2 melt jets in sub-cooled and saturated water at low pressure may develop a propagating event, although of very low efficiency (≤ 0.15%);

- Al_2O_3 melt jets (serving as a stimulant for the corium fuel) generally experience spontaneous strong steam explosions when dropped in low pressure sub-cooled water;

- Al_2O_3 melt jets dropped in saturated water at low pressure, in general, have to be triggered to experience strong steam explosions.

These significant observations point to the important role that the melt physical properties may be playing in the steam explosion process. Much research on this aspect is being pursued in Europe under the auspices of the European Commission. Some physical mechanisms have been identified. Nevertheless, it appears that the prototypic corium mixtures may not be as explosive (very low efficiency and/or explosiveness) as previously assumed.

1.3.1.1.5. Resolution Status

The conclusion from the NRC studies by SERG1 and SERG2 is that the α-mode failure due to explosive corium-water interactions is not sufficient to rupture the primary system or the containment vessel and therefore this failure mode is very unlikely. This conclusion is consistent with the results from several experimental studies performed in Europe and Japan.

Therefore, this issue of in-vessel steam explosion is considered as definitely resolved, especially in new reactor designs such as the EPR, and hence additional measures with respect to Accident Management Evaluations are not justified.

1.3.1.2. Ex-vessel steam explosion

Steam explosions in the reactor pit and spreading compartment are avoided by the EPR specific design features and the characteristics of the chosen mitigation strategy.

The related design measures in the pit involve the avoidance of water ingress into the pit either

- through penetrations, by restricting and shielding the entry cross-sections around the loop lines, or

- through the ventilation duct, by their pressure-tight design.

In addition, an effective limitation of the potentially interacting masses of melt and water is achieved by the small free space underneath the RPV.

The corresponding design measures in the core catcher involve:

- the avoidance of water inflow from sprays or leaks, which is achieved by:

  o the remote and isolated arrangement of the spreading compartment,

  o the controlled mode of flooding with low rate after melt spreading is complete.

In addition, layers of sacrificial concrete are provided in both the reactor pit and core catcher. The concrete in the reactor pit consists of iron-ore and siliceous pebbles in almost equal proportion, while the concrete in the core catcher is purely siliceous. The resulting admixture of concrete into the melt ultimately reduces the density of the oxidic corium fraction below that of the metallic one. As a result, the core melt will form a stratified molten pool in which the lighter oxidic fraction builds the upper and the metallic melt the lower layer. In parallel, the addition of siliceous concrete in the core catcher increases the viscosity of the oxidic melt, which results in the formation of a viscous layer at the free surface. In case of flooding this layer can inhibit the interaction between melt and water.

In the core catcher this configuration, in combination with the low flow rate of the added water and the fact that water pours onto the surface from the top, practically eliminate the risk of steam explosion, in particular those that could endanger containment leak tightness.

This was demonstrated in a number of representative experiments. Among these, the tests in the MACE [Ref-1] [Ref-2] and OECD-CCI project [Ref-3] demonstrate that especially an agitated MCCI pool and the related formation of non-condensable gas successfully inhibit FCI.

1.3.2   Recriticality

The sub-criticality of a PWR is maintained under all accidental conditions by the following features:

- the geometry of the fuel assemblies,

- the distribution of control assemblies containing neutron absorbers in the reactor core,

- the presence of burnable absorbers distributed within the fuel rods,

- boric acid in the reactor coolant.

In the progression of a severe accident, resulting from a loss of coolant and the loss of core cooling, the features listed above are significantly altered. For example the geometry and the position of the absorber rods, which will melt much earlier in the accident sequence than the other fuel assembly structures, will be altered. The loss of moderator is beneficial for preventing recriticality of the core, however in the event of flooding of the core during the core degradation the recriticality risk for the resulting configurations must be assessed. This assessment is presented in this sub-section.

For the melt mitigation and stabilisation proposed for the EPR, the following states are considered:

- an undamaged or only slightly damaged reactor core without control rods,

- a partially damaged fuel lattice with free fuel pellets, fragments of fuel elements, absorber elements and structural materials,

- a liquid fuel pool within the lower head of the RPV in combination with potentially remaining core fragments and liquid fuel within the core region,

- a molten fuel pool within the reactor pit which contains different fractions of sacrificial concrete,

- liquid corium equally distributed within the spreading area,

- solidified corium, partially fragmented and distributed on the cooling structure within the spreading compartment.

The potential for recriticality is assessed following the addition of water to the configurations described above. The source of the water could arise from RIS [SIS] reflooding before vessel failure or by flooding of the corium within the spreading compartment. The individual states listed above can be grouped into three categories as follows:

- in-vessel configurations,

- reactor pit configuration,

- spreading compartment configurations

The potential for recriticality in each of these categories is assessed in the sub-sections below.

1.3.2.1 In-Vessel Recriticality

The in-vessel configurations correspond to the earlier phases of a severe accident. At the start of the sequence the fuel is intact and starts to melt due to a loss of core cooling. As the temperatures in the core increase a molten pool forms and after a certain time a relocation of the corium into the lower head occurs. This lower head pool configuration can lead to vessel failure if reflooding is not effective.

The identification of fuel and absorber configurations enables the performance of bounding neutronic calculations with MCNP code [Ref-1] to evaluate the potential for reaching a critical condition (Keff = 1) during the different degradation phases for a UO_2 core with 5% enrichment. Temperature profiles in the core, and degradation configurations identified by MAAP4 code analysis of severe accident scenarios, are used to inform the choice of assumptions for the MCNP code. This is also complemented by the feedback of experimental results on for example the influence of early control rod degradation on fuel degradation, or the behaviour of neutron absorbing fission products (volatile and non volatile) [Ref-2], which are dependent on the core temperatures during the accident progression.

The results of the core reactivity analysis for all phases are dependent on the boron concentration of the in-vessel reflooding water. The reference value for the boron concentration of the IRWST water injected by the RIS [SIS] is between 2450 ppm and 2750 ppm natural boron for a UO_2 core.

The three selected time phases are:

- an undamaged or only slightly damaged reactor core (phase 1),

- a partially damaged fuel lattice with free fuel pellets, fragments of fuel elements, absorber elements and structural materials (phase 2),

- a liquid fuel pool within the lower head of the reactor pressure vessel in combination with potentially remaining core fragments within the core region (phase 3).

1.3.2.1.1 Assessment of the Potential for Recriticality during Phase 1

This phase represents the quenching of the core when only the control rods are partially melted and the fuel geometry is intact. The fuel surface available for heat transfer during reflooding is very high and consequently an effective fuel quench may be expected within a few minutes.

Due to radiation heat transfer, the control rods heat up simultaneously with the fuel rods. Partial AIC (control rod material) melting could alter the control rod functions. However, the neutron absorption properties will not be lost providing the stainless steel cladding remains intact. Following water injection, after a short time in which oxidation may accelerate core degradation, the core is rapidly quenched and all degradation stops, on both the fuel rods and the absorbers.

The MAAP4 code results for absorber temperatures show that at least 40% of the control rod length remains cold and does not melt. Consequently, the bottoms of the control rods are assumed to remain partially intact.

Before the start of quenching, the more the fuel is degraded, a greater amount of fission products are likely to be released. Therefore a long fuel degradation period results in the loss of phase 1 geometry. In this scenario the assessment considers only the core fission products not yet released for the delayed quench, which corresponds to the water injection at the time of fuel geometry loss. MAAP results for LBLOCA and SBLOCA core melt transients show that when 10% of fuel is melted, implying phase 1 geometry loss at least 50% of the gaseous fission products remain in the fuel matrix after quenching.

The assumptions addressing partial release of volatile fission products before significant fuel rod melting and incomplete degradation of the control rods lead to the conclusion that the IRWST boron concentration is sufficient to completely prevent recriticality in phase 1 with uncertainties of 125 ppm in the neutronic calculations included.

Consequently there is no potential for recriticality, especially as the likelihood of in-vessel injection during the time scale of a few minutes of phase 1, is very low.

1.3.2.1.2 Assessment of the Potential for Recriticality during Phase 2

When fuel melting begins in the top of the core the corium relocates and forms a molten pool. Upon reflooding, a crust forms around the molten pool preventing water ingress into a significant fraction of the corium molten pool. Therefore only a limited amount of the debris bed can be reflooded and cooled at the top of the molten pool, as in the TMI-2 accident [Ref-1].

The state of art of corium debris coolability for low pressure scenarios shows that the coolable mass of corium is limited and uncertain. A coolable mass under the 20-30 t observed in the TMI-2 accident should be expected [Ref-1], due to low Critical Heat Flux at low pressure.

Neutronic calculations for this phase assume that all the control rods have been lost and that all volatile absorbent fission products have been lost. The solid fission products are considered homogeneously mixed in molten matrix.

By assuming a homogeneous distribution of the corium components, but without mixing with the melted control rods, a configuration is assessed for a mass like that of TMI-2. Results show that the IRWST boron concentration is sufficient to prevent recriticality for the expected corium mass cooled and uniformly fragmented at the optimum porosity.

1.3.2.1.3 Assessment of the Potential for Recriticality during Phase 3

This phase starts when sufficient corium is relocated to the lower head of the Reactor Pressure Vessel. In this phase a scenario like that at TMI-2 can be expected, where only a limited corium mass is in the lower head after crust failure (relocation after quench), or a scenario with corium relocation that forms a pool later covered by cold water (relocation before quench). The assessment considers two different configurations for the corium geometry in the lower head, following the injection of water.

The first configuration with small masses of corium relocated and assumed totally fragmented in the lower head, has been studied using the same model as that used for phase 2. This assumes that all of the corium is fragmented at the optimum porosity. The neutronic study simulates small fragmented masses in the lower head, with an equivalent cylindrical geometry, and all control rods lost. For irradiated fuel, it assumes the complete loss of all volatile absorbent fission products. The results of the study are the same as for phase 2. This demonstrates that a TMI-2 like event does not present a risk of recriticality.

The second configuration studies higher masses of corium relocated in the lower head and forming a molten pool. When reflooding occurs the upper part of the pool is fragmented and cooled by forming a debris bed. With this configuration, vessel failure cannot be prevented. A specific model is used to study the geometry in which the bottom of the pool is without moderation (due to the high temperature of the pool centre, which prevents liquid water penetration) while the upper part is cooled and filled with water at the optimum porosity and is consequently moderated.

The results show that the potential for criticality is not determined by the dry corium mass, but by the small mass of debris deposited on the crust, because this material is moderated. Recriticality does not occur for a cooled thickness under 15 cm. However, this is more than the maximum cooled thickness calculated by the severe accident code MAAP, This is because water penetration in the debris bed is limited by steam production and the limited time before vessel failure.

Therefore, for phase 3 there is no real potential for recriticality.
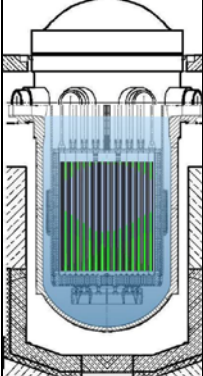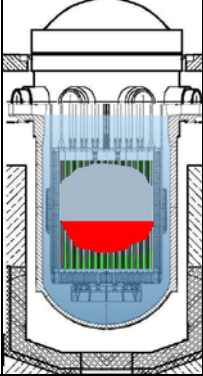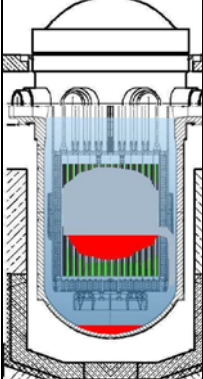
1.3.2.1.4 *Conclusion*

Without water injection in the vessel the corium has a large subcriticality margin with UO_2 fuel due to the negative void coefficient. Consequently there is no potential for recriticality.

In the case of Safety Injection System (RIS [SIS]) recovery during the core degradation, an injection at the IRWST boron concentration presents no recriticality risk in phase 1 of the core degradation, where the available fuel surface for heat transfer is high. In phases 2 and 3 there are uncertainties regarding the effective coolable mass in low pressure degraded scenarios. Therefore available estimations show that the effective coolable mass is not sufficient to reach the minimum mass required to produce a critical configuration under the relevant hypotheses described above. Even though the corium mass that may be fragmented and cooled remains limited, the operating strategy for severe accidents promotes the ability to add highly borated water when the corium is maintained in the vessel to allow for any uncertainty in the assessments.

SUB-SECTION 16.2.1.3.2.1 - TABLE 1

In-Vessel Recriticality Configurations and Results

Phase 1		<u>Start of core degradation</u> Safety injection with IRWST boron concentration **presents no recriticality risk**, when fuel geometry is quite intact.
Phase 2		<u>Formation of a molten pool in the core</u> There are uncertainties regarding the effective coolable mass in low pressure degraded scenarios. Expected coolable mass like that at TMI-2, uniformly fragmented at optimal porosity, **presents no recriticality risk.** In addition a higher amount of corium (although unlikely to be coolable) may present no recriticality risk since optimal and uniform porosity is not assured for large masses.
Phase 3		<u>Relocation of the corium into the vessel lower head</u> In this configuration vessel failure cannot be prevented, but reflooding may fragment corium in the upper part. The expected coolable thickness **presents no recriticality risk**, because water penetration in the debris bed is limited by steam production.

1.3.2.2. Ex-vessel recriticality

The following basic melt pools are considered in the assessment of recriticality during melt stabilisation within the core melt stabilisation system.

- Interaction of the molten corium pool with sacrificial concrete in the reactor pit

- A shallow molten corium pool of uniform depth in the core catcher

- Solidified, partially fragmented corium in the core catcher

Recriticality is only of concern if the molten corium pools listed above come into contact with a moderator for example water.

A potential source of water in the reactor pit is water arising from late reflooding of the reactor pit. In this scenario water is poured onto the open surface of the corium pool. This late reflooding occurs during scenarios when the dedicated depressurisation is delayed, i.e. after the core outlet temperature has exceeded 650°C.

Within the core catcher, the spread corium is flooded with water stored in the IRWST.

Due to the addition of water to the molten core during these scenarios a description of the molten pool configurations and an assessment of the potential for recriticality is required. This assessment is presented below for each scenario.

1.3.2.2.1. Assessment of the potential for recriticality in the reactor pit

Molten pool configuration

In accordance with section 2.4 of this sub-chapter, the corium pool is likely to form stratified layers within the reactor pit. Initially, the oxide melt will have a higher density than the metal melt, at this stage the pool will consist of three layers, a bottom oxide layer located underneath the metal melt and a third slag layer consisting mainly of concrete decomposition products will be located on top the metallic melt layer.

Once the oxide density has reduced to less than that of the metallic melt due to continuous mixing with the relatively light concrete decomposition products, the layer arrangement inverts and the metallic layer becomes located underneath the oxide melt layer. At the same time, the slag becomes mixed with the oxide melt and thus vanishes. Following the inversion of the oxide and metallic melt layers, the molten pool consists of two layers.

An additional, configuration, is that the chemically immiscible oxidic and metallic melts may be mechanically mixed by the stirring effect of the concrete decomposition gases, which rise through the molten pool. In this situation, the molten pool in the reactor pit would not form stratified layers as described above, but a single pool consisting of intimately mixed oxide and metal melt, whereby the concrete decomposition products would be dissolved in the oxide fraction.

Assessment

The geometry most prone to recriticality is the original core configuration. Any configuration departing from that while the core degrades will therefore reduce the risk of recriticality. The reason for this is that the degrading and melting core becomes increasingly compact, thus reducing the potential for moderator ingression and the likelihood of establishing a moderator volume/fuel volume ratio with the potential for recriticality.

As the molten pool in the reactor pit is compact, the potential for water ingression is highly limited regardless of whether the pool material is in stratified layers or mixed. Only the free surface of the melt is expected to interact with water, thus the water is kept away from the bulk of the melt. This situation is enhanced by mixing of the sacrificial material with the melt, which increases the melt volume whilst further diminishing the possibility of water ingression into the bulk of the melt.

In conclusion, for the reasons described above recriticality is not an issue for the corium pool within the reactor pit.

1.3.2.2.2. Assessment of the potential for recriticality in the core catcher

Molten pool configuration

Following the opening of the melt gate the molten corium spreads and undergoes interactions with the sacrificial concrete layer covering the internal, melt-facing surface of the core catcher. As is the case for the reactor pit, the pool will either form two layers or stay mixed due to agitation by concrete decomposition gases. In contrast to the reactor pit, the corium pool within the core catcher is, shallow. 300 seconds after the flooding valves have been triggered by the spreading of the melt, flooding of the pool free surface with water commences, whilst the molten corium concrete interactions continue. As a result, fragmentation of the free surface is likely to occur and water ingress into the corresponding fragment bed is possible. At the same time the melt becomes completely enclosed by water. Therefore, it is necessary to perform an analysis to assess the likelihood of recriticality in the core catcher.

Analysis

This analysis predicts the eigenvalue (k_∞) as a function of melt fragmentation level, which in turn determines the water ingression depth. A number of parameter variations are made to the base case used in the analysis. These include enrichment, boron concentration, melt temperature and porosity of the fragment bed, which is synonymous for moderator volume/fuel volume ratio. The following table compares these parameters for the base case with the parameters for the variation cases.

Parameter	Base case	Variation
Melt density	4680 kg/m^3	-
Height of the melt	0.429 m	-
Average fuel enrichment	2 w/o U235	3 w/o U235
Porosity of fragment bed	0.2	0.4
Melt temperature	200 °C	1850°C
Water conditions	20°C, 1bar	-
Boron concentration	0 ppm	2500 ppm B$_{nat}$

Further important assumptions and boundary conditions used in the analysis include:

- the melt expands infinitely in the xy-direction,

- a 1-dimensional model is adequate,

- the top and bottom surfaces of the melt are covered with layers of water (thickness: 0.2 m),

- the melt contains the total UO$_2$ mass of the core (approximately 142 t),

- the melt includes the total Zr mass of the core in oxidised form (ZrO_2, about 58 t),

- there is homogeneous distribution of all melt components, no stratification is present,

- the melt contains approximately 140t of decomposition products which have been mixed with the melt during the interaction with sacrificial concrete in the reactor pit and core catcher.

This set of conservative assumptions allows for uncertainties in the model parameters and the calculation method.

Sub-section 16.2.1.3.2.2 - Figure 1 presents k_∞ as a function of melt fragmentation for the base case and the parameter variations.

The analysis shows that the reactivity increases with increasing fragmentation of the melt. Regarding the base case, there is no risk of recriticality even with complete fragmentation, the result of this analysis is a maximum multiplication coefficient k_∞ of 0.72.

An increase in the porosity of the fragment bed from 20% to 40% increases the multiplication coefficient k_∞ by 0.09.

Fresh fuel is assumed for the calculations with no depletion of the fissionable isotopes and no fission products produced. The change of the multiplication coefficient for an increase in enrichment from 2 to 3 w/o U235 is $\Delta k_\infty \sim +0.1$.

Increasing the temperature of the melt (i.e. the uranium isotopes) at a constant density leads to a decrease in the multiplication coefficient by 0.05.

The boron concentration in the cooling water corresponds to 2500 ppm boron of natural composition. Relative to non-borated water, this boron concentration reduces the multiplication coefficient by 0.13.

In conclusion, the margins to recriticality are significant.

Higher enrichment

In addition, mixed melt configurations and the more conservative layered configurations with an enrichment of 4 w/o U235 were also studied with different boundary conditions (different melt composition, different scenarios):

Parameter	Layered case with 4 w/o U235
Melt density	Oxide 4515 kg/m³ Metal 6726 kg/m³
Height of the melt	Oxide 0.539 m Metal 0.102 m
Average fuel enrichment	4 w/o U235
Porosity of fragment bed	0.44, 0.20 to 0.50
Melt temperature	1650°C, 70°C
Water conditions	70°C, 3 bar
Boron concentration	0 ppm, 2300 ppm

The most critical configuration in the spreading area was found for the case listed in the table above.

To study the effect of the porosity of the melt, water penetration depth (i.e. fragmentation) and fuel temperature, these parameters were varied without consideration of any boron concentration in the cooling water and the most reactive configuration, $k_\infty \approx 1.21$, was found to result from a porosity of 44%, a water penetration depth of 51.6 cm and a fuel temperature of 70°C (conservative case).

When 2300 ppm natural boron concentration was considered the reactivity was found to be $k_\infty \approx 0.82$.

The most reactive porosity will decrease due to the competing effect between absorber and moderator. It was found that the highest eigenvalue k_∞ with boron occurs at a porosity of 24% (70°C fuel temperature, 2300 ppm boron concentration, 24% porosity and 51.6 cm water penetration depth).
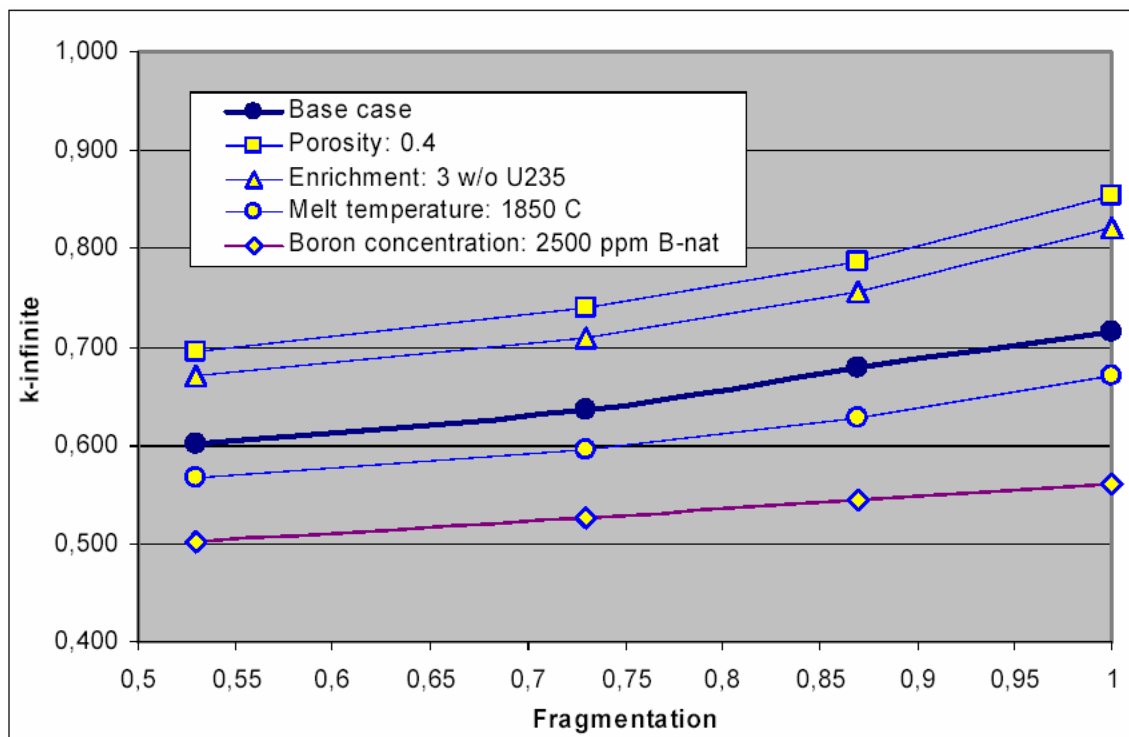
For this very conservative configuration results $k_\infty \approx 0.93$, i.e. large margins to criticality exist.

Thus also higher enrichments do not result in recriticality during ex-vessel melt stabilisation.

.

SUB-SECTION 16.2.1.3.2.2 - FIGURE 1

Eigenvalues (k_∞) as a function of fragmentation including parameter variations for the corium melt in the core catcher

2. ANALYSIS OF CORE MELT SEQUENCES

2.1. IN-VESSEL ACCIDENT PROGRESSION AND SELECTION OF RELEVANT SCENARIOS

2.1.1. Analysis of Core Melt Scenarios

Core degradation and in-vessel core melt progression provide the characteristics of melt relocation from the core into the vessel lower head and the energy released from the primary system, before and after vessel failure, and thus the initial conditions for assessing the loads on the surrounding structures and the containment.

In order to assess the effectiveness of design provisions and mitigation features intended to deal with the different consequences of a severe accident, boundary conditions and design safety requirements have been defined based on relevant core melt scenarios according to the following multi-step approach:

- the first step is to identify the relevant scenarios from a phenomenological point of view.

- the second step is to study the scenarios with integral codes and to classify different core melt scenarios which are representative for the situations which lead to a core melt. During this step, the following parameters are determined: primary circuit pressure level, mass and energy releases, steam, hydrogen and fission products releases, and melt release into the reactor pit after vessel failure.

- the third step is to select the relevant design scenarios associated with each severe accident challenge and to establish representative boundary conditions that provide the loads the mitigation feature(s) will have to cope with. These challenges are as follows:

  o primary coolant system depressurisation,

  o hydrogen risk in the containment,

  o ex-vessel melt stabilisation,

  o containment pressurisation, and

  o radiological releases into the containment.

In compliance with the safety approach for the exclusion of high-pressure core melt scenarios, the selection contains scenarios that cover a wide range of physical phenomena. Thus, a reasonable envelope for the phenomena is provided.

The selection of design-relevant scenarios is mainly based on deterministic principles; however, in some cases, additional probabilistic arguments are also used.

2.1.1.1. Definition of Relevant Cases of Core Melt Scenarios

For design measures and their assessment two relevant groups of scenarios are defined:

- Representative scenarios.

- Bounding scenarios.

The representative scenarios are used as a basis for the design measures proposed and/or the assessment of the specific measures or phenomena. Bounding cases are used to show the robustness of the proposed measures.

Representative scenarios:

The representative scenarios to be considered are consistent with the RCP [RCS] depressurisation strategy which means that they only cover low pressure cases. The progression of these scenarios will depend on the break size (if relevant), the heat removal capabilities from the secondary side, and the bleed actuation time. Without active safety injection recovery, vessel failure cannot be avoided for these cases.

The course of events leading from core uncovery to vessel failure involves the following phases, which are similar for the different scenarios, but have a different timing:

- core uncovery with core heat up resulting from gradual loss of cooling water,

- cladding oxidation with hydrogen and fission product releases from the gap,

- core melt onset with eutectic interactions between core materials and formation of a molten pool and additional release of fission products and inactive aerosols,

- onset of corium relocation to the water filled lower head of the vessel: dry-out of debris which re-melt and vaporisation of residual water, and

- heat up and failure of the vessel.

The representative cases are composed of:

- early low pressure core melt scenarios which do not necessitate bleed valve opening because RCP [RCS] depressurisation is achieved due to a sufficient break size, and/or secondary side heat removal capacities, or normal pressuriser safety valves opening. Even for such scenarios, one Primary Depressurisation System (PDS) line is opened at severe accident signal and will remain opened to avoid high pressure vessel failure.

- scenarios that require opening one PDS line to prevent core melting at high pressure. The RCP [RCS] depressurisation strategy aims at opening only one PDS-line, at least for a period of time that allows total accumulator water injection before the start of a significant oxidation of rods. The intention of this accident management strategy is to:

  o delay the onset of core melt,

  o reduce hydrogen production as much as possible,

      o   depressurise the primary system to avoid high pressure melt ejection from the reactor vessel and the risk of direct containment heating.

Any delay in opening the severe accident relief valves may lead to potential disadvantages which would increase containment loads; this is addressed in the section covering RCP [RCS] depressurisation and hydrogen risk.

Bounding scenarios:

Two kinds of bounding scenarios are considered:

- high pressure core melt scenarios with late primary system depressurisation, which can lead to passive accumulator water injection on the partially molten core or active water injection when the safety injection is available.

- all scenarios with active reflooding due to recovery of pumps and water sources.

The important parameters are the timing of the onset of water injection and the flow-rate of injection (dependent on the number of pumps available).

The following consequences are possible:

- reflooding, particularly during the first stage of oxidation with a slightly degraded geometry, may increase hydrogen production in-vessel. The increase in hydrogen production will depend on the level of core damage, the temperature level and the level of cladding oxidation prior to reflooding and the reflooding flow rate, because of the competing effects between the cooling by the water and the increase in temperature caused by the exothermal reaction of the zirconium with the steam.

- reflooding may lead to reactor vessel pressurisation due to the corium/coolant interaction. The degree of pressurisation depends on the level of corium fragmentation and the effectiveness of thermal transfer. It is limited by the RCP [RCS] discharge capacity. The reflooding time may affect the phenomena of corium relocation and solidification and blocking in the core. The discharge of steam from the RCP [RCS] also contributes to the increase in the containment pressure.

- early addition of water to the core with a sufficiently high flow rate during the first oxidation phase may quench the core and thus the core degradation may be stopped. It is possible that the molten core may be retained in the reactor vessel. However, if the water addition flow rate is insufficient, the core will heat up and reach the next stage of degradation.

- if the water injection is performed too late, i.e. when the corium can no longer be cooled, reactor vessel failure is inevitable and corium and water will be released from the reactor vessel into the reactor pit.

Sensitivity analyses on reflooding time have been carried out. A scenario is considered bounding when boundary conditions corresponding to the most onerous reflooding time are selected for the evaluation.

UK EPR

PRE-CONSTRUCTION SAFETY REPORT

CHAPTER 16: RISK REDUCTION AND SEVERE
ACCIDENT ANALYSES

SUB-CHAPTER : 16.2

PAGE : 31 / 295

Document ID.No.
UKEPR-0002-162 Issue 05

2.1.1.2. Analyses of Core Melt Scenarios

2.1.1.2.1. Analysis Methodology

Core melt scenarios are modelled, as far as possible, using a best estimate approach. The conservative assumption of the unavailability of MHSI and LHSI at the start of the accident results in a minimum time for the onset of uncovery.

The reactor vessel core melt scenarios are calculated using the MAAP code (Appendix 16A), which has been extensively benchmarked.

During the heat-up and melting of the fuel rods, volatile fission products are released and it is assumed that, the decay heat is divided between the remaining core, the containment atmosphere, the IRWST and the corium relocated into the reactor vessel lower head.

2.1.1.2.2. Main Assumptions for In-Vessel Core Degradation Analysis

Overpressure protection system, depressurisation system and engineered safeguards systems:

Data is given in Section 16.2.2.1 - Table 1. These values correspond to the assumptions taken into account in the severe accident studies.

Core characteristics and main steel mass in vessel:

Data is given in Section 16.2.2.1 - Table 2. These values correspond to the assumptions taken into account in the severe accident studies.

Main initial conditions:

See Section 16.2.2.1 - Table 3. These values correspond to the assumptions taken into account in the severe accident studies.

Initial fission product inventory:

See Section 16.2.2.1 - Tables 4 and 5. These values correspond to the assumptions taken into account in the severe accident studies.

Decay heat used for severe accident studies:

See Section 16.2.2.1 - Table 6. These values correspond to the assumptions taken into account in the severe accident studies.

Timing of the accident progression of main scenarios without in-vessel reflooding:

The chronology of the core melt scenario events is shown in Section 16.2.2.1 - Tables 7 to 11.

The different stages considered during core degradation are as follows:

- Time t0: Core uncovery resulting from the loss of primary coolant.

- Time t1: Core heat-up, cladding oxidation and start of fission product release.

- Time t2: Onset of core melt with eutectic interactions among the core materials, candling of the cladding, structural materials and fuel, and formation of blockage zones at the bottom of the core, followed by the appearance of a pool of corium.

- Time t3: Beginning of mass relocation to the reactor vessel lower head. The generic behaviour of natural convection for a molten mass heated volumetrically first leads to sideways relocation via the heavy reflector which occurs before a downward relocation through the thick support plate of the core.

  o This initial relocation always takes place into the water-filled lower plenum of the reactor pressure vessel. Some or all of the relocated material may become converted into debris (i.e. particles or fragments of different sizes) made up of both metal and oxides.

  o Between t3 and vessel failure (t4) a period of corium heating occurs after the first relocation in the water. The debris dries out, re-melts and progressively forms a pool of corium, which includes successive downflows from the melting core. A crust develops on the top of the pool and along the wall of the reactor vessel.

  o The calculation uses the assumption of a homogeneously mixed oxidic debris pool which exchanges heat by natural convection with the crust. A metallic layer is above the oxidic molten pool and particulate debris is assumed to rise to the top. A convective circulation together with conduction in the metallic layer may remove decay heat from the oxidic molten pool and may distribute it along the interface between the metal layer and the vessel wall.

- Time t4: Reactor vessel failure due to one of various possible mechanisms:

  o The layer of molten metal may thermally attack and weaken the reactor vessel wall,

  o The remaining internal pressure, the weight of the corium and the thermal loads may cause a creep rupture,

  o Jet forces during the relocation phase may cause a localised failure of the reactor vessel lower head. Analysis does not predict this type of failure but instead predicts fragmentation of the corium and the formation of a crust at the moment of the first flow into the water-filled reactor lower head.

2.1.1.2.3. Identification of Main Scenarios for Representative Cases

The main core melt scenarios to be considered are:

- total loss of the RRI-SEC [CCWS-ESWS] cooling train,

- total loss of offsite power (LOOP) combined with the loss of 6 diesel generators,

- total loss of ultimate heat sink,

- small break LOCA (SB(LOCA)),

- large break LOCA or break of the surge line (LB(LOCA)),

- steam generator tube rupture (SGTR),

- total loss of residual heat removal,

- total loss of the steam generator feedwater (TLOFW),

- primary break outside the containment (V(LOCA)),

- loss of primary system water inventory in shutdown state.

This list of core melt scenarios covers all the cases of water loss which lead to core uncovery and damage. Since safety injection is unavailable, the progress of the accident is influenced by the size of the break (in case of LOCA) and the heat removal capacity by the steam generators. The scenarios in which the coolant train is lost, LOOP, and small break LOCA may be classified in families according to the possibility of secondary side heat removal. In the first approach, a steam generator tube rupture, a failure of primary pump seals after a total loss of power or a break in one of the primary pumps themselves after a loss of RRI-SEC [CCWS-ESWS] are similar to a LOCA.

In the case of a small break LOCA, if the break of the RCP [RCS] is not sufficiently large to remove all decay heat, some energy is transferred to the secondary side and the primary pressure stabilises at the SG safety valves setpoint value plus a few bar when saturation point is reached in the RCP [RCS].

In the case of partial automatic cooldown failure due to a factor other than the loss of the main valves, the operator will activate maximum manual depressurisation 30 minutes after reactor trip by fully opening the main steam atmospheric dump valves.

Most studies have been performed for core melt scenarios initiated at full power conditions (status 100% Nominal Power).

For shutdown scenarios, the analysis is limited to checking the effect of low decay heat on the main boundary conditions: i.e. pressure in the RCP [RCS], hydrogen production, reactor failure mode and corium release from the vessel.

2.1.1.2.3.1.   Full Power Conditions

The scenarios analysed for each family are described below:

Family 1: SB(LOCA) and SGTR with partial and fast secondary cooldown (Table 7).

SB(LOCA): several break sizes were analysed [Ref-1].

At initial time (t = 0), a break in the cold leg is opened instantaneously. Sub-cooled water is discharged through the break and the RCP [RCS] coolant inventory decreases. Failure of MHSI and LHSI is assumed. The pressuriser is the part of the primary system which empties first. The reactor trip signal is sent when the pressuriser pressure drops to 130 bar. The reactor trip signal is set to 6 seconds. At this time, the main feedwater is instantaneously shut off and the emergency feedwater is activated with a delay of 50 seconds. The RCP [RCS] water reaches saturation and voiding appears in the core. Due to water draining through the break and to RCP [RCS] water vaporisation, the upper and the hottest regions (such as the upper plenum, the hot legs and steam generator tubes) start to void. The main coolant pump coasts down very quickly (time 4 minutes). When the safety injection system setpoint is reached at a low pressure of 110 bar, a partial cooldown is automatically realised by opening of the SG relief valves in order to depressurise the secondary side down to 60 bar in 20 minutes (equivalent to a cooldown rate of 100°C/h).

At 30 minutes after reactor scram, the operator initiates maximum depressurisation of the secondary side by total opening of the main steam atmospheric dump valves (VVP [MSSS]).

Due to the full opening of these valves and the size of the break, the primary pressure drops to the accumulator threshold value before the onset of core uncovery. The accumulator water depletion happens 35 minutes into the LOCA scenarios with a small 5 cm break in the cold leg. Thus reflooding and subsequent core cooling give a delay before core uncovery.

In all cases, when the temperature at the core outlet reaches 650°C, the dedicated severe accident relief valve is opened, even if the primary system has already been depressurised by the secondary cooldown.

The 650 °C criterion is met only after drying out of the SGs and that the refill-up of the SG feed-water tank until 100 hours is not taken into account, which is conservative.

For evaluation of the calculation, as an example, selected parameters like water inventory, pressure, mass of molten material and maximum fuel rod temperature of a 5 cm break are shown in Section 16.2.2.1 - Figures 1 and 2.

SGTR: core melt scenario [Ref-2]

This has been analysed to identify the leak tightness functional requirements for the secondary system consistent with the radiological source term targets. The scenario and assumptions are as follows:

- an SGTR (a double-ended tube rupture) at the top of the tube plate,

- no leak from the steam isolation valves,

- emergency boron system (RBS [EBS]) unavailable,

- failure of the (AAD [SSS]) and the (GCT [MSB]),

- reactor trip and turbine trip on (RCP [RCS]) low pressure criterion,

- at reactor trip, loss of the SEC [ESWS], the RRI [CCWS], RCV [CVCS], RIS [SIS] and Reactor Coolant Pumps,

- manual isolation of the 4 steam generators on reactor trip. SEC [ESWS] initiated on the 3 intact steam generators (4 ASG [EFWS] tanks available). Cooling partly achieved on 4 SGs on the actuation of the safety injection signal (on RCP [RCS] low pressure). Cooling rapidly achieved on the 3 intact SGs at the safety injection signal + 30 minutes and rising of the VVP [MSSS] threshold of the SG to 96 bar. No re-filling of ASG [EFWS] tanks,

- opening of the dedicated severe accident relief valve when the maximum core outlet temperature reaches 650°C.

For evaluation of the calculation, selected parameters such as RCP [RCS] pressure, water level in the core, masses of water in the primary circuit and pressuriser, temperature of vapour in SG and pressure in SG are shown in Section 16.2.2.1 - Figure 7 to Figure 9.

__Family 2: LB(LOCA) and SB(LOCA) with partial secondary cooldown only (Section 16.2.2.1 - Table 8)__ **[Ref-3]**

Breaks of different sizes have been analysed. The evolution of primary pressure is connected to the steam discharge rate at the break:

- in the case of large break LOCA scenarios, the break is sufficient to remove the residual heat. Heat exchange in the water-fed SG is achieved from the secondary side to the primary side (the secondary becomes a heat source and transfers its energy to the primary): the primary pressure drops below the secondary pressure.

- in the case of smaller breaks, e.g. a break of 46 cm^2 (7.5 cm), since the steam discharge rate at the break is insufficient to completely remove the heat generated by the core, a part of the decay heat is transferred to the secondary side by the vaporisation of the feedwater which supplies water to the steam generator. The heat flux goes from the primary side of the steam generator tubes to the secondary side; the temperature of the primary side coolant is slightly higher than the saturation temperature of the secondary side pressure of the water-fed SG. The primary pressure consequently stabilises at a value higher than that of the secondary pressure which corresponds to the steam generator relief valve setpoint. In the case of a break of 46 cm^2, the primary pressure follows the evolution of the secondary pressure: during partial cooldown, the pressure falls then stabilises just below 60 bar.

- For evaluation of the calculation a LB(LOCA) and a 5 cm SB(LOCA), the same parameters as indicated above are depicted in Section 16.2.2.1 - Figures 3 to 6.

__Family 3: Scenarios without RCS break and with SG dryout (Section 16.2.2.1 - Table 9)__

Two scenarios were analysed: LOOP [Ref-4] and TLOFW [Ref-4].

The description of a LOOP scenario with loss of the emergency diesel generators and loss of emergency feedwater system is as follows:

- the loss of offsite power at time t = 0 seconds causes the shutdown of the primary pumps and the ARE [MFWS] pumps, reactor and turbine trip. The turbine isolation valves close and a signal is sent to start up the emergency feedwater injection. The emergency feedwater and emergency power (diesel generators) are unavailable, thus preventing the use of active systems. Only the passive components are available: discharge valves and pressuriser, steam generator and accumulator safety valves.

- 6 seconds after accident initiation, the control rods are fully inserted into the core, but the core heat generation is such that the primary pressure rises to the opening pressure of the pressuriser valves.

- from this time, the steam generators are removing enough decay heat from the core by secondary water vaporisation to allow the primary pressure to decrease to around 140 bar. Subsequently, there is no longer enough water in the SG secondary side resulting in an increase of primary system pressure to the cycling point of the pressuriser valves. When the lowest opening pressure of the valves is reached, the decay heat removal begins by the loss of primary water inventory. The steam generators have dried out after just 2 hours.

- manual depressurisation of the RCP [RCS]: the severe accident criterion for opening the severe accident relief valve is reached at approximately 3 hours 20 minutes.

The total loss of feedwater scenario differs from the above LOOP only in that the automatic shut down does not occur at time t = 0 seconds but is initiated on the low SG level criterion and the shutdown of the primary pumps on the very low SG level. Due to the higher quantity of energy transmitted to the RCP [RCS], SG dryout occurs earlier.

2.1.1.2.3.2.   Shutdown Conditions

Shutdown conditions have only been examined for LOOP scenarios, with different levels of decay heat, with or without the availability of accumulators and two levels of RCP [RCS] water (full and mid-loop).

From a phenomenological point of view, these scenarios are representative of many other scenarios, such as those with the loss of coolant.

Three reactor conditions have been analysed:

- B: hot shutdown, RHR not connected, RCP [RCS] full of water, RCP [RCS] closed.

- C: intermediate cold shutdown, RHR connected, RCS level at mid-loop, SG pressure at 1 bar.

- D: cold shutdown, RHR connected, RCP [RCS] level at mid-loop, SG pressure at 1 bar.

Condition C is subdivided into two subsidiary conditions, Ca and Cb.

Condition Ca is characterised by:

- an RCP [RCS] full of water (nominal level) and closed,

- a primary pressure between 1 bar and 25 bar,

- a primary temperature between 55°C and 120°C.

For all calculations, the initiating event occurs 6 hours (time 0 on the MAAP calculation) after the reactor scram with a primary pressure of 25 bar and a primary temperature of 120°C.

Condition Cb is characterised by:

- a mid-loop level of RCP [RCS],

- a primary pressure of 1 bar,

- a primary temperature of 55°C.

For all calculations (conditions Ca and Cb) the following assumptions have been adopted:

- the RHR is lost,

- the accumulators are isolated,

- the primary pumps are stopped,

- the pressuriser safety valve setpoints are at 40 bar for opening and 30 bar for closing,

- the setpoint for main steam atmospheric dump valves is 2 bar,

- the thermal-hydraulic conditions of the secondary side are:

    o P = 2 bar,

    o T = 120°C,

    o Level = nominal level at 100% ≈ 16 m.

In condition D, the accumulators are isolated, the steam generators are empty, the primary system is assumed to be open above the pressuriser, and the accident is assumed to have occurred 38 hours after reactor scram.

2.1.1.2.3.3. Non Mitigated Scenarios

In order to be able to assess the consequences of late RCP [RCS] depressurisation on hydrogen production, creep failure risk due to high pressure scenarios, and to identify the available time for the operator to depressurise the primary circuit manually, scenarios without opening of severe accident relief valves were studied. These are TLOFW and SB(LOCA) with no partial or fast secondary cooldown, and SB(LOCA) with only partial secondary cooldown with one steam generator (Tables 10 and 11).

2.1.1.2.4. Identification of Bounding Scenarios

An assessment of the importance of in-vessel reflooding and the consequences for all challenges in the case of severe accidents must take into account the likelihood of a late depressurisation of the RCP [RCS] leading to water injection, or a recovery of active safety injection and the accident management strategy.

Various families of reflooding scenario have been identified:

- the scenario involving high pressure core melt with safety injection available (late depressurisation of the RCP [RCS] leads water injection),

- core melt scenarios with failure of the MHSI/LHSI pumps. Repair of at least one pump allows the reactor vessel to be reflooded.

- core melt scenarios with loss of the RRI [CCWS]/SEC [ESWS] cooling system

- LOOP core melt scenario with failure of emergency diesel generators. Repair of the diesel generators may allow the reactor vessel to be reflooded,

- LOOP core melt scenario. Recovery of offsite supplies may allow the reactor vessel to be reflooded.

The consequence of reflooding the reactor vessel due to accident management procedures are analysed in a parametric manner: the parameters are the time of onset of safety injection and the flow rate. The variations in these parameters are studied for two groups of scenarios:

- a scenario in which the RCP [RCS] is intact: LOOP and total loss of feedwater,

- a core melt scenario with a break of the RCP [RCS]: SB(LOCA) with partial secondary cooldown only for the late RCP [RCS] depressurisation and SB(LOCA) with fast secondary cooldown for active reflooding by safety injection.

2.1.2. Selection of Relevant Scenarios to Design Mitigation Features

The boundary conditions used in the design of mitigation measures are derived from the results of representative or bounding scenarios which may reasonably fall within the range of the phenomena which must be controlled by mitigation features. These are used as a basis for designing the mitigation measures for the following risks:

- risk of reactor vessel failure at high pressure (scenarios of core melt at high pressure):

  o prevention of induced steam generator tube rupture (SGTR) and the risk of containment bypass by radioactive materials,

  o preventing the corium from being dispersed in the containment under high pressure and leading to direct containment heating (DCH).

- hydrogen risk:

  o preventing a global detonation or local transition from deflagration to detonation,

  o limiting the global deflagration pressure peaks to below the containment proof pressure of 6.5 bar, for both representative and bounding scenarios.

- risk of ablation of foundation raft:

  o avoiding corium ablation of the concrete foundation raft and in particular the penetration of the liner.

- risk of excess containment pressure for a long period of time:

  o limiting the containment pressure peaks to below the containment design pressure of 5.5 bar.

- risk of not meeting radiological targets:

  o limiting the leak rate from the internal containment to 0.3% per day of the gas volume inside the containment at the design pressure of 5.5 bar, under accident conditions without direct leaks to the environment,

  o prevention of containment bypass.

2.1.2.1. Prevention of High Pressure Core Melt Scenarios

2.1.2.1.1.   Parameters of Interest to Select Reference Scenarios

Concerning prevention of HP core melt scenarios, the main parameters to be considered are as follows:

- Actuation signal for depressurisation.

- Time available for successful depressurisation until RPV melt-through.

For actuation of one Primary Depressurisation System (PDS) line, which includes two motor operated valves in series in the discharge line to the pressuriser relief tank, the appropriate criterion is the temperature of the primary fluid. In order to determine the necessary bleed capacity, the relevant criterion is the time which is available between actuation signal and RPV melt-through. In addition, the conditions (pressure and temperature) of the fluid at valve opening are important.

It is assumed that in-vessel reflooding, which occurs after onset of core relocation into the lower head, cannot guarantee to save the vessel because the geometry of the debris is unknown and efficient debris cooling cannot consequently be guaranteed. So, in the case when reflooding is too late, the time of reflooding and the flow-rate will only influence the pressure spike and the pressure at vessel failure, but reflooding will not necessarily lead to in-vessel melt stabilisation.

2.1.2.1.2.   Reference Scenarios

Section 16.2.2.1 - Table 12 presents the reference scenarios studied to assess the efficiency of the mitigation approach to prevent high pressure vessel failure. LOOP with unavailability of 6 diesel generators and TLOFW both have scenarios with and without in-vessel reflooding. For the main scenarios without in-vessel reflooding, the vessel failure pressure will be below 5 bar. For core melt scenarios for which in-vessel reflooding is too late to save the vessel, the vessel failure pressure could be up to 20 bar [Ref-1].

2.1.2.2. Hydrogen Risk

2.1.2.2.1.   Parameters of Interest to Select Representative Scenarios

The selection of scenarios and relevant boundary conditions is made to determine the parameters which influence the main risk in the containment.

The important parameters are the release mode of hydrogen, hydrogen production and the associated steam content. The main risks in the containment are:

- the risk of global detonation or local deflagration to detonation transition (DDT), which should be prevented, and the pressure peak due to fast local deflagration. The main parameters affecting this risk are the maximum hydrogen production rate, hydrogen release rate and steam content; a higher steam content reduces the risks of fast deflagration and transition to detonation;

- the adiabatic isochoric (constant volume) complete combustion (AICC) pressure (p_{AICC}) which was calculated systematically in all analysed scenarios. The worst cases are those which combine a large mass of hydrogen with the largest amount of steam possible below the inerting limit;

UK EPR

PRE-CONSTRUCTION SAFETY REPORT

CHAPTER 16: RISK REDUCTION AND SEVERE
ACCIDENT ANALYSES

SUB-CHAPTER : 16.2

PAGE : 40 / 295

Document ID.No.
UKEPR-0002-162 Issue 05

- the thermal loads on the containment and the steel liner due to recombination or combustion; the available mass of hydrogen in the containment which may burn is the main parameter influencing these loads.

2.1.2.2.2. Hydrogen Production

2.1.2.2.2.1. Representative Scenarios

The amount of hydrogen produced has been determined for all scenarios studied (Section 16.2.2.1 - Table 13). These "representative scenarios" are selected on the basis of their likelihood and are used to demonstrate the efficiency of hydrogen mitigation features.

Several phases of hydrogen production are identified:

- The first oxidation phase including relocation of oxidic and metallic materials in the core. This corresponds to the highest H_2 production as predicted by the MAAP4 code [Ref-1] and mainly depends on the oxidation surface area, kinetic rate, steam availability (dependent on the water supply and the flow blockages in the core), and the diffusion of steam and hydrogen in the gas mixture in the uncovered part of the core.

- The second phase during relocation of corium into the lower head which depends on the relocation flow rate and debris fragmentation level; there is no significant H_2 production in phase 2 according to predictions by the MAAP4 code [Ref-1].

- The ex-vessel production phase, which depends on the interaction between melt and sacrificial concrete in the reactor pit and on the spreading area.

Only the hydrogen produced during the first oxidation phase is considered to be relevant because the rate of recombination is greater than the production rate during later phases of the accident progression [Ref-1] and leads to good mixing of the containment atmosphere, thus reducing the risk of fast deflagration.

Many sensitivity studies and code comparisons have been performed for this phase which confirms the suitability of MAAP4. In general, it can be stated that MAAP4 hydrogen production rates bound other calculations for scenarios without reflooding.

Thus, by using MAAP4 results, the relevant scenarios for hydrogen production have been chosen which have the highest amount of hydrogen produced in one phase and a high flow rate.

In order to assess the local H_2 risk in different compartments, SB(LOCA) studies have been performed not only for different break sizes but also for different locations, with breaks in the cold leg, hot leg, and the pressuriser [Ref-1].

In order to investigate the effect of hydrogen released after RPV failure and the effect of thermal loads resulting from standing flames, the SB(LOCA) "20 cm² cold leg scenario with only partial secondary cooldown" has been investigated [Ref-1]. This is a representative scenario which leads to the production of significant amounts of burnable hydrogen and which minimises the period between in-vessel and ex-vessel hydrogen production.

2.1.2.2.2.2. Bounding Scenarios

The production of hydrogen with in-vessel passive or active reflooding, which are considered as bounding scenarios, have been determined in a conservative manner. Additional production of hydrogen has been calculated for many reflooding times with MAAP4 code and only the worst case, corresponding to maximum hydrogen production together with the most unfavourable moment of reflooding is selected. MAAP4 predicts significant additional hydrogen production rate, only for reflooding which occurs during the autocatalytic oxidation phase of the rods**.** Passive accumulator water injection in the case of late depressurisation in a high pressure scenario or active reflooding with MHSI or LHSI pumps running provide an additional supply of steam, which sustains and reinforces the oxidation process.

The reflooding scenarios are "bounding scenarios" selected they include phenomena that might aggravate the hydrogen risk. They are used to demonstrate the robustness of the concept of preventing early containment failure with regard to "cliff-edge" effects.

2.1.2.2.3. Hydrogen Release Mode

Direct discharge into the containment is via the pressuriser relief tank which has discharge pipes installed lower than the pressuriser safety valves to avoid any water plug downstream of the valves. A large pressuriser relief tank is needed to collect the pressuriser safety valve discharge to avoid contaminating the containment in the most frequent events and to collect discharges in case the pressuriser safety valve is stuck in the open position for a few minutes during testing.

A 40 m^3 tank is compatible with the present layout. Its location is at the 1.5 m level. The tank is in series with the discharge piping and is separated by a wall from the neighbouring generator blowdown system flash tank. It is equipped with two rupture disks which direct the discharge of the pressuriser relief tank to two reactor coolant pump compartments (2 and 3).

According to the behaviour of the pressuriser relief tank rupture disk, which ruptures at 19 bar differential pressure, three different release modes are possible:

- release only through the break as in SB(LOCA) scenarios with fast secondary cooldown because the RCP [RCS] is depressurised to below 20 bar due to the break size or steam generator heat removal before the core outlet temperature reaches 650°C and a PDS line is opened. [Ref-1]

- release only through the pressuriser valves for core melt scenario without any RCP [RCS] break, such as LOOP with failure of 6 diesel generators or TLOFW.

- release of gas mixture through the break and through pressuriser valves for scenarios such as SB(LOCA) with only secondary partial cooldown. A mixed release scenario could influence:

    o The hydrogen content in pump compartments 2 or 3 in the case of additional releases: break release + PDS release.

    o The risk of flame propagation from areas having leaner mixtures into areas with richer mixtures (or the contrary) in the case of two different release locations.

UK EPR

PRE-CONSTRUCTION SAFETY REPORT

CHAPTER 16: RISK REDUCTION AND SEVERE
ACCIDENT ANALYSES

SUB-CHAPTER : 16.2

PAGE   : 42 / 295

Document ID.No.
UKEPR-0002-162 Issue 05

2.1.2.2.4. Selection of Hydrogen Releases into the Containment

Section 16.2.2.1 - Figure 11 shows the mass of hydrogen produced against time for different reflooding times for the SB(LOCA) scenario, "20 cm² break in cold leg with fast secondary cooldown" [Ref-1], which is a scenario with high hydrogen production and low steam content.

The scenarios selected for the analysis of the different hydrogen risks: dynamic pressure due to fast deflagration, AICC pressure and thermal loads due to recombination or combustion are given in Section 16.2.2.1 - Table 13.

The different masses of hydrogen produced in-vessel selected for the containment analysis are presented in Section 16.2.2.1 - Figure 10.

2.1.2.3. Risk of Basemat and Reactor Pit Ablation

2.1.2.3.1. Parameters of Interest to select Reference Scenarios

Relevant scenarios are selected to justify the functioning of temporary melt retention in the reactor pit as a principal prerequisite for successful melt spreading and long-term melt stabilisation. The corium releases from the vessel are the boundary conditions of the mitigation approach. The scenarios are chosen with reference to the following relevant parameters:

Pressure at reactor vessel failure:

For the main representative scenarios without in-vessel reflooding, gravity driven flow is the main release mode of the corium from the vessel because the vessel failure pressure is expected to be below 5 bar. Only for low likelihood bounding scenarios such as late in-vessel reflooding, can a corium dispersal mode occur since the vessel failure pressure could be in the range up to 20 bar.

Modes of reactor vessel failure:

In spite of remaining R&D uncertainties, there is a high likelihood that in most cases the lower vessel head failure will be as a consequence of creep which may be accompanied by partial melting of the vessel wall.

For the main core melt scenarios, the first relocation of melt into the lower head occurs through breaches in the heavy reflector and vessel baffle.

According to MAAP4 predictions, there is no vessel failure due to ablation caused by a corium jet. Instead, MAAP 4 predicts the formation of a molten oxidic pool in the lower head [Ref-1].

Different configurations of corium phases may exist which can lead to different stratification layers in the lower head. A particular assumption of stratification is taken into account in the studies: the oxidic debris pool is homogeneously mixed and the metal layer rises to the top of the debris pool. The same convective circulation in the metal layer which transfers the decay heat of the debris bed upward is responsible for the sideward heat transfer between the bulk metal layer and the vessel wall, which is at the melting point.

Therefore, the main first failure mode considered for representative melt release corresponds to a small discharge hole located at the lateral part of the lower head where the molten metal and the wall are in contact. The size of the hole increases by wall ablation during the molten corium discharge. The growth of the initial failure is sufficient to discharge the part of the corium pool that is available above the location of the hole very rapidly; a small initial hole is predicted to grow to around 40 cm (the exact value is MAAP4 code specific).

The standard MAAP4 mechanical model has a two step RPV failure mode: increased heat transfer to the vessel wall from the metallic layer leads to a local rupture near the transition between oxidic and metallic layers if load stress is greater than the yield stress. Alternatively, the vessel may fail by creep according to the temperature distribution in the vessel. The location of the hole could be at a lower level if corium pressure becomes significant. All the corium above the failure location drops into the reactor pit. However, a large part remains in the vessel until a second failure occurs due to creep rupture, which results in a discharge of the residual corium located in the lower head.

The corium in the lower head continues to transfer heat to the core support plate by radiation. This accelerates its thermal failure and consequently the release of corium.

Due to the high thermal flux to the vessel from the metallic layer on the top surface of the corium pool in the lower head, it is theoretically possible that quasi-uniform symmetrical thermal loads could lead to a circumferential failure. The failure mode with a full circumferential shear of the lower head leads to an instantaneous release of the corium located in the lower head. Such a failure is assumed to occur for higher vessel pressures (< 20 bar), which can evolve in scenarios with late reflooding. Such a failure conservatively taken into account to bound the hydrodynamic loads in the reactor pit and to evaluate the risk of debris entrainment.

However, because of inherent local variations in the heat flux distribution in the lower head and in the local vessel wall thickness, it is more likely that the initial failure will be significantly less than 360°. Assuming 3D loads and local failure, only a limited amount of melt may be released into the reactor pit at vessel failure while the rest is released later in parallel with the progressive weakening of the remaining part of the vessel lower head.

The MAAP4 calculations assume that the lower part of the vessel insulation is destroyed after the first melt release. The heat-up of the vessel takes thermal radiation into account using an iterative process and the temperature of the slag layer of the molten core-concrete pool which represents the corium/sacrificial material interactions in the pit. The radiation emissivities of the vessel wall and the surface of slag are assumed to be 0.85.

Amount of corium:

A total mass of molten material of 300,000 kg is assumed, which constitutes a decoupling value, as it bounds the MAAP4 results ranging from 230,000 kg to 285,000 kg according to the scenario [Ref-2].

For a total inventory of Zr of 38,300 kg, the range of in-vessel Zr oxidation is 30% to 60% according to the scenario.

The temperature of the oxidic melt can be in the range 2300°C to 2500°C. 2500°C corresponds to the liquid temperature of a melt consisting of 141,000 kg UO_2, 21,000 kg ZrO_2 and 21,000 kg Zr. This composition corresponds to an in-vessel Zr-oxidation level of 40% and the assumption that most of the unoxidised Zr dissolves in the oxidic melt**.**

The temperature of the metallic melt is found to be in a range between 1500°C to 1700°C. The amount of Fe is a function of the scenario and can reach up to 100,000 kg.

2.1.2.3.2. Selection of Corium Releases into the Reactor Pit

The release sequences given in Section 16.2.2.1 - Figure 12 are from representative scenarios, i.e. scenarios without late in-vessel reflooding. For the scenarios LB(LOCA) and LOOP during power and shutdown states, the mass of oxidic corium (UO_2, ZrO_2) is around 160 tons. The remaining part of 60 tons is metallic corium mainly consisting of Fe. For SB(LOCA) scenarios the metallic mass is about 100 tons. Given the assumed failure mode of the lower head as well as the effect of radiant heat exchange between the melt free surface and the lower structures of the RPV, the core melt inventory is completely released into reactor pit within 40 to 80 minutes according to the scenario. [Ref-1]

2.1.2.4. Containment Pressurisation

Taking into account all the energies released into the containment for a severe accident scenario, the design pressure and temperature of the inner containment must ensure leak tightness without operation of the containment heat removal systems for a period of at least 12 hours.

A 12 hour period corresponds to the minimum passive energy storage capacity of the containment (mainly thermal inertia of the containment structures and the IRWST). The different parameters that influence the containment pressurisation rate are:

- The early mass and energy release, which depends on the RCP [RCS] break size.

- The hydrogen release, which depends on the specific scenario.

- The decay heat, which depends on the timing of the accident. The time from the initiating event influences:

  o the decay heat in the corium.

  o the decay heat in fission products released into the containment.

- The ex-vessel corium interaction with sacrificial material, which depends on the content of sacrificial material and includes both exothermic and endothermic reactions.

- Corium quenching in the spreading area, which depends on corium fragmentation and water flow rate in the spreading area.

- The MHSI availability, which depends on many parameters and, in particular, on the IRWST water temperature (and LHSI availability).

The pressuriser surge line LOCA (35.6 cm) is the relevant scenario because it leads to the most rapid core degradation leading to:

- The highest initial mass and energy release from the vessel into the containment because the IRWST is completely by-passed.

- The shortest time to corium quenching on the spreading area.

- The highest decay heat.

Mass and energy releases from the vessel are given on Section 16.2.2.1 - Figures 13 and 14. Mass and energy release into the containment resulting from ex-vessel processes is described in section 2.4 of this sub-chapter.

SECTION 16.2.2.1 - TABLE 1

MAAP4 data – Assumptions for severe accident studies
Overpressure protection system, depressurisation system [Ref-1]

PORV opening pressures	174, 178, 178 bar
Assumption of total RCP [RCS] severe accident discharge through one PDS-line	250 kg/s at 176 bar
Secondary side relief valves opening pressure	95.5 bar
Secondary side safety valves opening pressure	104 bar

Pump head table: 1 MHSI pump		
Height (m)	Volumetric flow rate (m^3/s)	Mass flow rate (kg/s)
800	0	0
700	$1.417\ 10^{-2}$	14.16
600	$2.278\ 10^{-2}$	22.8
400	$3.444\ 10^{-2}$	34.44
0	$5.111\ 10^{-2}$	51.1
Pump head table: 1 LHSI pump		
Height (m)	Volumetric flow rate (m^3/s)	Mass flow rate (kg/s)
200	0	0
160	$4.028\ 10^{-2}$	40.3
120	$6.611\ 10^{-2}$	66.1
60	$9.528\ 10^{-2}$	95.3
0	$1.156\ 10^{-1}$	115.5

Accumulators:

– Number
   (all injecting into downcomer, MAAP 4 assumption): 4

– Total volume: 47 m³ for each accumulator

– Initial water mass: 31700 kg

– Initial pressure: 45 bar

SECTION 16.2.2.1 - TABLE 2

MAAP4 Data – Assumptions for severe accident studies
Core characteristics and main steel mass In Vessel [Ref-1]

The EPR core has 241 fuel bundles (17x17) and 89 control rod clusters (each containing 24 absorber rods). Each bundle contains 265 fuel rods, 24 guide tubes for control rods. The mass of Ag is 3,167 kg, mass of In is 594 kg and mass of Cd is 198 kg. This mass corresponds to the total amount of Ag-In-Cd and B4C in the EPR hybrid control rods.

The total mass of UO_2 is 140,800 kg (fuel pellets).

Zircaloy is located in the fuel cladding, the guide tubes for control rods, the instrumentation tubes and the grids.

The main contributor to hydrogen production is the Zircaloy. Steel also may be an additional source of H_2 production.

Zircaloy inventory (kg)	Fuel cladding	Guide tubes	Grids	Top and bottom plugs
Active part	29925	3001	1504	
Non-active part	2494	250	364	554

Hydrogen production potential as function of Zircaloy masses:

	Active fuel clad	Total fuel clad	Active	Total Zircaloy
Zircaloy (kg)	29925	32419	34430	38092
H2 (kg)	1312	1422	1510	1684

Main steel mass in the vessel:

- Core barrel below the elevation of top of the core: 32,600 kg

- Core barrel above the elevation of top of the core: 24,100 kg

- Heavy reflectors: 94,300 kg

- Core upper plate: 4,000 kg

- Core support plate: 24,300 kg

- Vessel: 1,150 kg/m²

SECTION 16.2.2.1 - TABLE 3

MAAP4 Data – Assumptions for severe accident studies
Main Initial Conditions [Ref-1]

PRIMARY SYSTEM AND STEAM GENERATORS	
RPC [RCS] pressure	155 bar
Average RPC [RCS] temperature	313°C
Secondary side pressure	78 bar
Average secondary temperature	287°C
Mass of water in RPC [RCS], not including pressuriser	269000 kg
Mass of water in pressuriser	24800 kg
Mass of water in steam generator (secondary side)	4 x 81000 kg
SG heat transfer area (5980 tubes/SG)	7960 m² (secondary side)/SG
CONTAINMENT	
Pressure of air in containment	1 bar
Initial temperature of air in containment	30°C in accessible part 42°C in non accessible part
Mass of water in IRWST	2,066,000 kg
Temperature of water in IRWST	42°C

SECTION 16.2.2.1 - TABLE 4

Initial Fission Product Inventory – Assumptions for severe accident studies

Mass of elements (kg)	
Results obtained with ORIGEN-S without uncertainty [Ref-1]	
Elements	**Masses (kg)**
Xe	833.82
Kr	53.98
I	39.10
Rb	49.18
Cs	505.79
Sr	131.37
Ba	238.76
Y	68.82
La	196.46
Zr	511.17
Nb	4.67
Mo	524.24
Tc	124.55
Ru	415.64
Sb	2.67
Te	77.68
Ce	437.52
Pr	176.19
Nd	602.49
Sm	118.69
Np	75.36
Pu	4204.78

UK EPR

PRE-CONSTRUCTION SAFETY REPORT

CHAPTER 16: RISK REDUCTION AND SEVERE
ACCIDENT ANALYSES

SUB-CHAPTER : 16.2

PAGE   : 50 / 295

Document ID.No.
UKEPR-0002-162 Issue 05

SECTION 16.2.2.1 - TABLE 5

Initial fission products inventory – Assumptions for severe accident studies

Fission product groups, masses (kg)			
Results obtained with ORIGEN-S without uncertainty [Ref-1]			
1	Noble gases	Xe	833.82
		Kr	53.98
		Tot	887.80
	Structural materials	Cd	198
		In	594
		Ag	3167
		Sn	527.20
		Mn	115.00
		Tot	4601.20
2	CsI + RbI		79.96
3	TeO_2		0
4	SrO		158.24
5	MoO_2		715.37
6	CsOH + RbOH		586.40
7	BaO		269.90
8	$La_2O_3 + Pr_2O_3 + Nd_2O_3 + Sm_2O_3 + Y_2O^3$		1364.50
9	CeO_2		550.03
10	Sb		2.78
11	Te_2		78.29
12	$UO_2 + NpO_2 + PuO_2$		145640

UK EPR

PRE-CONSTRUCTION SAFETY REPORT

CHAPTER 16: RISK REDUCTION AND SEVERE ACCIDENT ANALYSES

SUB-CHAPTER : 16.2

PAGE : 51 / 295

Document ID.No.
UKEPR-0002-162 Issue 05

SECTION 16.2.2.1 - TABLE 6

Decay heat – Assumptions for severe accident studies

Time after Shutdown	Decay heat assumption used for severe accident analyses (% of nominal power) [Ref-1]
0.1 s	6.008
1 s	5.612
5 s	4.828
10 s	4.391
50 s	3.402
100 s	2.996
1800 s	1.612
1 h	1.307
5 h	0.846
10 h	0.718
24 h	0.575
36 h	0.514
111 h	0.359
8 d	0.292
11 d	0.258
13 d	0.242
15 d	0.229
20 d	0.209
32 d	0.170

UK EPR

PRE-CONSTRUCTION SAFETY REPORT

CHAPTER 16: RISK REDUCTION AND SEVERE ACCIDENT ANALYSES

SUB-CHAPTER : 16.2

PAGE : 52 / 295

Document ID.No.
UKEPR-0002-162 Issue 05

SECTION 16.2.2.1 - TABLE 7

Event chronology for core melt scenarios without in-vessel reflooding (MAAP 4 Code) - SG partial and fast secondary cooldown [Ref-2]

Event	LOCA cold leg 5 cm (20 cm²)	LOCA cold leg 7.5 cm (46 cm²)	LOCA hot leg 5 cm (20 cm²)	LOCA hot leg 7.5 cm (46 cm²)	LOCA cold leg 5 cm (20 cm²)	LOCA hot leg 7.5 cm pressuriser break	SGTR one double ended tube
(condition)		Full power, 1 SG feed			Full power, 4 SG fed	Full power, 1 SG fed	
One PDS line opening	24h19min	9h45min	12h52min	4h58min	40h18min	14h27min	48h45min
Core uncovery	20h37min	8h12min	9h30min	3h36min	38h46min	11h56min	47h59min
Accumulator depletion	35 min	35 min	3h17min	35 min	33 min	34min	4h47min
Core melt onset	25h	9h58min	13h03min	5h10min	40h21min	14h39min	49h36min
Start of core relocation into lower head	28h31min	12h35min	15h55min	7h40min	43h23min	17h33min	56h56min
First vessel failure	30h07min	13h54min	18h37min	8h41min	46h18min	17h45min	58h31min

SECTION 16.2.2.1 - TABLE 8

Event chronology for core melt scenarios without in-vessel reflooding (MAAP 4 Code) - SG partial cooldown only [Ref-2]

	LOCA cold leg 3.8 cm (11.4 cm²)	LOCA hot leg 3.8 cm (11.4 cm²)	LOCA cold leg 5 cm (20 cm²)	LOCA hot leg 5 cm (20 cm²)	LOCA cold leg 7.5 cm (46 cm²)	LOCA hot leg 7.5 cm (46 cm²)	LOCA surge line 35.6 cm (993 cm²)
				Full power, 4 SG fed			
One PDS line opening	3h33min	3h02min	2h01min	1h43min	57 min	47min	23 min
Core uncovery	3h01min	2h19min	1h41min	1h23min	44min	35min	11min
Accumulator depletion	3h40min	3h10min	2h07min	1h50min	1h02min	53min	17min
Core melt onset	4h50min	4h12min	3h09min	2h44min	1h52min	1h38min	28min
Start of core relocation into lower head	6h58min	6h17min	4h52min	4h43min	4h16min	3h14min	1h54min
First vessel failure	8h19min	6h58min	6h30min	4h58min	5h05min	4h26min	2h45min

UK EPR

PRE-CONSTRUCTION SAFETY REPORT

CHAPTER 16: RISK REDUCTION AND SEVERE ACCIDENT ANALYSES

SUB-CHAPTER : 16.2

PAGE : 54 / 295

Document ID.No.
UKEPR-0002-162 Issue 05

SECTION 16.2.2.1 - TABLE 9

Event chronology for core melt scenarios without in-vessel reflooding (MAAP 4 Code) - Scenarios without RCS break and with SG dry-out [Ref-3]

	LOOP 24 H FULL POWER	LOOP 24 H NORMAL FEED AND BLEED DURING 3 H	LOOP SHUTDOWN CONDITION CA (6H AFTER SCRAM)	LOOP SHUTDOWN CONDITIONS Cb (23H AFTER SCRAM)	LOOP SHUTDOWN CONDITIONS Cb (35H AFTER SCRAM)
SG dryout	2h13min	2h13min	7h	9h37min	
One PDS line opening	3h20min	7h28min	10h12min	12h34min	
Core uncovery	3h	3h	9h43min	11h51min	1h18min
Accumulator depletion MHSI injection [3h05mn-6h] LHSI injection [3h14mn-6h]	3h39min	6 h	-	-	
Core melt onset	4h49min	7h35min	10h33min	13h03min	2h15min
Start of core relocation into lower head	6h36min	9h31min	13h04min	10h16min	7h09min
First vessel failure	7h54min	11h21min	14h34min	18h19min	8h45min

UK EPR

PRE-CONSTRUCTION SAFETY REPORT

CHAPTER 16: RISK REDUCTION AND SEVERE ACCIDENT ANALYSES

SUB-CHAPTER : 16.2

PAGE : 55 / 295

Document ID.No.
UKEPR-0002-162 Issue 05

SECTION 16.2.2.1 - TABLE 10

Event chronology for core melt scenarios without mitigation no PDS-line opening (MAAP 4 code) [Ref-2]

	TLOFW	SB LOCA COLD LEG WITHOUT SG PARTIAL COOLDOWN			
		3.8 cm cold leg (5 cm²)	3.8 cm cold leg (11.4 cm²)	5 cm cold leg (20 cm²)	7.5 cm cold leg (46 cm²)
Core oxidation onset	1h20min	5h55min	2h38min	1h32min	47min
Core melting	1h40min	5h57min	2h40min	1h36min	50min
Start of core relocation into lower head	3h29min	8h04min	5h52min	3h52min	6h18min
Accumulator/injection /depletion	-	7h07min / 8h46min	3h10min / 6h29min	1h45min / 6h03min	4min / 3h49min
MHSI/LHSI shutoff reached	-	6h24min / 8h45min	2h45min / 6h28min	1h27min / 6h02min	36min / 3h49min
Vessel failure	3h51min	8h45min	6h28min	6h03min	7h56min

UK EPR

PRE-CONSTRUCTION SAFETY REPORT

CHAPTER 16: RISK REDUCTION AND SEVERE ACCIDENT ANALYSES

SUB-CHAPTER : 16.2

PAGE : 56 / 295

Document ID.No.
UKEPR-0002-162 Issue 05

SECTION 16.2.2.1 - TABLE 11

Event chronology for core melt scenarios without mitigation no PDS-line opening (MAAP 4 code) [Ref-2]

SB LOCA COLD LEG ONLY 4 SG PARTIAL SECONDARY COOLDOWN	2.5 cm cold leg (5 cm²)	3.8cm cold leg (11.4 cm²)	5 cm cold leg (20 cm²)	7.5 cm cold leg (46 cm²)
Core oxidation onset	8h36min	3h45min	2h07min	1h54min
Core melting	8h39min	3h52min	2h13min	2h41min
Start of core relocation into lower head	11h42min	7h35min	9h51min	6h21min
Accumulator/injection /depletion	9h36min / 13h20min	4h / 8h12min	2h13min / 9h51min	57min / 4h17min
MHSI/LHSI shutoff reached	23min / 13h19min	17min / 8h12min	14min / 5h24min	11min / 2h15min
Vessel failure	13h18min	8h12min	12h26mn	7h47min

SECTION 16.2.2.1 - TABLE 12

Relevant scenarios for high pressure core melt prevention [Ref-3]

Kind of Scenario	Relevant Scenario	Reasons for the Choice
Core melt scenarios without in-vessel reflooding	LOOP (unavailability of 6 DG) full power reactor state A	High energy to be released only with bleed capacity, most severe for RCP [RCS] pressure level (no break other than bleed discharge; no SG heat removal) Bound all core melt scenarios with breaks or/and with SG heat removal
	TLOFW with unavailability of feed is a scenario with a negligible likelihood. Full power reactor state A	Highest energy in RCP [RCS] (late reactor trip and pumps stop). However in the context of a deterministic approach with identification of margins, the available time to successfully depressurise such scenario is also studied.
Core melt scenarios with in-vessel reflooding	LOOP with SI recovery	Bound all scenarios with late reflooding (most severe for pressure level because lowest discharge capacity: bleed valve only)
	TLOFW with delayed RCS depressurisation and reflooding	Highest energy in RCP [RCS] (late reactor trip and pumps stop)

SECTION 16.2.2.1 - TABLE 13

Relevant scenarios for H_2 risk [Ref-2]

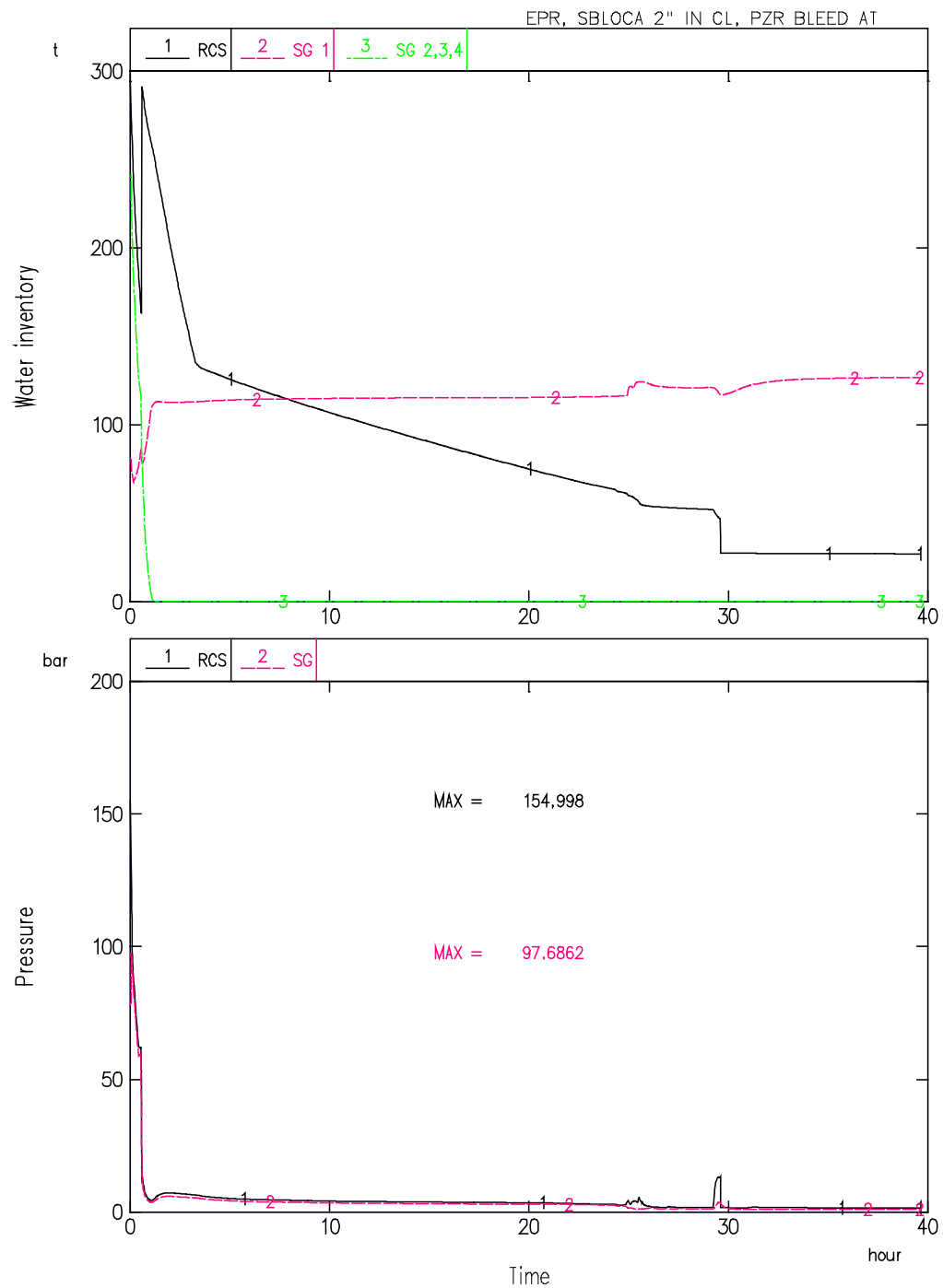| Mode of Release	Relevant H_2 Release for Representative Senarios	Relevant H_2 Release for Bounding In-vessel Passive or Active Reflooding Scenarios
Break release only	1 SB(LOCA) 5 cm (20 cm²) cold leg fast secondary cooldown 2. Local risk dynamic pressure SB(LOCA) 7.5 cm (46 cm²) pressuriser leak fast secondary cooldown Higher H_2 stratification than 1 Other SB(LOCA) with different break locations (as hot leg SB(LOCA))	SB(LOCA) fast secondary cooldown if no disk rupture of pressuriser relief tank during reflooding (< 19 bar) bounded with 1.
PDS release (pumps compartments 2 and 3)	LOOP bounded by LOOP with refloat	4. LOOP with refloat 4 MHSI Inerted containment (no combustion) Highest H_2 release (100 kg) Influence thermal loads due to H_2 recombination
Mixed release: break and pressuriser	3. SB(LOCA) 5 cm (20 cm²) cold leg with secondary partial cooldown Significant burnable H_2 release. Limited time window between in vessel H_2 production and ex-vessel H_2 production	5. SB(LOCA) 5 cm (20 cm²) cold leg partial secondary cooldown delayed depressurisation Highest amount of burnable H_2 with significant steam content Influences pressure dynamic loads and thermal loads on metallic liner 6. SB(LOCA) 5 cm (20 cm²) cold leg fast secondary cooldown (reflooding 4 MHSI highest H_2 production with lowest steam content

UK EPR

PRE-CONSTRUCTION SAFETY REPORT

CHAPTER 16: RISK REDUCTION AND SEVERE
ACCIDENT ANALYSES

SUB-CHAPTER : 16.2

PAGE   : 59 / 295

Document ID.No.
UKEPR-0002-162 Issue 05

SECTION 16.2.2.1 - TABLE 14

Relevant scenario for melt release conditions from the vessel for scenario without in-vessel reflooding [Ref-4]

| Scenario	Time Window between First Relocation and Vessel Failure	First Vessel Failure Time	Duration of Vessel Failure	Duration of Melt Release
Surge line break LOCA	51min	2h45min	20min	40min
LOOP with unavailability 6 diesels	1h20min	7h55min	23min	50min
5b cm SB(LOCA) with fast secondary cooldown	1h36min	29h35min	14min	1h15min
LOOP on shutdown condition (case D, 35h)	4h30min	4h50min	14min	51min

SECTION 16.2.2.1 - FIGURE 1

SB(LOCA) (5 cm) with fast secondary cooldown: RCP [RCS], SG water inventory and pressure versus time (5 cm cold leg, Table 7) [Ref-1]

EPR, SBLOCA 2" IN CL, PZR BLEED AT

Legend (top plot): 1 RCS, 2 SG 1, 3 SG 2,3,4

Legend (bottom plot): 1 RCS, 2 SG

MAX = 154,998

MAX = 97,6862

SECTION 16.2.2.1 - FIGURE 2

SB(LOCA) (5 cm) with fast secondary cooldown: mass of molten material in lower head and fuel rod/fuel temperature versus time (5 cm cold leg, Table 7) [Ref-1]


EPR, SBLOCA 2" IN CL, PZR BLEED AT

Lower Head

MAX = 105.905

Tmax rods

MAX = 3137.19

Time

hour
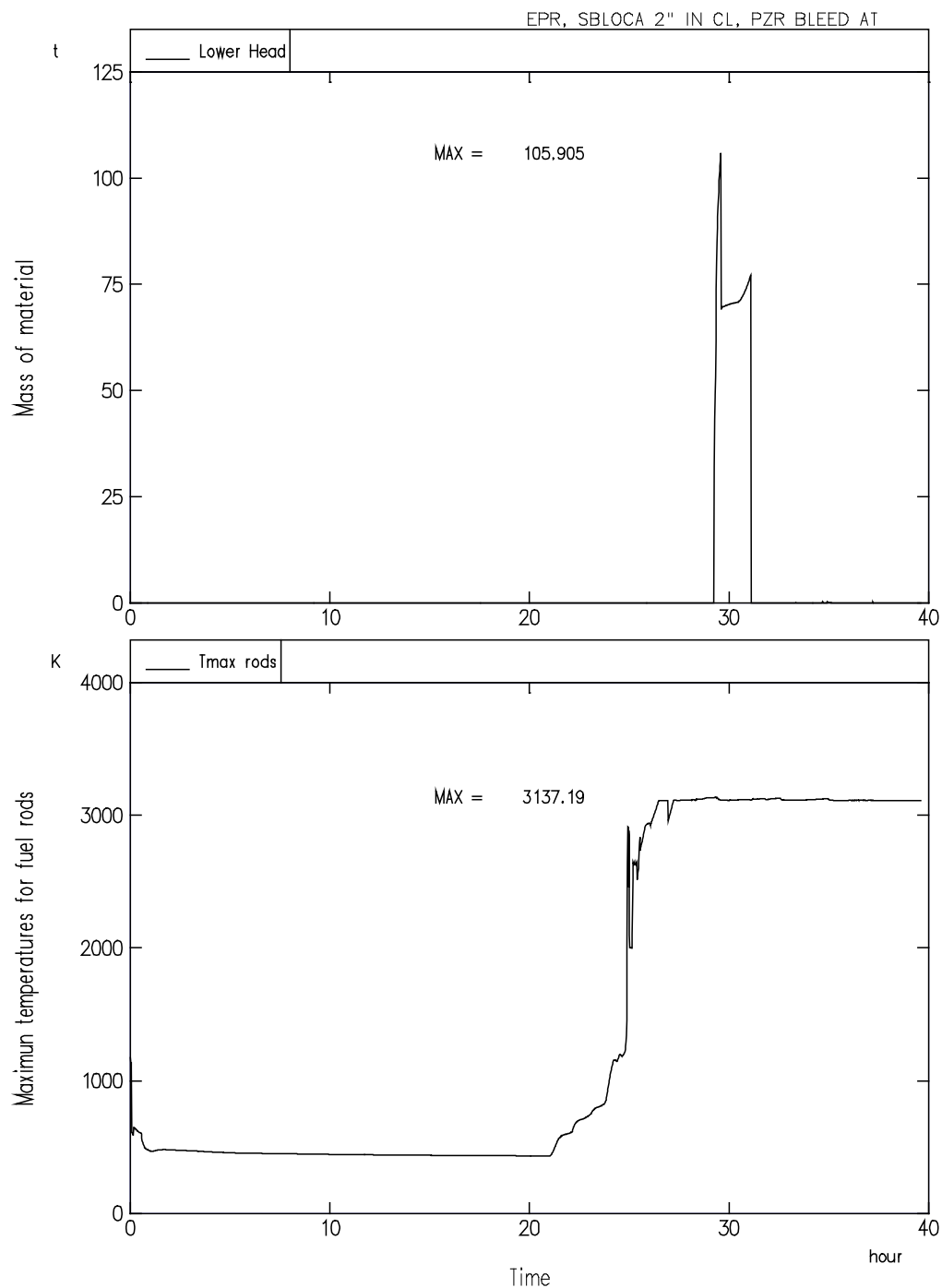
SECTION 16.2.2.1 - FIGURE 3

LB(LOCA): RCP [RCS], SG water inventory and pressure (surge line 35.6 cm, Table 8) [Ref-1], [Ref-2]

EPR, LBLOCA (SURGE LINE BREAK), PZR
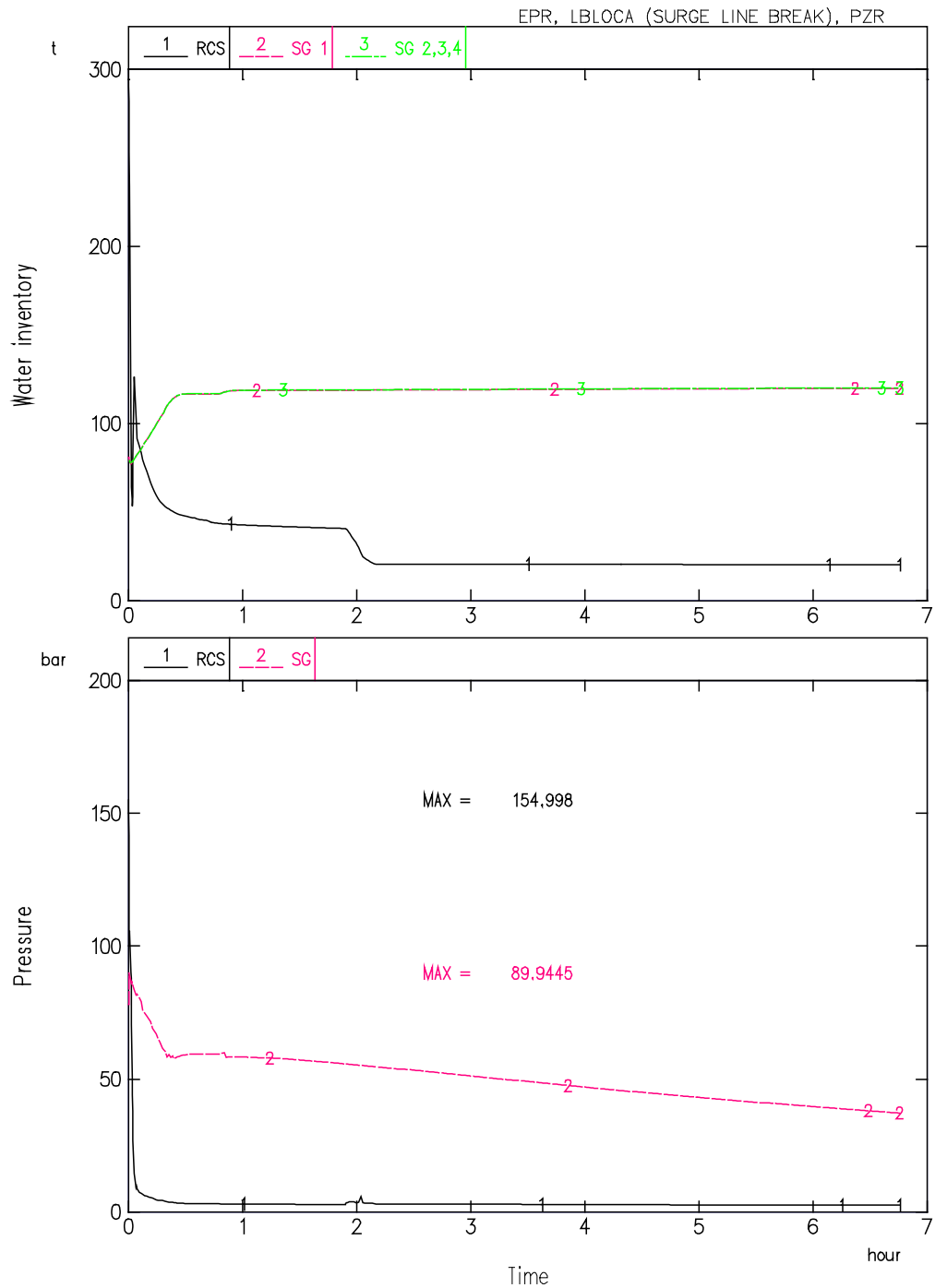
SECTION 16.2.2.1 - FIGURE 4

IB(LOCA): mass of molten material in lower head and fuel/rod temperature versus time (surge line 35.6 cm, Table 8) [Ref-1], [Ref-2]

EPR, LBLOCA (SURGE LINE BREAK), PZR
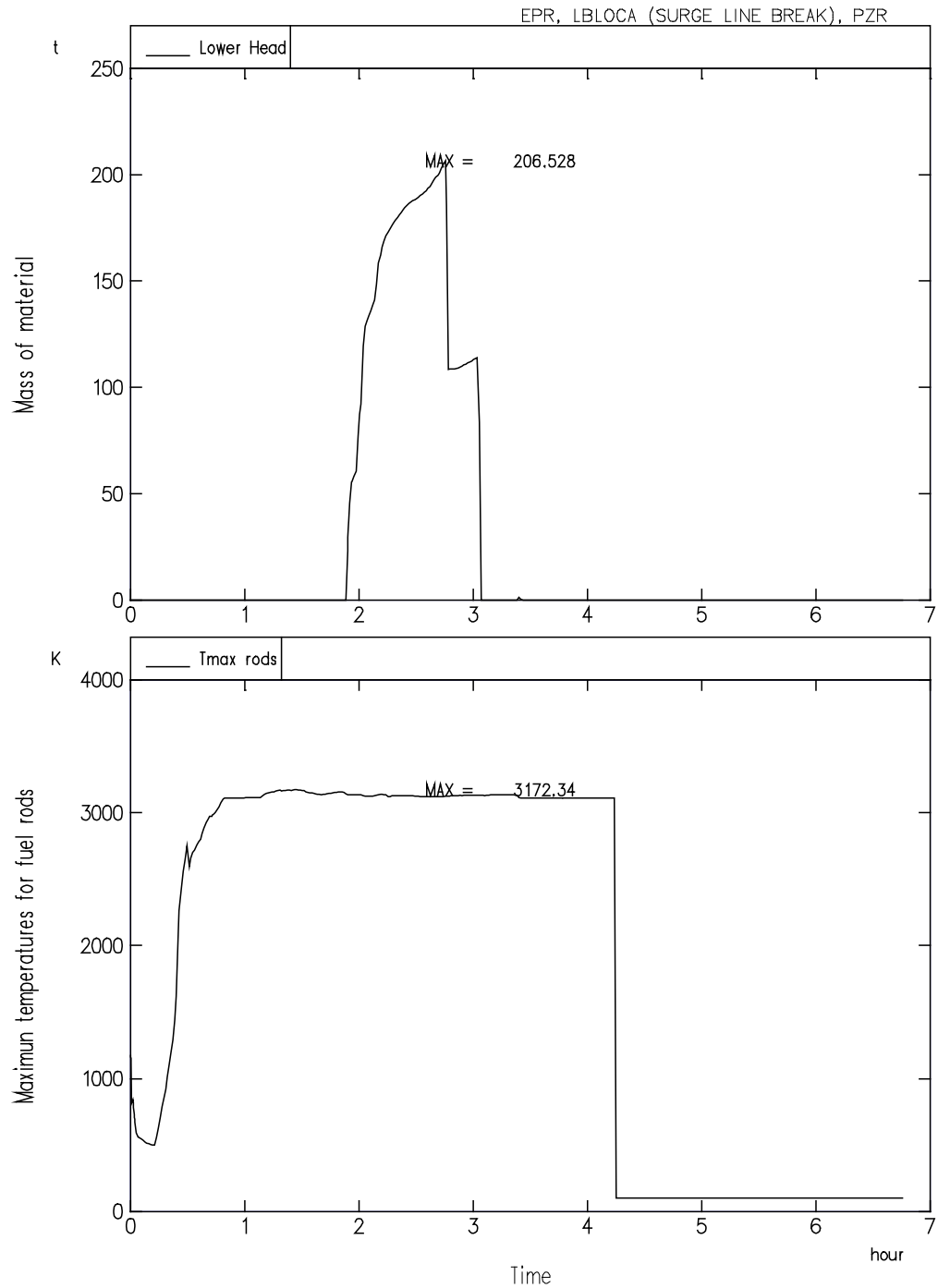
SECTION 16.2.2.1 - FIGURE 5

SB(LOCA) (5 cm) with partial secondary cooldown: RCP [RCS], SG water inventory and pressure versus time (5 cm cold leg, Table 8) [Ref-3]

EPR, SBLOCA 2" IN CL, PZR BLEED AT

MAX = 154.998

MAX = 97.6815
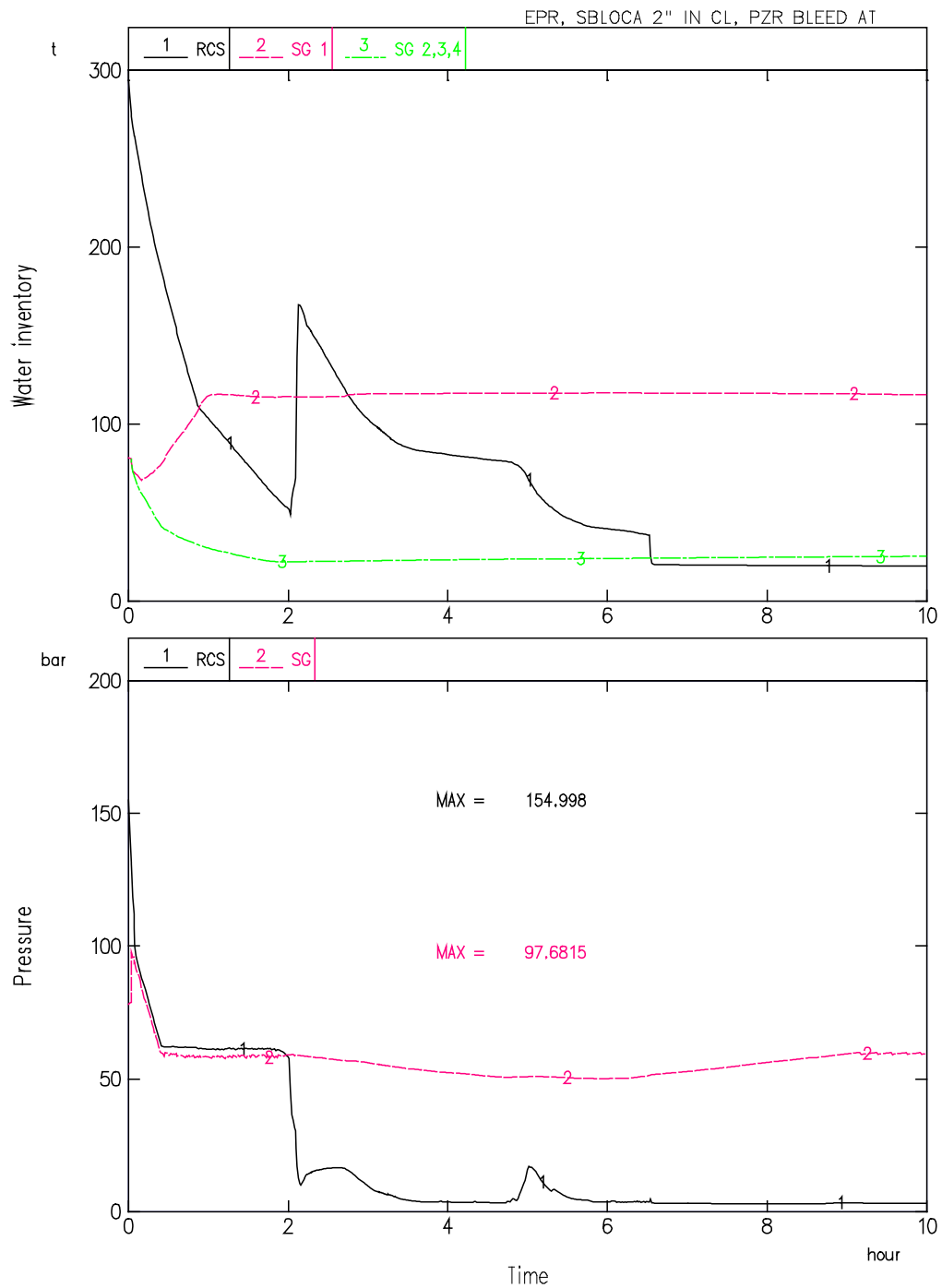
SECTION 16.2.2.1 - FIGURE 6

SB(LOCA) (5 cm) with partial secondary cooldown, mass of molten material in lower head and fuel rod/fuel temperature versus time (5 cm cold leg, Table 8) [Ref-3]

EPR, SBLOCA 2" IN CL, PZR BLEED AT

Lower Head

MAX = 127.023

Tmax rods

MAX = 3209.54

Time

hour
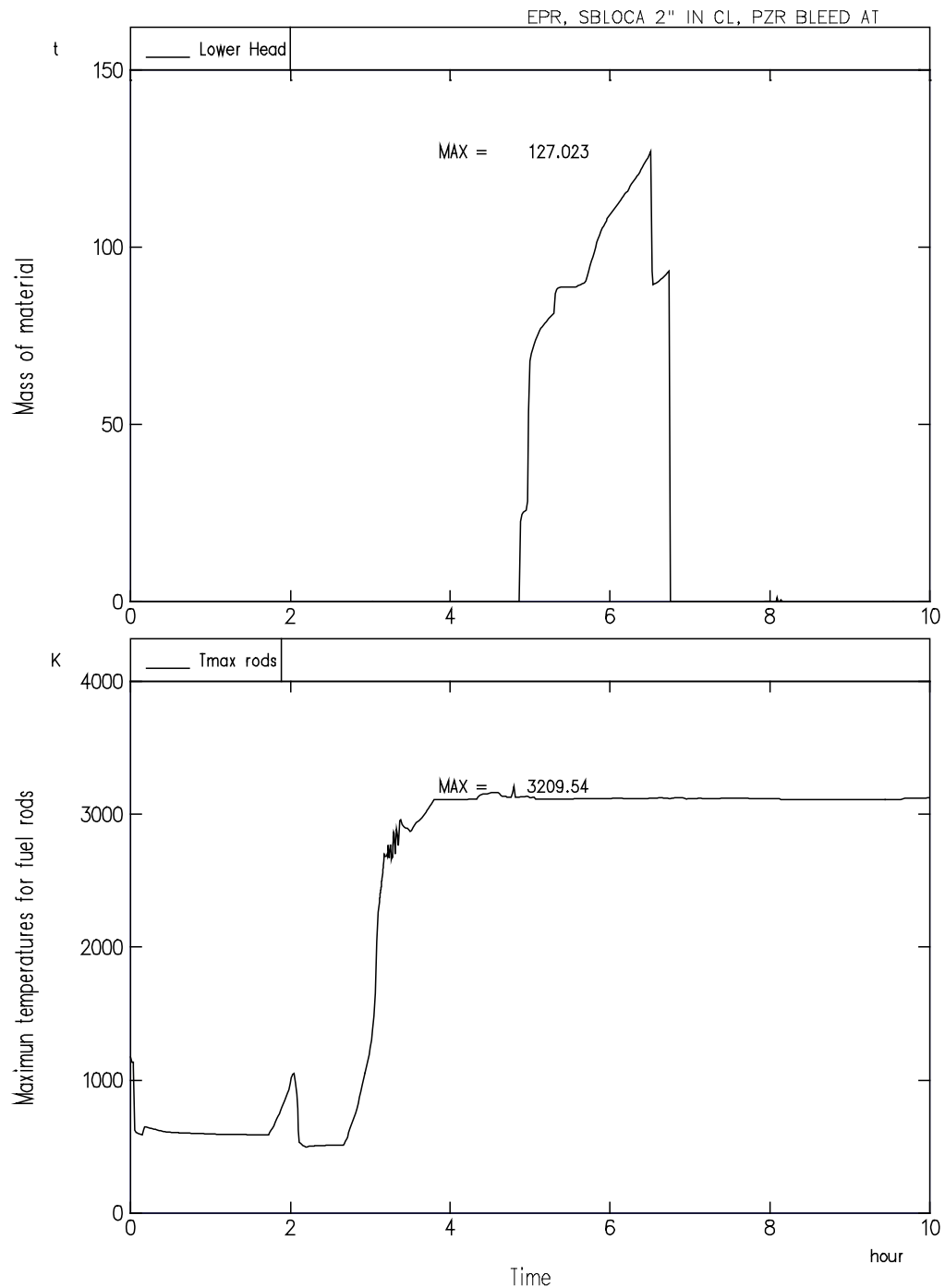
SECTION 16.2.2.1 - FIGURE 7

SGTR one double-ended tube: RCP [RCS] pressure, boiled-up water level in the CORE (Table 7) [Ref-4]
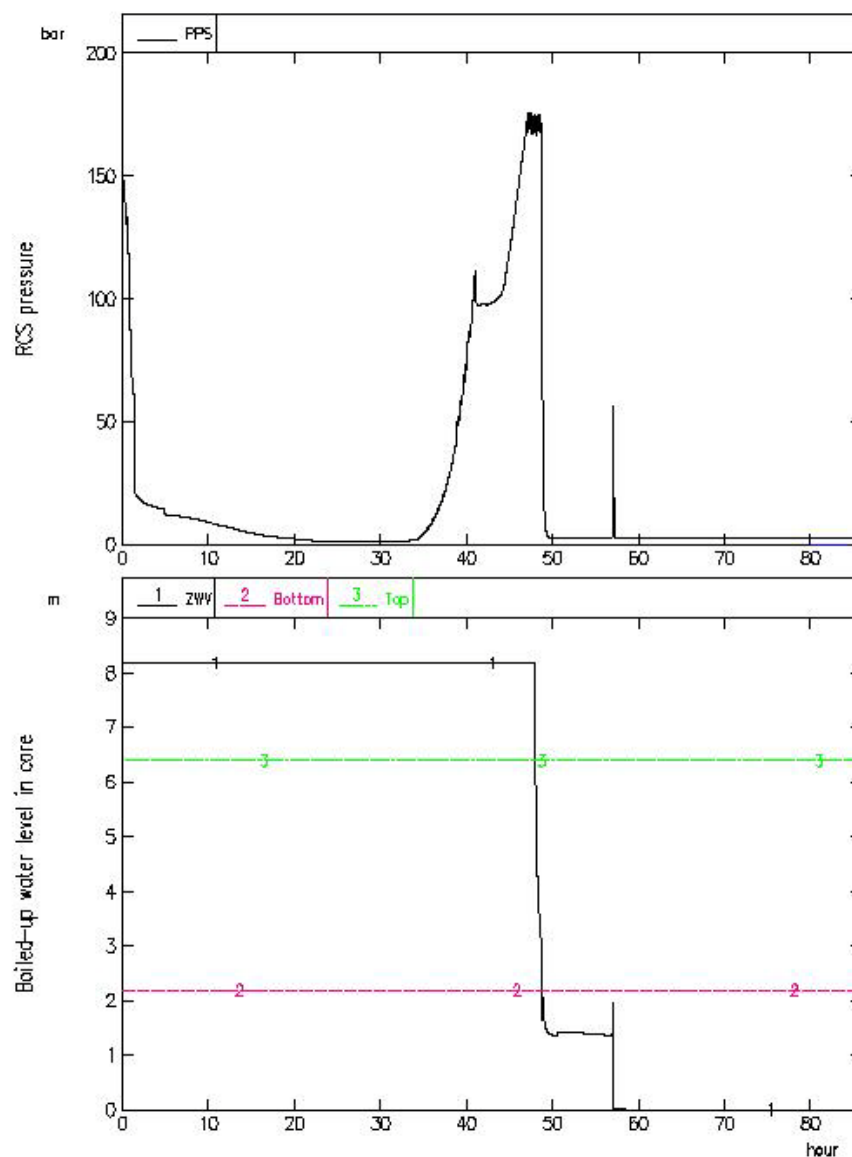
SECTION 16.2.2.1 - FIGURE 8

SGTR one double-ended tube: Mass of water, in primary system, in PRESSURISER (Table 7) [Ref-4]
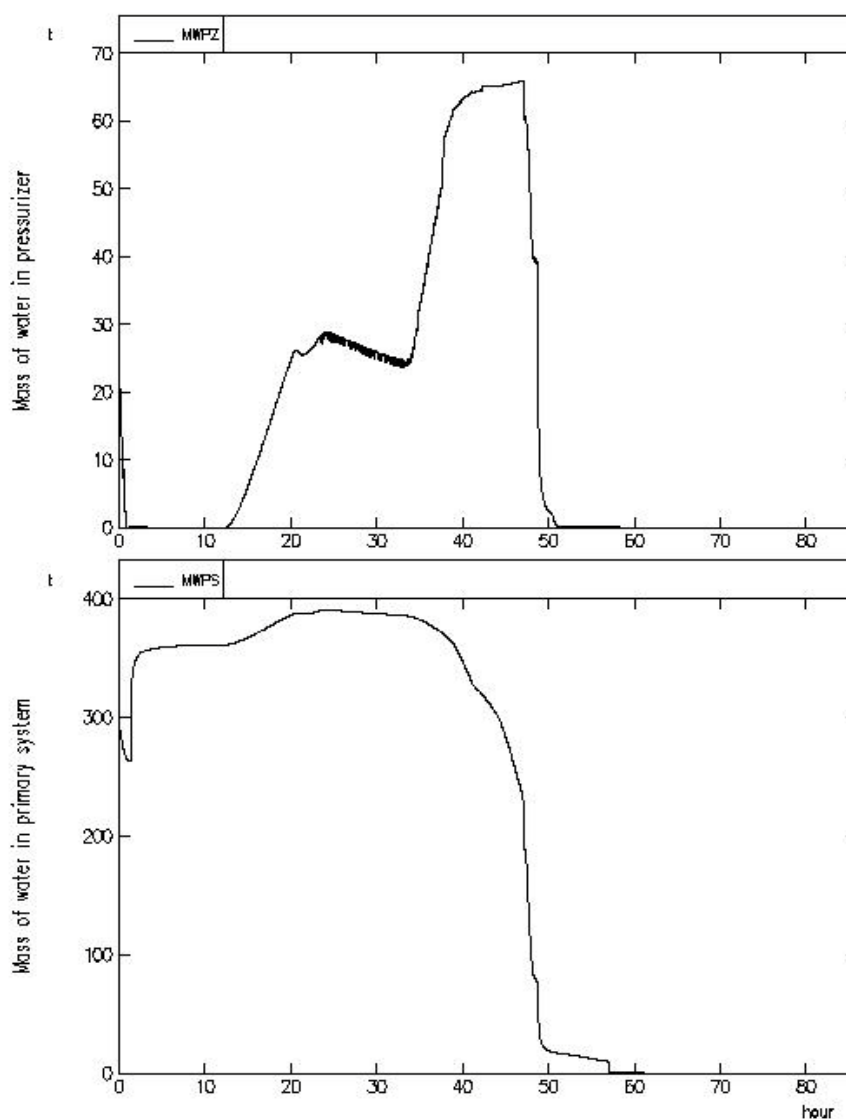
SECTION 16.2.2.1 - FIGURE 9

SGTR one double-ended tube: Temperature of gas in SG, pressure in SG (Table 7) [Ref-4]

SUB-CHAPTER : 16.2

PAGE   : 69 / 295

PRE-CONSTRUCTION SAFETY REPORT

UK EPR

CHAPTER 16: RISK REDUCTION AND SEVERE
ACCIDENT ANALYSES

Document ID.No.
UKEPR-0002-162 Issue 05
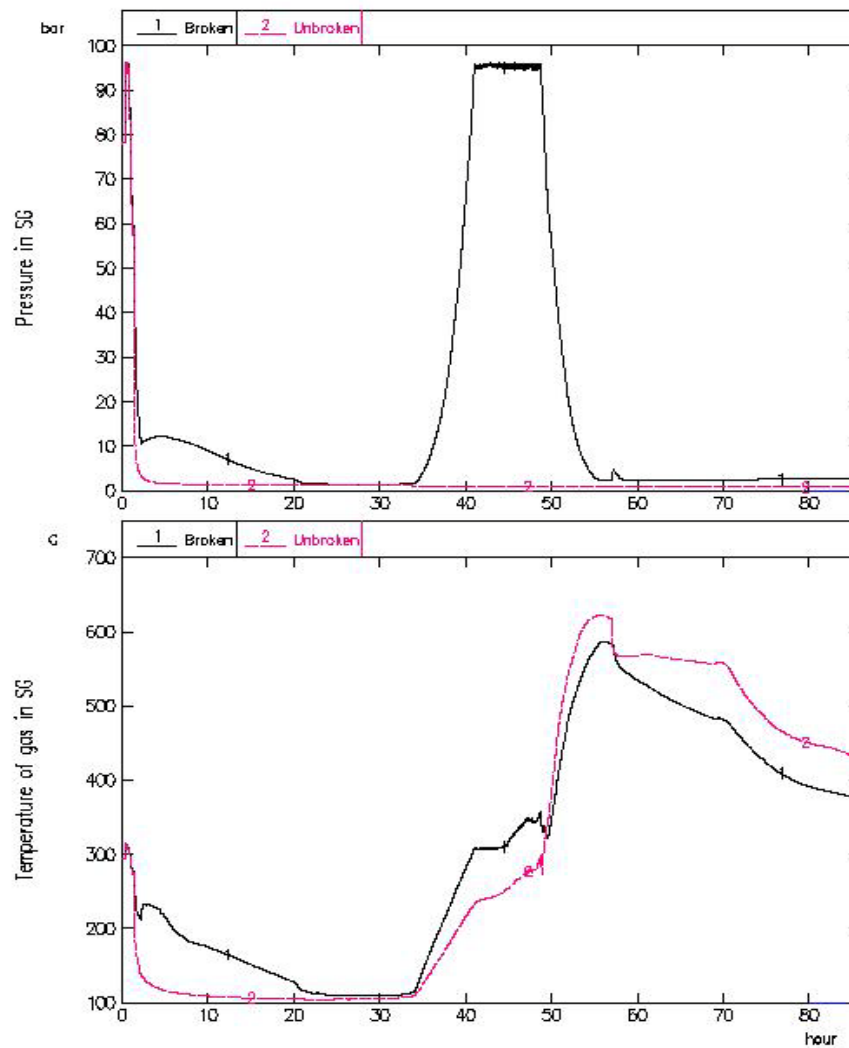
SECTION 16.2.2.1 - FIGURE 10

Hydrogen production for relevant core melt scenarios [Ref-1]
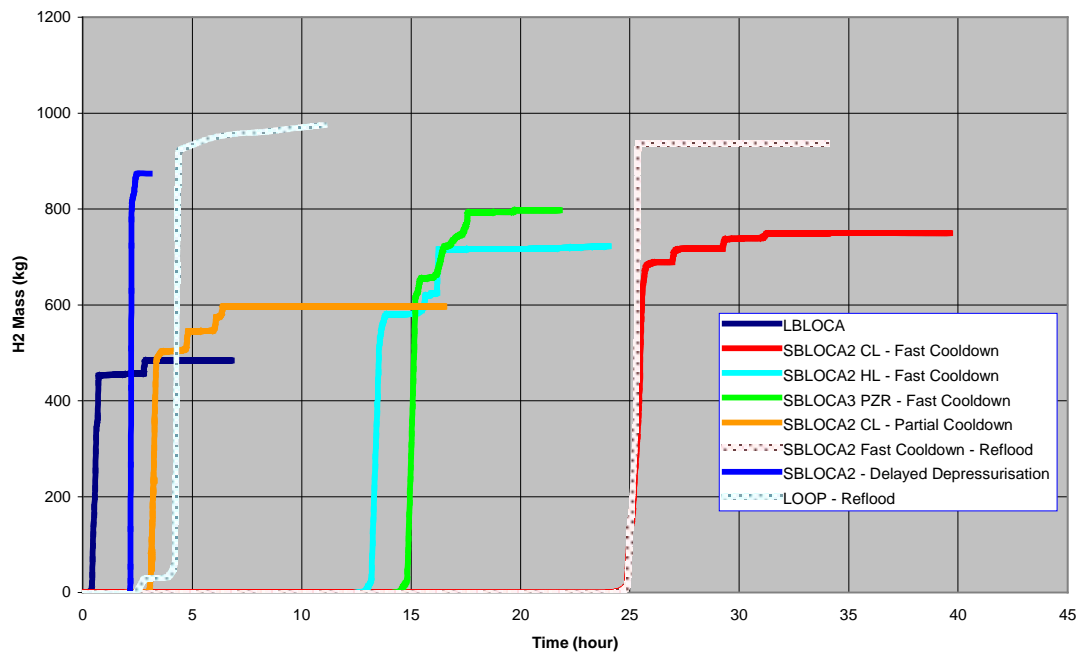
SECTION 16.2.2.1 - FIGURE 11

Hydrogen production for in-vessel reflooding SB(LOCA) 5 cm (different reflooding times) [Ref-1]
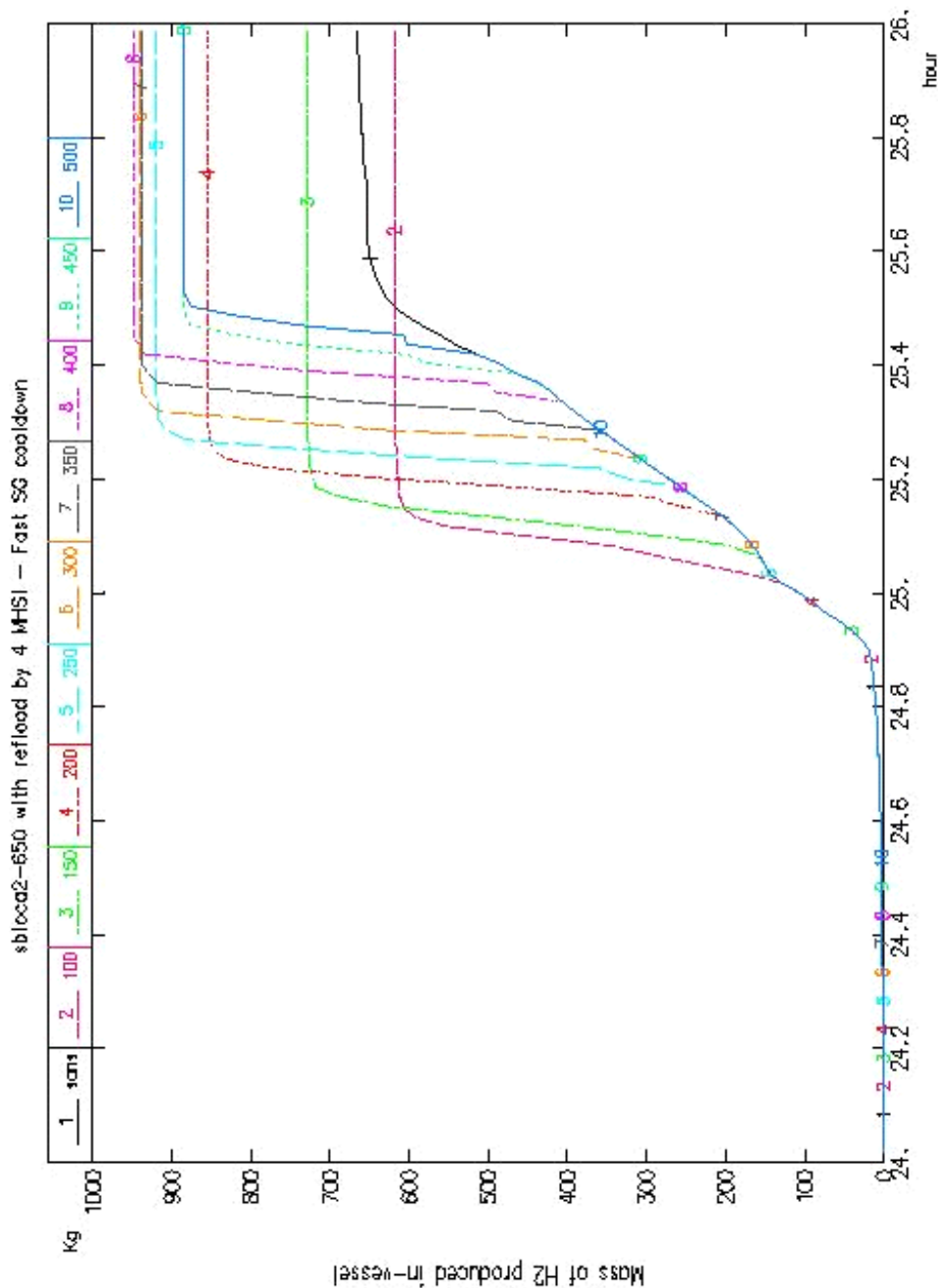
SECTION 16.2.2.1 - FIGURE 12
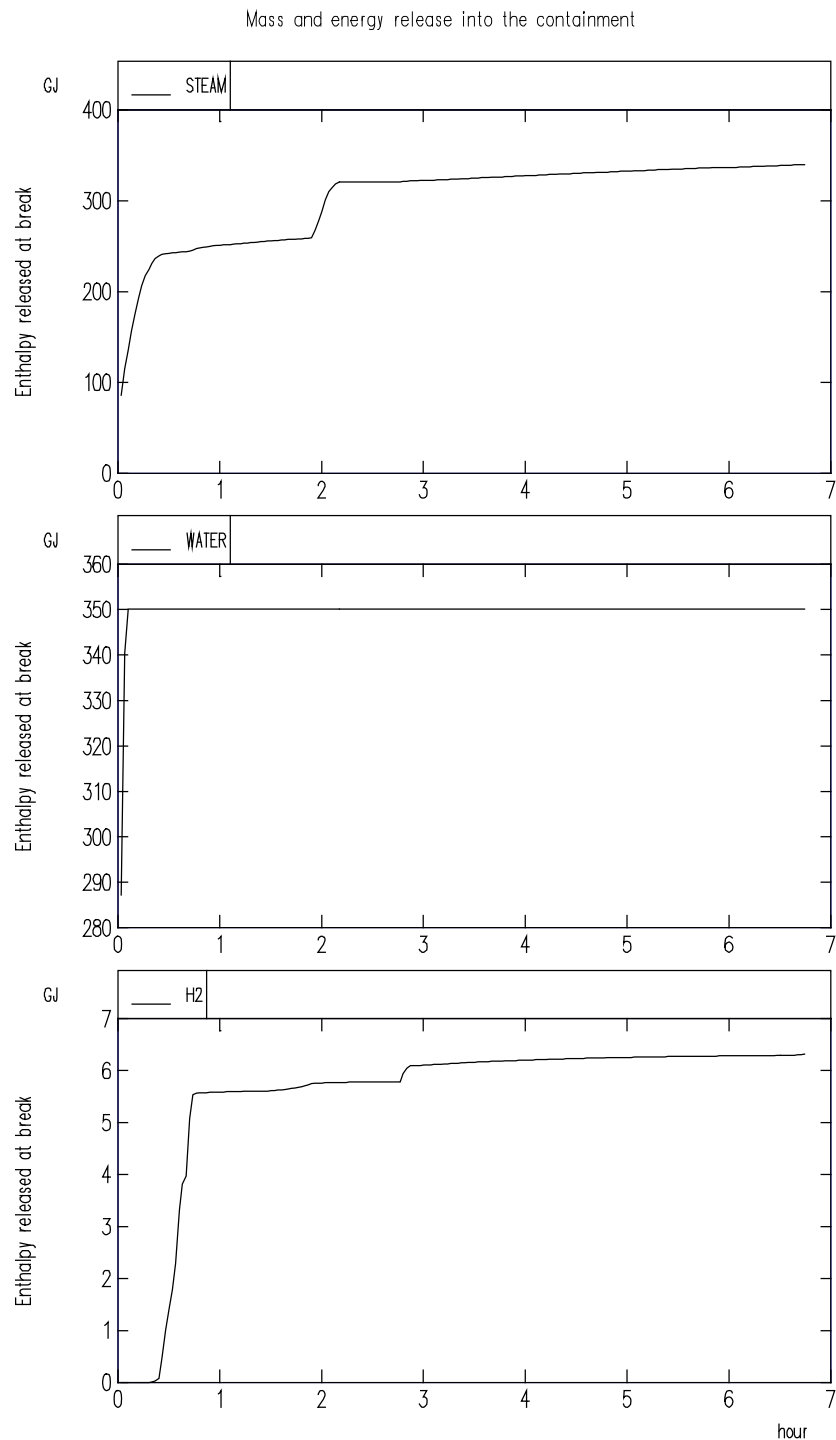
Melt release from the vessel [Ref-2]
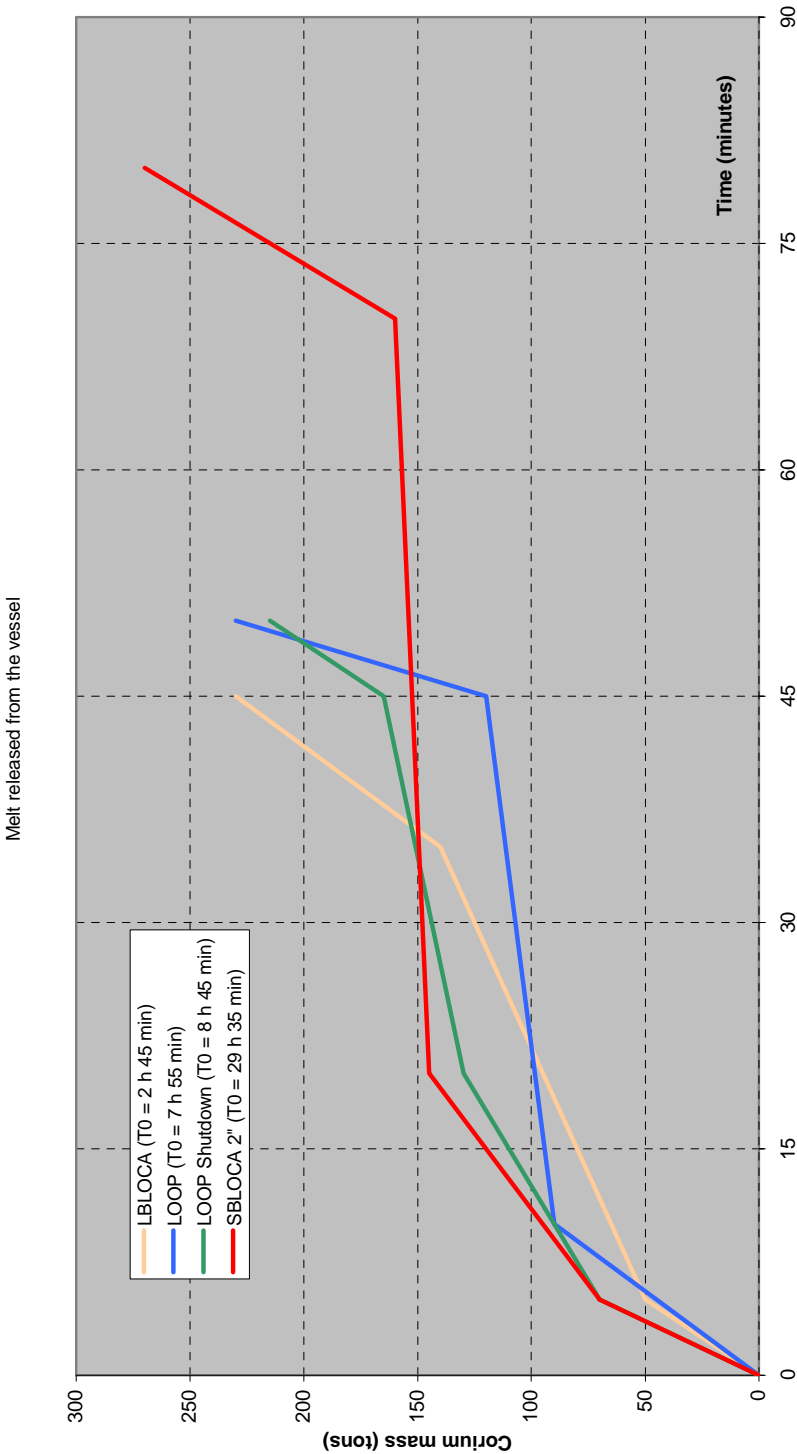
SECTION 16.2.2.1 - FIGURE 13

Mass and energy release into the containment surge line break [Ref-5]

Mass and energy release into the containment
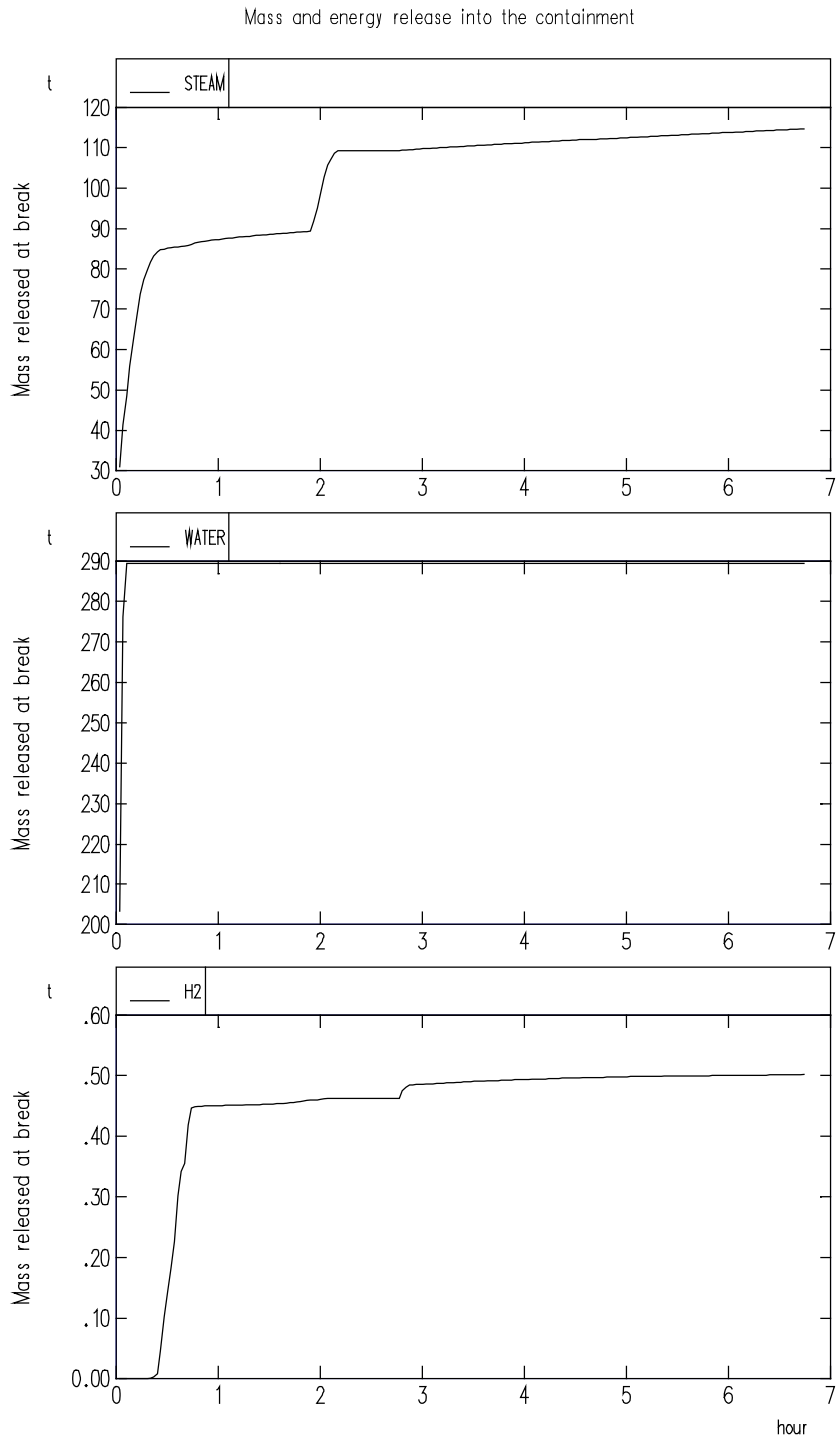
SECTION 16.2.2.1 - FIGURE 14

Mass and energy release into the containment surge line break [Ref-5]

Mass and energy release into the containment

2.2. ASSESSMENT OF PRIMARY SYSTEM DEPRESSURISATION

Failure of the reactor pressure vessel (RPV) under high internal pressure is of importance to severe accident risk as missiles could be created from vessel movement. Also high pressure melt ejection (HPME) could lead to direct containment heating (DCH) by melt dispersal inside the containment atmosphere which could result in subsequent containment failure.

The general safety requirements which apply to the primary depressurisation system (PDS) of the EPR are:

- the containment should be designed so that the pressures and temperatures attained inside the containment as a consequence of a severe accident will not result in its uncontrolled failure,

- as containment design takes into account consequences related to a severe accident (SA) but without considering loads induced by the high pressure melt ejection (HPME), rupture of the reactor coolant system (RCP [RCS]) at high pressure must be excluded by design.

Therefore, the ability to reduce the primary system pressure in high pressure severe accidents should be ensured so that occurrence of a SA at high pressure can be prevented.

The primary coolant system should therefore be equipped with pressure reduction systems that must be able to perform their safety function appropriately under high pressure severe accident conditions.

Depressurisation could either be intentional by operator action or unintentional by creep induced rupture of the RCP [RCS] pipework due to heat-up if steam natural circulation is established within the RCP [RCS].

One of the main provisions of the EPR design in this respect is the severe accident primary depressurisation system (PDS) with its dedicated severe accident valves. A short description of the primary depressurisation system is provided in the following section.

2.2.1. Description of the Primary Depressurisation System (PDS)

Even though RPV failure at high pressure is physically unlikely, the EPR is designed with an objective to transfer high pressure core melt sequences into low pressure sequences with high reliability so that a high pressure vessel breach can be practically eliminated. This is achieved through two dedicated SA depressurisation valves (PDS valves) on two discharge lines on top of the pressuriser that are part of the PDS.

The PDS consists of PDS valves, discharge lines, and the pressuriser relief tank (PRT). Each line includes two valves in series that are connected to the same pressuriser nozzle, located at the same elevation as the nozzles of the safety valves, and discharge into the pressuriser relief tank via the same line as the safety valves.

The total steam flow capacity of one PDS valve is 900 te/h at 17.6 MPa, under saturated steam conditions. For both, Feed & Bleed (F&B) and SA functions, the motor operated valves of one line only can be opened manually during high pressure accident sequences when the severe accident criterion (core exit temperature = 650°C) is reached, which corresponds to a pressuriser steam temperature of 350°C.

A general view of the primary depressurisation system is shown in Section 16.2.2.2 – Figure 1.

2.2.2. Characteristics of the Considered Scenarios

The depressurisation capacity of the primary system and the time required to open the relief valves in the case of a severe accident have a significant impact on the core degradation kinetics. They affect all the severe accident in-vessel source terms (depressurisation rate and pressure peak, hydrogen release, corium release from the reactor vessel).

The analysis to justify the effectiveness of the RCP [RCS] discharge capability is performed based on the capacity of the severe accident relief valves with a mass flow rate of 900 te/hour. In fact, in many core melt scenarios, the pressuriser relief valves will also be available and may provide a similar additional discharge capacity of 3 x 300 te/hour.

Taking into account the selection of the most relevant scenarios, the specific detailed description of two bounding scenarios considered for the analysis of the discharge capacity through the PDS is provided in the following two sections.

2.2.2.1. Station Blackout Sequence [Ref-1]

This sequence is initiated by loss of off-site power (LOOP) with loss of the emergency diesel generators (EDG) and loss of emergency feedwater system (ASG [EFWS]). It is considered as the basic high pressure scenario. During this sequence, the liquid level in the steam generator decreases causing the primary system to heat-up and pressurise until the opening setpoint pressure of the pressuriser safety valves is reached 1 hour 20 minutes after accident initiation. The safety valves start to cycle to control the pressure. The decay heat starts to be removed by loss of RCP [RCS] water. About 2 hours after accident initiation, the steam generators become completely dry while the pressuriser safety valves discharge into the PRT. At this time, the differential pressure limit of the rupture disk will be exceeded and the RCP [RCS] water will immediately start to discharge into the containment.

As the energy released with the water flowing through the pressuriser safety valves is smaller than the decay heat produced in the core, the RCP [RCS] average water temperature continues to increase until it reaches the saturation temperature at the opening pressure of the pressuriser safety valves. This occurs at about 2 hours 30 minutes after accident initiation. After this time, the fluid discharged through the pressuriser safety valves is a two-phase water and steam mixture.

About 3 hours after accident initiation, the core uncovers and the accident progression will depend upon the opening time of the PDS valves.

2.2.2.2. Total Loss of Feed Water Sequence [Ref-1]

Total loss of feedwater sequence (TLOFW) is initiated by the failure of the main feedwater system (ARE [MFWS]) and emergency feedwater system (ASG [EFWS]).

The TLOFW scenario differs from the LOOP scenario because of the following two events:

- reactor automatic shutdown is activated by the signal of low steam generator water level about 30 seconds after loss of main feedwater and emergency feedwater (time t = 0 seconds).

- when the water level in the steam generators becomes very low, after about 20 minutes, the primary coolant pumps are stopped by operator action.

These delays for reactor scram and for stopping of the pumps will result in a higher internal energy of the RCP [RCS] and, thus, acceleration of the accident progression. Steam generators dry out at 44 minutes, and core uncovery occurs at 1 hour 17 minutes. Because core heat-up is very rapid, this scenario is studied only for the consequence of a delayed depressurisation. The efficiency of the bleed capacity is also verified.

2.2.3. Criteria for RCP [RCS] depressurisation and identification of available time periods

2.2.3.1. Criteria for RCP [RCS] depressurisation

2.2.3.1.1. Steps for RCP [RCS] depressurisation

If heat removal from the Steam Generators (SG) is unavailable, or the partial secondary cooldown and/or fast secondary cooldown fail, the operator must perform Feed & Bleed to prevent core melt.

The principle of the accident management is the following:

- SG depressurisation, action performed in Emergency Operating Procedures (EOP),

- if not successful, primary Feed & Bleed which is performed by PDS actuation (first level of PDS actuation), action performed in EOP,

- PDS valves actuation for mitigation of a consequence of severe accident, if not yet open (second level of PDS actuation), action performed in Operating Strategies for Severe Accidents (OSSA).

2.2.3.1.2. Criteria for primary Feed & Bleed

The success of operator action to depressurise the RCP [RCS] depends on the availability of plant state diagnostics, which may indicate to the operator the need for Feed & Bleed operation. It is also assumed that the operator has completed preparations to perform the Feed & Bleed operation. The diagnostic criteria that indicate the need for Feed & Bleed depend on the accident scenario as follows:

- scenario with SG dryout and no RCS break (as LOOP with failure of 6 EDGs): low SG water level (3 m) for the 4 SGs,

- small break loss-of-coolant accident (SB(LOCA)) scenario with SG feed and without secondary partial cooldown: low PZR pressure and high SG pressure will identify failure of both partial cooldown and MHSI,

- SB(LOCA) scenario with successful partial cooldown and operator failure to perform fast secondary cooldown: the strategy which relies on the longest allowed operator time for secondary depressurisation also reduces the available time for a manual primary Feed & Bleed.

Safety injection is assumed to be actuated at PZR pressure (< 112 bar); the safety injection signal automatically starts the MHSI+LHSI pumps and initiates a partial cooldown of the secondary system. If the automatic partial cooldown is not successful, the operator will have time (at least 30 minutes) to perform a manual partial cooldown. For this reason, it is assumed that preparation for primary Feed & Bleed starts 30 minutes after low PZR pressure and the identification of failure of partial cooldown.

Two criteria can be used to decide to perform primary Feed & Bleed:

- water level measurement (bottom of hot leg) and primary pressure

- overheating at core outlet and secondary pressure

2.2.3.1.3. Severe accident criteria

If the PDS is not already actuated for primary Feed & Bleed, the ultimate criterion for the actuation of the PDS valves has the objective of depleting the accumulator tanks before the onset of core melt, in order to prevent potential high levels of oxidation due to accumulator water injection onto a hot core.

This criterion (temperature of 650°C at the core outlet) is the ultimate criterion for opening one PDS line for the mitigation of oxidation. However, for all high pressure scenarios, the operator is aware that at the time at which the criterion for primary Feed & Bleed is met he will be asked to open one PDS line. Section 16.2.2.2 - Table 1 shows the evolution of the TLOFW scenario with late opening of PDS valves.

2.2.3.2. Justification of PDS valve discharge capacity for in-vessel reflooding

With the strategy of opening PDS valves at the maximum core exit temperature of 650°C, the discharge capacity of 900 te/hour at 176 bar for each PDS line (including two valves in series) is sufficient to enable a very low pressure (below 4 bar) to be reached before the onset of relocation of molten core materials into the reactor vessel lower head, giving an adequate time margin before vessel failure. The differential pressure between the RCP [RCS] and the containment will thus be negligible at the time of reactor vessel failure (Section 16.2.2.2 - Figure 2).

The discharge capacity of the PDS valves influences the pressure spike at the time of corium relocation into the lower head; this spike is in the range of 20 to 60 bar. This uncertainty depends mainly upon corium fragmentation level and corium/water heat transfer which depends on assumptions used in the code. However, the high discharge capacity allows a rapid decrease of pressure following this spike because the steam is easily removed. Thus, low pressure is reached early before vessel failure without any significant amount of water in the lower head. The pressure difference with the containment is negligible at vessel failure time. No risks of Direct Containment Heating (DCH) or significant uplift forces on the vessel supports are expected. The corium release into the reactor pit will be a gravity driven flow.

The main results of a core melt scenario LOOP with 6 EDG unavailable and opening of one PDS line at 650°C are given in Section 16.2.2.2 - Figures 2 to 8.

For late in-vessel reflooding which may occur after the onset of relocation, vessel failure might not be prevented. On the other hand, the capacity of one PDS line is sufficient to remove decay heat and to keep the equilibrium pressure below 20 bar at vessel failure, whatever the safety injection flow rate (1 pump or several pumps). The pressure spike in the primary system, which occurs at reflooding, decays rapidly due to high discharge capacity of the PDS valves.

SUB-CHAPTER : 16.2

PAGE : 78 / 295

UK EPR

PRE-CONSTRUCTION SAFETY REPORT

CHAPTER 16: RISK REDUCTION AND SEVERE
ACCIDENT ANALYSES

Document ID.No.
UKEPR-0002-162 Issue 05

At the time of water injection, the pressure spike can be above 50 bar but the vessel failure always occurs the range 12 to 20 bar. The results for different in-vessel reflooding times are given in Section 16.2.2.2 - Table 2.

Although RPV failure at 20 bar is only conceivable in case of late depressurisation or late in-vessel reflooding, 20 bar is considered as a design basis for the RPV supports and for the design of the pit walls against the resulting differential pressure. With the assumption of instantaneous circumferential vessel rupture at 20 bar, the resultant of calculated uplift forces on the vessel and support are shown in Section 16.2.2.2 - Figure 16.

2.2.3.3. Identification of margins for delayed depressurisation

The available period of time to actuate the PDS valves in a high pressure scenario varies according to the primary circuit break size and steam generator conditions: SG dryout, failure of partial cooldown, or a scenario with success of partial cooldown only and failure of fast secondary cooldown.

For SB(LOCA) scenario with very small break size such as 2.5 cm (5 cm²), the action time available to the operator will be longer due to the slow rate of water depletion. For a large break size, which would enable rapid injection by the accumulators, the primary pressure will already be low when severe accident signal of 650°C at the core outlet is reached and the accumulator water depletion will also increase the time to reach the signal. Therefore, a range of break sizes around 5 cm (20 cm²) and 7.5 cm (46 cm²) exists for which the break size is:

- too small to take benefit of accumulator injection before reaching the signal,

- but sufficient to maximise the available time before reaching the signal.

The bleed capacity of one PDS line is sufficient to provide much extra time to have a delayed depressurisation, which enables pressure to be below 20 bar at vessel failure.

This period of time represents a margin for a successful mitigation in cases where the PDS line is not opened at the core exit temperature of 650°C.

A delayed depressurisation can have some disadvantages such as:

- higher hydrogen production due to possible accumulator water injection on a hot core,

- risk of RCP [RCS] piping rupture by creep (steam generator tubes).

For the worst scenario with highest decay heat, which is expected for TLOFW, vessel failure at 170 bar is expected to occur at 3 hours 51 minutes after reactor trip if no depressurisation valves are actuated and without consideration of other RCP [RCS] creep failures [Ref-1]. For half an hour before vessel failure, it is possible to actuate the bleed valve to decrease RCP [RCS] pressure below 20 bar at vessel failure.

Section 16.2.2.2 - Table 1 presents the main results for TLOFW core melt scenarios.

The main results of core melt scenario TLOFW with late PDS line opening are given in Section 16.2.2.2 - Figures 9 to 15. Opening of the PDS line with safety injection is actuated after the onset of core melt relocation into the lower head at 3 hours 33 minutes.

UK EPR

PRE-CONSTRUCTION SAFETY REPORT

CHAPTER 16: RISK REDUCTION AND SEVERE
ACCIDENT ANALYSES

SUB-CHAPTER : 16.2

PAGE   : 79 / 295

Document ID.No.
UKEPR-0002-162 Issue 05

The bleed discharge capacity enables a more tolerant design An additional period of time of 1 hour 30 minutes is available after the severe accident signal (650°C), which represents an increased margin for the operator to actuate the PDS valves to achieve bleed flow and to manage RCP [RCS] pressure to be below 20 bar at vessel failure.

2.2.3.4. Temperatures in the Primary System

2.2.3.4.1. Maximum Gas Temperature

- For scenarios with the opening of one PDS line at the temperature criterion of 650°C (such as the LOOP scenario (see Section 16.2.2.2 - Figures 6 and 7)), the pressuriser is almost full of water so that the gas temperature equals the saturation temperature of water, which is 350°C. Superheated steam exiting the core is cooled down to saturation temperature while going through the pressuriser plug. This pressuriser plug is discharged partly when the PDS line is opened, but some water can still remain in it and not flow down into the hot leg due to insufficient differential pressure between pressuriser and hot leg; the gas temperature does not increase before complete pressuriser dryout. The temperature of the gas flow through the valves of the opened PDS line remains below 350°C for a long time and reaches 600°C only very late, just before time of vessel failure.

- In the case of delayed depressurisation in the TLOFW scenario (Section 16.2.2.2 - Figures 13 and 14), the pressuriser gas temperature reaches 620°C at valve opening. For valves opening at 650°C, the expected hot gas temperature through the valves should be below 600°C taking into account MAAP 4 code uncertainties.

- In the time period between the onset of core melting and the onset of core relocation into the vessel lower head, for the LOOP scenario, gas natural circulation from the upper plenum increases the temperature of the hot leg of the pressuriser loop up to 880°C (Section 16.2.2.2 - Figure 8). For the TLOFW scenario with delayed RCP [RCS] depressurisation, the hot leg temperature reaches 1000°C (Section 16.2.2.2 - Figure 15). Because of uncertainties in the calculation of natural circulation in the primary system, 1000°C can be considered as a maximum gas temperature through the valves of the opened PDS line before vessel failure occurs.

These temperature values meet the functional requirements of the PDS lines (long term increase of temperature and increase of temperature followed by a cold thermal shock in case of short term spike due to a delayed depressurisation or a reflooding).

2.2.3.4.2. Risk of Creep Rupture in RCS Pipes in case of Delayed Depressurisation

Three distinct natural circulation patterns can be established in the RCP [RCS] under high pressure severe accident conditions:

- in the reactor vessel between the core and upper plenum regions,

- between the reactor vessel upper plenum and the steam generator inlet plenum,

- between the inlet and outlet plena of the steam generator.

Section 16.2.2.2 - Figure 17 shows the steam flow in each of these patterns. Natural circulation usually results in heat-up of the structural material, which will be subjected to elastic-plastic and creep behaviour.

Creep behaviour occurs when the material is kept at a sufficiently high temperature for sufficient time. Creep strain increases with time and temperature until it reaches a critical value at which creep rupture occurs.

For a TLOFW scenario without opening of any PDS line, the heat-up of the primary loop structures is very rapid. The maximum wall temperatures are [Ref-1] [Ref-2]:

- 1000°C for hot leg, and

- 500°C for SG tubes, or 355°C if the SA valves are opened at the severe accident criterion of 650°C core exit temperature.

In the EPR, the high ratio of the total cold surface of the SG tubes to the nominal core thermal power contributes to limiting the temperature in SG during loop natural circulation. The advantageous behaviour of SG tube material (Inconel 690) with respect to creep also limits the risk of tube rupture under high pressure scenarios. With delayed RCP [RCS] depressurisation, creep rupture would occur at the weakest point of the primary system.

Studies on various parts of the RCP [RCS] which have the potential to fail (bimetallic welds in the hot leg, pitting in the surge line, the lower part of the surge line, upper bimetallic welds in the surge line, pressuriser, steam generator tubes and steam generator tube plates) have shown that the weakest point is the bimetallic weld (between the austenitic and ferritic steels) of the hot leg, with no risk of SG tube rupture and hence no risk of containment by-pass.

Even though the induced rupture of the steam generator tubes is unlikely, the related risk will be evaluated for various core melt scenarios within the framework of the Level 2 probabilistic safety assessment (PSA).

SECTION 16.2.2.2 - TABLE 1

TLOFW scenario, delayed RCP [RCS] depressurisation [Ref-1]

Onset of core melt without any PDS line opening	1h 40 min
Onset of core relocation into lower head without any PDS line opening	3h 29 min
Period after the 650°C signal to actuate PDS valves to be below 20 bar at time of vessel breach (without safety injection)	2h

SECTION 16.2.2.2 - TABLE 2

LOOP with unavailability 6 DG, vessel failure pressure for late in-vessel reflooding (4 MHSI + 4 LHSI) time events [Ref-1]

	LOOP with 6 DG unavailable Late in-vessel reflooding (4 MHSI + 4 LHSI) Time of events				
Onset of in-vessel reflooding	No reflooding	Relocation	Relocation + 30 min	Relocation + 60 min	Relocation +90 min
Vessel failure pressure	2 bar	18 bar	18 bar	18 bar	20 bar

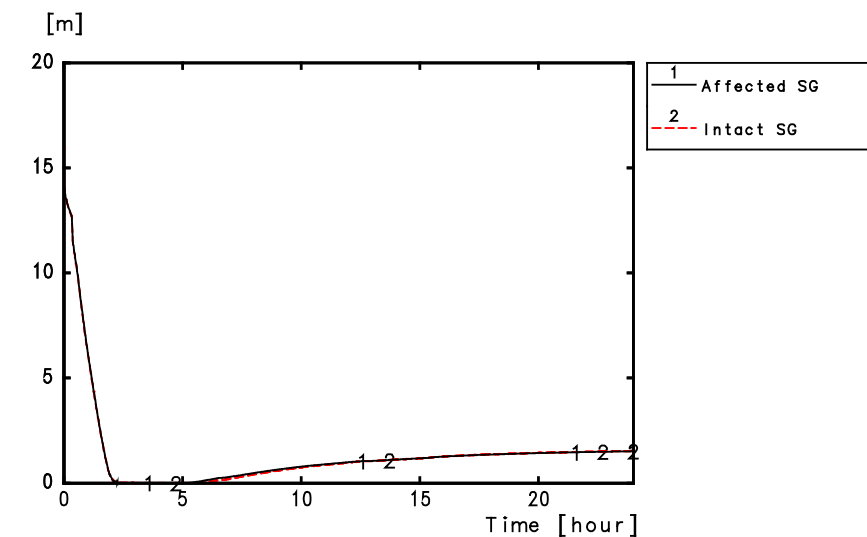## SECTION 16.2.2.2 - FIGURE 1

General view of the PDS

SECTION 16.2.2.2 - FIGURE 2

RCP [RCS] and SG pressure, collapsed level in SG (LOOP) [Ref-1]
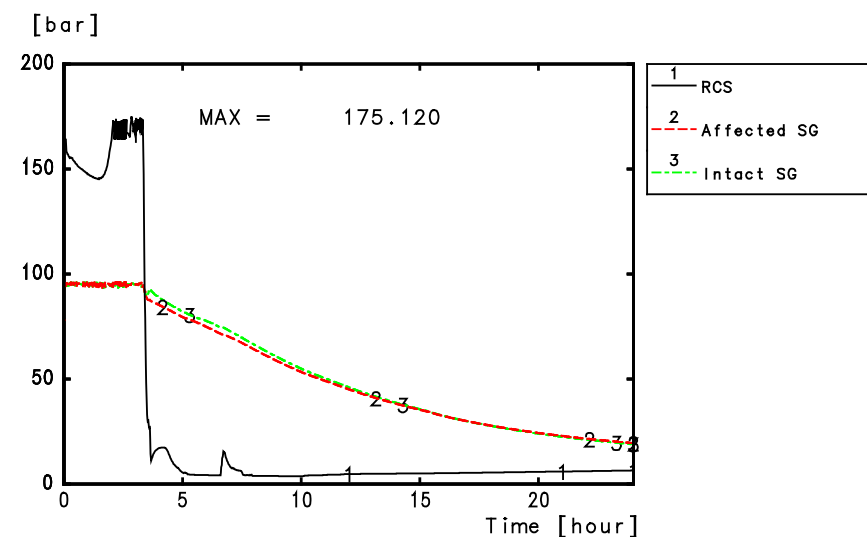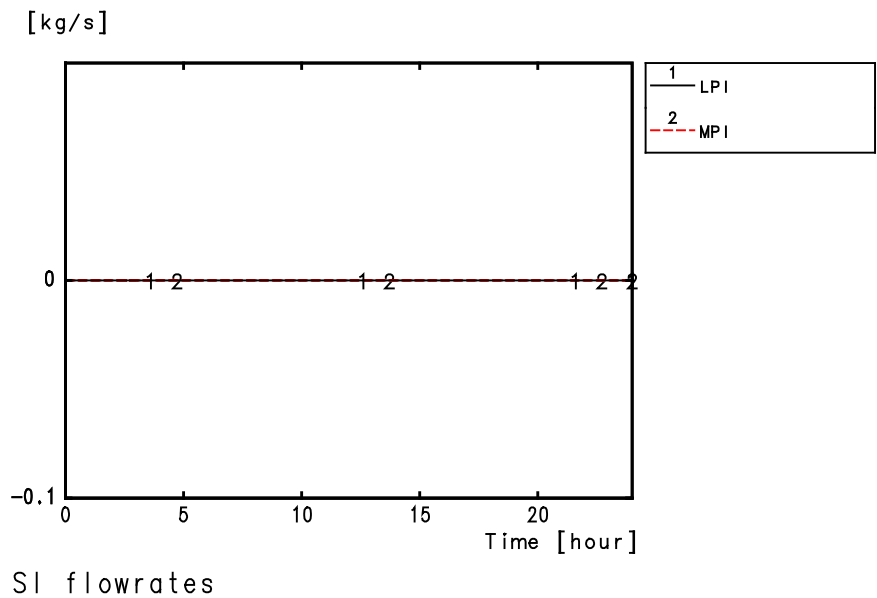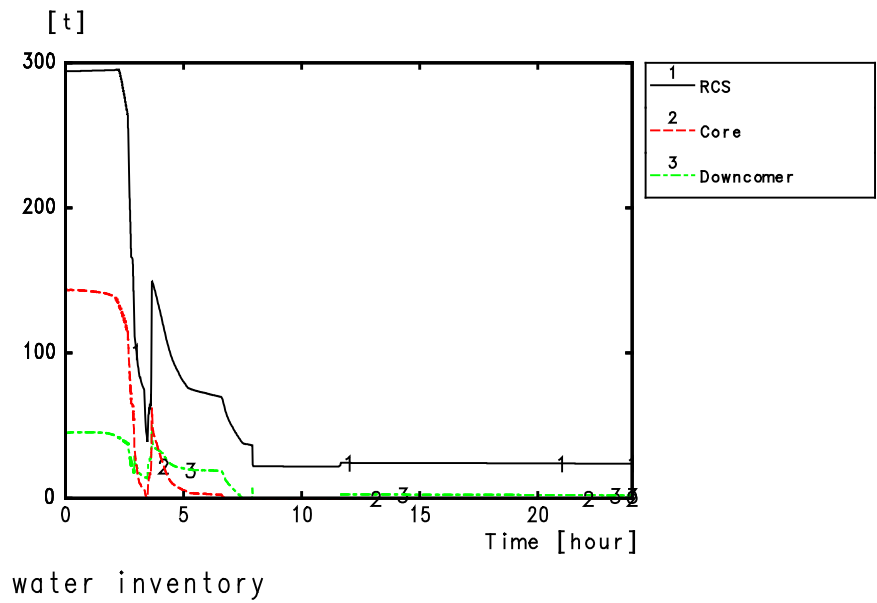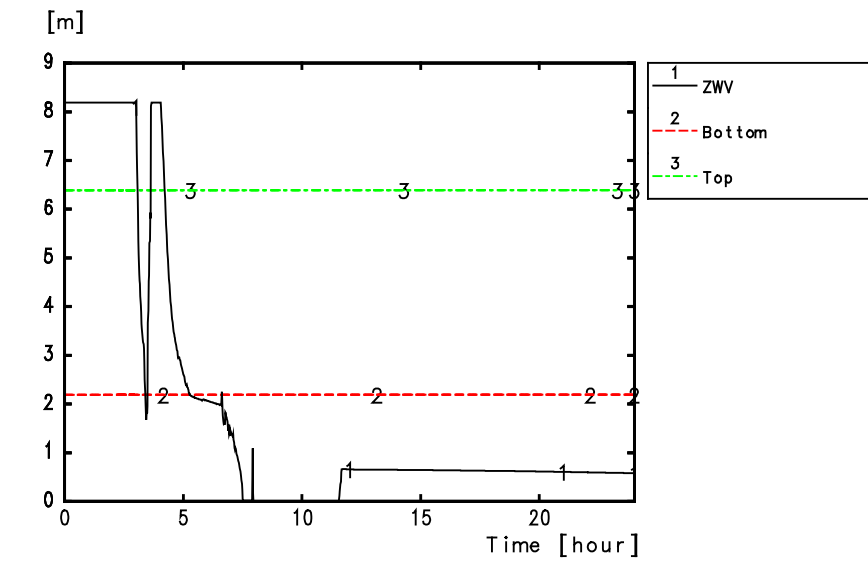

Pressure

Collapsed level in SGs

SECTION 16.2.2.2 - FIGURE 3

Water mass in RCP [RCS], core and downcomer; Safety injection flow rates (LOOP) [Ref-1]
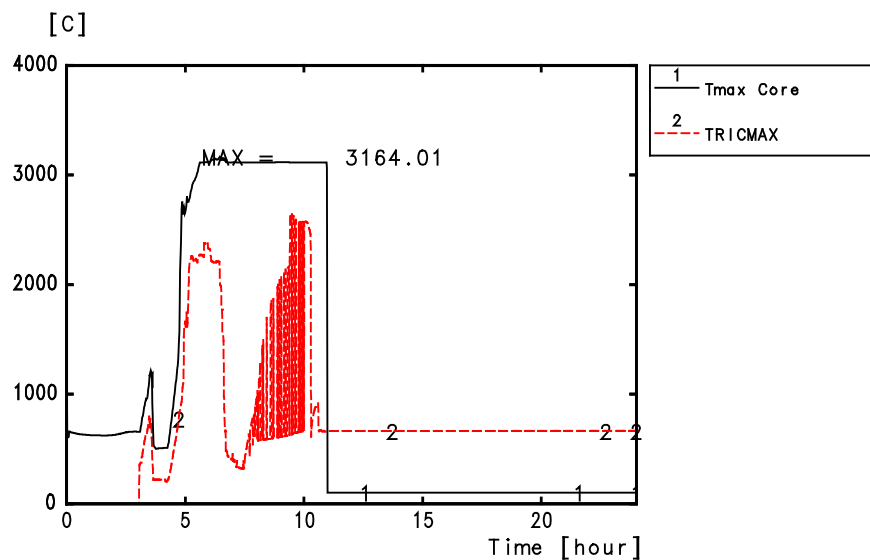

water inventory

SI flowrates

SECTION 16.2.2.2 - FIGURE 4

Core level, maximum core temperature and maximum core outlet gas temperature (LOOP) [Ref-1]
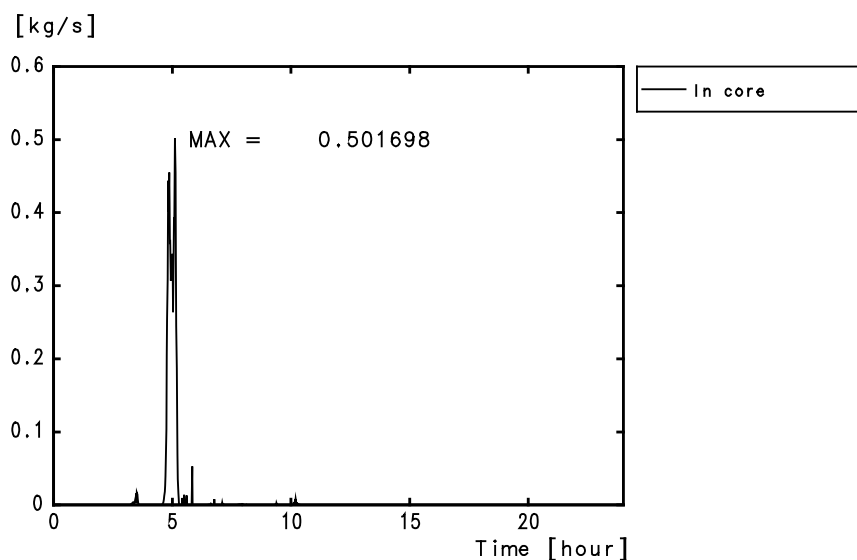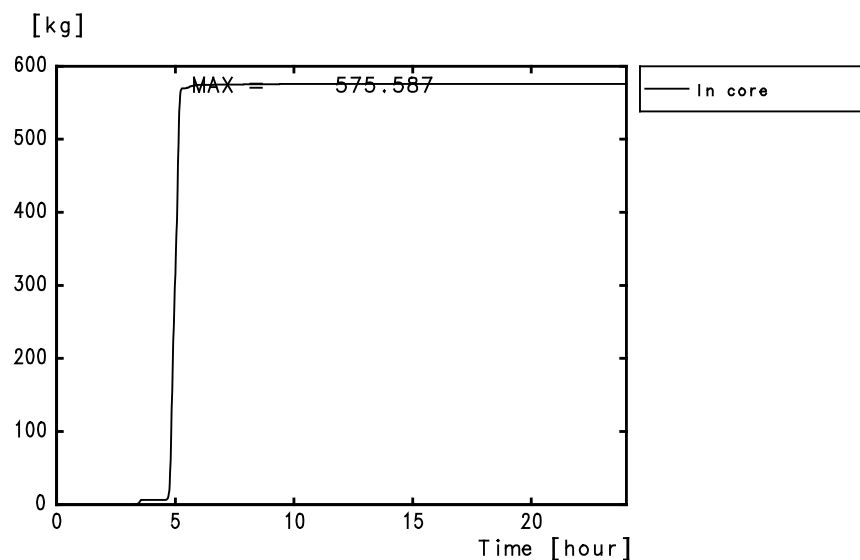

Core level

Maximun core temperature and max. core outlet gas temp.

SECTION 16.2.2.2 - FIGURE 5

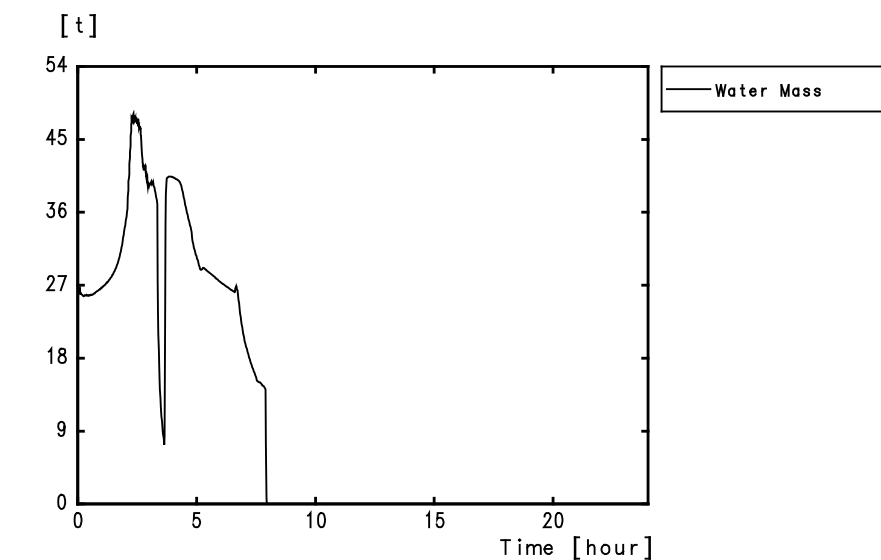**Hydrogen release rate and mass production in core (LOOP) [Ref-1]**

[kg/s]

MAX = 0.501698

In core

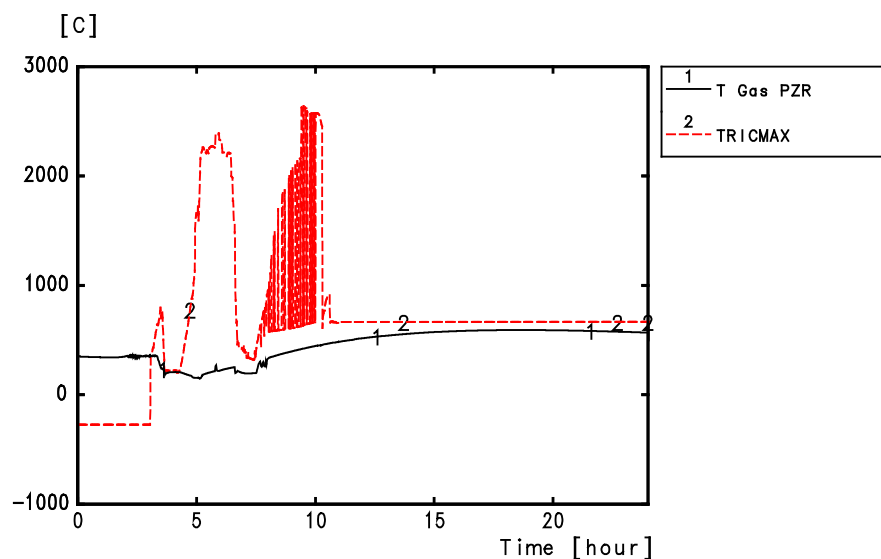Hydrogen Release Rate

[kg]

MAX = 575.587

In core

H2 production in-vessel

SECTION 16.2.2.2 - FIGURE 6

Water mass in PZR, TRICMAX* and PZR gas temperature (LOOP) [Ref-1]

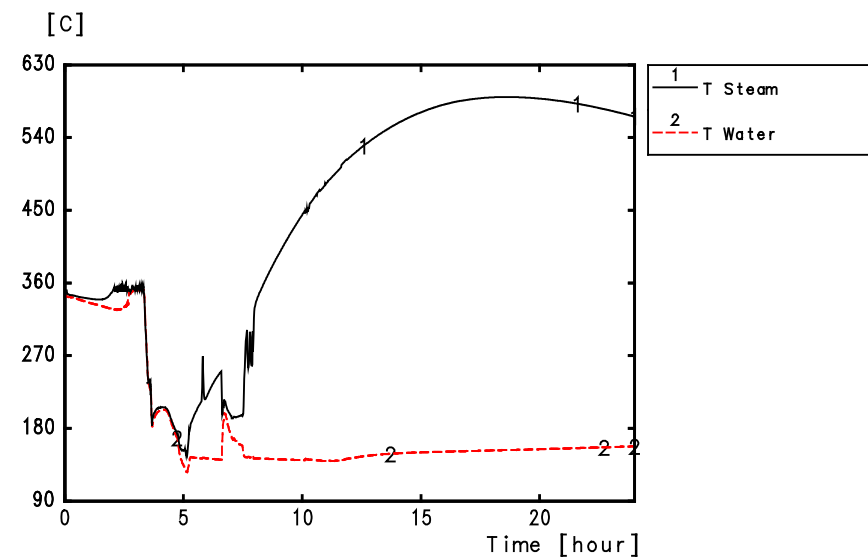Water mass in pressurizer

Temperature in PZR and Core
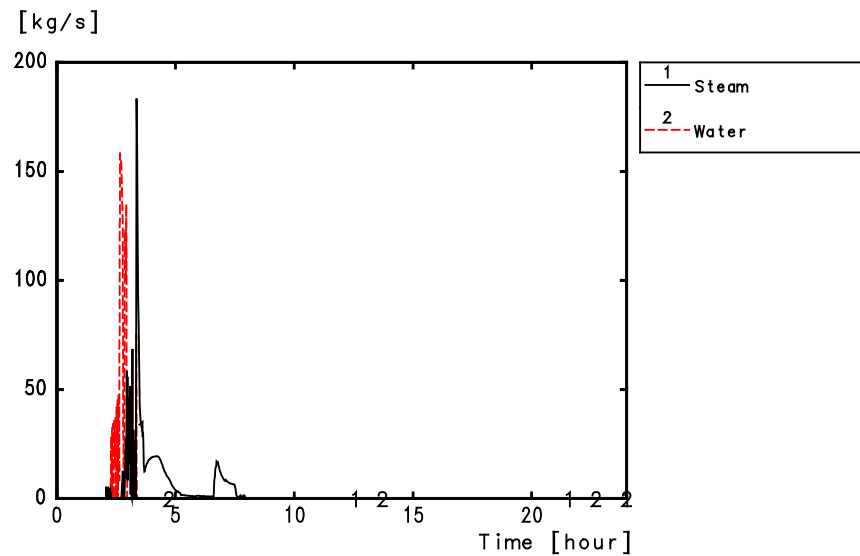
* TRICMAX is the maximum core outlet gas temperature

SECTION 16.2.2.2 - FIGURE 7

Flow rates out of PZR, PZR water and steam temperatures (LOOP) [Ref-1]

Flowrate out of pressurizer

Temperature in Pressurizer

SECTION 16.2.2.2 - FIGURE 8

Maximum hot leg, surge line and SG tubes temperatures (LOOP) [Ref-1]
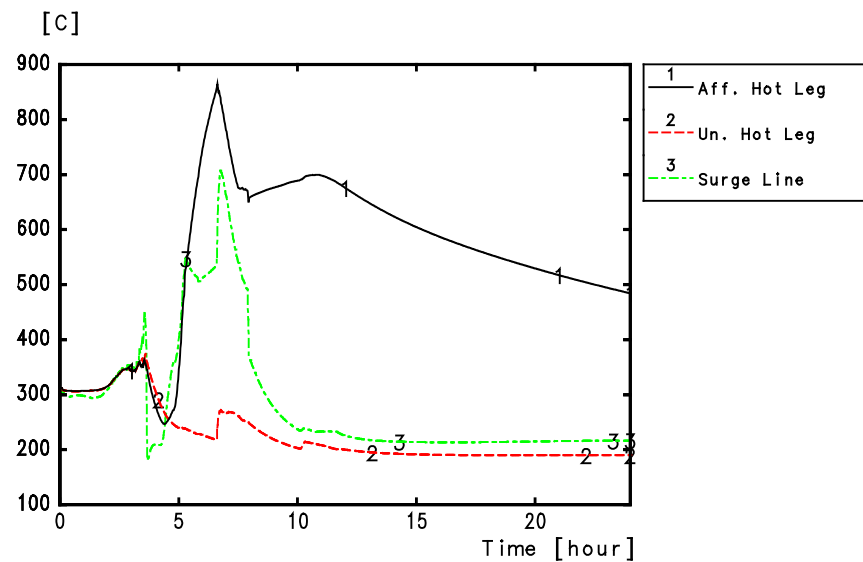
Maximum surface temperatures
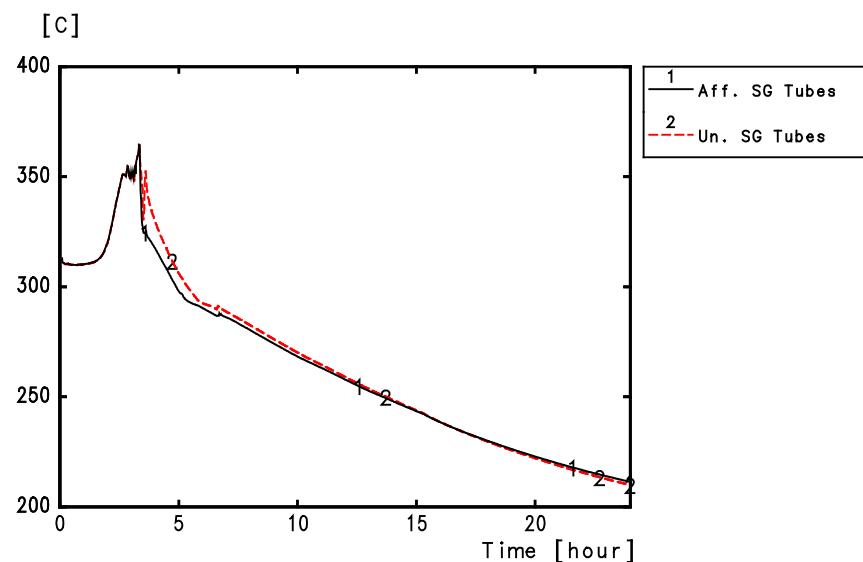
Maximum SG tubes temperature

SECTION 16.2.2.2 - FIGURE 9

RCP [RCS] and SG pressure, collapsed level in SG (TLOFW) [Ref-1]
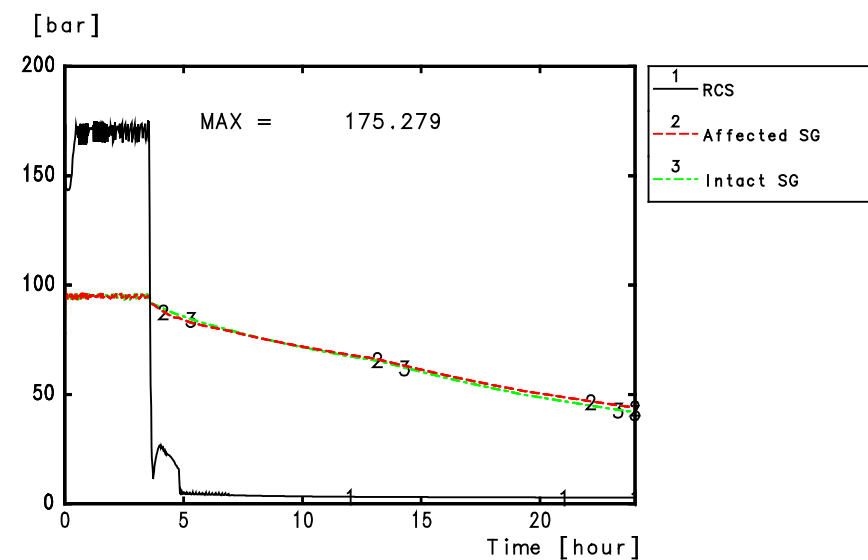
Pressure
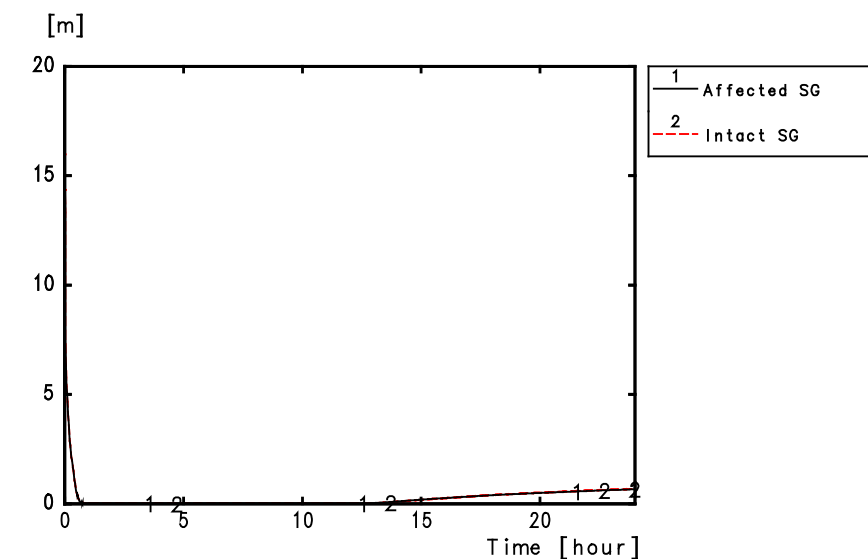
Collapsed level in SGs

SECTION 16.2.2.2 - FIGURE 10

**Water mass in RCP [RCS], core and downcomer;
Safety injection flow rates (TLOFW) [Ref-1]**
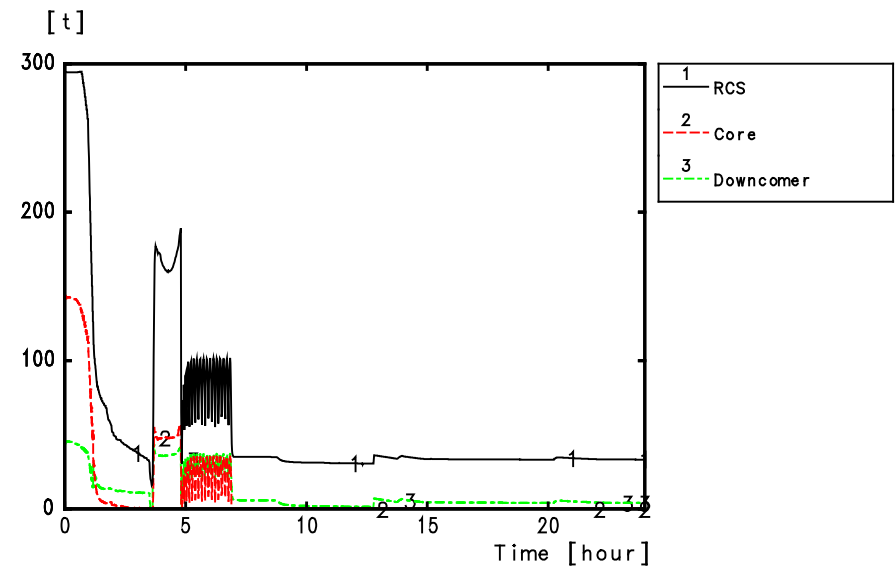
water inventory
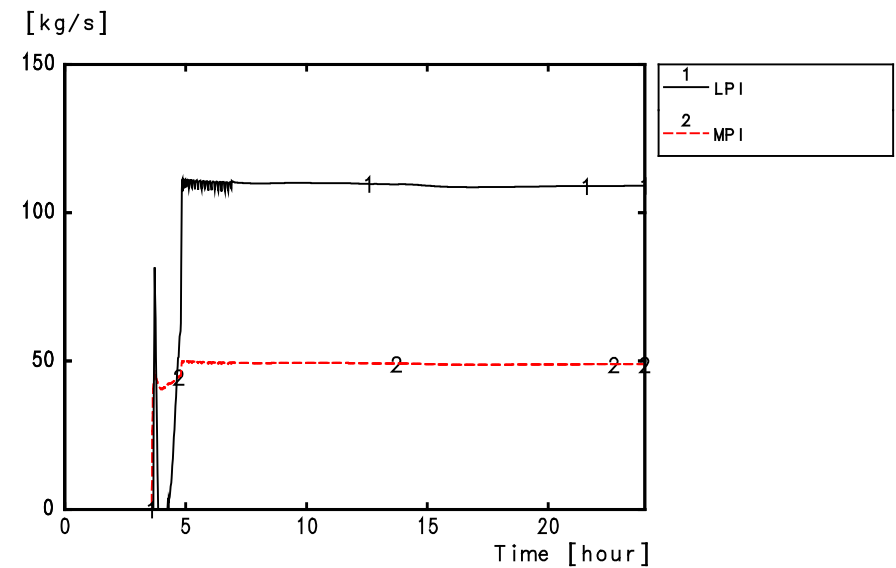
SI flowrates

SECTION 16.2.2.2 - FIGURE 11

Core level, maximum core temperature and maximum core outlet gas temperature (TLOFW) [Ref-1]
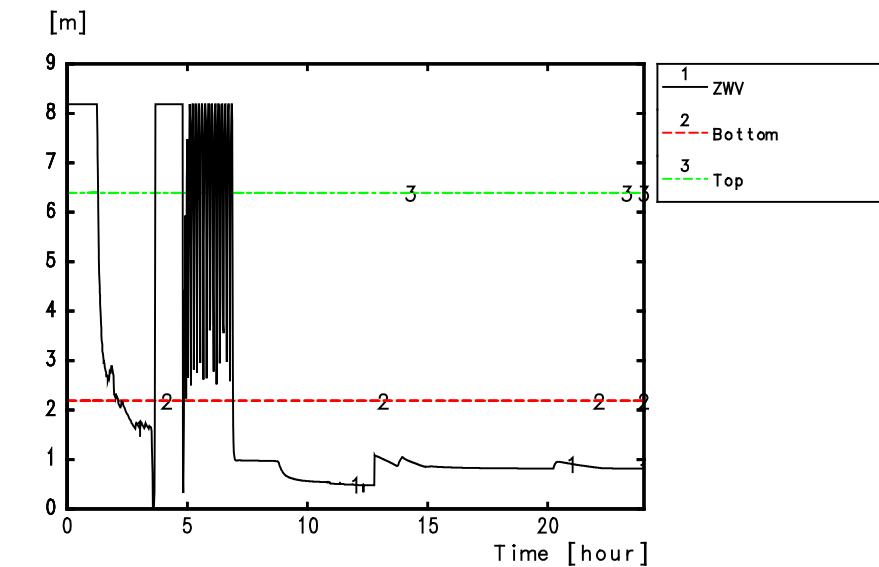
Core level
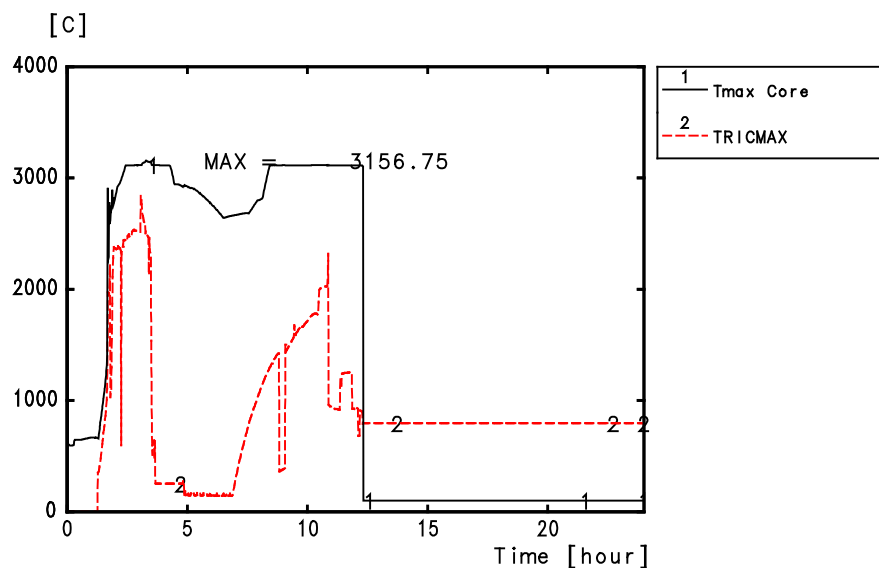
Maximun core temperature and max. core outlet gas temp

SECTION 16.2.2.2 - FIGURE 12

Hydrogen release rate and mass production in core (TLOFW) [Ref-1]
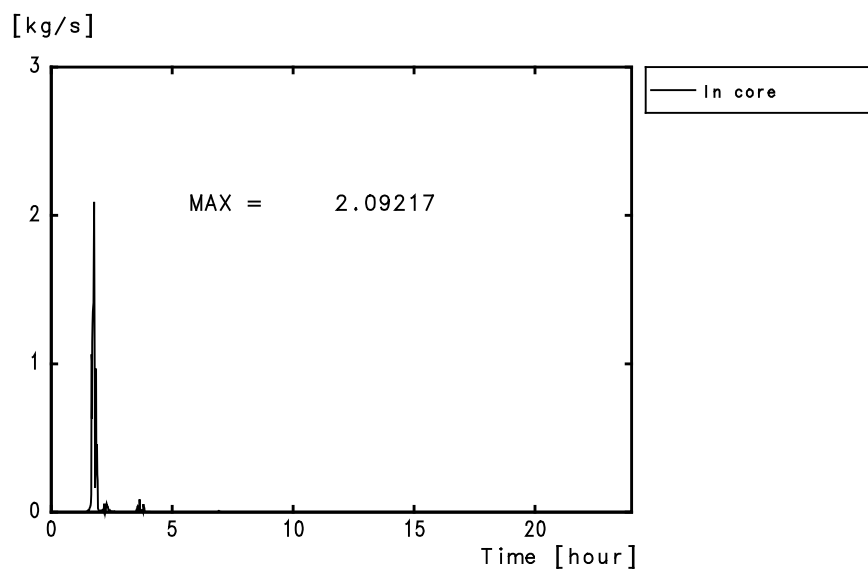
Hydrogen Release Rate
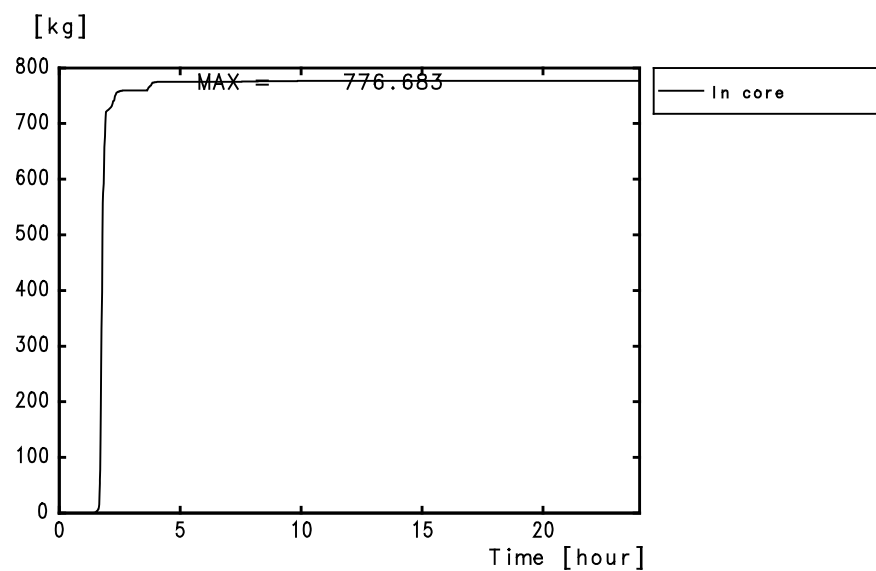
H2 production in-vessel

SECTION 16.2.2.2 - FIGURE 13

Water mass in PZR, TRICMAX* and PZR gas temperature (TLOFW) [Ref-1]
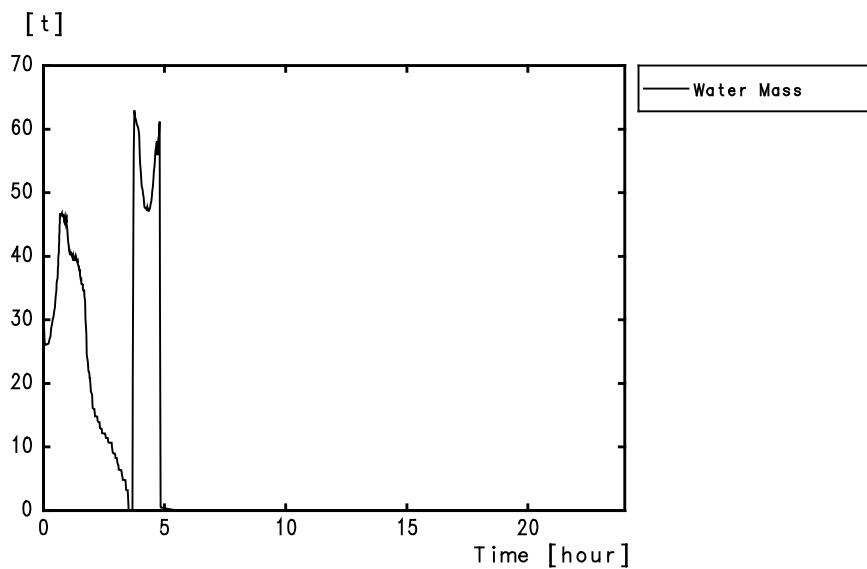
Water mass in pressurizer
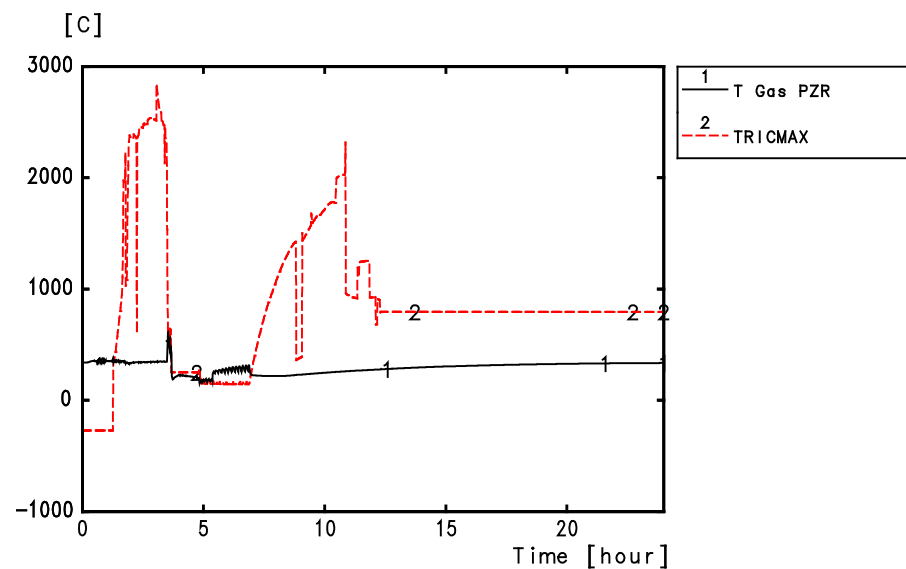
Temperature in PZR and Core

* TRICMAX is the maximum core outlet gas temperature

SECTION 16.2.2.2 - FIGURE 14

**Flow rates out of PZR, PZR water and steam temperatures (TLOFW) [Ref-1]**
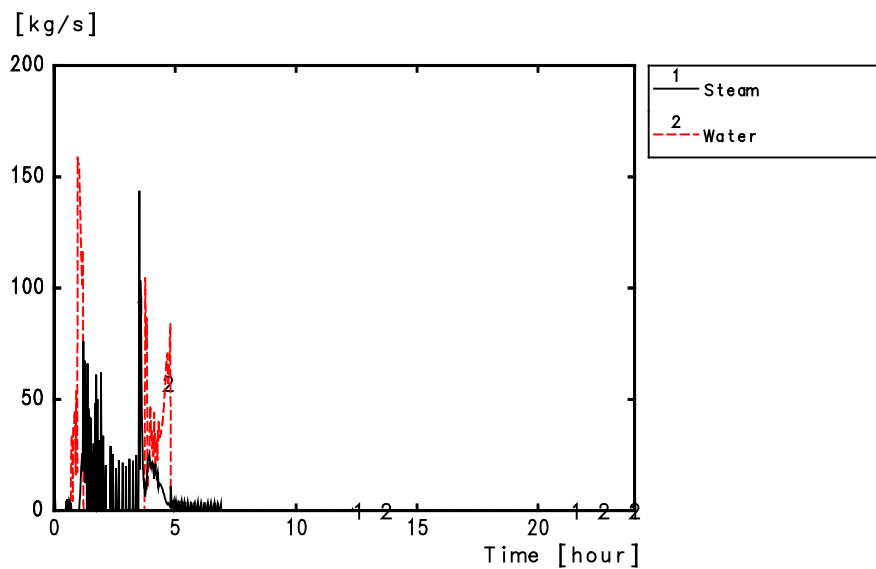
Flowrate out of pressurizer
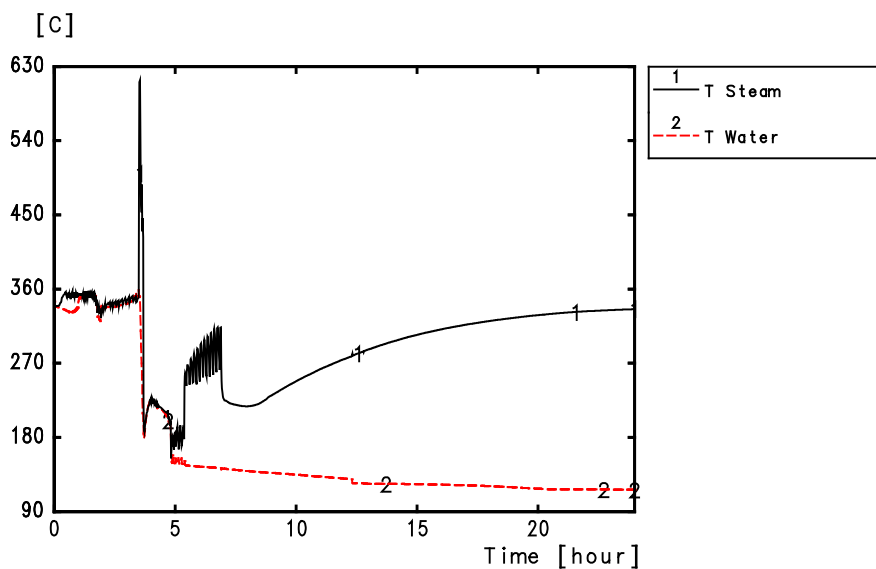
Temperature in Pressurizer

SECTION 16.2.2.2 - FIGURE 15

Maximum temperature in hot legs, surge line and SG tubes (TLOFW) [Ref-1]
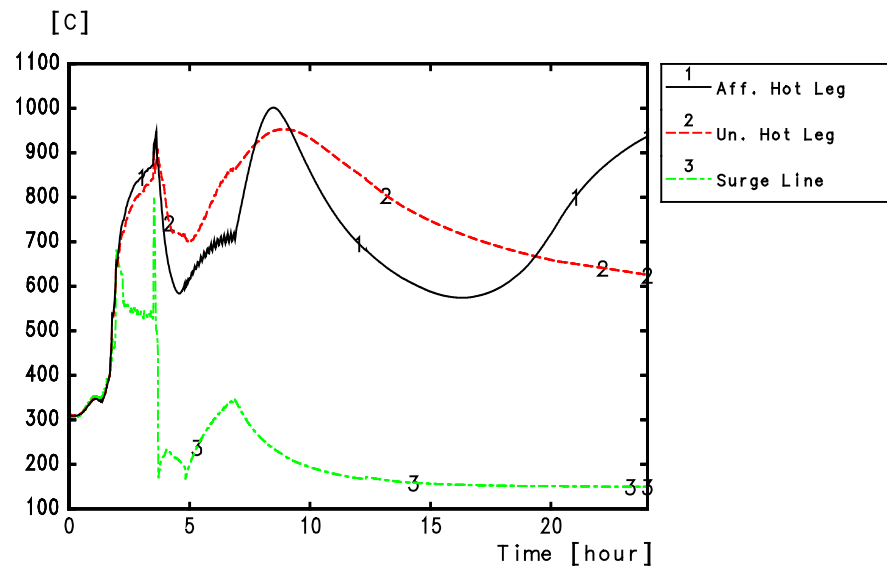
Maximum surface temperatures
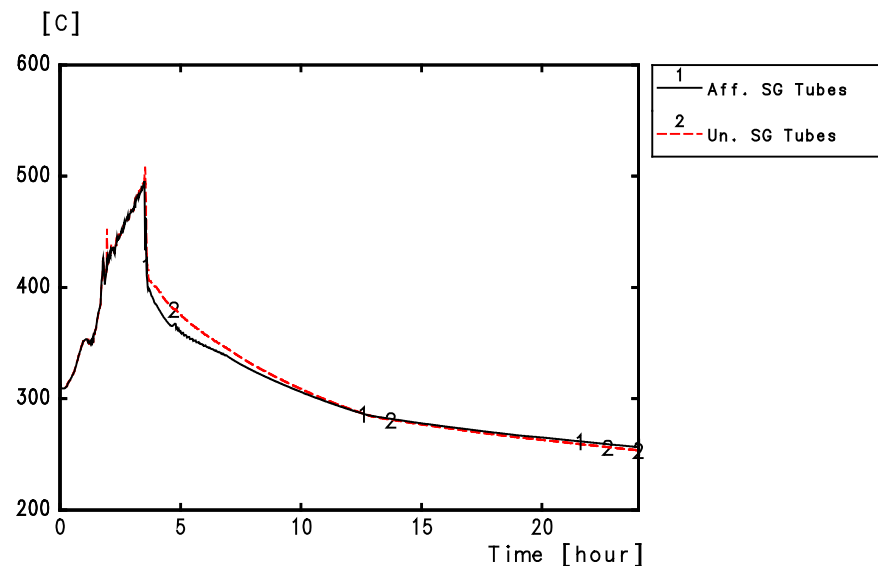
Maximum SG tubes temperature

SECTION 16.2.2.2 - FIGURE 16

Uplift forces on the vessel and support [Ref-1]
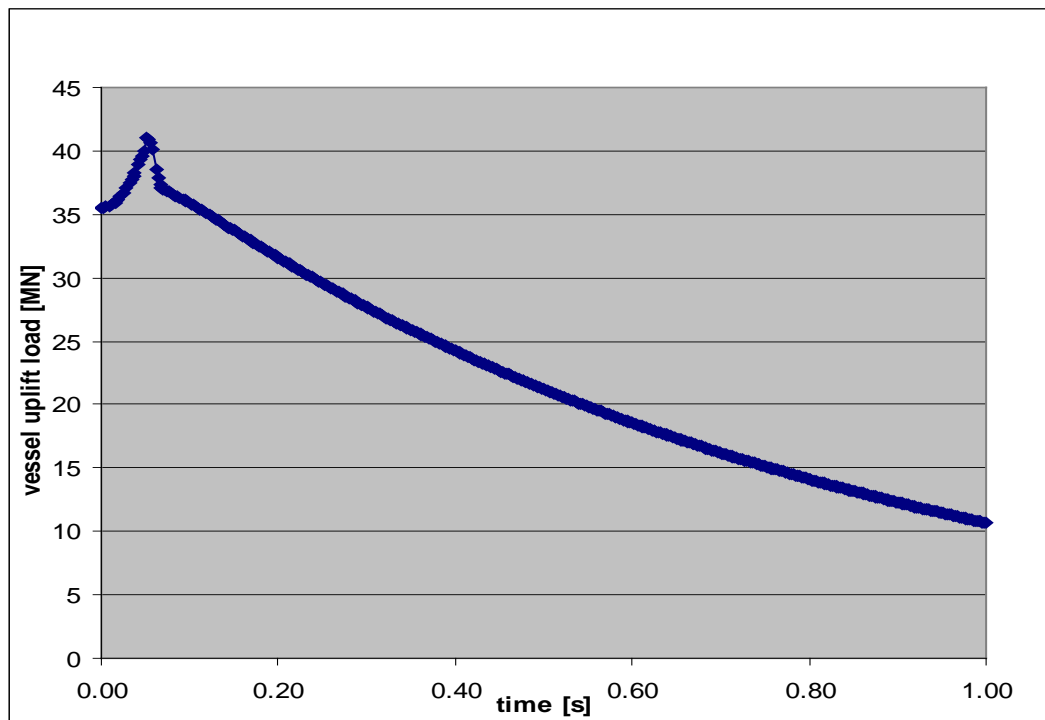
SECTION 16.2.2.2 - FIGURE 17

Natural circulation patterns in RCP [RCS]
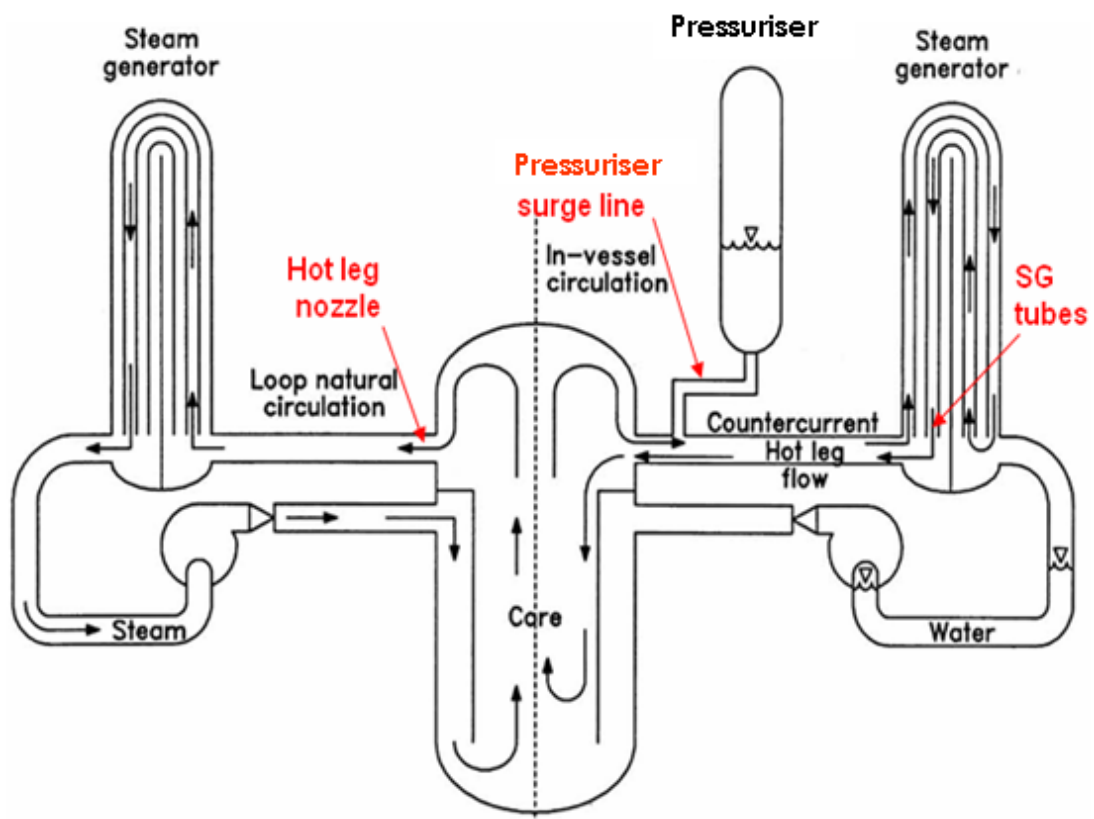
2.3. ASSESSMENT OF HYDROGEN CONTROL

2.3.1. Approach to Verifying the Efficiency of the Combustible Gas Control System

The combustible gas control system (CGCS) is described in detail in section 4 of Sub-chapter 6.2. The procedure to verify the efficiency of the CGCS consists of four steps:

1. Modelling of the scenarios relevant to hydrogen risk with MAAP-4 (see Appendix 16A) up to the point of RPV failure in order to provide mass and energy release data. Representative and bounding scenarios are selected. The classification of scenarios is outlined in section 2.1 of this sub-chapter. In brief, representative scenarios form the basis for the design and the verification of the severe accident design measures, while bounding scenarios are used to demonstrate their robustness and to explore their limits. Mass and energy release (including hydrogen release) into the containment due to ex-vessel melt stabilisation is modelled with COSACO (see Appendix 16A) in combination with an engineering model to address steam discharge due to melt flooding and quenching. The approach and results are described in section 2.4 of this sub-chapter.

2. Modelling of the gas and temperature distribution in the containment for the selected scenarios with the computational fluid dynamics (CFD) code GASFLOW (see Appendix 16A), taking into account the recombiners. These calculations are necessary for the time period in which there is a risk of hydrogen combustion. This is typically from the start of hydrogen release to the achievement of a uniform gas distribution in the early ex-vessel phase. In order to apply the correct boundary conditions during the period of hydrogen combustion risk, in particular steam concentration and wall temperatures, the history of the thermo-hydraulic parameters must be considered from the beginning of the accident in an appropriate way.

3. The assessment of the hydrogen risk is based on GASFLOW (see Appendix 16A) results and consists of analysing the possible Adiabatic Isochoric Complete Combustion (AICC) pressure, the potential for flame acceleration and deflagration to detonation transition (DDT). The assessment of flame acceleration and DDT is based on experimentally proven criteria. The most important of these criteria is the "sigma" criterion. This relates the non-isochoric combustion expansion ratio ('gas density before combustion' divided by 'gas density after combustion') to a threshold value determined by experiment. The assessment of the hydrogen combustion mode is based on the gas and temperature distribution under the assumption that ignition can occur at any time and any place if the gas mixture is ignitable. Following this deterministic approach, the likelihood of ignition is not considered and it is conservatively assumed that maximum accumulation of hydrogen occurs prior to ignition. Explicit calculations of hydrogen combustion are necessary to assess temperature loads, in particular on the containment shell. To calculate these temperature loads, GASFLOW is also used, as its laminar combustion model is sufficient for this purpose. (COM3D, a CFD code for modelling fast hydrogen deflagration (see below) is not appropriate for these calculations because it does not account for heat transfer to the walls.)

4. If fast combustion cannot be excluded by the criteria, an explicit calculation of the combustion process and the resulting pressure history is necessary. COM3D (see Appendix 16A) is used for this purpose. In order to perform COM3D calculations, one (or more) instant(s) for ignition must be selected. Usually a compromise has to be found between decreasing likelihood of flame acceleration (i.e. increasing homogenisation of the atmosphere) and increasing amount of hydrogen (i.e. potential energy) in the containment with time. For the selected cases, the GASFLOW results (gas and temperature distribution) have to be transferred as input values to COM3D. Next, a location for the ignition must be selected, taking into account hydrogen and steam concentrations in the vicinity and the available path for flame acceleration. The combustion process itself needs to be analysed only for a period of about one second. Dynamic effects with high, sharp pressure peaks normally only occur in the first tenth of a second. It is not necessary to calculate the total maximum pressure from the entire combustion process by COM3D because it is covered by the AICC pressure. The calculation of the AICC pressure is based on gas composition and temperature as a function of time.

The justification process described above focuses on pressure loads resulting from global deflagration and on flame acceleration with the potential for DDT. It is based on particular scenarios, i.e. on calculated hydrogen release histories. For these scenarios the in-vessel production of 450 to 900 kg of hydrogen up until core slumping is predicted by MAAP-4 [Ref-1]. It has been shown by comparisons with other codes and by validation calculations with MAAP-4 of QUENCH experiments [Ref-2], that MAAP-4 provides reasonably conservative results. In the ex-vessel phase, another 830 kg of hydrogen are generated by corium-concrete interactions in the reactor pit and core catcher. Consequently, the system verification considers a total amount of hydrogen that significantly exceeds the amount that would be generated by hypothetically assuming 100% oxidation of core cladding.

Hydrogen production is not an instantaneous process. It occurs over a time defined by the core degradation process and by ex-vessel reactions. Generally, slow core degradation leads to a large amount of hydrogen because the time available for oxidation is longer. Because of the depletion by recombiners, the amount of hydrogen present in the containment is lower than the generated amount of hydrogen except for a short period during the beginning of release (before the start of recombiner operation). This difference is most pronounced for slow hydrogen generation. This can be seen in Sub-section 16.2.2.3 - Figure 1, which shows the amount of hydrogen generated during the core melt process, the amount of hydrogen depleted by the recombiners and the amount of hydrogen present in the containment for a SB(LOCA) scenario with fast cooldown. About 900 kg of hydrogen are recombined within 5.5 hours, which corresponds to an average recombination rate of 163 kg/h. The total amount of hydrogen resulting from 100% oxidation of core Zr corresponds to 1320 kg and would thus be removed within 8 hours. This satisfies a design aim of the EPR to complete hydrogen removal before spraying might be required (12 hours).

Hence the total generated hydrogen mass is not the most important parameter for estimating the hydrogen risk. The hydrogen release rate and the steam concentration in the containment are more important for fast combustion.

A high hydrogen release rate leads temporarily to a non-uniform hydrogen distribution with high peak concentrations. This unfavourably affects both the possibility for flame acceleration and the detonation cell widths. High hydrogen release rates can be associated with re-flooding of a hot core. Therefore, re-flood scenarios must be considered.

A low steam concentration in the containment also unfavourably influences both the flammability of the mixture and the detonation cell widths. Therefore, scenarios with fast secondary cooldown, which result in low steam concentration in the containment, must be investigated.

The calculations presented here were performed for a representative configuration of the EPR (i.e. the basic design phase configuration), assuming a one-room containment and without considering the steel liner. It is a justified simplification to not explicitly model the transformation of the two-room containment into a one-room containment by means of rupture and convection foils and passively activated dampers, as this happens very early in the course of a severe accident, well before hydrogen release into the containment. Consequently, at the time of hydrogen peak release, the foils and dampers connecting the equipment rooms affected by hydrogen release to the annular rooms and the dome are already open, and efficient convection throughout these compartments has been established [Ref-3].

A detailed assessment of the performance of recombiners with regard to depletion performance, exhaust characteristics and local atmospheric heating is part of the analysis of the selected accident scenarios. The analyses show that the passive autocatalytic recombiners succeed in removing a significant amount of hydrogen from the containment atmosphere during the hydrogen release phase and in the period shortly after, resulting in the long term in a depletion of hydrogen below the combustibility limit within 12 hours after the start of the severe accident. In general, the temperature loads from the recombination of hydrogen are rather localised, as each operating recombiner emits a hot exhaust plume which rises upwards due to buoyancy and chimney effects. A detailed assessment of the exhaust gas temperatures and the quantification of surface temperatures at the surface of the containment shell liner in areas close to the recombiners demonstrates that the distance between recombiner exhausts and the liner is sufficiently large to avoid critical temperature loads.

An extensive programme of recombiner qualification tests has been performed in parallel with the development of the recombiners [Ref-4]. In addition, recombiner modelling in computational programs has been validated based on extensive, international, qualification testing and significant margins in the modelling of the recombiners for the CGCS have been demonstrated [Ref-5]. Additionally, a sensitivity study of the hydrogen distribution inside the EPR containment atmosphere during a severe accident and the removal of hydrogen by recombination was performed, assuming a postulated reduced performance of the passive auto-catalytic recombiners [Ref-6]. It is shown that a global reduction of the nominal hydrogen depletion rate by 25% has only a limited and significantly less than proportional impact on the overall performance of the recombiners.

The following section presents the results of the calculations of gas distribution, pressure and temperature loads for the selected representative and bounding scenarios.

2.3.2. Potential Pressure Loads

2.3.2.1. Overview of the Analysed Scenarios

In order to determine potential pressure loads, different representative and bounding scenarios have been analysed following the procedure described in section 2.3.1 of this sub-chapter. The AICC pressure, which is a purely theoretical upper limit for pressure, is calculated for all scenarios, whereas the combustion process itself has been modelled only for the most important scenarios. Sub-section 16.2.2.3 - Table 1 lists these scenarios analysed for pressure and thermal loadings. Bounding scenarios are given in the lower part of the table and are shaded with grey. The abbreviations used are as follows: f.s.c. is fast secondary cooldown and p.c. is partial cooldown. For some scenarios, the process of laminar combustion has also been calculated with GASFLOW (see Appendix 16A). The main emphasis of these calculations is to quantify thermal loads. However, they also highlight the margins for AICC pressure.

2.3.2.2. Hydrogen Distribution

The gas and temperature distributions, which are the prerequisites for the assessment of combustion loads, have been calculated for all scenarios with GASFLOW. This code has been developed and validated by the Research Centre Karlsruhe and is described in Appendix 16A. The containment is divided into about 100,000 cells using cylindrical coordinates and non-equidistant grid spacing in the radial and vertical directions [Ref-1].

Sub-section 16.2.2.3 - Table 2 gives an overview of the main characteristics of the scenarios investigated. The maximum amount of hydrogen present in the containment varies from 450 to 860 kg. Due to the recombiners, this value is always less than the amount of hydrogen released from the RCP [RCS] as discussed above. The extent of this difference depends on the release rate. In case of slow release, e.g. from a 5 cm (20 cm^2) SB(LOCA) in the cold leg with fast secondary cooldown, the maximum amount of hydrogen in the containment is significantly lower than the cumulative release. In contrast, for a fast release, e.g. in a SB(LOCA)/D scenario (where 'D' signifies delayed depressurisation), the difference is marginal. The maximum hydrogen concentration also depends on the steam concentration. The hydrogen concentration is relatively high with respect to the mass of hydrogen for scenarios with low steam concentration, as in the case of a fast secondary cooldown, and relatively low for scenarios with high steam concentration, as in the case of a partial cooldown. For all scenarios the average hydrogen concentration in the containment is always below 10% by volume. The size of the region of high concentration ($\geq$ 13% by volume) gives some first indication of the risk from fast deflagration of hydrogen. A maximum size of this region of 20,000 m^3 is found for two scenarios: 7.5 cm (46 cm^2) SB(LOCA) at the top of the pressuriser with fast secondary cooldown, and 5 cm (20 cm^2) SB(LOCA) in the cold leg with fast secondary cooldown and re-flood. For both scenarios the combustion process is analysed with COM3D (see section 2.3.3 of this sub-chapter). Generally, the maximum size of the region with 13% hydrogen by volume is reached soon after hydrogen release starts, when the gas distribution is still quite inhomogeneous, and long before the end of release, when the size of the region with 4% by volume reaches its maximum. These values are also indicated in Sub-section 16.2.2.3 - Table 2.

In this discussion, SB(LOCA) type scenarios are selected because of the low steam content in the containment. This property results in an aggravated hydrogen combustion risk compared to LB(LOCA) scenarios for example, where the high steam concentration yields significantly more inert containment conditions. In addition, probabilistic studies show that SB(LOCA) scenarios are much more likely severe accident scenarios than LB(LOCA) scenarios.

2.3.2.3. AICC and Expected Combustion Pressure

Hydrogen combustion can proceed in different modes. For hydrogen concentrations below about 10% by volume, the flame speed is expected to be subsonic, i.e. no shock waves occur. The maximum possible peak pressure from such a combustion is given by the AICC pressure. However, this pressure cannot be reached in a realistic containment for the following reasons:

- As the flame velocity is low, heat is efficiently transferred to structures, inert gases such as steam, and also to droplets. This is a departure from the adiabatic condition.

- If hydrogen concentration is below 8% by volume, combustion is not complete. Also the complex structure of the large containment leads to incomplete combustion in case of a deflagration. This is a departure from the completeness condition.

Therefore, examples of both AICC pressure and laminar combustion pressures calculated with GASFLOW are presented. Laminar combustion leads to a quasi-static pressure increase, which means that the pressure rise is isotropic and steady.

Four representative scenarios have been analysed with respect to AICC pressure history [Ref-1]:

- 5 cm (20 cm^2) SB(LOCA) in the cold leg with fast secondary cooldown (f.s.c.),

- 5 cm (20 cm^2) SB(LOCA) in the hot leg with fast secondary cooldown (f.s.c.),

- 7.5 cm (46 cm^2) SB(LOCA) at the top of the pressuriser with fast secondary cooldown (f.s.c.),

- 5 cm (20 cm^2) (SB)LOCA in the cold leg with only partial cooldown (p.c.; with consideration of ex-vessel hydrogen).

In addition, as another severe accident test case a LOOP scenario with loss of all diesel generators, which yields a higher steam concentration in the containment than a SB(LOCA) type scenario, has also been analysed with GASFLOW. However, for these scenarios with depressurisation at a core outlet temperature of 650°C, it has been found that steam concentration is sufficiently high so that no global combustion can occur [Ref-2].

In addition, two bounding scenarios have been analysed [Ref-1]:

- 5 cm (20 cm^2) SB(LOCA) in the cold leg with partial cooldown (p.c.) and delayed depressurisation (SB(LOCA)/D),

- 5 cm (20 cm^2) SB(LOCA) in the cold leg with fast secondary cooldown (f.s.c.) and re-flood (SB(LOCA)/R).

Sub-section 16.2.2.3 - Figure 2 shows the histories of the potential AICC pressure (solid curves) for all scenarios on a shifted time scale (hydrogen release starts at time zero) together with the calculated combustion pressure histories (dashed curves) for three scenarios: SB(LOCA) cold leg f.s.c., SB(LOCA)/D and SB(LOCA) cold leg p.c. for the ex-vessel phase. The pressure calculated with GASFLOW does not exceed 5.5 bar. The maximum AICC pressure of 6.3 bar was calculated for the bounding scenario SB(LOCA)/D. The highest pressure increase of 4.2 bar was calculated for the SB(LOCA)/R scenario with a peak pressure of 5.6 bar. Note that the AICC pressure curves show the pressure value that would result from combustion at any given time. They do *not* describe combustion histories, in contrast to the curves resulting from GASFLOW calculations.

2.3.3. Assessment of the Combustion Mode

Flame acceleration up to sound velocity has been found in many hydrogen combustion experiments, when the hydrogen concentration was above about 10% by volume. Flame acceleration originates from turbulence generated by structures in the flow path (e.g. orifices in tube experiments). Fast hydrogen combustion leads to dynamic pressure loads, which means non-isotropic loads with strong variation in time.

In extreme cases, a fast flame can even evolve into a detonation (DDT). Direct initiation of a detonation is not possible within a containment due to the high energy required. Peak pressures are comparable to those generated by fast deflagration, but the dynamic variation of the pressure with time (and thus the slope of pressure variation) is much higher.

Potential hydrogen combustion in a nuclear reactor containment is quite well understood today. This is the result of many experiments performed under different conditions in previous years. Hence, procedures are now available for the direct prediction of the possible mode of combustion, either based solely on the distribution of gases and temperature, or additionally using information about the containment geometry.

Flame acceleration can only occur if the expansion ratio, which is the ratio of the atmospheric density before the combustion to the density after the combustion, exceeds a threshold value (sigma criterion). This threshold value is derived directly from experiments and depends only on the gas concentration and the temperature.

In order to reach sound velocity, the flame must be sufficiently accelerated, and thus the path of the flame must be long enough. This so-called run-up distance is less well established and was not applied in the analyses of this section. The minimum distance for reaching sound velocity also depends on the gas concentration. Finally, DDT can only happen if the characteristic spatial extent of the compartment(s) under consideration is more than seven times the detonation cell size (lambda), which depends on the mixture composition (7 lambda criterion). This factor of seven has been derived from experiments.

These criteria define conditions for the corresponding phenomena, such as flame acceleration or DDT. When comparing the predicted behaviour based on these criteria against the calculations of the combustion process in a containment, e.g. performed with COM3D (see section 2.3.3 of this sub-chapter), it appears that these criteria are very conservative. The criteria are necessary but not sufficient to determine the behaviour accurately. They have usually been derived from 1D closed tube experiments and do not account for any gas relief perpendicular to the axis of propagation, which would be more realistic for the compartment structure of a containment. By investigating this effect experimentally in vented tube experiments, a correction factor to the sigma criterion for flame acceleration has been established based on the relative area of the vertical openings. However, this correction was not considered in the conservative analyses in this section.

Because of the large degree of conservatism described above, the criteria are often violated locally and temporarily during the course of a severe accident. Therefore, the process of combustion has been explicitly calculated using COM3D (see Appendix 16A), which was developed by Research Centre Karlsruhe to assess flame acceleration and fast deflagration.

The four representative scenarios and the two bounding scenarios listed in sub-section 2.3.2.3. have been examined. The potential combustion mode has been analysed for all scenarios under consideration. As an example, this section treats two scenarios, which are the most conservative in their particular class, the 7.5 cm (46 cm^2) SB(LOCA) at the top of the pressuriser with fast secondary cooldown (f.s.c.), which is a representative scenario, and the 5 cm (20 cm^2) SB(LOCA) in the cold leg with fast secondary cooldown (f.s.c.) and re-flood at the most unfavourable time (SB(LOCA)/R), which is a bounding scenario. These scenarios have also been analysed in detail with COM3D to assess whether flame acceleration and fast deflagration really occur (see section 2.3.3.4 of this sub-chapter).

Combustion risk is analysed using the sigma criterion, which states that there is no risk of flame acceleration as long as the sigma index is less than 1. For regions with sigma index greater than 1, flame acceleration cannot be excluded by this procedure alone, but does not necessarily occur. The geometrical conditions must also favour flame acceleration (obstacles, no vent openings). All combustion calculations performed at AREVA with COM3D for situations with sigma index greater than 1 show that there is still a large margin before fast combustion with significant loads to the containment shell or DDT can occur.

2.3.3.1. 7.5 cm (46 cm^2) SB(LOCA) at the Top of the Pressuriser with Fast Secondary Cooldown

Combustion risk can be expected to be higher for this scenario compared to a scenario with hydrogen release at a lower elevation in the containment because of hydrogen stratification in the upper part of the containment.

The region with sigma index > 1 can best be seen in horizontal cross-sections. Sub-section 16.2.2.3 - Figures 3a to 3c show the volume with sigma index > 1 at the elevation of the break at 29,250, 29,600 and 29,700 seconds after the start of the accident, respectively. The situation is nearly constant in time for this period, showing a sigma index > 1.4 in the upper pump compartments of loop 3.

At the elevation of the polar crane, the volume with sigma index > 1 grows in size with time. At 29,250 seconds, only the plume above the steam generator (SG) compartment of loop 3 shows a sigma index > 1. Later in the accident, the volume with sigma index > 1 grows in regions away from the containment shell, where steam condensation still occurs, towards the centre of the containment. At 29,700 seconds, the sigma index is > 1 for about 70% of the containment at this elevation.

At 50 m elevation a ring-shaped region of high sigma index can be identified at 29,250 seconds (see Sub-section 16.2.2.3 - Figure 4a), similar to the hydrogen concentration distribution. This volume also grows in regions away from the containment shell towards the centre. At 29,700 seconds, the sigma index is > 1 for nearly the entire top of the containment (see Sub-section 16.2.2.3 - Figures 4b, 4c).

2.3.3.2. 5 cm (20 cm^2) SB(LOCA) in the Cold Leg with Fast Secondary Cooldown and Re-Flood

In order to get an idea of the extent of the region where flame acceleration might be possible, the volume with sigma index > 1 is analysed (Sub-section 16.2.2.3 - Figures 5 to 7).

At 19,300 seconds, the volume with sigma index > 1 is limited to both affected pump rooms, as can be seen in the upper part of Sub-section 16.2.2.3 - Figure 5a, which shows a horizontal cross-section through the containment at elevation 14.1 to 14.7 m. Due to superposition of the release through the break and the Pressuriser Relief Tank (PRT), the hydrogen plume on the left is larger and has higher sigma index values, up to 1.75. A sigma index > 1 can be roughly correlated with hydrogen concentration above 15% by volume in this case.

At 19,400 seconds, (see Sub-section 16.2.2.3 - Figure 5b) the volume with sigma index > 1 is slightly extended to the neighbouring SG compartments. On the other hand, the sigma index values are now generally smaller and remain below 1.4.

For the time period of 19,550 to 21,000 seconds, the sigma index remains below 1 at this elevation.

For the dome region, the elevations 37.2 to 39.7 m and 46.8 to 49.2 m are selected to facilitate a direct comparison with the hydrogen concentration.

Sub-section 16.2.2.3 - Figures 6a and 6b show the sigma index at the lower dome elevation for the relevant times of 19,400 seconds and 19,550 seconds. At 19,300 seconds, the dome is not yet filled with hydrogen at a high concentration and, at 21,000 seconds, the hydrogen concentration has started to decrease.

At 19,400 seconds, the two plumes related to the two release locations can be clearly identified. Again the plume on the left is somewhat larger due to the superposition of the break and PRT release. Also in some annular regions the sigma index is slightly > 1 as a result of down-streaming gas. The maximum sigma index is around 1.4.

At 19,550 seconds, the sigma index is slightly > 1 for around 75% of the cross-sectional area. All sigma index values are below 1.2.

Sub-section 16.2.2.3 - Figures 7a and 7b show the sigma index at the upper dome elevation for the same times. There are no significant differences compared to the lower dome elevation.

In summary, in relation to the times under consideration, the volume with sigma index > 1 is limited to

- the equipment rooms at 19,300 seconds,

- the equipment rooms and the plume in the dome at 19,400 seconds,

- the entire dome region at 19,550 seconds,

- a very small region at the bottom of the containment at 21,000 seconds.

2.3.3.3. Influence of Activating the Spray System

The effect of the spray system on the hydrogen risk has been investigated with GASFLOW for the bounding scenario 5 cm (20 cm^2) SB(LOCA) in the cold leg with partial cooldown and delayed depressurisation (SB(LOCA)/D) [Ref-1]. The spray system is actuated at the worst case time, when the amount of hydrogen and the risk of fast deflagration are close to their maximum. It can be shown that activation of the spray system does not negatively affect the hydrogen risk.

Moreover, beneficial aspects seem to prevail: the competition between increased volumetric hydrogen concentration and homogenisation of the atmosphere leads to favourable sigma and lambda values in the case when spraying is activated. This means that flame acceleration is less likely in this case. In addition, the presence of droplets in the atmosphere leads to a further reduction of the risk because

- flame velocity is lower, and

- droplets can pick up energy in case of combustion, thus lowering the pressure.

However, these effects are not explicitly taken into account in the formula for the sigma and lambda index.

The main results from this investigation of the SB(LOCA)/D scenario are as follows:

- Activation of the spray system reduces the risk of hydrogen combustion globally and locally by homogenising the hydrogen-air-steam atmosphere.

- No complete combustion is possible for either case, with or without spraying. In case of spray activation, the maximum potential AICC pressure is reduced from 6.3 to 6.1 bar.

- The maximum average hydrogen concentration is below 10% by volume with and without spraying. The average hydrogen and steam concentrations are shown in Sub-section 16.2.2.3 - Figure 8.

- The risk of flame acceleration is slightly reduced in case of spray activation. However, the effect of turbulence induced by spraying is not taken into account by the GASFLOW calculations.

- Flame acceleration is only possible in loop 2 and loop 3 for about 3 minutes during the release period. At that time, the hydrogen plume of 16% concentration by volume is smaller than 1000 m^3.

- The volume of the plume with sigma index > 1 decreases rapidly when the spray system is activated, and the duration when the sigma index > 1 is about 100 seconds shorter. Sub-section 16.2.2.3 - Figure 9 shows the history of the plume with sigma > 1. Without spraying the cloud has a maximum volume of close to 12,000 m^3. This value is reduced to 9,000 m^3 in the case of spray actuation.

To conclude, in the case of spray activation, the slow increase in hydrogen concentration is mitigated by enhanced mixing of the containment atmosphere by the spraying and also by more efficient hydrogen reduction through the recombiners.

2.3.3.4. Dynamic Pressure Loads

The consequences of fast combustion on the containment shell are analysed with COM3D (see Appendix 16A), which is a CFD code specially developed by Research Centre Karlsruhe for the analysis of fast combustion processes. Combustion is modelled in the code on the basis of an eddy break-up model. Initial conditions for the code are taken from the respective GASFLOW calculation; ignition time and location are selected taking into account the sigma criterion for flame acceleration.

The simulation of turbulent combustion requires detailed spatial resolution of the reacting flows. Therefore, the containment is modelled with finer resolution than required for GASFLOW (distribution and laminar combustion). COM3D uses a cubic Cartesian grid (**41**·41 cm ^{3}) to achieve this high resolution within the calculation. The total number of cells in the whole containment exceeds 2,000,000.

Two representative scenarios and two bounding scenarios have been analysed to envelop all scenarios where there is the possibility of hydrogen combustion:

- 5 cm (20 cm^2) SB(LOCA) in the cold leg with fast secondary cooldown (f.s.c.); rationale: steam depleted condition, large amount of hydrogen,

- 7.5 cm (46 cm^2) SB(LOCA) at the top of the pressuriser with fast secondary cooldown (f.s.c); rationale: steam depleted condition, stratification,

- 5 cm (20 cm^2) SB(LOCA) in the cold leg with partial cooldown (p.c.) and delayed depressurisation (SB(LOCA)/D); rationale: high release rate and thus temporarily large local concentrations, large amount of hydrogen, mixed release mode,

- 5 cm (20 cm^2) SB(LOCA) in the cold leg with fast secondary cooldown (f.s.c.) and re-flood (SB(LOCA)/R); rationale: steam depleted condition, large amount of hydrogen, high release rate.

These scenarios are a subset of those listed in section 2.3.2.3 of this sub-chapter.

2.3.3.4.1. 5 cm (20 cm^2) SB(LOCA) in the Cold Leg with Fast Secondary Cooldown [Ref-1]

Based on the time dependent hydrogen distribution as calculated with GASFLOW, the criteria for the exclusion of flame acceleration (sigma index < 1) is violated for a short period of time in particular rooms (local violation). Fast secondary cooldown is very onerous for hydrogen combustion because of the low steam concentration within the containment when hydrogen is released. The event is characterised by release only through the break, and the combustion process is analysed to assess the consequences of the sigma criterion being violated in events which are significant contributors to core melt frequency. An accidental ignition is assumed at the most unfavourable time (just before the maximum amount of hydrogen has been released into the containment and at the end of the time period of violation of the sigma criterion) and at the most unfavourable location (above the break and just below the upper pump room).

Flame acceleration occurs in the upper part of the pump room in which the break is located and the two adjacent SG compartments. Here pressure pulses typical of a fast deflagration are found. On its way through the containment, the flame decelerates in the dome due to the lower hydrogen concentration compared to the loop compartments. Only at a level close to the top of the SG tower, e.g. at the top of the cylindrical part of the containment, dynamic effects can be observed. At the top and bottom of the containment the pressure rise is quasi-static.

The pressure history at two locations of the containment shell is plotted in Sub-section 16.2.2.3 - Figure 10 for the top of the cylindrical region of the containment. On the side where the ignition spot is located, pressurisation starts at the top of the cylindrical part of the containment at the same time as at lower locations around the material hatch. On the opposite side, the pressure rise is delayed by about 0.05 seconds.

Strong oscillations in pressure, more pronounced than at the elevation of the material hatch, are limited to the time range before 0.3 seconds. Later, a quasi-static pressure rise dominates. At the top of the containment only weak oscillations occur. The maximum dynamic pressure found anywhere on the containment shell is 2.7 bar. The pressure load on the containment shell is thus essentially quasi-static.

In summary, the observed combustion is a mild fast deflagration starting quite violently within the affected loop but damped on its way towards the containment shell because of the lower hydrogen concentration in the dome.

2.3.3.4.2. 7.5 cm (46 cm²) SB(LOCA) at the Top of the Pressuriser with Fast Secondary Cooldown [Ref-1]

This scenario has been selected for analysis with COM3D because of the presence of hydrogen stratification above the break location. Ignition has been assumed at the most unfavourable time (29,700 seconds into the accident) which is characterised by a hydrogen concentration in the dome of about 12% by volume. Hydrogen concentration is above 24% by volume in the pressuriser room and above 12% in the adjacent SG compartment, which is connected to the dome. Steam concentration within the hydrogen plume is between 20 and 25% by volume. The sigma criterion is violated in the pressuriser and SG compartment as well as in parts of the dome at the time of ignition. Ignition is assumed at the worst location, that is in the SG compartment at the elevation of the connection to the upper pressuriser room.

Apart from short pressure spikes up to 4 bar close to the ignition location, no dynamic effects on the containment shell are found. Therefore, combustion pressure is bounded by the AICC pressure for this scenario (4.3 bar).

UK EPR

PRE-CONSTRUCTION SAFETY REPORT

CHAPTER 16: RISK REDUCTION AND SEVERE ACCIDENT ANALYSES

SUB-CHAPTER : 16.2

PAGE : 109 / 295

Document ID.No.
UKEPR-0002-162 Issue 05

2.3.3.4.3. 5 cm (20 cm^2) SB(LOCA) in the Cold Leg with Partial Cooldown and Delayed Depressurisation [Ref-1]

This bounding scenario results in a large release of hydrogen with high release rates due to flooding of the hot core by the accumulators. This is a result of the assumption that depressurisation of the RCP [RCS] by the operator is delayed. The sigma index is > 1 only for a short period between 7900 and 8100 seconds. Later, homogenisation of the atmosphere and recombination eliminates the possibility of flame acceleration. The maximum sigma index occurs very early between 7900 and 7950 seconds, when the amount of hydrogen in the containment is still small. During this period the lambda criterion is also violated (leading to a risk of DDT). The most severe consequences of combustion can be expected when the maximum amount of hydrogen in the containment is present during the period of DDT risk. Consequently, ignition was assumed at 8000 seconds just above the break, where the potential for flame acceleration is highest.

The calculation was performed for one second. Less than 200 kg hydrogen is burnt in this period of time, with a peak burning rate of 240 kg/s. The maximum flame velocity was always less than 60 m/s. Thus, no significant dynamic loads occurred, either on the containment shell or on the inner walls. Extrapolating the burning rate to complete combustion, a pressure increase of 2.8 bar is expected. Adding the 2.8 bar to the initial pressure of 2.9 bar, the total pressure is close to the AICC pressure. The maximum dynamic pressure found locally on the containment shell is 3.8 bar. Note that the assumption of no heat transfer to the wall in the COM3D calculation is valid because of the short period of calculation time for fast deflagration.

Generally, for the SB(LOCA) scenario with delayed depressurisation and initial conditions as calculated with GASFLOW, no extensive fast deflagration is predicted and thus no significant dynamic loads on the structures occur.

As no substantial fast combustions occurred under these particular conditions, a set of parametric calculations was performed as a sensitivity study:

- reducing the initial steam concentration to show the effect on flame velocity and combustion rate,

- adding additional obstacles to show the effect on flame acceleration,

- changing the location of ignition to investigate the flame propagation from poor to rich mixture, and

- closing all radial openings of the SG compartments.

From these calculations, it was concluded that:

- some flame acceleration occurred in the SG compartments but was followed by deceleration in the dome, resulting in small pressure loads on the containment shell,

- radial venting has a significant effect on the process of flame acceleration, and thus the transfer of results from closed tube experiments to a realistic containment probably leads to very conservative results.

High local pressure peaks on the containment shell did not occur because flame acceleration within the SG compartment is limited by radial venting and deceleration in the dome. The latter seems to be an effect of general importance. The risk of flame acceleration with the potential to jeopardise the containment integrity only exists, if at all, in the early period after onset of hydrogen release. At that time, the distribution is not homogeneous and regions of high concentration exist in the equipment rooms but little hydrogen is in the dome. Later, when the concentration in the dome rises, the overall gas distribution is quite homogeneous, with hydrogen concentration well below 10% by volume. This effect is mainly due to convection but also supported by the recombiners.

2.3.3.4.4. *5 cm (20 cm^2) SB(LOCA) in the Cold Leg with Fast Secondary Cooldown and Re-Flood [Ref-1]*

This is the most conservative bounding scenario analysed because it combines low steam concentration in the containment (from fast secondary cooldown) with a high peak hydrogen concentration (from re-flood). Two cases were investigated:

- ignition in the pump room at the elevation of the main coolant lines,

- ignition in the dome at the elevation of the polar crane above the affected SG compartment.

In the case of the lower ignition point, flame acceleration in the SG compartment occurred, leading to flame speeds above 400 m/s at the top of the SG compartment. Deceleration in the dome reduced the flame speeds to around 100 m/s when the flame touches the containment shell. Hence, dynamic effects were limited to the first 0.2 seconds and were well below the AICC pressure.

In the case of ignition in the dome, a laminar combustion occurred with flame velocities around 30 m/s. After 2 seconds, flame acceleration down into the SG compartments occurred, leading to flame velocities of around 100 m/s. Loads on the containment shell were benign compared to ignition in the pump room.

However, despite the smooth pressure history on the containment shell, pressure differences across inner walls are important. Sub-section 16.2.2.3 - Figure 11 shows the pressure histories for two different locations on the inner wall of the SG tower together with a typical pressure history for the inner pump room walls and the annular compartments for the first 0.2 seconds. The maximum pressure difference across any wall is 0.4 bar.

2.3.3.5. Temperature Loads

In the case of a severe accident, thermal loads on the containment shell may result from hydrogen oxidation, both by recombiners or during combustion. The following sub-sections present typical results of calculations performed with GASFLOW that are relevant to thermal loads.

2.3.3.5.1. Temperature Loads Due to Recombination

When there is no combustion, containment shell temperatures are determined by hydrogen recombination. A specific investigation of thermal loads was performed for the LOOP scenario with re-flood at the most unfavourable time (LOOP/R) [Ref-1], because this scenario leads to the largest amount of hydrogen released into the containment (nearly 1000 kg). However, this specific LOOP scenario was investigated with an early version of the GASFLOW code that did not include radiation from gas to walls. This means that gas temperatures, in particular close to the walls, are over-predicted, while wall temperatures are under-predicted. Note that the steel liner was not modelled explicitly in any of the calculations.

In general, no wall temperature above 121°C was identified in any of the calculations. Sub-section 16.2.2.3 - Table 3 lists the calculations performed and the major findings. The maximum wall temperature depends on the amount of hydrogen recombined and thus on the amount of hydrogen available as well as other parameters such as steam concentration. Sub-section 16.2.2.3 - Figure 12 gives some time histories for containment shell temperatures at different positions at the top of the vertical containment cylinder wall for the 5 cm (20 cm^2) SB(LOCA) cold leg f.s.c. scenario. The maximum temperature observed for this scenario was 90°C. For other scenarios, temperatures up to 121°C were found. The table only gives a lower bound for the temperature in the SB(LOCA) scenario with re-flood because the calculation was performed for only a relatively short period of time and more hydrogen might be expected to be involved in the reaction than was actually accounted for in the calculation. The highest containment shell temperatures were found for the SB(LOCA) scenario with delayed depressurisation.

This study on the thermal loads from recombination led to the conclusion that containment shell temperatures are tolerable. Although there are local high temperatures of up to around 800°C in the exhaust gas from the recombiners and although large areas of the dome can have gas temperatures around 200°C, the containment shell temperatures are well below the saturation temperature of steam at the design pressure. This is due to the arrangement of the recombiners, which are all located sufficiently far away from the containment shell in the configuration of the EPR utilised for these calculations (i.e. the Olkiluoto 3 plant).

2.3.3.5.2. Temperature Loads Due to Combustion

Higher local containment shell temperatures can be expected from hydrogen combustion compared to recombination, because combustion heat can be released in a much shorter period of time. As the EPR is not equipped with igniters, ignition can only occur accidentally. On the other hand, without immediate combustion, hydrogen can accumulate locally despite the presence of recombiners with the potential of a late ignition. Recombiners or sparks from electrical equipment can be regarded as potential triggers for combustion.

The analysis is based on three scenarios:

- 5 cm (20 cm^2) SB(LOCA) in the cold leg with fast secondary cooldown (f.s.c.). This scenario covers combustion from in-vessel generated hydrogen.

- 5 cm (20 cm^2) SB(LOCA) in the cold leg with partial cooldown (p.c.). This scenario also addresses combustion of ex-vessel generated hydrogen in a "standing flame" above the un-flooded melt.

- 5 cm (20 cm^2) SB(LOCA) in the cold leg with partial cooldown (p.c.) and delayed depressurisation. This scenario covers combustion from in-vessel generated hydrogen.

2.3.3.5.2.1.   5 cm (20 cm^2) SB(LOCA) in the Cold Leg with Fast Secondary Cooldown [Ref-1]

Accidental ignition was assumed in the dome just above the SG compartment of the affected loop 2 to maximise thermal loads on the containment shell. Two cases were analysed:

a) Continuous combustion starting just after the onset of the hydrogen release above the SG of loop 2 and ending with the termination of hydrogen release 4000 seconds later. Thus, the duration of combustion was about 40 minutes. This calculation was performed for an additional 2000 seconds after combustion to allow for heat exchange between atmosphere and walls.

b) Instantaneous combustion 1500 seconds after the onset of the hydrogen release, corresponding to an accumulation of 520 kg hydrogen in the containment. The duration of global combustion was about 50 seconds, where 250 kg of hydrogen was burnt. After global combustion, the released hydrogen is continuously burnt as in case a) close to the source with no significant further energy input (combustion of only 30 kg hydrogen). This calculation was carried out for an additional 1300 seconds to allow for heat exchange to the walls as in case a).

In both cases the combustion as calculated with GASFLOW was incomplete (less than half of the released hydrogen was burnt).

Continuous Combustion:

The conditions in the containment above the SG compartment of loop 2 at the time of ignition are:

- Average atmospheric temperature: 64°C

- Pressure: 1.3 bar

- Amount of hydrogen: 91.2 kg

- Amount of hydrogen in the dome: 72.5 kg

- Average hydrogen concentration: 1.5% by volume

- Average hydrogen concentration in the dome: 2.9% by volume

- Average steam concentration in the 4% plume: 15% by volume

- Average steam concentration in the plume in the dome: 16% by volume

- Internal wall surface temperatures: 61 to 62°C

- Containment shell surface temperature: 60°C

The average hydrogen concentration in the dome at the time of ignition is well below the ignition limit. However, above the SG of loop 2 the local hydrogen concentration is 6.4%.

At the beginning of the combustion, the hydrogen release rate exceeds the hydrogen burning rate and therefore the amount of hydrogen present in the containment increases. The peak value of 200 kg is reached 800 seconds after ignition. This peak value can be compared with the total hydrogen release up to that time (760 kg) and with the amount of hydrogen present in the containment if hydrogen is removed by recombiners only (580 kg).

As a consequence of this incomplete combustion, the pressure and atmospheric temperature are far below AICC values. The maximum inner wall surface temperatures can be found close to the combustion area with a peak value of 240°C about 1500 seconds after ignition, which corresponds to an increase of 178°C. The maximum surface temperatures of the other inner walls are below 180°C.

The peak values for the containment shell surface temperatures are reached later, around 2200 seconds after ignition, with the highest value in the dome of 145°C corresponding to an increase of 85°C.

Instantaneous Combustion:

The conditions in the containment above the SG compartment of loop 2 at the time of ignition, about 1500 seconds after the start of hydrogen release, are:

- Average atmospheric temperature: 87°C

- Pressure: 1.48 bar

- Amount of hydrogen: 516 kg

- Amount of hydrogen in the dome: 250 kg

- Average hydrogen concentration: 7.8% by volume

- Average hydrogen concentration in the dome: 9.4% by volume

- Average steam concentration in the 4% plume: 16% by volume

- Average steam concentration in the plume in the dome: 17% by volume

- Internal wall surface temperatures: 61 to 67°C

- Containment shell surface temperatures: 61 to 64°C

Because of combustion, the pressure rises within 50 seconds to 2.2 bar and the average gas temperature increases to 290°C. This is well below the corresponding AICC values (4.1 bar and 770°C, respectively) and indicates that combustion is far from complete. The increase of both pressure and temperature occurs within 50 seconds, while the respective decline to the half value takes 150 seconds. At the end of the period under consideration the average gas temperature is 114°C.

Only 250 kg of hydrogen is burnt immediately, and another 56 kg is burnt slowly until the end of the period under consideration, 1300 seconds after ignition.

The maximum surface temperature of the inner walls is around 155°C, whereas the maximum containment surface temperature is around 82°C at half height and 140°C at the top of the containment. Thus, at around 20°C, the increase is rather low at half height, but may be as high as 80°C at the top of the dome.

2.3.3.5.2.2.   5 cm (20 cm2) SB(LOCA) in the Cold Leg with Partial Cooldown (With Consideration of Ex-Vessel Hydrogen) [Ref-1]

To conservatively address the ex-vessel hydrogen risk, a scenario was selected with

- minor Zr oxidation in the in-vessel phase (a large amount of Zr remains in the ex-vessel melt leading to fast early dissolution of the sacrificial concrete and to high release rates of hydrogen), and

- early vessel failure to reduce the time available for the recombination of in-vessel hydrogen

A 5 cm (20 cm^2) SB(LOCA) in the cold leg with only partial cooldown (p.c.) was assumed. This is a so-called "mixed release" scenario, which means that, in addition to the break, in-vessel hydrogen is also released from the relief tank by operator action (at the 650°C core outlet temperature signal) into the lower part of the containment following depressurisation.

Melt-concrete interaction and the corresponding hydrogen release has been calculated with the COSACO code (see Appendix 16A), which has been developed for the EPR core melt stabilisation system.

As the ex-vessel hydrogen is released mainly in two distinct phases at two different locations, the combustion calculation is subdivided into 2 calculations:

a) Temperature loads from hydrogen released in the reactor pit. This phase lasts about 30 minutes and about 200 kg of hydrogen are released.

b) Temperature loads from hydrogen released in the spreading compartment during the second phase (after gate failure) where about 230 kg of hydrogen are released. For this calculation it is assumed that no combustion occurs prior to gate failure, but that recombiners remain active. Recombiners can cope with the small amounts released between the two phases (release rate 39 g/s) and a "standing flame" is not thought to be stable during this long period of time because of the small release rate.

As hydrogen is released at a very high temperature, well above its auto-ignition temperature, for the calculation it is assumed that ignition occurs whenever the gas mixture is flammable. Despite the average steam concentration in the containment being relatively high, the steam is stratified to some extent and thus combustion is possible in the lower part of the containment. Combustion in the core catcher leads to the highest temperature loads. Consequently, combustion in the pit is not considered here.

The calculation of the combustion process in the core catcher is performed under the assumption that no combustion had occurred prior to gate failure. An initial combustion of 280 kg hydrogen (consisting of the initial release in the spreading compartment plus the remainder from the earlier release in the in-vessel phase, corresponding to the 2% lower limit reached by the recombiners in the cold state, see Sub-chapter 6.2 section 4.2.2.1) occurred, followed by continuous combustion of the hydrogen produced by melt-concrete interaction in the core catcher. The amount of hydrogen released in the core catcher is comparable to that released in the reactor pit, but the release duration is shorter and the connection to the upper part of the containment is better.

The maximum concrete temperature, which occurred in the spreading compartment, was 450°C at the end of the combustion period (which is just before the flooding of the melt). The maximum wall temperature for steel internals was reached earlier and was 520°C. The maximum surface temperature of the liner was 220°C, which dropped only slightly until the end of the calculation period. It is not expected that the maximum temperature of the containment shell significantly exceeds the calculated maximum liner temperature.

2.3.3.5.2.3.   5 cm (20 cm2) SB(LOCA) in the Cold Leg with Partial Cooldown and Delayed Depressurisation [Ref-1]

To find the bounding containment shell temperature, the SB(LOCA) cold leg scenario with partial cooldown (p.c.) and delayed depressurisation was calculated assuming continuous combustion. In total, about 640 kg of hydrogen were burnt.

Accidental ignition was assumed above the steam generator compartment of loop 2. Ignition started in a region above the loop 2 compartments and was allowed everywhere in the containment provided that the hydrogen mixture was flammable and the temperature was above 800 K (527°C). Due to the early ignition no fast combustion was expected.

The flame propagates downwards, burning the hydrogen just after its release from the RCP [RCS] close to the break and the PRT release location. In this phase the temperature increase on the containment shell is only caused by the hot gases rising from the break location. Hot gases from combustion in the equipment rooms reach the dome only via the SG towers. These hot gases mix with those from combustion in the dome itself (which is most violent above the SG tower) and lead to high rates of heat transfer to the ceiling in some places.

The initial conditions at the moment of ignition are as follows:

- Time since start of the accident: 7840 seconds

- Time since start of hydrogen release: 40 seconds

- Accumulated amount of hydrogen in the containment: 19 kg

- Accumulated amount of hydrogen in the dome: 9 kg

- Pressure in the containment: 2.2 bar

- Hydrogen cloud above 4% by volume: 70 m^3

- Average gas temperature in the containment: 110°C

- Average gas temperature in the hydrogen cloud: 200°C

- Initial containment shell surface temperature (hot spot):   101°C

- Average hydrogen concentration in the 4% plume: 6% by volume

- Average steam concentration in the 4% plume: 65% by volume

Hydrogen release rate:

- Through the break: < 0.05 kg/s

- Through the relief tank: 0.9 kg/s

Steam release rate:

- Through the break: 10 kg/s

- Through the relief tank: 57 kg/s

At the time of maximum ceiling temperature (8025 seconds), the containment pressure peaked at 3.9 bar. The maximum average containment atmospheric temperature was 330°C.

An amount of 566 kg hydrogen was burnt within 175 seconds (3 minutes) up to the time of maximum hot spot temperature. At the end of the calculation at 8500 seconds, 640 kg hydrogen was burnt, corresponding to 76% of the released hydrogen. Thus, more than twice as much hydrogen was burnt as in the SB(LOCA) case without delayed depressurisation.

As expected, the highest containment shell temperatures occurred at the ceiling of the containment above the loop 2 compartments. Peak temperatures were around 320°C and occurred at the same time as the maximum gas temperature around 7975 seconds. These surface temperatures drop continuously towards 220°C at the end of the calculation (8500 seconds).

The containment shell surface temperature for the vertical wall was significantly lower, declining from top to bottom.

At high elevations above 45 m, peak temperatures were around 136°C at 8220 seconds. The temperatures decrease slowly to about 131°C at the end of the calculation (8,500 seconds).

At lower elevations the temperatures were below 122°C at all times during combustion. Thus for the material hatch no temperature above 122°C can be expected for this extremely challenging scenario.

The temperatures mentioned above are surface temperatures. Inside the containment shell the temperatures decrease within 25 cm towards the steady state temperature that existed before the hydrogen combustion event.

High temperatures were spatially limited to a hot spot above the SG compartments on the side where combustion started and lasted only a few hundred seconds. Sub-section 16.2.2.3 - Figure 13 shows the time histories of the ceiling temperature at different locations.

2.3.4. Conclusions from the Verification Process

The EPR CGCS has been evaluated in a consistent manner utilising state-of-the-art CFD codes, using an adequate nodalisation scheme, and taking into account current knowledge on combustion behaviour, such as criteria for the non-occurrence of flame acceleration and DDT. A summary of corresponding current and future research and development work is presented in [Ref-1].

Several representative and bounding scenarios have been specified to justify the EPR CGCS.

The major findings are as follows:

- Average hydrogen concentration does not exceed 10% by volume for any scenario.

- AICC pressure is at no time > 5.5 bar for representative scenarios.

- AICC pressure can reach 6.3 bar for a bounding scenario. The realistic pressure is much lower because combustion is neither complete (hydrogen concentration too low) nor adiabatic (relatively slow combustion).

- Recombination rate of hydrogen is several hundred kg/hour. This is sufficient to ensure that hydrogen removal is sufficiently advanced when spraying might be required (12 hours).

- Temperature loads on the containment shell resulting from recombination are below 120°C.

- Temperature loads on the containment shell are below 170°C for representative scenarios when considering combustion of in-vessel generated hydrogen. Ex-vessel generated hydrogen may lead to containment shell temperature of at most 220°C due to continuous combustion (standing flame). These temperatures are reached in the dome only.

- Peak temperature on the containment shell from combustion is around 300°C for bounding scenarios (SB(LOCA) with delayed depressurisation, steel liner explicitly modelled). However, this peak temperature is only reached in the dome and involves only an area of around 10 m^2.

- Combustion temperatures are considerably lower in the cylindrical part of the containment where the penetrations for ducts, material hatch and personnel airlock are located.

- Dynamic loads on the containment shell are benign. Pressurisation is bounded by AICC pressure. Although the flame accelerates in the SG tower, it decelerates in the dome, which results in small dynamic loads on the containment shell.

There seems to be no restriction for the activation of the spray system with regard to hydrogen risk. The positive effect of mixing the atmosphere by the spray system compensates the negative effect of increasing the relative hydrogen concentration due to steam condensation.

SUB-SECTION 16.2.2.3 - TABLE 1

Scenarios analysed for pressure and thermal loadings

Scenario	AICC	Laminar combustion pressure	Dynamic pressure from fast deflagration	Combustion of ex-vessel hydrogen	Thermal loads from recombination	Thermal loads from combustion
LOOP with reflood					x	
5 cm (20 cm^2) SB(LOCA) cold leg f.s.c.	x	x	x		x	x
5 cm (20 cm^2) SB(LOCA) hot leg f.s.c.	x					
7.5 cm (46 cm^2) SB(LOCA) pressuriser f.s.c.	x		x			
5 cm (20 cm^2) SB(LOCA) cold leg p.c.	x	x		x		x
5 cm (20 cm^2) SB(LOCA) cold leg f.s.c. with reflood	x		x		x	
5 cm (20 cm^2) SB(LOCA) cold leg p.c. with delayed depressurisation	x	x	x		x	x

(p.c.: partial cooldown, f.s.c.: fast secondary cooldown; shaded rows: bounding scenarios)

SUB-SECTION 16.2.2.3 - TABLE 2

Hydrogen distribution [Ref-1]

Scenario	Maximum mass of H_2 present in the contain-ment (kg)	Maximum average H_2 concentra-tion (% by volume)	Maximum size of the 4% H_2 plume (m³)	Time when 4% plume reaches maximum after start of H_2 release (s)	Maximum size of the 13% H_2 plume (m³)	Time when 13% plume reaches maximum after start of H_2 release (s)
5 cm (20 cm²) SB(LOCA) cold leg p.c.	500	5	80000	2000	210	1000
5 cm (20 cm²) SB(LOCA) hot leg f.s.c.	450	5.5	60000	2500	1000	100
7.5 cm (46 cm²) SB(LOCA) pressuriser f.s.c.	580	7	52000	3200	20000	1500
5 cm (20 cm²) SB(LOCA) cold leg f.s.c.	580	8	74000	3500	9500	1500
5 cm (20 cm²) SB(LOCA) cold leg f.s.c. with reflood	860	9.5	75000	2000	20000	1500
5 cm (20 cm²) SB(LOCA) p.c. cold leg with delayed depressurisation	800	7	75000	600	5000	200

(p.c.: partial cooldown, f.s.c.: fast secondary cooldown; shaded rows: bounding scenarios)

UK EPR

PRE-CONSTRUCTION SAFETY REPORT

CHAPTER 16: RISK REDUCTION AND SEVERE
ACCIDENT ANALYSES

SUB-CHAPTER : 16.2

PAGE   : 120 / 295

Document ID.No.
UKEPR-0002-162 Issue 05

SUB-SECTION 16.2.2.3 - TABLE 3

Hydrogen release and temperature for various scenarios

Scenario	Mass of hydrogen released	Major finding
LOOP with reflood	1000 kg	Wall temperature: 89°C to 121°C Gas temperature in the dome around 200°C
5 cm (20 cm^2) SB(LOCA) cold leg f.s.c.	760 kg	Wall temperature: 66°C to 90°C Gas temperature in the dome around 185°C
5 cm (20 cm^2) SB(LOCA) cold leg f.s.c. with reflood	920 kg	Wall temperature > 100°C
5 cm (20 cm^2) SB(LOCA) p.c. with delayed depressurisation	850 kg up to core quenching	Wall temperature < 121°C

(p.c.: partial cooldown, f.s.c.: fast secondary cooldown; shaded rows: bounding scenarios)

SUB-SECTION 16.2.2.3 - FIGURE 1

History of accumulated mass, depleted mass and present mass of hydrogen in the containment for a 5 cm (20 cm^2) SB(LOCA) cold leg f.s.c. [Ref-1]
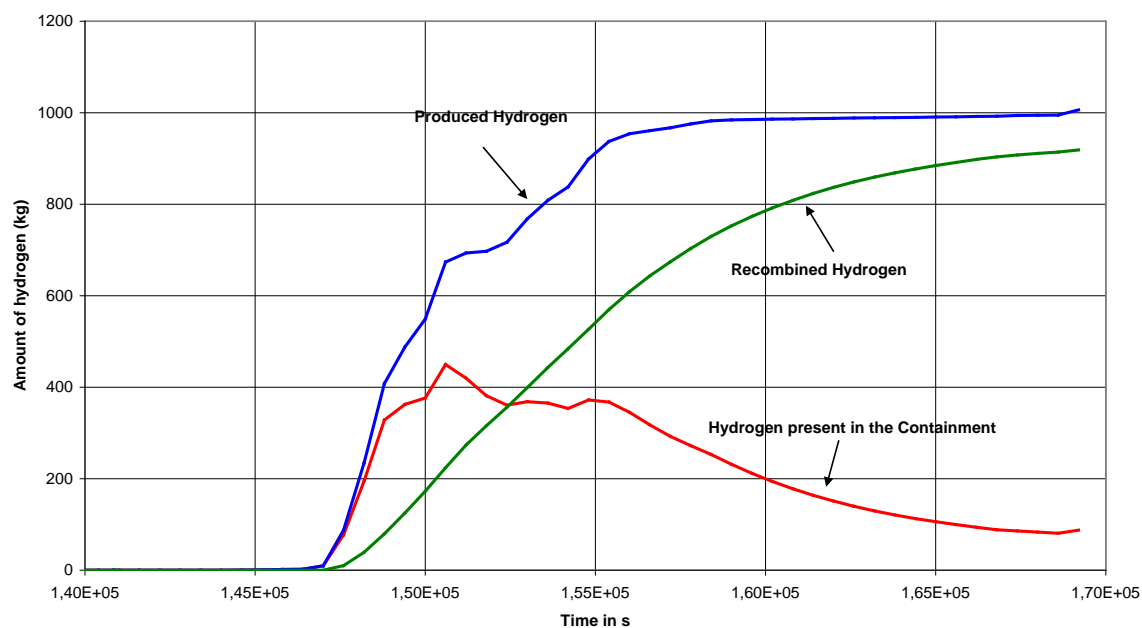
SUB-SECTION 16.2.2.3 - FIGURE 2

History of AICC pressure and expected combustion pressure for various scenarios [Ref-1]
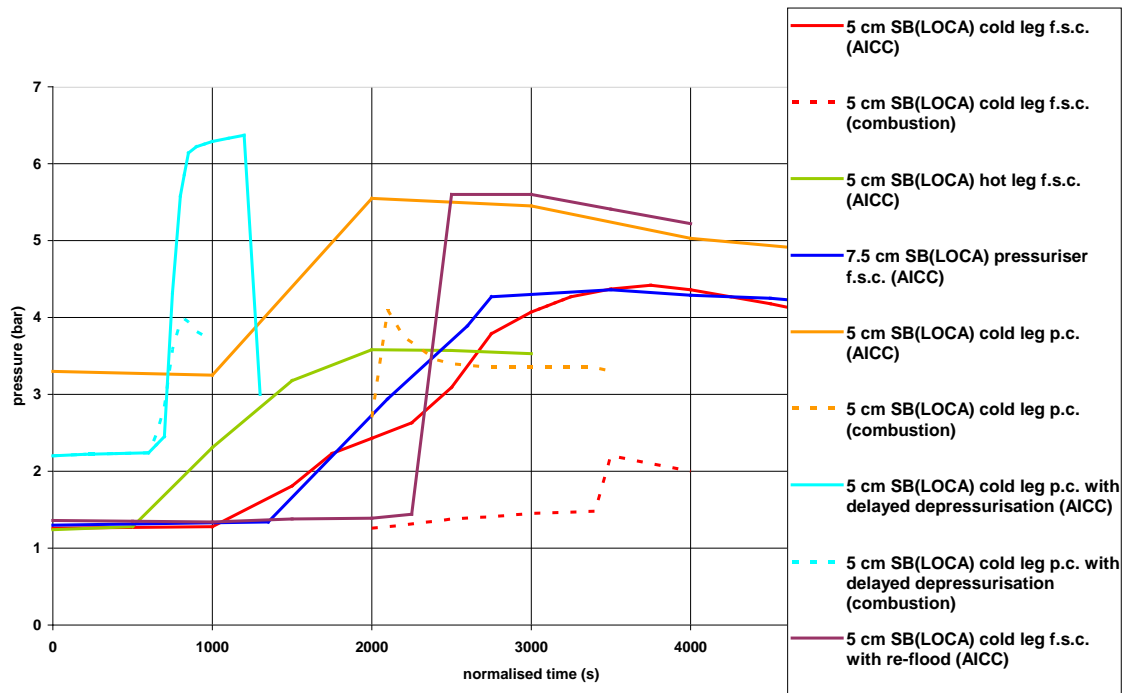
SUB-SECTION 16.2.2.3 - FIGURE 3

Region of sigma index > 1 at elevation of the break for a 7.5 cm (46 cm^2) SB(LOCA) pressuriser f.s.c. at various times [Ref-1]
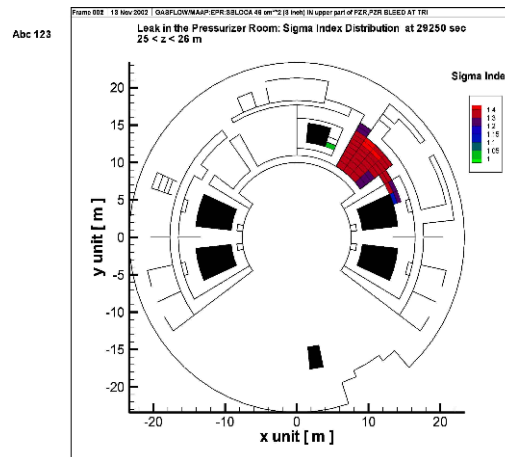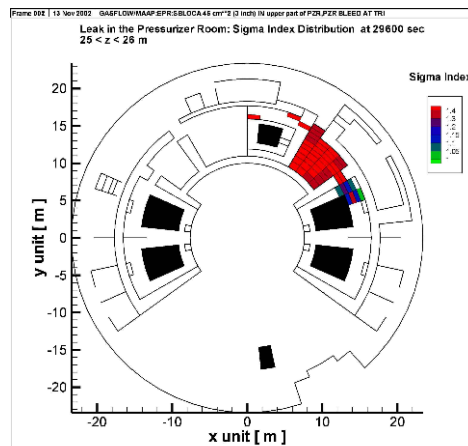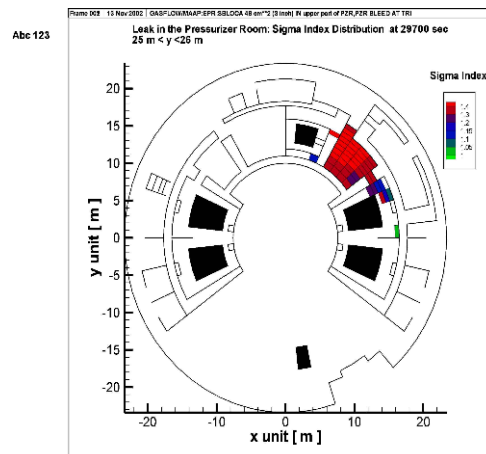
(a) 29250 s

(b) 29600 s

(c) 29700 s

SUB-SECTION 16.2.2.3 - FIGURE 4

Region of sigma index > 1 at the top of the containment for a 7.5 cm (46 cm^2) SB(LOCA) pressuriser f.s.c. at various times [Ref-1]
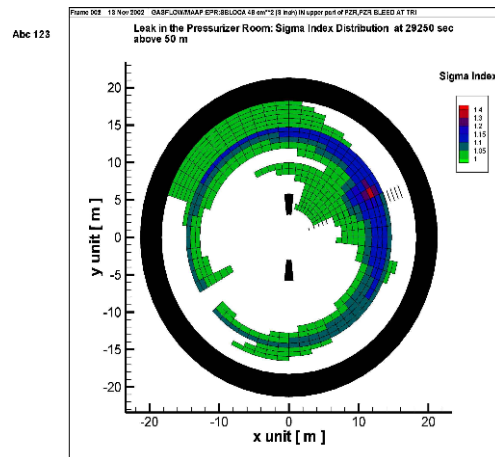
(a) 29250 s
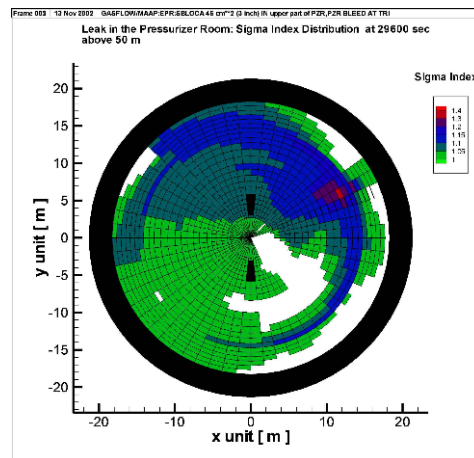
(b) 29600 s
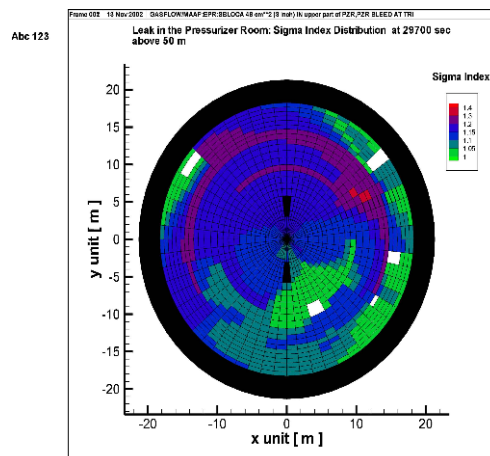
(c) 29700 s

SUB-SECTION 16.2.2.3 - FIGURE 5

Region of sigma index > 1 at elevation 14.1 to 14.7 m for a 5 cm (20 cm^2) SB(LOCA) cold leg f.s.c. with re-flood at various times [Ref-1]
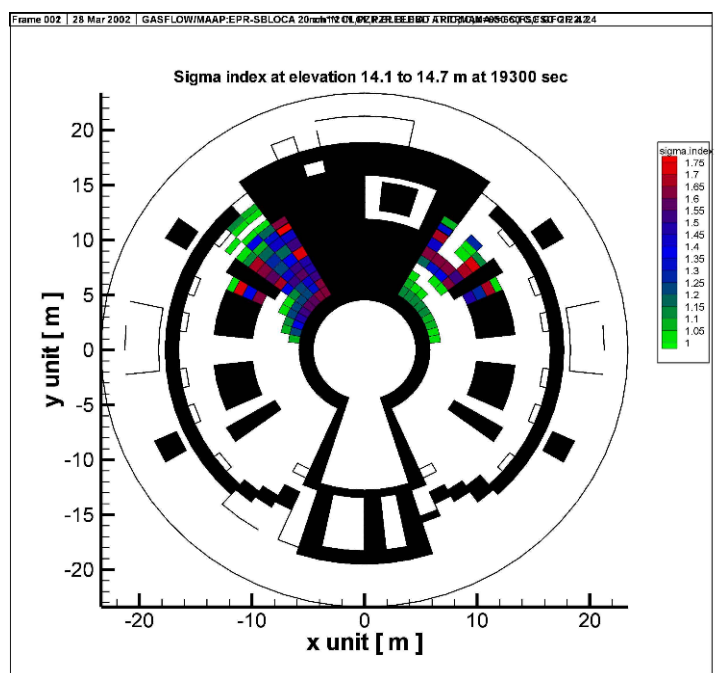
a) 19300 s corresponding to 25.33 h accident time
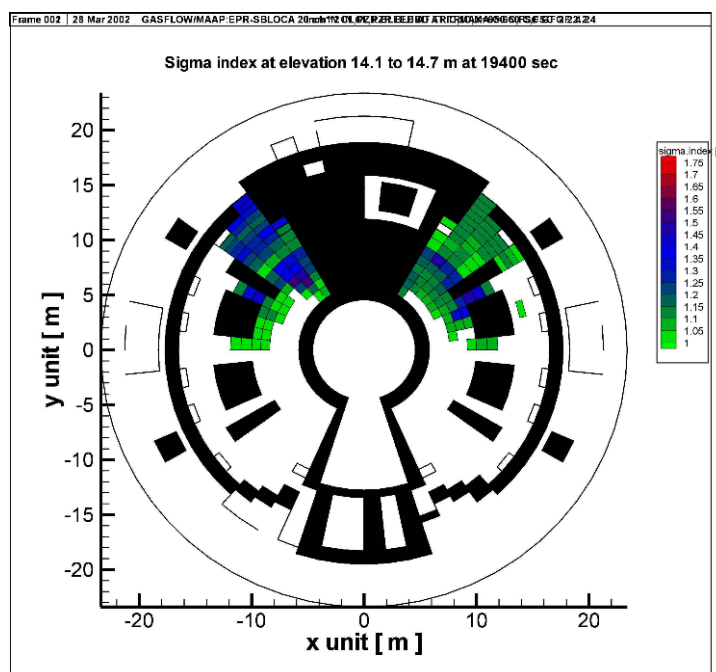
b) 19400 s corresponding to 25.36 h accident time

SUB-SECTION 16.2.2.3 - FIGURE 6

Region of sigma index > 1 at elevation 37.2 to 39.7 m for a 5 cm (20 cm^2) SB(LOCA) cold leg f.s.c. with re-flood at various times [Ref-1]
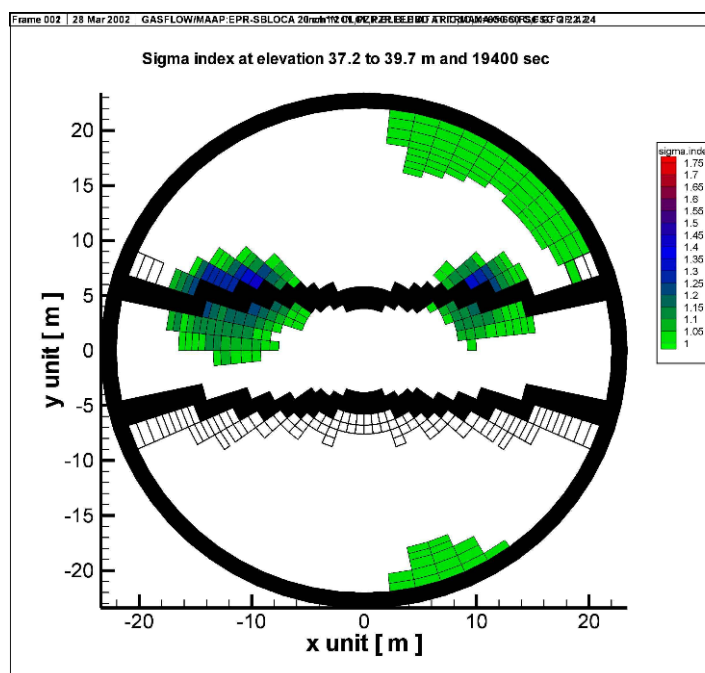
a) 19400 s corresponding to 25.36 h accident time
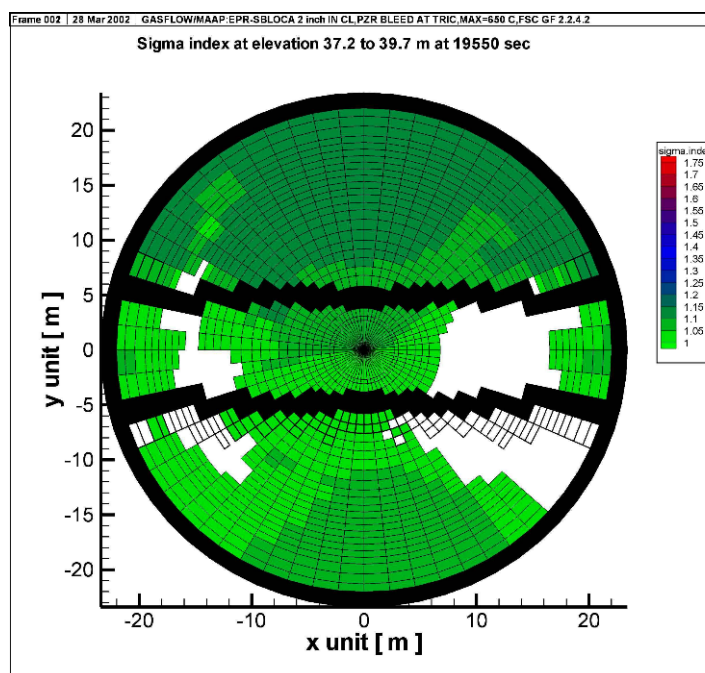
b) 19550 s corresponding to 24.4 h accident time

SUB-SECTION 16.2.2.3 - FIGURE 7

Region of sigma index > 1 at elevation 46.8 to 49.2 m for a 5 cm (20 cm^2) SB(LOCA) cold leg f.s.c. with re-flood at various times [Ref-1]
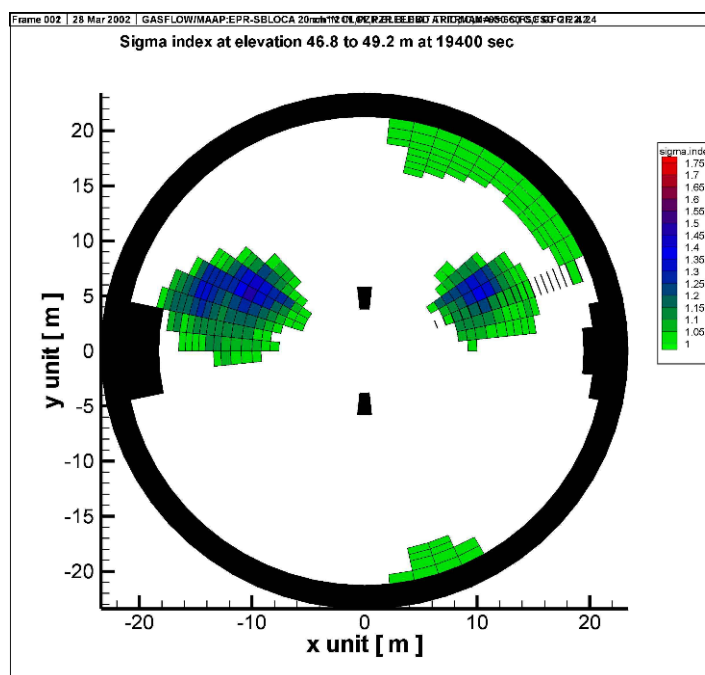
a) t=19400 s corresponding to 25.36 h accident time
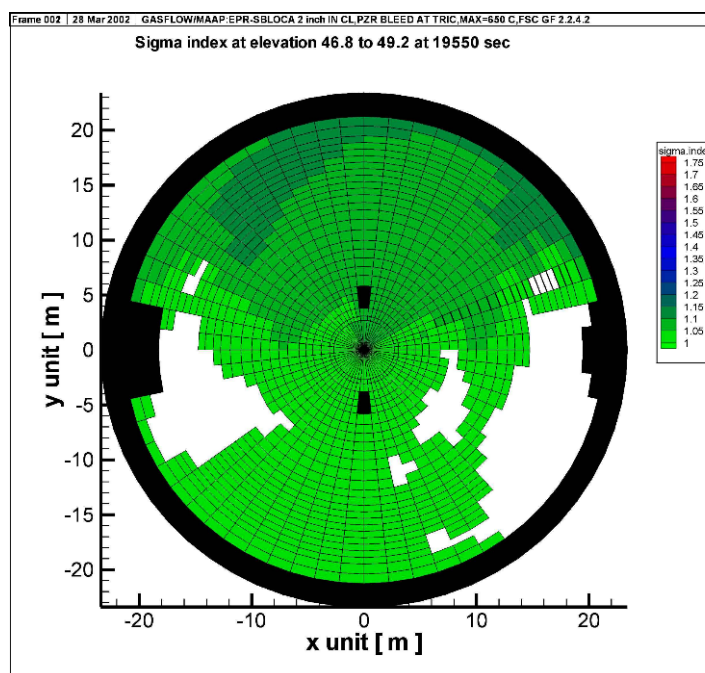
b) t=19550 s corresponding to 25.4 h accident time

SUB-SECTION 16.2.2.3 - FIGURE 8

Hydrogen and steam concentration history for a 5 cm (20 cm^2) SB(LOCA) cold leg p.c. with delayed depressurisation, with and without spraying after 8000 s [Ref-1]
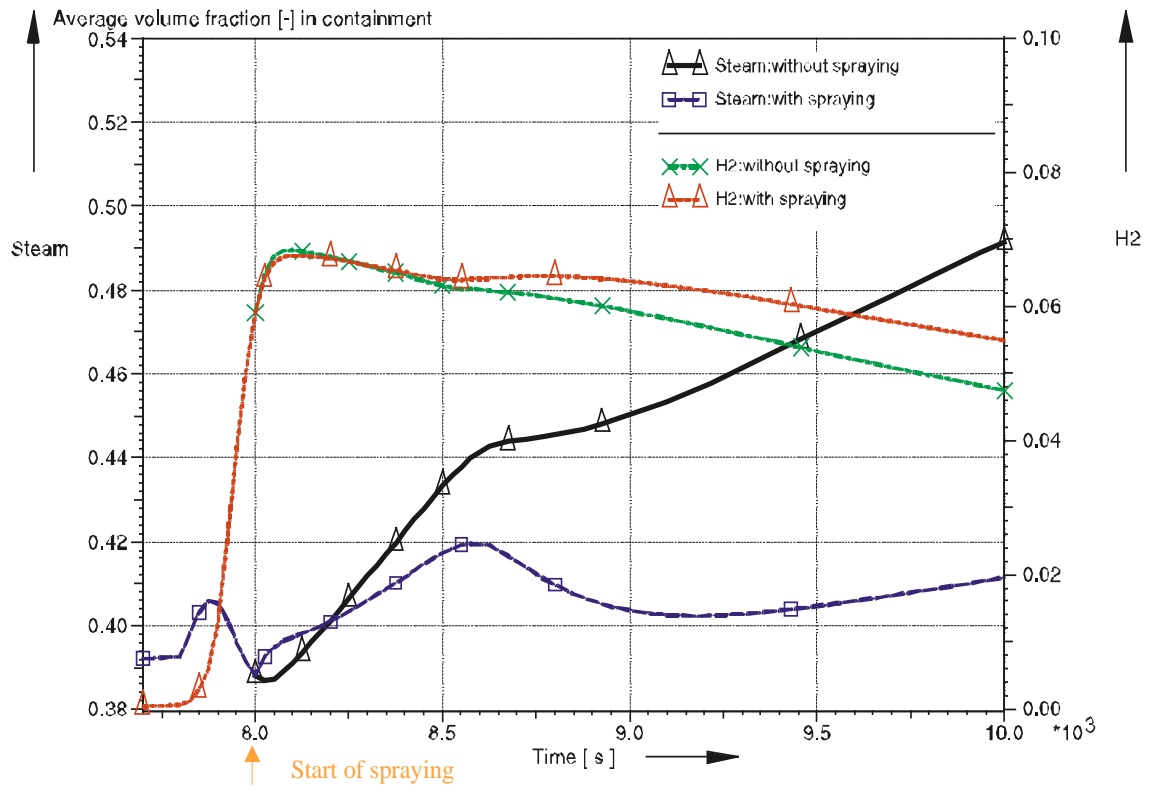
SUB-SECTION 16.2.2.3 - FIGURE 9

History of plume volume with sigma index > 1 for a 5 cm (20 cm^2) SB(LOCA) cold leg p.c. with delayed depressurisation, with and without spraying after 8000 s [Ref-1]
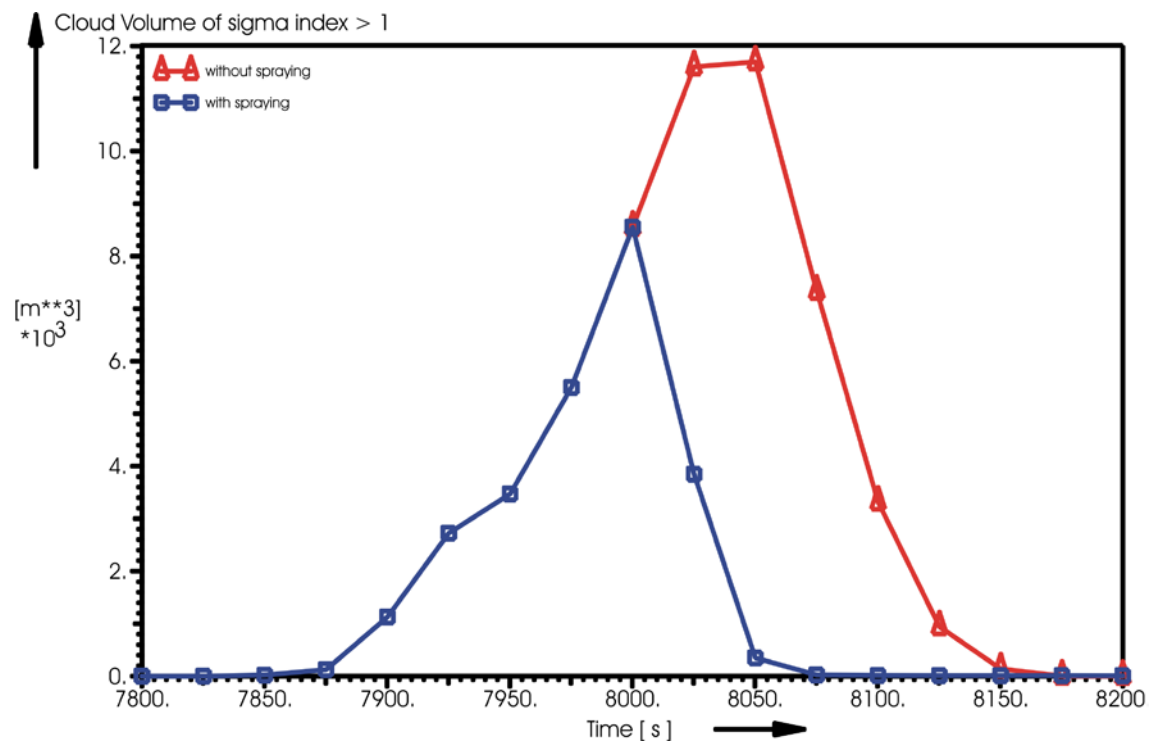
SUB-SECTION 16.2.2.3 - FIGURE 10

Pressure history (in Pa) for a 5 cm (20 cm^2) SB(LOCA) cold leg f.s.c. at two opposite locations at the top of the cylindrical containment part [Ref-1]

Time, s
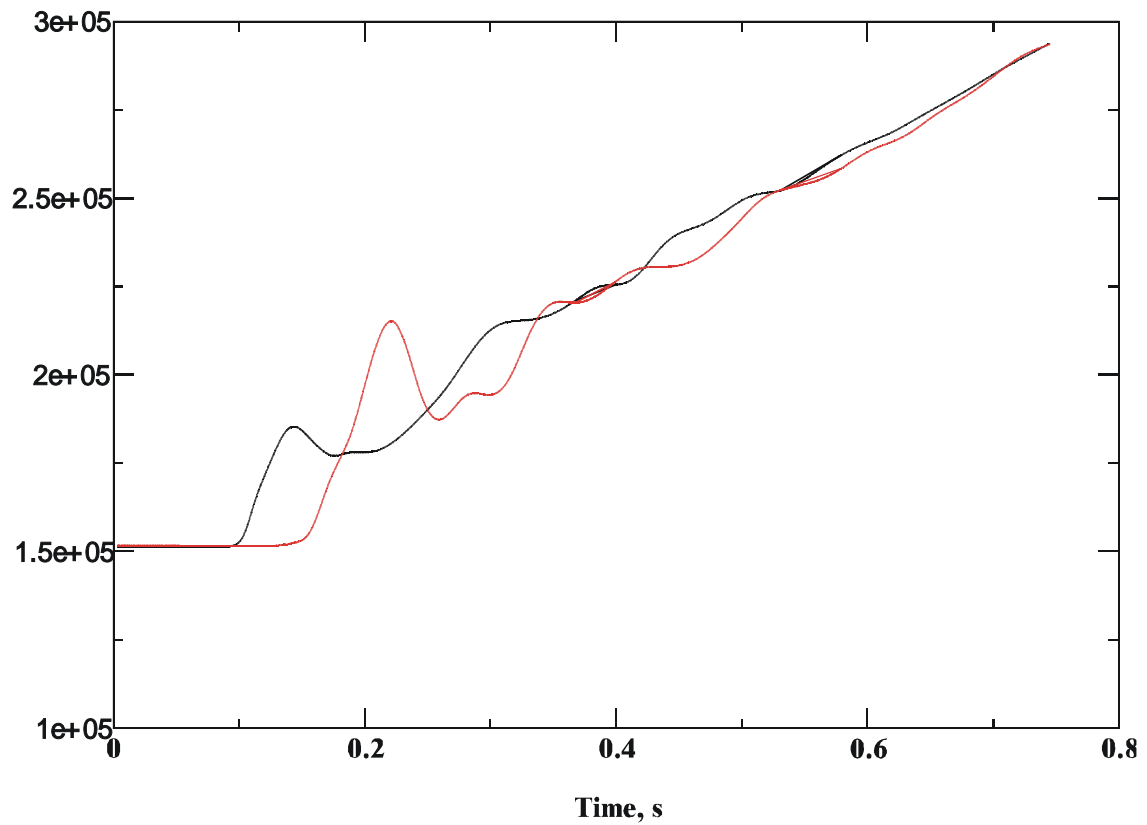
SUB-SECTION 16.2.2.3 - FIGURE 11

Pressure history for a 5 cm (20 cm^2) SB(LOCA) cold leg f.s.c. with re-flood at different locations on the SG compartment inner wall, in the upper pump room and in the annular room, with ignition in the pump room [Ref-1]

UK EPR

PRE-CONSTRUCTION SAFETY REPORT

CHAPTER 16: RISK REDUCTION AND SEVERE
ACCIDENT ANALYSES

SUB-CHAPTER : 16.2

PAGE : 132 / 295

Document ID.No.
UKEPR-0002-162 Issue 05
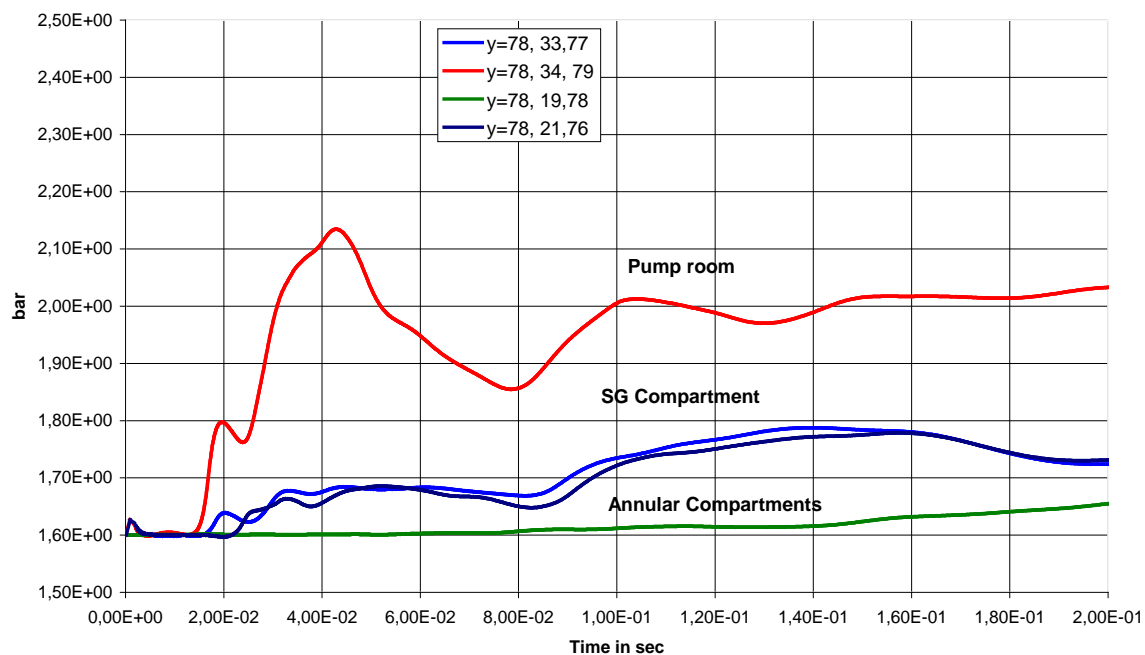
SUB-SECTION 16.2.2.3 - FIGURE 12

Containment shell temperature history for a 5 cm (20 cm^2) SB(LOCA) cold leg f.s.c. at various locations at the top of the cylindrical containment part [Ref-1]
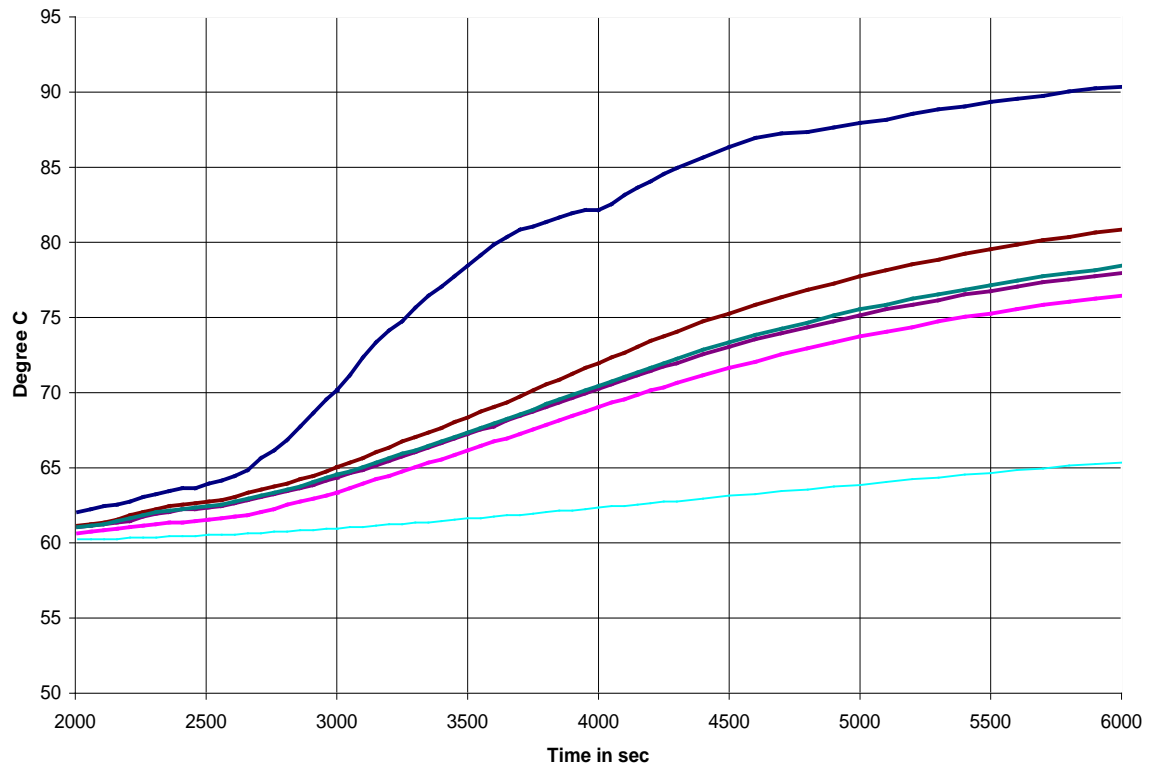
SUB-SECTION 16.2.2.3 - FIGURE 13

Wall surface temperature history for a 5 cm (20 cm^2) SB(LOCA) cold leg p.c. with delayed depressurisation at various locations of the containment inner surface, with continuous combustion [Ref-1]
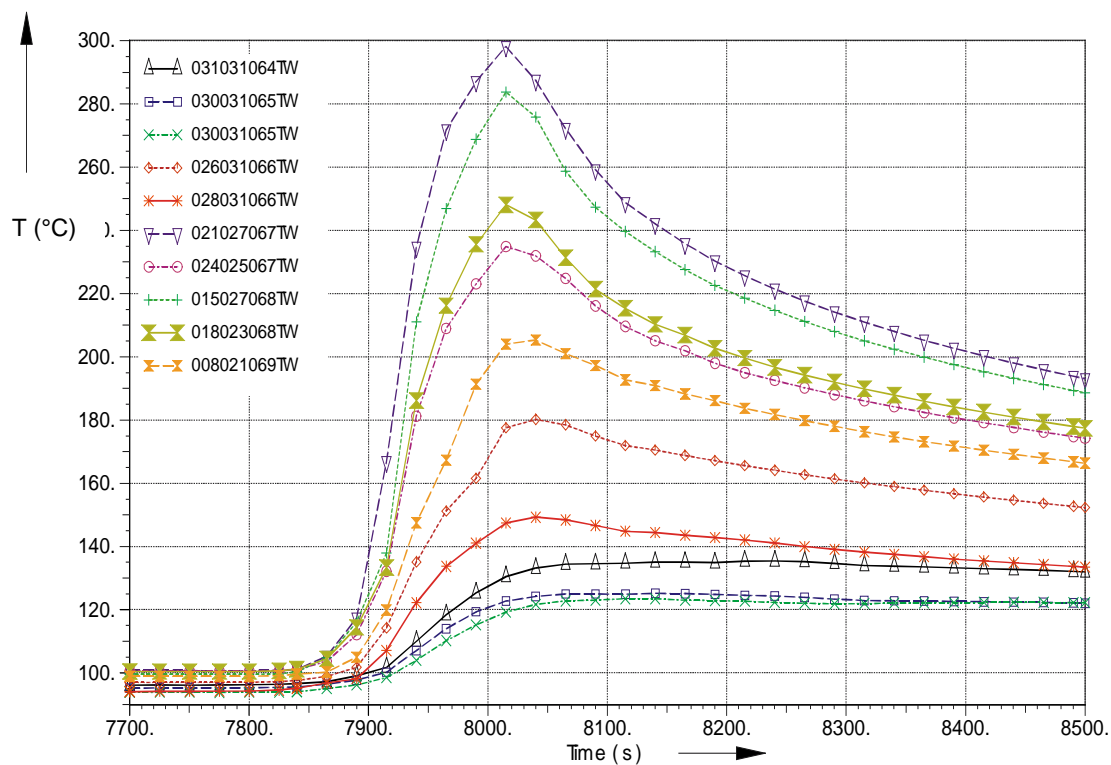
2.4. ASSESSMENT OF MELT STABILISATION

2.4.1. Basic strategy

Due to the high projected power rating of the EPR and the related low margins, In-Vessel melt Retention (IVR) by outside cooling of the Reactor Pressure Vessel (RPV) has been dismissed from the beginning. Instead, an ex-vessel Core Melt Stabilisation System (CMSS) is being implemented. Its function is based on the spreading of the melt onto the surface of a water-cooled metallic and concrete core catcher, followed by subsequent quenching with water drained passively from the In-containment Refuelling Water Storage Tank (IRWST). The efficiency of the stabilisation process strongly benefits from the achieved increase in the surface-to-volume ratio of the melt [Ref-1].

The core catcher is located in a dedicated compartment adjacent to the pit. Under normal operating conditions the connection between pit and spreading compartment is closed. In the case of a severe accident it will be opened by the thermal destruction of a separating plug by the core melt. Thanks to the spatial separation between pit and spreading compartment, the core-catcher is safe from potentially critical loads related to the failure of the RPV. Furthermore, unintentional flooding of the core catcher during power operation is not critical to the safety of the plant. As a consequence of this decoupling, power operation and design-basis mitigation measures remain unaffected by the existence of the core catcher.

The relocation of the melt from the pit into the core catcher is preceded by a phase of temporary retention in the reactor pit. This measure allows for the likelihood that the release of the molten material from the RPV will not take place in one pour, but in stages. Temporary retention is based on the provision of a layer of sacrificial concrete that must be penetrated by the melt prior to its release from the pit. The resulting delay and the admixture of sacrificial concrete make the characteristics of the melt during relocation and subsequent spreading and stabilisation predictable and independent of the inherent uncertainties associated with in-vessel melt pool formation and RPV failure.

Melt arrival in the core catcher initiates the gravity-driven overflow of water from the IRWST which cools the core catcher from the outside and brings the melt into a stable state by means of passive systems only. As an option, the Containment Heat Removal System (EVU [CHRS]) can be used to provide water to the core catcher actively. This will completely submerge the spreading compartment and the reactor pit and stop further steam discharge into the containment as a pre-condition for reaching atmospheric pressure conditions in the long-term without the need for a venting system.

The provision of the CMSS avoids the interaction of the molten core with the structural concrete and with it the risk of:

(i) penetrating the embedded liner,

(ii) weakening and mechanically deforming load-bearing structures and the basemat itself, and

(iii) sustained release of non-condensable gas into the containment atmosphere.

The melt stabilisation process involves the following stages, (see Sub-section 16.2.2.4 – Figure 1):

- The failure of the RPV and the subsequent release of the molten core

- The temporary retention of the released material in the pit

- The opening of the gate and the relocation of the accumulated melt

- The passive flooding and quenching of the melt in the spreading compartment

- Long term cooling and heat removal

During this sequence, a transformation of the molten corium into a coolable and cooled configuration is achieved on the basis of simple physics and without requiring further operator action or the use of internal or external active systems. The above-listed stages of the CMSS are described in detail in the following sections.

2.4.1.1. Assessment of the general robustness of the concept

2.4.1.1.1. Tolerance to melt release conditions from the RPV

In a postulated severe accident, the initial conditions of the melt release from the RPV are determined by the preceding scenario, by the course of in-vessel core degradation, relocation and quenching, and finally by the failure sequence of the lower head. All these processes involve a significant degree of uncertainty.

To make the EPR CMSS tolerant to these uncertainties, the design allows for an initial phase of temporary melt retention and accumulation in the reactor pit. This strategy, which incorporates a sacrificial concrete layer has a favourable, self-adjusting characteristic, which is based on the fact that a well-defined amount of energy is needed to melt and incorporate a concrete-layer of given type and thickness.

As this energy must come from the decay heat produced within the released melt, a postulated lower initial release fraction, or a later time of release at correspondingly lower decay power level, will result in longer retention times in the pit and thus also compensate for the longer period of melt release from the RPV under these conditions.

The sensitivity to the conditions of the initial melt release from the RPV is further reduced by the fact that the lower RPV is not only heated from the inside by the residual core debris in the lower head, but also from the outside by thermal radiation from the released melt.

In the pit, the interaction of the melt with the concrete results in vigorous gas production and intense gas-induced mixing. This favours an isotropic heat flux distribution inside the Molten Core Concrete Interaction (MCCI) pool and adjusts the heat flux radiated off the pool surface relative to that carried into the surrounding concrete. Consequently, the heat-up of the RPV lower head is coupled to the progression of the melt front into the sacrificial concrete in such a way that, for all relevant scenarios, the lower RPV will be thermally destroyed before the concrete above the gate is ablated [Ref-1].

The total amount of sacrificial concrete ablated during the retention period is limited and largely determined by the position of the surrounding refractory layer. As the amount of concrete in the molten corium determines the properties of the melt, these properties - including temperature and mass - become adjusted into narrow, well-defined ranges at the end of the retention period.

Therefore, the addition of sacrificial concrete not only results in the inclusion of most of the core inventory into the molten pool prior to the release of the melt from the pit, but also leads to an equalisation of the spectrum of possible melt states. In consequence, all subsequent stabilisation measures become widely independent of the inherent uncertainties related to the melt release conditions from the vessel.

2.4.1.1.2. Tolerance to loads during RPV failure

The core catcher is located in a dedicated compartment adjacent to the pit. The connection between pit and spreading compartment is normally closed and will only be opened by the melt in case of a severe accident. Due to this separation, the core-catcher in the spreading room is safe from potentially critical loads related to the failure of the RPV.

The design element that provides this functional separation is the melt plug at the bottom of the pit. This plug closes the entrance of the transfer channel and avoids an early release of melt before the end of the accumulation process as described in the previous section. The function of the melt plug must not be endangered by loads potentially connected with the failure of the RPV for any relevant scenario.

The design of the CMSS is based on the assumption that after primary depressurisation and after reaching a non-coolable melt state, there will be no late active injection of water into the primary circuit. As a consequence, the RPV will fail under dry conditions at an internal overpressure significantly below 5 bar, which strongly reduces the loads on the surrounding structures.

Higher RPV failure pressures are only possible following a postulated late active injection. In such cases, the open depressurisation valve will limit the pressure in the primary circuit to values below 20 bar at the time of RPV melt-through. To demonstrate that the melt stabilisation function is invulnerable against late re-flood scenarios it has to be shown that RPV melt through at this pressure level does not lead to fatal consequences caused by pressure build up in the pit, mechanical impact of the detaching lower head, erosive effects of the outflowing melt or melt dispersal. These phenomena are discussed in turn.

Pressure build-up in the pit

As an upper-limit decoupling value for the pressure in the pit following RPV failure in case of late re-flood, a quasi-static internal pressure of 20 bar has been adopted. This corresponds to the predicted maximum pressure inside the primary circuit at the time of vessel failure (see section 2.2 above). Since RPV failure leads to an increase in volume, the pressure after expansion will be correspondingly reduced, which justifies the conservatism of the chosen value.

To achieve a sufficient load-carrying capacity, the surrounding walls and the melt plug have been provided with an adequate reinforcement. The melt plug is further provided with a steel frame, which transfers the pressure forces into the structural concrete.

Mechanical impact of the detaching lower head

According to the results of related experiments, e.g. in the framework of the MVI-project [Ref-1], the most likely initial failure position of the RPV under the conditions of elevated internal pressure is located in the upper region of the melt, where heat fluxes are highest. Due to unavoidable asymmetries in the heat-up process, a local failure appears likely. Nevertheless, it cannot be excluded that the entire lower head will detach from the residual RPV at once. This results in upward-directed forces on the RPV support and downward-directed forces on the concrete bottom.

To avoid a direct mechanical impact of the accelerated lower head on the melt plug, concrete blocks are provided around the centre of the bottom of the pit. Besides absorbing the related impact loads, these blocks also limit the maximum distance the lower head can fall, which shortens the time for preceding acceleration by gravity and internal pressure. Consequently, its kinetic energy is reduced to a value low enough to be absorbed by the concrete blocks and the underlying structural concrete.

Erosive effect of the out-flowing melt

If the RPV fails under elevated internal pressure, melt can be pushed out of the leak and hit the surface of the surrounding concrete. The expected size of the initial leak in the RPV is determined by the preceding thermal history. In the case of a molten pool in the lower head, the highest heat fluxes into the RPV will occur near the top of the melt, near the interface between the metal and oxide layer. A failure in this region will result from local melt-through. Melt ejection through such a lateral hole is characterised by:

- A limited amount of released melt (because the leak is near the surface)

- A short duration of the release

- A non-focussed, dispersed flow field

This kind of melt jet cannot cause any significant erosion at the adjacent concrete walls. In addition, erosion of the sacrificial concrete at any location other than the melt plug would not impede the retention function of the pit, thanks to the back-up provided by the protective layer.

Compared to this, jets exiting through the bottom of the lower head could potentially be more critical because of their possible impact on the melt plug. However, the EPR does not have pre-existing penetrations in the bottom that could create a focused, long lasting jet. In addition, the released melt would accumulate on top of the melt plug, which is at the lowest position in the pit, and increasingly absorb and dilute any further impact.

For gravity-driven melt pours, the erosive effect on concrete was experimentally observed to be negligible, e.g. in the COMET experiments [Ref-2], for oxidic and even superheated metallic melt. This is attributed to the fact that the decomposition of concrete creates large amounts of gas, which counteracts the flow of melt and creates a protective cushion at the impact location.

Melt dispersal

Melt dispersal occurs during the interaction between released melt and the flow of gas and steam. Very small particles can be created, which can be carried into the containment. The extent of melt dispersal during vessel failure at elevated internal pressures of < 20 bar has been investigated experimentally in the DISCO program at Research Centre Karlsruhe [Ref-3] using a scaled-down EPR-type pit geometry. The tests were performed for hypothetical central or lateral holes in the RPV lower head, as well as for a hypothetical "unzipping" of the lower head. The DISCO results yield information on the flow regime and the extent of melt dispersal for the investigated configurations, and complement those obtained in the Lower Head Failure (LHF) experimental program at Sandia National Laboratory [Ref-4] and in the FOREVER tests performed by RIT [Ref-5] [Ref-6].

The DISCO tests showed that for lateral holes, seen as the most likely failure location in the RPV, a considerable reduction of the dispersal rate was found as compared to central holes. Large differences were observed between the results with different corium simulants.

The amount of dispersed material was found to be strongly dependent on the failure mode and failure location of the RPV. The influence of the driving pressure is smaller but varies considerably with failure mode and location. For central holes in the bottom of the lower head, the driving pressure and the size of the hole have significant influence on the dispersed amount, while for lateral holes, slot type openings or in case of a complete unzipping of the RPV lower head, this influence remains low.

The hot DISCO tests with Al-Fe-thermite melts, which were closest to the prototypic situation among the tests performed, demonstrate that the dispersed melt fraction is generally low and deposited predominantly within neighbouring lateral compartments, while practically no melt is carried into the containment dome. Based on the experimental results and the codes and correlations developed from them, the melt fraction that is dispersed and carried into the containment is predicted to be < 5%. This low value for the EPR design results from the absence of a direct path from the pit to the containment dome. Gas discharge is limited by the narrow circumferential gap around the RPV through which the gas has to pass before leaving the pit.

To assess the heat transport to the containment atmosphere, a bounding dispersed melt fraction of ~10% of the initial total corium mass was conservatively assumed. Even for this conservative assumption, the increase in containment pressure caused by the combined effect of heat transfer and hydrogen combustion remains below 1 bar. Because the dispersed material is finely fragmented, it can be assumed to be coolable and cooled after deposition in local sumps.

2.4.1.1.3. Tolerance to a postulated late re-flood

The design basis of the EPR CMSS involves the assumption that, after primary depressurisation and after reaching a non-coolable melt state in the lower head, there will be no late active injection of water into the RPV. Consequently, it is assumed that the RPV fails under dry conditions and that there is no later addition of water on top of the MCCI-pool.

Nevertheless, it is required that a postulated late active injection at any time must not lead to a failure of the melt stabilisation function, which is discussed below.

Water injection before initial RPV failure

Here, cases only need to be considered for which, according to the definition of a "late" re-flood, a non-coolable molten pool has formed in the lower head. In this situation, a second molten pool can also be present on top of the lower support plate. However, because of the preceding relocation of the melt into the lower head, either the heavy reflector, or the lower support plate can be assumed to be already penetrated by the melt.

This only allows the presence of a shallow melt pool on top of the lower support plate, which can be quenched and cooled by the added water. The intense steam production during flooding of the hot degraded core results in an increase in the pressure in the primary circuit, which is limited by the flow through the open depressurisation valves. Analysis has shown that this release will keep the primary pressure at the time of RPV melt-through below 20 bar.

The contact of the molten pool with the lower head will finally lead to RPV failure, which will release that part of the molten core above the failure into the pit. The melt release will be followed by water, leading to the situation of a flooded MCCI pool in the pit.

Water injection after initial RPV failure

Due to the preceding failure of the RPV lower head, the added water can fill the entire pit region and cool the RPV from the outside. In addition, because the enclosures, formed by the lower head and by the heavy reflector and the lower support plate were previously penetrated by the melt, no deep molten pools can exist inside the RPV. Therefore, it is evident that, under these conditions, the water addition will quench, cool, and arrest all material still present within the remains of the RPV.

The final situation is characterised by some unknown fraction of core material remaining in the vessel in a stable configuration and the rest being incorporated in a flooded ex-vessel MCCI pool. What remains to be shown is that the melt in this MCCI pool will ultimately be transferred into a coolable and cooled configuration.

For this, it is necessary to consider the phenomenology of the MCCI process. As experimentally confirmed, e.g. by the MACE experiments [Ref-1] to [Ref-3], the heat flux distribution in the molten pool and the rate of concrete erosion during MCCI do not significantly depend on whether the surface of the molten pool is flooded or not. This is because the upward directed heat flux is dominated by the intensity of convection within the molten pool, which again is mainly driven by the gas release at the melt-concrete interface and therefore not influenced by the presence of water at the upper surface.

What will be influenced, though, are the thermodynamic conditions at the surface. The presence of water and the resulting switch to nucleate boiling heat transfer will drastically reduce the surface temperature and result in the formation of an oxidic crust, which insulates and isolates the melt from the water on top. Underneath this crust, the molten pool will progress towards the gate, and finally relocate into the core catcher, in the same way as in the dry case. Any molten debris that was quenched in the pit during re-flood will remain there, as long as water is provided by either the RIS [SIS], or the EVU [CHRS].

To summarise: though flooding of the pit may extend the MCCI period and delay gate failure due to the stabilisation of part of the core material in the RPV or the pit, which reduces the decay power in the molten pool, late flooding is not able to change the ultimate course of events, leading to gate failure and melt spreading into the core catcher.

2.4.1.2. Assessment of melt retention in the pit

Temporary retention is based on the provision of a layer of sacrificial concrete that must be penetrated by the melt prior to its escape from the pit. This layer is backed-up on the outside by a protective layer (see Sub-section 16.2.2.4 - Figure 1), except at the position of the melt plug, which therefore acts as a predefined weak point. The ultimate purpose of the protective layer is to contain the melt in a predefined volume and to avoid contact between melt and structural concrete. The protective layer consists of a zirconia-based refractory material, which is able to withstand the attack of the core melt during the retention period.

First contact between melt and protective layer is likely to occur in the region of the top metal layer, where the heat flux to the concrete and the resulting erosion speed are higher than in the oxide region below. The zirconia material is fully stable when in contact with the metallic melt fraction [Ref-1].

The material is also stable against the oxidic fraction, under ongoing MCCI conditions [Ref-1]. This is due to the steady introduction of "cold" concrete decomposition products into the bulk of the molten pool, which leads to the formation of a sub-cooled mixture consisting of:

(i) a dispersed solid phase containing the high-melting refractory components zirconia and urania, and

(ii) a liquid phase having a high content of low-melting concrete decomposition products.

Therefore, the melt is always "saturated" in refractory components, so any significant dissolution of potentially exposed zirconia is avoided.

The provision of a layer of sacrificial concrete of defined thickness has a favourable self-adjusting characteristic. This stems from the fact that to ablate a defined amount of concrete the melt must generate a defined integral amount of decay heat. Therefore, a lower initial mass of released melt and/or a lower level of decay heat will result in correspondingly longer retention times, and vice versa. This feedback makes the accumulation process independent of the melt release sequence and the time of RPV failure (decay heat level).

This independence is further reinforced by the fact that, due to the zirconia layer having a low thermal conductivity, the RPV, residual core, MCCI pool and sacrificial concrete form a coupled quasi-adiabatic system. The RPV lower head is not only heated from the inside, but also from the outside by thermal radiation from the surface of the MCCI pool. Due to the gas-induced mixing within the MCCI pool, the corresponding radiant heat flux is of the same order as the heat flux into the surrounding concrete. This inherent coupling links the process of concrete ablation with the heat-up and ultimate thermal failure of the RPV lower head.

The geometrical constraint imposed by the refractory layer pre-determines the total amount of concrete ablated during the retention period, which adjusts the final melt properties, including temperature and viscosity, into a narrow and predictable range. This is because these properties mainly depend on the melt concrete fraction. The admixture of sacrificial concrete leads to an equalisation of the spectrum of possible melt states at the end of the retention process and therefore makes the spreading process and all subsequent events independent of the inherent uncertainties associated with in-vessel melt pool formation and RPV failure.

Selection of sacrificial concrete

The composition of the sacrificial concrete in the reactor pit is specifically selected to meet the requirements of temporary melt retention. The concrete aggregate consists mainly of Fe_2O_3 and SiO_2 in approximately equal proportions, with 15% by weight common Portland cement in the dry concrete mixture as a binder.

Fe_2O_3 helps to oxidise the chemically aggressive metallic components Zr and U in the sub-stoichiometric melt. The reaction by-product, Fe, does not alter the thermo-chemical characteristics of the melt. In addition, after the dissolved metal inventory in the oxide decreases, surplus Fe_2O_3 accumulates as FeO and Fe_3O_4 in the oxide melt, which reduces the liquidus temperature and, correspondingly, the temperature level at which the MCCI takes place. This effect is beneficial as, in combination with the formation of silicates, it contributes to reducing the fission product release from the MCCI pool.

Fe_2O_3 and SiO_2 are provided in their natural form as iron ore (hematite) and siliceous pebbles. This also introduces, $MgCO_3$ (dolomite) and $CaCO_3$ (limestone) into the concrete system, but only in small quantities. Ordinary Portland cement is used to bind the concrete aggregates. Hardening tests with the described composition have shown that a steady state water content of less than 5% can be achieved. Sub-section 16.2.2.4 - Table 1 lists the composition, density and decomposition properties of that concrete called FeSi/PZ15/8 for a water-content of 5%.

2.4.1.2.1. Validation strategy

A precondition for the corresponding analysis is the characterisation of the melt release from the RPV. This information includes the masses of oxidic and metallic components, their corresponding thermo-dynamic and thermo-chemical states, and their order of discharge into the reactor pit. These parameters can be obtained from integral codes such as MAAP-4 (Appendix 16A).

However, because late in-vessel melt progression is an ongoing R&D issue, the models incorporated in these codes and the resulting predictions involve a high level of uncertainty. Moreover, the feedback of thermal radiation emitted from the MCCI pool in the pit to the RPV lower head, which, under EPR conditions, contributes substantially to lower head failure, is not adequately reflected.

Due to these deficiencies, the validation of the accumulation function of the pit for the EPR is performed based on generalised melt release sequences. Though still being supported by MAAP-4 predictions for the state and amount of the released melt, they involve a wider variation of key assumptions and thus envelop the release sequences and conditions obtained with MAAP-4. This strategy drastically reduces the spectrum of melt release scenarios and release modes to be considered.

The principal tool to perform the assessment is the MCCI code COSACO (Appendix 16A), which has been extended by models that simulate the lower RPV and its coupling with the MCCI.

2.4.1.2.2. Modelling approach

Generalised release cases

The applied generalised melt release sequences are based on the modelling scheme outlined in Sub-section 16.2.2.4 - Figure 2.

As the core of the EPR is enclosed by a heavy reflector, which, due to its significant thermal capacity, prevents early sideward melt-through, it is assumed that a large molten pool forms on the lower support plate before the melt can penetrate the heavy reflector and discharge into the lower head [Ref-1]. Ultimately, two partially molten pools can coexist, one located in the lower head, the other above the core support plate, see Sub-section 16.2.2.4 - Figure 2a. In the further course of the in-vessel melt-down, material may relocate from the upper into the lower pool, even after penetration of the lower head and start of MCCI in the pit.

The prediction of the amount of melt in the lower head, which is initially released into the pit after local failure of the RPV, does involve significant uncertainties. The approach followed here is to envelop these uncertainties by a parametric variation of the amount of melt that is initially released into the pit and by considering the feedback between the MCCI in the pit and the heat-up and failure of the RPV. This variation yields various initial melt masses in the residual RPV and pit.

In considering the effective thermal interaction by radiant heat transfer between the lower head and lower support plate, see Sub-section 16.2.2.4 - Figure 2b, both masses are combined as a single equivalent mass, thereafter called RPV-bottom, see Sub-section 16.2.2.4 - Figure 2c. The RPV-bottom is assumed to be heated by thermal radiation emitted from the MCCI pool in the pit and by a fraction of the decay heat generated in the molten material remaining in-vessel.

The RPV-bottom is assumed to detach from the RPV as soon as it reaches a predefined failure temperature. Upon failure, the melt fraction remaining in-vessel, along with the RPV-bottom, is discharged into the reactor pit and added to the MCCI pool. The temperature at which this failure takes place is taken as the temperature at which the ultimate strength of the steel approaches zero. Data for high temperature tensile steel indicate that this will occur at ~1300°C. Most likely, the lower head will fail below 1300°C due to progressive, creep-induced reduction of the load-bearing cross-section.

In-line with this phenomenology, the applied generalised melt release sequences involve two distinct melt pours. The first pour initiates the MCCI in the pit and the second pour completes the melt release from the RPV. As the MCCI continues, the newly released second pour heats up and becomes mixed into the existing molten pool.

The amount of the first pour varies between 40% and 80% of the total released mass (metal plus oxide) as obtained from MAAP-4 calculations, see section 2.1, sub-section 2.1.2.3.1, and Sub-section 16.2.2.4 - Table 2. Furthermore, the time of the first pour is independently varied between 10,000 seconds (around 3 hours) and 86,400 seconds (1 day) to investigate the influence of the level of decay heat on the failure time of the RPV-bottom/melt plug and the retention time in the pit. The selected time interval yields a variation in the decay heat level of ~30%. This variation is bounding for the different initiating scenarios, e.g. LB(LOCA) and SB(LOCA), and envelops the vast majority of possible melt release sequences.

To describe the configuration within the MCCI pool, it is assumed that the immiscible metallic and oxidic melt fractions stratify into layers according to their density. The reasons for assuming stratified layers are:

- The initially high density difference between the (heavier) oxide and metal of ~2 te/m³

- The expected formation of an oxidic crust at the oxide-metal interface caused by the fact that the temperature of the metal melt is initially about 500°C lower than that of the oxide

In the stratified mode, the downward MCCI is governed initially by the heavier oxidic melt. Due to the admixture of lightweight concrete decomposition products, the density of the oxide steadily approaches that of the metal melt until finally, the metallic melt relocates underneath the oxide. During this layer inversion, the slag layer which formed on top of the metal melt mixes with the oxide. As the slag layer consists of lightweight material, namely of concrete decomposition products and oxidation-products formed in the metal layer, this admixture results in a strong decrease of the oxide density and a new stable stratification.

In addition to the described changes of the configurations of the layers, an assumed permanent mixing of the oxidic and metallic phases during the entire MCCI was also analysed. These two cases (fully stratified and fully mixed) bound all intermediate configurations, including a partial mixing of the metal into the oxide at the common interface. Sub-section 16.2.2.4 - Table 3 gives an overview of all analysed cases.

The analysis performed [Ref-2] had demonstrated that the calculated retention times are practically independent of the initial Zr-oxidation level, because the Zr-fraction is fully oxidised within a short period. Therefore, in most of the following calculations a best-estimate value of 40% by weight was chosen for the degree of Zr-oxidation in the oxidic melt at the time of its release from the RPV.

The decay power distribution between oxidic and metallic melt fraction was assumed to be 90:10, in accordance with the experimental results obtained of the MASCA projects [Ref-3].

<u>First large pour consisting of metallic melt only</u>

In order to supplement the described best-estimate release sequences, a postulated initial release of a large amount of metal melt (without oxide) was also analysed. The scenario relates to an initial breach of the RPV near the lower level of the metallic pool after practically all the metal has already accumulated in the lower head. The resulting fast axial erosion is considered the most onerous case for the retention function.

The assumptions made for the mass and temperature of the metal melt release are compatible with those for the generalised sequences. The chosen amount of 70 te corresponds to the full mass of the metallic melt release as considered in the other scenarios.

While the composition of the ternary Fe/Cr/Ni subsystem is kept constant and taken equal to that given in Sub-section 16.2.2.4 - Table 2, the degree of Zr-oxidation was varied between 30% and 70% to parametrically investigate the effect of the Zr-chemistry. In addition, to assess the influence of the initial temperature of the metal melt, its value was varied between 1550°C and 1700°C. Sub-section 16.2.2.4 - Table 4 summarises the investigated cases for the metal melt release.

2.4.1.2.3. Results

This sub-section presents the results of the analysis performed to examine the ability of the reactor pit to accumulate the core inventory. Melt accumulation is considered successful if, for each analysed case, the following two targets are fulfilled, significantly before the MCCI pool comes into contact with the melt gate:

- The lower head plus lower support plate ("RPV-bottom") have failed thermally and dropped into the MCCI pool together with the residual in-vessel melt

- All incorporated material is molten and diluted in the MCCI-pool and conditions that favour melt spreading are achieved

The compliance of the concept with these targets is demonstrated in the following sections.

2.4.1.2.3.1.   Melt accumulation

<u>Generalised release cases</u>

Regarding the first criterion, it is necessary to track melt front progression into the sacrificial concrete in the axial direction (downward) and to relate it to the failure history of the RPV-bottom, in particular to the time of the final discharge of the melt inventory into the reactor pit.

In Sub-section 16.2.2.4 - Table 3 and in this section the different cases considered are annotated by a percentage and two letters (e.g. 80%E-M). The percentage refers to the initial melt mass as a percentage of that predicted by MAAP; the first letter to the time of melt release (Early or Late); and the second letter to the mode (Layered/Mixed).

In this respect, Sub-section 16.2.2.4 - Figure 3 shows the calculated course of axial ablation for the cases analysed with the "layered mode" assumption. To evaluate the influence of the "layered mode" assumption, the figure also includes two cases (80%E-M and 80%L-M) analysed with the "mixed mode" assumption. The figure demonstrates that, for all cases, the failure of the RPV-bottom will occur long before the melt reaches the gate, at a time when less than half of the sacrificial concrete is ablated. This holds true despite a substantial variation in the calculated total melt-concrete interaction time, which results from the variations in the decay heat level and the initial mass of melt in the pit.

The calculated duration of the MCCI in the pit for a typical low-power scenario is ~35% greater than for a high power scenario with an equal amount of initial melt. This correlates well with the decrease in decay power of ~34% resulting from the corresponding shift in the onset of MCCI from 10,000 seconds to 1 day and thus confirms the statement made in section 2.4.1.1 of this sub-chapter about the self-adjusting characteristic of the MCCI in the pit, which comes about because a given amount of energy (integral decay power) is needed to ablate a concrete-layer of a given thickness.

The initial amount of melt affects the duration of temporary melt retention because an increased mass not only results in a higher absolute decay power, but also in a lower surface-to-volume ratio. This leads to higher heat flux densities at the melt-concrete interface and higher erosion rates. Furthermore, at the same time, there is an increase in the heat flux to the upper surface of the pool, which faces the RPV lower head. The higher thermal radiation from this surface accelerates the heat-up of the RPV-bottom in the same proportion as the MCCI rate.

The latter becomes obvious from a comparison of the times needed for the heat-up of the RPV-bottom for the two cases 80%E-L and 40%E-L. Though the masses of melt initially released into the pit differ by a factor of two, the obtained failure times of the RPV-bottom of 3100 seconds and 4400 seconds are much closer. The result illustrates the self-adjusting effect of the thermal coupling between ex-vessel melt and RPV-bottom, which ensures a sufficiently fast failure of the lower head.

The cases conducted using the "mixed mode" assumption are characterised by an initially low erosion rate. This is caused by the large fraction (> 90%) of solid oxide, which results from the postulated mixing of the "cold" metallic melt into the oxidic melt at the beginning of the MCCI. Consequently, a high fraction of the oxidic melt first solidifies and must be re-melted before concrete ablation can become effective. This prolongs the MCCI as compared to the "layered mode" cases.

Despite the increase in the duration of the MCCI, the failure of the RPV-bottom in the "mixed mode" cases takes place at about the same erosion depth as in the corresponding layered cases. This again confirms that, because the RPV-bottom and the MCCI pool form a coherent system, achieving the failure criterion of the RPV-bottom is more a function of erosion depth than interaction time. As Sub-section 16.2.2.4 - Figure 4 shows, the criterion for the failure of the RPV-bottom is achieved at an axial ablation depth of about 20 cm for all investigated cases. Moreover, it shows that, for a given initial melt mass, the influence of the actual decay heat level on the ablation depth at the time of RPV-bottom failure is not significant.

This feature of the chosen retention concept is attributed to the fact that the failure of the RPV-bottom takes place after it has absorbed a certain amount of energy, which - in the applied model - is mainly emitted from the melt by thermal radiation. The time needed to absorb this energy is governed by the radiant heat flux at the melt surface. For a low heat flux, because of a low decay heat level in the melt, the time to achieve the failure temperature of the RPV-bottom is correspondingly increased. This is compensated by the fact that, in this case, the heat flux into the concrete, which determines the ablation rate, is also lower. As heat fluxes to the top and bottom in the gas-mixed molten pool are at least equal (may be higher to the top), both heat flux values change in roughly the same proportion. Consequently, the failure of the RPV-bottom always takes place at a similar axial ablation depth, independent of the actual level of decay heat. If the heat flux distribution within the MCCI pool is anisotropic, the energy transport to the top would be proportionally increased, which would lead to an even earlier failure of the RPV-bottom.

Considering that the calculated residual thickness of concrete at the position of the gate at the time of the failure of the RPV-bottom is approximately 55% of the initial thickness, the margins with respect to melt accumulation are high.

Sub-section 16.2.2.4 - Figure 5 compares the results obtained for the generalised melt release sequence with specific scenario-dependent release sequences, obtained with MAAP-4. The figure shows the bounding character of the generalised melt release sequences, in particular for LB(LOCA) and LOOP scenarios. The melt release sequences obtained with MAAP-4 for these scenarios are covered by each of the generalised sequences analysed in the parametric study independently of whether the metallic and oxidic phases in the MCCI pool are assumed as mixed or layered.

The melt release sequence for a SB(LOCA) scenario, which is characterised by a late first melt release 29 hours after scram, is consistent with the generalised melt release sequences that assume a late first melt release after 1 day. Among the cases that assume stratified conditions, the case 60%L-L is most representative for the SB(LOCA) scenario and in good agreement with the MAAP-4 prediction. The cases 40%L-L and 80%L-L bound the duration of melt release compared by MAAP-4. All cases that assume mixing of the metallic and oxidic melt phases yield longer release times and are thus bounding for the MAAP-4 SB(LOCA)-case. This verifies the assumption that the generalised melt release sequences lead to bounding melt release curves as compared to those calculated with the integral code MAAP-4.

First large pour consisting of metallic melt only

The results given in Sub-section 16.2.2.4 - Figure 6 show that for this case also the melt temperature is predicted to rise initially due to the oxidation of the Zr. Due to this, the temperature increases with increasing Zr concentration in the initial melt. After the Zr content is depleted, temperatures decrease to the solidifying temperature, where they remain for the rest of the MCCI. Concurrent with this transient cooldown, the melt erodes into the concrete at a rate of about $\sim 2.5 \times 10^{-4}$ m/s, almost independently of the melt initial temperature and Zr-content. Following the transient phase, the ablation front progression is quasi-steady and predominantly driven by the decay heat, see Sub-section 16.2.2.4 - Figure 7.

While the characteristics of the transient phase are widely independent of the varied parameters, its duration increases with increasing temperature and Zr-content from ~500 seconds to ~1000 seconds and, accordingly, the ablation depth at the end of the transient phase varies between ~0.125 m and ~0.25 m. The minimum residual thickness of the concrete of at least 0.25 m provides a favourable margin against premature failure of the gate. The ablation rates during the quasi-steady phase are at least one order of magnitude lower than the transient rates. Therefore, the gate will not be reached within the considered period of 1000 seconds, which bounds the duration of all melt release sequences predicted by MAAP-4.

In conclusion, a first pour consisting exclusively of metallic melt is not critical to the melt accumulation function of the reactor pit.

2.4.1.2.3.2. Melt conditioning

Regarding the second issue, it is necessary to check whether the final characteristics of the melt at the end of the temporary retention phase are similar and favourable with respect to the succeeding spreading process. This task comprises a comparison of the final values obtained for liquidus temperature, melt temperature and composition, as well as for the resulting volumetric solid fraction. The latter value is of importance, as it influences viscosity and thus influences the ability of the melt to spread.

The melt compositions obtained for all calculated cases are summarised in Sub-section 16.2.2.4 - Figure 8. The figure shows the following variation in the composition of the melt: core oxides: ~69-74%, SiO_2 ~13-16%, iron-oxides from ~6-9%. The fraction of other concrete decomposition products is always about ~5.5%. It should be noted that the material properties are determined rather by the volumetric (molar) composition rather than fraction by weight. The content of lightweight concrete decomposition products is much higher than the mass fraction given above.

The total mass of ablated concrete varies between 90 te and 100 te depending on the initially released melt mass, time of first release, and assumed melt configuration during MCCI. Notably, the results show that, for all considered cases, any metallic uranium and zirconium present in the initial melt are completely oxidised.

The next task is to investigate to what extent the achieved terminal melt states are similar in their relevant characteristics and in particular if they favour melt spreading. To this end, the resulting liquidus and melt temperatures, as well as the corresponding volumetric solid fractions are determined and compared on the basis of their time-dependent evolution, to demonstrate the equalising character of the MCCI.

Sub-section 16.2.2.4 - Figure 9 shows the evolution of the liquidus temperature for all cases conducted assuming either a layered or mixed melt mode. In terms of the analyses conducted in the layered mode, the main events that disrupt the continuous decrease in liquidus temperature during MCCI are: (i) the second melt pour which causes a steep increase in the liquidus temperature due to the addition of molten core material and (ii) the density-driven layer inversion between oxide and metal layer, which acts in the opposite direction due to the admixture of the low-melting point slag to the oxidic phase. Layer inversion is obviously not an issue in the mixed mode.

Despite substantial differences in the preceding course of the MCCI, the predicted liquidus temperatures at the end of temporary melt retention fall into a narrow band, which is only about 50 K wide. The temperature of the oxidic melt generally follows the evolution of the liquidus temperature, see Sub-section 16.2.2.4 - Figures 9 and 10.

Sub-section 16.2.2.4 - Figure 10 indicates that the predicted temperature of the oxidic melt at the time of spreading is always approximately 2050°C. Compared to the initial temperature of the melt during release from the RPV of about 2500°C, this temperature reduction of about 500°C is caused by the change in melt chemistry and by the admixture of concrete decomposition products. The lower temperature helps to reduce the radiant heat losses at the upper surface and the conduction heat losses into the bottom during spreading.

The calculated sub-cooling of the oxidic melt at the end of the MCCI, i.e. the temperature difference between liquidus and melt temperature, is generally only ~25°C. This must be compared to a difference of several hundred degrees between the liquid and the immobilisation temperature of the melt. The latter is characterised as the temperature at which the volumetric solid fraction reaches about 50%.

The low volumetric solid fraction in the oxidic melt (see Sub-section 16.2.2.4 - Figure 11) confirms the ability of the melt to spread. Essentially, the values vary between 0.03 and 0.05 for all cases, despite substantial differences in the preceding course of temporary melt retention. These values are an order of magnitude below the value at which immobilisation occurs.

In the mixed mode, the volumetric solid fraction is initially very high, due to the postulated addition of "cold" metal to the oxidic melt, but steadily decreases due to melt reheating. The same effect arises after a mixture of oxidic and metallic melt is added to the MCCI pool after failure of the RPV-bottom.

A low volumetric solid fraction relates to low viscosities [Ref-1]. The calculated low values of viscosity (see Sub-section 16.2.2.4 - Table 5) and the low sub-cooling at the time of gate contact establish very favourable conditions for melt spreading. Due to the unifying characteristic of the temporary melt retention, this result holds true independently of the underlying scenario.

2.4.1.2.3.3. *Mass and energy release by the MCCI in the reactor pit*

The prediction of mass and energy release by the MCCI in the reactor pit is based on initial and boundary conditions that yield conservative results regarding the containment response.

Such conditions are provided by a surge line break scenario, which leads to vessel failure and melt release into the reactor pit as early as 2 hours 45 minutes after scram and thus involves a high decay power level in the melt. At the same time, the duration of melt release for this scenario is relatively short. Relative to other scenarios, the selected scenario therefore yields high concrete ablation rates, which translate into conservative off-gas rates. The integral gas release is predominately determined by the amount of available concrete, which is determined by the thickness of the sacrificial layer in combination with the presence of the refractory shielding and thus is almost independent of the scenario and the related melt release sequence.

Sub-section 16.2.2.4 - Figures 12 to 15 show the release of H_2O, H_2, CO_2 and CO as a function of time, while Sub-section 16.2.2.4 - Figure 16 gives the corresponding release temperature. The release temperature is assumed to correspond to the temperature of the particular melt phase, which forms the upper layer of the MCCI pool. Hence, it corresponds to the temperature of the slag layer before layer inversion and of the oxide melt afterwards. As the oxide melt exhibits the highest temperature in the MCCI system, the release temperature increases by ~310°C as a consequence of the layer inversion at 16120 seconds. Furthermore, with successive layer inversions the gas release rates strongly increase. This effect results from the high transient ablation rates, mainly in the downward direction due to the interaction of the concrete with superheated metal, which prevails until the end of the retention phase in the pit.

UK EPR

PRE-CONSTRUCTION SAFETY REPORT

CHAPTER 16: RISK REDUCTION AND SEVERE ACCIDENT ANALYSES

SUB-CHAPTER : 16.2

PAGE   : 148 / 295

Document ID.No.
UKEPR-0002-162 Issue 05

2.4.1.2.4. Conclusion on temporary melt retention in the pit

Given the inherent characteristics of the MCCI to adjust the ablation front progression to the amount of initially released melt, combined with the fact that the MCCI forms a coherent system with the lower structures of the RPV, the analysis performed demonstrates that the core melt inventory will be collected in the reactor pit sufficiently before the melt attains contact with the melt gate, independent of the underlying scenario.

Another important result concerns the state of the molten pool at the end of the retention phase in the reactor pit. The analysis predicts excellent spread of the oxidic melt fraction, due to its low volumetric solid fraction and viscosity at the time of spreading. This is consistent with the proposed phenomenological description of the MCCI [Ref-1].

Furthermore, the composition of the melt at the end of the retention period was found to be fairly insensitive to the mode and time of the initial melt release from the RPV as well as to the melt initial conditions, including the degree of Zr-oxidation and the Zr-partitioning ratio between oxide and metal. In all cases the final melt is fully oxidised and includes an amount of concrete decomposition products of the order of 50% by volume.

This unification is supported by the geometrical constraints established by the refractory layer, which spatially restricts the melt front progression in radial and axial directions and thus limits the amount of incorporated concrete. In this sense, temporary melt retention in the pit makes all subsequent measures independent from the initiating scenarios as well as from the inherent uncertainties related to in-vessel melt progression and RPV-failure.

The retention function is sufficiently resistant to deviations from design-base conditions as it tolerates late flooding as well as highly conservative assumptions regarding the melt release from the RPV.

2.4.1.3. Assessment of gate failure

This sub-section describes the function of the melt gate, the tools used for its validation and the main results obtained.

The implementation of a removable melt plug in the pit bottom results from the requirement to access the lower pit for inspection, if necessary. The melt plug consists of a sacrificial concrete layer on top of an aluminium plate, the so-called "gate". The gate is mounted on top of a steel frame, which establishes mechanical support against potential pressure loads acting on the melt plug from above. The steel frame has the shape of an open mesh and provides the necessary cross-section for melt release after gate melt-through. The melt plug can be moved into its position and locked against the outer steel frame by means of a remote-controlled cart.

In its locked-in state, the melt plug is functionally an integral part of the sacrificial concrete layer. The thickness of its concrete layer is identical to that covering the surrounding lower pit region. As the sacrificial concrete is not backed by protective material at the position of the melt plug the melt plug acts as the predefined weak point of the melt enclosure during the phase of temporary melt retention and accumulation in the pit.

The corresponding analysis shows that the entire melt will be collected in the MCCI pool after less than half of the sacrificial concrete in axial direction is eroded, see section 2.4.1.2.3.1 of this sub-chapter.

A significant heat-up on the embedded frame during this first phase is avoided by the small thickness of the upper part of the steel frame and by the fact that the "chutes" on its outer periphery have a low profile and do not reach into the upper half of the concrete. The lower part of the steel frame, which extends below the level of the gate, is also much thicker and thus represents a high thermal inertia, which helps to prevent early failure. This is because the energy needed to melt a certain volume of steel is higher than the energy to decompose the same volume of concrete (based on the materials physical/chemical properties).

As a consequence, the embedded support frame is expected to support the gate until the sacrificial concrete cover of the melt plug is eroded and the melt reaches the level of the gate. The frame is additionally supported mechanically by a circumferential weld that connects the vertical and horizontal part of the frame at the bottom, at a position directly above the zirconia bricks. This connection is able to carry the weight of the melt and the residual melt plug, even without crediting the surrounding chutes.

In the unlikely case that the support frame would thermally fail before the gate is locally penetrated by the melt, the entire frame, including locked-in gate would completely drop-out into the transfer channel under the hydrostatic pressure of the accumulated melt. This will instantaneously open a large cross-section for melt release.

In all other cases, after penetrating the sacrificial concrete, the melt will expose and melt through the aluminium gate with the support frame intact. The outflow cross-section is determined by the size of the initial contact area between melt and gate and by the growth of the resulting hole in the gate due of the heat transfer between flowing melt and surrounding concrete. The aluminium gate itself does not act as a thermal resistance for the flow because of the low melting point of the material and the fact that it will interact exothermically with the melt.

2.4.1.3.1. Validation strategy

Due to the large diameter of the reactor pit and the fact that the surface area of the gate is less than a tenth of the total surface area of the pit bottom, it can be expected that concrete ablation, across the surface of the gate, will be practically homogeneous and therefore the erosion front will be fairly even.

Therefore, a large region of the gate is predicted to contact the melt within a short period of time. Such quasi-uniform contact is further promoted by the low thermo-mechanical stability of residual, dried-out concrete layer that would surround the initial contact area. This would cause a large area of the gate to open, thus allowing a very fast release of the accumulated melt into the transfer channel and core catcher. It is evident that for this most likely case no specific analysis is necessary.

However, because the assumption of a large initial contact area cannot be reliably proven due to the absence of MCCI experiments at reactor-scale, the possibility of a small contact area also needs to be assessed. The cross-section and location of the initial contact area cannot be predicted, as they are determined by the course of the preceding MCCI. Therefore, a minimum conceivable size is chosen consistent with observations from available large-scale experiments.

The most relevant MCCI experiments are the tests performed at ANL in the framework of the MACE [Ref-1] to [Ref-3], and OECD-CCI projects [Ref-4]. They combine large cross-sections (from 50cm*50cm to 1.2m*1.2m) with the use of a prototypic oxidic melt. Among these experiments, the OECD-CCI tests are the best-documented with respect to tracking local erosion. Tests CCI-1 and CCI-3 are most representative for the EPR due to the use of a silicate-type concrete.

2.4.1.3.2. Modelling approach

For the postulated case of a local initial contact between melt and gate, bounding assumptions are made for the size and location of the initial contact area as well as for the state of the melt, including its mass, temperature and the distribution of the immiscible metallic and oxidic phases. In addition, a variation of relevant assumptions is performed to demonstrate the large margins involved in the design.

2.4.1.3.3. Results

The expected case of a large initial contact area between the melt and the aluminium gate is expected to lead to a quasi instantaneous melt-through of the gate and a fast release of the accumulated melt inventory.

Regarding outflow time, this case is bounded by the more conservative case of a limited initial contact area. For the related small initial contact areas, it is shown [Ref-1] that, for the entire spectrum of considered cases, the melt release will be complete in less than 200 seconds. This is due to the predicted growth of the initial hole by heat transfer to the residual concrete of the melt plug that surrounds this initial hole. This heat transfer is highly effective in particular in the best-estimate case of a layered molten system when the denser metal layer is located below the lighter oxide and thus is the first phase to be released through the hole.

The final size of the opening at the end of the release process is typically on the order of 0.5 m² which results from the assumption of an average hole size during outflow of ~0.25 m², corresponding to about 10% of the total gate area.

2.4.1.4. Assessment of melt spreading

After penetration of the gate the melt enters the melt discharge channel which guides it into the core catcher. Due to its large cross-section of more than 1 m² and the fact that the walls are covered with a thermally insulating ceramic layer, the transfer channel is not expected to have a significant effect on the flow, especially when the failure cross-section of the gate is less than that of the channel.

The inlet level of the melt discharge channel into the core catcher is above the maximum melt level. Therefore, once the melt has covered the bottom of the core catcher any melt arriving later does not have to physically move from the inlet to its final position. Instead, the melt will find its own level and rise uniformly across the entire core catcher.

Within the core catcher, the melt spreads under practically dry conditions, as the spreading compartment is a dead-end room and isolated from the rest of the containment. There is no inflow of water from sprays or leaks and only a limited amount of condensate may form inside the room. Though dry conditions are not required for a successful spreading, they make the distribution of the melt more predictable because fuel coolant interactions are avoided.

2.4.1.4.1. *Validation strategy*

Two redundant tools are used to validate the assumption that the melt will relocate into and distribute within the core catcher after gate opening. First a detailed analysis with the AREVA code CORFLOW (see Appendix 16A) and a confirmatory assessment with the phenomenological spreading model developed at RIT [Ref-1], which was validated against a wide set of spreading experiments. In addition, the ability of an EPR-type melt to spread has also been confirmed independently [Ref-2] by the CEA with the code THEMA within the framework of the European ECOSTAR project.

Based on the accumulated knowledge base, the success of melt spreading under EPR conditions is generally considered a non-critical issue because:

- as a result of the preceding MCCI in the pit, the out-flowing oxidic melt will be fully liquid

- the liquid metallic melt is expected to be released first and thus the oxide will spread on a hot smooth surface

- the surrounding structures, in particular in the melt discharge channel, have only a limited heat absorption capability

- the average melt level in the core catcher after spreading will be as high as 50 cm

This evaluation is reflected in the corresponding positive assessment given by a group of European experts within the framework of the EUROCORE project [Ref-3].

2.4.1.4.2. *Modelling approach*

2.4.1.4.2.1. *CORFLOW code*

CORFLOW (Appendix 16A) uses a 3D-model in Cartesian coordinates for the reactor pit, channel and spreading compartment, as shown in Sub-section 16.2.2.4 - Figure 17. To reduce the complexity of the actual geometry, several simplifications are included:

- a flat bottom, neglecting the step at the end of the melt discharge channel

- each phase (oxide/metal) is released and spread separately, which neglects the additional driving hydrostatic pressure head of the other overlying melt phases in the reactor pit during outflow through the gate

All the above simplifications are conservative with respect to front propagation, as they reduce the mechanical energy of the fluid. With respect to the opening characteristics of the melt gate, various cases were modelled, in accordance with the findings in section 2.4.1.3.3 of this sub-chapter. They include:

- a complete, instantaneous opening of the entire cross-section

- a partial opening with a cross-section of 0.24 m² , which corresponds to about 10% of the total gate area

Cases with an initial release of either an oxidic or mixed melt were included in the analysis despite the fact that an initial release of metallic melt is predicted to be most likely, consistent with the COSACO calculations described in section 2.4.1.5.2.1 of this sub-chapter, and the deduced release sequences:

- first metal, then oxide plus slag (RS-A, after layer inversion)

- suspension of metal in oxide plus slag (RS-B)

- first oxide, then metal, then slag (RS-C, layer inversion suppressed)

As CORFLOW is restricted to the analysis of single-component flow, the above release sequences had to be reduced to the following simplified cases:

1a Spreading of metallic corium onto concrete

1b Spreading of oxidic corium with slag, onto a metallic melt

2 Spreading of oxidic corium without slag, onto concrete

3 Spreading of a mixed corium (oxide, slag and metal) onto concrete

Mixed corium spreading is considered as the best estimate release model (indexed as "Ref."), since an intense mixing of phases during the release process has also been observed in the 2D-COMAS EU-4 spreading test [Ref-1] performed with initially layered oxidic and metallic corium. This test was simulated by CORFLOW with good accuracy by assuming a single-component-fluid with properties of the mixture of metal and oxide [Ref-2].

In addition to the analysis of the four cases 1 a/b, 2 and 3 listed above, the CORFLOW analyses for the EPR [Ref-3], also include separate calculations to assess the effects of:

- a lower initial temperature of the oxidic corium

- a reduced cross-section of the gate area

- a non-Newtonian rheology of the oxidic corium

The initial melt conditions for the CORFLOW analyses [Ref-3] were extracted from the COSACO results for the melt retention phase in the pit for an SB(LOCA) scenario. This scenario represents a conservatively low decay heat level and is thus bounding for examining the ability of the melt to spread.

2.4.1.4.2.2.   RIT model

As compared to the former approach, the methodology developed at the Royal Institute of Technology Stockholm (RIT) is not based on a numerical, but on an empirical-phenomenological approach. It is based on an in-depth review of the state-of-the-art knowledge of melt spreading (database, simulation, analysis methods and scaling considerations) [Ref-1] together with a complete description of the RIT model. The underlying methodology was first developed for spreading in 1D-channels, but has recently been extended to cover spreading in 2D-channels and, more importantly, spreading into an open area.

In the RIT method, the terminal spread melt thickness δ_{spr} is shown to be a function of the time scales of two competing processes: hydrodynamic (convective) spreading τ_{conv}, and solidification τ_{sold}. In the gravity-inertia regime, the hydrodynamic spreading time scale τ_{conv}, is determined as the time period required for liquid (melt) to reach its capillary thickness, δ_{cap}. The characteristic solidification time, τ_{sold}, is defined as the time period needed to cool the melt to an immovable state. For this, not only the superheat, but also a part η of the latent heat of fusion, has to be removed from the bulk melt. Based on the mass and momentum conservation equations, a square-root relation was established between the dimensionless length scale (representing ratio $\delta_{spr} / \delta_{cap}$) and the dimensionless time scale (representing ratio $\tau_{conv} / \tau_{sold}$). The square-root law was shown to be valid in both gravity-inertia and gravity-viscous regimes, employing a dimensionless viscosity number, which was analytically derived.

An experimental program - "Scaled Simulant Spreading Experiments" (S3E) - was performed at RIT. The S3E data was analysed and found to fit very well with the scaling rationale developed. The RIT method was then used to predict the spreading distance in one-dimensional high-temperature oxidic melt spreading tests at RIT. Very good agreement between the pre-test prediction results and data was obtained. The validation success confirmed assumptions made in deriving the model equations (e.g., $\eta = 0.5$) and justified the use of the heat transfer correlations employed.

Extensive validation of the RIT method was performed against the data from a large number of spreading experiments. The method was found to predict the spreading distance in one- and two-dimensional channels with reasonable accuracy. It was also found that the spreading in two-dimensional channels is bound by the channel sidewalls and hence essentially one-dimensional.

The RIT method was employed to perform pre-test predictions for the COMAS EU-2b core melt spreading experiment [Ref-2] with good agreement between the predicted and observed spreading distance. Validation of the RIT method for melt spreading into an open area was also performed on the database obtained from the RIT simulant-material experiments. It was found that melt spreading into an open area is significantly different from 1D-spreading. As the melt can spread in all directions, the hydrodynamic spreading time-scale is remarkably reduced, and hence the spreading area significantly enhanced. As a result, the terminal melt thickness may decrease by a factor of 3 to 10, as compared to the corresponding 1D-case.

As the EPR core catcher is somewhere between a 1D- and 2D-geometry, both RIT methods for (i) an open area and (ii) a channel were employed to predict the core melt spreading characteristics for the EPR. The latter represents a conservative lower bound estimate for the melt-covered area.

The characteristics of core melt spreading in the EPR case were evaluated for selected core melt accident scenarios, in which the melt superheat and flow rate, and the physical properties are subject to uncertainties. The effect of both the scenario and the phenomenological (modelling) uncertainties are outlined. A probabilistic assessment framework, incorporating the deterministic and parametric models, was developed to test both phenomenological and scenario uncertainties in the evaluation of the safety-important parameters, i.e. the terminal spread-melt thickness, or the coverage of the melt retention area by core melt. Such treatment of uncertainties achieves an integrated assessment, showing the influence of uncertainties of different parameters on the results obtained.

The assessment was performed for two basic cases with either a low (case A) and high (case B) amount of sacrificial concrete slag added to the oxidic corium before spreading. Again, only the oxidic melt fraction was considered. In addition, a lower range of core melt discharge rate was chosen for a bounding evaluation of the spreading characteristics for case B.

2.4.1.4.3. Results

2.4.1.4.3.1. CORFLOW code

Cases 1a, 2 and 3 simulate the spreading of various kinds of corium with various initial temperatures onto cold concrete [Ref-1]. Case 1b describes the spreading of oxidic corium, including slag, onto an already spread, hot metallic corium. Sub-section 16.2.2.4 - Table 6 summarises selected results. In all the cases considered, the melt reached all parts of the spreading area within about 10 seconds. An almost homogeneous distribution is generally achieved in less than one minute.

For the standard cases, Sub-section 16.2.2.4 - Table 7 lists selected results after one minute and summarises information on corium heat transfer. Due to the applied symmetry, the heat source and sink terms relate to only one half of the real geometry (~85 m²).

Due to its high heat conductivity and low emissivity, heat conduction to the substratum is the major heat sink for the spreading metal in case 1a. For all other standard cases, radiation to the surroundings is the dominant heat removal process. The comparison between heat loss and heat generation terms indicates that, over the period of one minute, the total decay heat production is one order of magnitude lower than the heat losses.

Variants of the standard cases were assessed with more conservative conditions. These include: initial temperatures that were 200°C lower than for the reference case, a reduction of the release cross-section of the gate, and the consideration of the non-Newtonian rheology of the oxidic melt. It was found that these variations have only minor influence on melt propagation, see Sub-section 16.2.2.4 - Table 8.

The CORFLOW calculations demonstrate that, for a variation of the open cross-section between 10% and 100% of the total gate area of 2.4 m², outflow times range from 100 seconds (0.24 m²) to 10 seconds (2.4 m²). If smaller gate failure cross-sections are assumed, the outflow time through the hole will be correspondingly extended. The CORFLOW analysis demonstrates that melt spreading is sufficiently fast and complete even for the most conservative case considered of a core oxide melt without the preceding release of liquid metal. For this case, melt temperatures are much higher than in the other cases because the oxidic corium has not yet incorporated the slag layer.

The calculated evolution of height profiles of the melt along the centreline within the transfer channel and spreading compartment shows that, even for the most conservative assumed case, the release and spreading of the melt will be complete in less than 200 seconds. The additional consideration of metal/slag layers above the melt in the pit would further increase the outflow velocity for the oxide due the increased hydrostatic pressure.

2.4.1.4.3.2. RIT model

For all selected cases, it was found that even the one-dimensional spreading model predicts a nearly complete spread (A_{theo}/A_{EPR} = 0.85 to 1), which, for a width of the channel equal to that of the melt discharge channel of the EPR, corresponds to a 1D spreading length of >100 m [Ref-1].

In comparison, the spreading-into-open-area model predicts ratios of $A_{theo}/A_{EPR} \gg 1$. The higher ratio in the 2D-case relates to the easier spreading, caused by the fact that even if the melt becomes locally immobilised, the obstacle can be by-passed, in contrast with the situation in a channel, where melt flow is constrained by the channel sidewalls.

Results of the sensitivity analysis indicate that besides initial melt temperature and superheat, for which conservatively low values were assumed, the total mass of the melt and its discharge rate are the most important parameters. Within the range of parameters investigated, other influential parameters, like scenario and phenomenological uncertainties were found to only have a small impact on the results of the assessment.

To summarise: the results of the assessment of core melt spreading in the EPR melt retention device show that for the given melt delivery conditions the entire spreading area will be covered uniformly. This confirms the predictions of the code CORFLOW.

2.4.1.5. Assessment of melt flooding and quenching

The EPR core catcher into which the melt relocates after its release from the pit is a shallow metallic crucible [Ref-1]. Its bottom and sidewalls are assembled from a large number of individual elements made of cast iron. They are connected using a slot-and-feather technique. Due to these flexible connections, the structure is highly insensitive to thermal expansion and deformation as a result of temperature gradients after melt contact. To enhance downward heat transfer, the bottom elements have fins that form rectangular, horizontal cooling channels.

The sidewall elements are thinner than those at the bottom and are stacked inside vertical beams for mounting purposes and for fixing to the wall. Also for the lateral elements, a flexible connection is provided by a similar slot-and-feather technique as used for the bottom plate. The vertical beams are attached to the surrounding concrete walls and preserve a sufficient gap for outside cooling and for the escape of the generated steam. The top of the steam vent is covered with a lid-type structure, which prevents the entry of material that was potentially splashed by local fuel coolant interactions during melt entry. The inside of the crucible structure is covered with a layer of concrete.

In the reactor pit the objective of the sacrificial concrete is to achieve a sufficiently long period of temporary melt retention to modify the properties of the melt and to oxidise excessive metallic Zr. In contrast, no such strong requirements exist for the spreading area. In particular, no specific conditioning of the melt has to be achieved at the end of the MCCI. Nevertheless, the presence of the sacrificial concrete layer has a few advantageous consequences, namely to:

- provide an easily-to-handle closed surface

- mechanically protect the structure during melt spreading

- reduce temperature and density of the melt

- delay the contact between melt and cooling structure

- promote melt fragmentation at the surface during flooding

- reduce the probability of FCI by the introduction of glass-formers, namely silica

- further improve the capability of the melt to retain fission products

The preceding MCCI, in combination with the high thermal inertia of the thick metallic cooling structure, ensures that heat fluxes to the water remain within tolerable limits for all reasonably expected melt states and spatial distributions with a high margin.

The arrival of the melt in the core catcher triggers the opening of valves that initiate the gravity-driven flow of water from the IRWST into the spreading compartment. The water first fills the central supply duct underneath the core-catcher. From there, it enters the horizontal cooling channels and then submerges the space behind the sidewall cooling structure from where the water pours onto the surface of the melt. The cross-section of the flow-limiter and valves establish an initial flooding rate of about 100 kg/s. At this rate the filling process described takes about 5 minutes.

In the initial phase of melt flooding, when the surface of the melt is still hot, all added water is expected to evaporate. Later a saturated water pool will form on top of the developing crust. This crust is predicted to steadily expand from the circumference towards the centre. Water overflow continues until the spreading compartment is flooded and the hydrostatic pressure levels between IRWST and spreading room are balanced. After the core catcher is submerged (see Sub-section 16.2.2.4 - Figure 18), the amount of steam discharged into the containment will be determined by the level of decay heat power in the melt.

In parallel with the flooding process, the spread melt interacts with the sacrificial concrete covering the horizontal and vertical cooling plates. The resulting delay before exposing the metallic structure and the high thermal inertia of the cooling plates ensure that the transient heat fluxes to the water in the cooling channels remain low. There is sufficient margin so that, even without the preceding cooldown, the heat flux can be absorbed by the water.

During MCCI, the temperature and the density of the oxidic melt fraction are steadily reduced by the incorporation of concrete decomposition products. Therefore, the formation of a density-stratified system with the lighter oxide on top and the heavier metal at the bottom is expected. Alternatively, part of the metal could be suspended within the oxidic phase during MCCI, in which case, the properties of the resulting "suspension" are also dominated by the oxidic phase. As a consequence,

- water that pours onto the melt will always contact the oxidic melt fraction:

According to the results of the MACE project [Ref-2] [Ref-3] substantial superficial fragmentation and improved coolability can be expected in this situation, which would significantly shorten the period of liquid melt states. Further, the formation of an oxidic crust and the avoidance of contact between metal and water are expected to strongly reduce the probability of FCI.

- the sacrificial concrete will always interact with the metallic melt fraction:

Due to the high heat loss during metal concrete contact and ablation, the metal temperature will quickly drop below the solidification temperature, which leads to the formation of a metallic crust at the bottom, as observed in the LACOMERA (COMET-L) experiments [Ref-4]. Such a crust is expected to reduce the transient thermal loads during the subsequent contact of the melt with the cooling plate. For contact between the cooling structure and the oxidic melt at the sidewall structure, these transient loads are lower than in the case of metal contact, due to the formation of thermally insulating crusts.

The tolerance of the cooling structure to the expected thermal loads was confirmed experimentally by dedicated tests in a full-scale rectangular horizontal channel [Ref-5]. Its length of 5 m corresponds to the maximum distance between the central water supply duct and the sidewalls in the EPR. The melt was simulated by electric heating from above. The sides of the channel were thermally insulated to establish symmetrical conditions. The setup operated at atmospheric pressure (1 bar) and was able to generate a maximum heat flux into the top of the plate of ~120 kW/m². In reality, the cooling structure can transfer even higher heat fluxes to the water in the cooling channels. This is because, under relevant severe accident conditions, the flooding of the melt inside the core catcher will generate large amounts of steam which automatically increase the pressure in the containment. The higher pressure causes a higher steam density which, in the relevant nucleate boiling regime, makes the heat transfer to the water more efficient.

The predicted heat flux from the melt to the water during the phase of the initial contact between molten steel layer and cooling structure peaks at a value below 100 kW/m². After this transient phase, the heat flux declines to values below 60 kW/m² [Ref-6].

The corresponding analysis is performed using the code WALTER (Appendix 16A). This code simulates the evolution of temperature within melt and cooling structure after melt flooding and quenching and thus yields the corresponding time-dependent heat flux to the water.

The fact that the experimentally measured heat fluxes to the water, even at low pressure exceed the analytically predicted maximum heat flux imposed by the melt confirm that the heat transfer to the water in the cooling channels is sufficiently effective over the entire course of melt quenching and cooling. This establishes comfortable margins and results in a high tolerance to local deviations in the final melt depth and in the spatial distribution of the metallic and oxidic phases.

The experiments [Ref-5] also confirmed that the heat transfer is independent of the direction of the water flow. Similar characteristics were measured for co-current and counter-current flow of steam and water. These two regimes correspond to an inflow of water from either the IRWST (co-current case) or from the saturated water pool on top of the melt after filling of the core catcher is complete (counter-current case). The related insensitivity avoids the need for defined flow conditions in the channels. Instead, it is sufficient to keep the core-catcher submerged, which, in the EPR design, is automatically achieved by the open connection between the IRWST and the core catcher [Ref-7].

This way, the melt can be cooled in a fully passive way without requiring pumps and/or an external water supply. The generated steam is condensed on containment structures or on spray droplets after availability of the containment heat removal system (EVU [CHRS]). As the stabilisation of the melt is exclusively based on heat transfer and crust formation, there are no limiting thermo-chemical constraints with respect to the stability of materials used in the design with respect to the core melt. This reduces the requirements to establish a certain range of melt compositions that had to be placed on earlier measures.

In addition to the described passive cooling mode, which allows for the removal of heat from the melt by boiling and evaporation, an active injection of water into the central supply duct by the EVU [CHRS] is a possible option. While the active mode is not relevant with respect to meeting the radiological targets for the EPR, it is nevertheless suggested in the long-term, to eliminate containment overpressure caused by the sustained steam release from the boiling water pool on top of the melt.

Due to the high capacity of the EVU [CHRS] coolers, one train is sufficient to achieve this target. Therefore, the second EVU [CHRS] train could still be used temporarily for containment sprays and thus for removing decay heat produced by airborne and deposited fission products from the containment atmosphere.

Specifically, active cooling would be conducted by closing the valve for water supply to the spray ring and opening the valves for water supply to the core catcher in the relevant EVU [CHRS] train. To prevent most of the coolant from flowing back into the IRWST through the open connection between IRWST and core catcher, a passive outflow reducer (POR) is provided between the IRWST and the connection to the flooding line. The POR has a high flow resistance in the direction towards the IRWST and a low resistance in opposite direction. Therefore, this element effectively limits direct backflow of water to the IRWST and ensures that most of the coolant will reach the core catcher.

During active core catcher cooling, the water in the spreading compartment would rise to the top of the chimney where it spreads on the heavy floor and, from there, flows back into the IRWST. As the spreading compartment and the reactor pit are connected via the open melt gate, the water level in the pit would also rise to the approximate level of the RPV nozzles. In this way, the residual RPV and the structural concrete around the reactor pit, which were exposed to high temperature during the phase of temporary melt retention, would be better cooled, resulting in a faster temperature decrease in this area.

The temperature at the core catcher/basemat interface and thus the temperature gradient through the base-slab will also be reduced relative to passive cooling, as the temperature boundary condition will be lower than the saturation temperature.

Another positive side effect is that the sub-cooled pool terminates the re-suspension of fission products during boiling at the water surface. Together with the achieved pressure reduction (ultimately to ambient pressure), this leads to a decrease of the fission product inventory in the containment atmosphere and in consequence, a reduction of the potential activity release in the event of leaks.

For the parts of the EVU [CHRS] located outside the containment, the active mode of core catcher cooling will imply the same requirements as the active spray mode. The water levels in the spreading compartment, reactor pit and IRWST during active cooling are shown schematically in Sub-section 16.2.2.4 - Figure 19.

2.4.1.5.1. Validation strategy

The interaction of the melt with the sacrificial concrete layer in the spreading compartment is analysed with the code COSACO (Appendix 16A). As an initial condition, it applies the melt state at the end of the temporary melt retention phase in the reactor pit, obtained by the analysis described in section 2.4.1.5.2.1 of this sub-chapter. The time to ablate the sacrificial concrete is compared with the time needed to flood the pipes and channels of the cooling system and to fill the freeboard between the concrete wall and the core catcher.

The exclusion of highly energetic FCI is based on the results of this analysis and on the experience gained from an extensive set of tests with top flooding of a spread melt [Ref-1] to [Ref-5]. In these tests either prototypic, urania-based core melts or stimulant melt have been flooded with water under the conditions of ongoing interaction with concrete. The stimulant melts used included those with oxidic phases containing large amounts of alumina, which is commonly known for its high likelihood to engage in FCI. No type of energetic interaction has been observed in any of these tests, despite the fact that the gas-induced mixing was often more intense and the concrete content lower than predicted for the melt flooding process in the EPR core catcher.

The mass and energy release into the containment is determined using an engineering model which is based on conservative assumptions with respect to quenching and superficial fragmentation.

2.4.1.5.2. Modelling approach

2.4.1.5.2.1. MCCI

The concrete walls of the core catcher are modelled assuming cylindrical geometry. To adjust the model, and in particular the ratio between bottom area and circumferential length, to that of the real core catcher, only a sector of the full cylinder and an inner inert region are assumed. In the calculations a sector width of 5.125 rad, an inert radius of 5.346 m and an outer radius of 9.83 m are used.

At the free surface, radiant heat transfer to the overlying concrete structure is considered. Due to the complexity of the flooding process, the presence of water at the surface is not taken into account. Therefore, the determination of the gas release from the MCCI is decoupled from the evaluation of the steam production resulting from the flooding of the free surface. The latter is addressed separately in the next section and in section 2.4.1.5.3.2

The MCCI ends at the time when the residual concrete thickness at the bottom is zero.

2.4.1.5.2.2. Melt flooding and quenching

As a consequence of the preceding admixture of concrete decomposition products and the resulting density inversion between the oxidic and metallic melt fraction during and after MCCI, the water at the surface will necessarily be in contact with an oxidic-type of melt.

The probability of FCI during flooding is low because of the formation of viscous oxidic layers and crusts, which inhibit the contact between liquid melt and water.

The events during flooding and quenching of oxidic prototypic corium melts have been extensively studied in the framework of the MACE and OECD MCCI projects [Ref-1] to [Ref-4]. The results obtained unanimously demonstrate that water distributes smoothly on the molten corium and that a substantial superficial fragmentation and improved coolability can occur. Fragmentation is promoted by the gas release from the ongoing interaction with the concrete and by the substantial shrinkage of the material during solidification.

At the time flooding starts, the melt is subject to an intense convective mixing driven by concrete decomposition gases. This causes a steady introduction of hot material to the surface and keeps the surface temperature high. Under these conditions film boiling is the dominant heat transfer mode. In this regime efficient heat transfer is anticipated due to conduction and radiation across the agitated (i.e. area enhanced) melt-water interface. In addition, melt droplets will be entrained into the water layer by gas emerging from the melt. The resulting heat fluxes, as measured in the MACE program, are in the range of ~3 MW/m².

Related to the EPR core catcher area of ~170 m² this compares to a total heat flux of ~510 MW, which is twice the value of ~240 MW needed to evaporate all incoming water. Therefore, only part of the melt surface can be covered with water in the initial phase of flooding.

After complete flooding, the melt enters a transient bulk-solidification phase. Solid oxidic corium has a higher density than the liquid, therefore solid fragments mix into the molten pool and cause an overall decline in temperature. This leads to a collapse of the gas-film and eventually to the formation of a slurry-type, viscous oxidic melt. The related drop in surface temperature, which results from the switch to gas-enhanced nucleate boiling, is accompanied by the formation of a stable surface crust.

The late bulk-solidification phase is accompanied by a decline in superficial heat-flux. Consequently, temperatures start to rise again and convection is re-established. The steady-state values of melt bulk temperature and crust thickness are defined by the actual level of decay heat generated internally.

After formation, the crust can provide support for melt particles and droplets carried through cracks and holes into the water with the flow of concrete decomposition gas. Melt ejections through volcano-like structures have been observed in many experiments with both simulant and prototypic material. The decay heat created within this particle bed is transferred directly to the water.

Cooling can also be established within porous crust regions or thermal cracks caused by volumetric shrinkage. The relevance and extent of this process is the subject of ongoing R&D.

For the analysis performed, a coolable melt fraction of 20% by weight [Ref-5] is assumed, created by the combination of the following mechanisms for melt fragmentation at the surface:

- initial mixing of water and liquid melt at the agitated interface

- formation of a partially porous crust

- crust cracking with water ingress

- gas driven ejection of material into the water pool on top of the crust.

Based on this best-estimate value and incorporating the phenomena described above, the heat transfer during the individual quenching phases is determined as described in the following sections.

Initial melt flooding

This phase starts with the first pour of water onto the melt and ends with the complete flooding of the entire melt surface. During this phase, as the total heat transport to the surface exceeds the power needed for the evaporation of all added water, the rate of steam generation is limited by the flooding rate. As a bounding estimate, the steaming rate over the entire period of melt flooding is taken equal to the rate of water addition of ~100 kg/s.

The duration of the flooding period depends on the assumption about what fraction of the energy initially stored in the melt can be released to the water by the two main mechanisms of bulk cooling and superficial fragmentation. The initial quenching phase ends when this amount of heat plus all newly generated decay heat is used up in the generation of steam.

For the quenching process, only the upper oxidic part of the melt is considered because, after the preceding MCCI, the temperature of the metallic melt below is lower than that of the oxide. Thus, no energy can be transferred from the metal to the oxide. Neglecting the metal is therefore conservative as in reality it will serve as an additional heat sink for the oxide.

The energy release from bulk cooling and quenching is calculated conservatively using the following assumptions:

- The total fraction of the fragmented oxidic corium is 20% by weight

- The quenched debris cools to the saturation temperature of the surrounding water

- The temperature after bulk-cooling is the corium immobilisation temperature

- The decay heat power is kept constant

The immobilisation temperature of the oxidic corium is the temperature at which the solid fraction reaches 50% by volume.

With these assumptions, the duration of the initial flooding period can be calculated. It is typically in the range of 1000 to 2000 seconds. The generated steam is released into the containment at saturation temperature.

This conservative model concentrates the energy release from the melt into the shortest possible time and is thus conservative with respect to the pressure build-up in the containment.

Water fill-up phase

According to the conservative approach taken, convection in the melt ceases after the initial flooding phase so further heat transport to the water is very low. All the decay heat is initially used up in the reheating of the melt pool. This results in the accumulation of a water pool on top of the crust. The water inflow rate remains relatively constant as it is defined by the fixed height of the circumferential overflow.

The bounding case is established by assuming that the heat flux from the bulk melt to the water remains zero until the average melt temperature has reached the pre-quench level and adequate convective heat transport is re-established. The only heat entering the water in this period is the decay heat produced in the fragmented melt.

Consequently, the accumulating water pool on top of the melt will stay sub-cooled and steam discharge into the containment is completely stopped. After the melt is again at high temperature, the decay heat generated in the bulk contributes to the heating of the water. The total decay power is sufficient not only to bring the newly arriving water to saturation conditions but also to heat the accumulated pool. As soon as this pool becomes saturated, steam discharge into the containment restarts.

2.4.1.5.3. Results

2.4.1.5.3.1. MCCI

During the MCCI, the density of the oxidic melt is reduced by the incorporation of concrete decomposition products. Due to this, the melt is expected to form a stable stratified system with the lighter oxide layer on top of the heavier metal. Therefore, the sacrificial concrete on top of the bottom cooling structure interacts exclusively with the metallic melt. At the beginning of this process, the cooldown of the initially superheated metal can result in high rates of concrete ablation and gas release.

When the metal layer temperature approaches the solidification temperature, erosion rates decline. The further course of the MCCI is dominated by the energy transport from the decay-heated oxidic melt.

This behaviour is illustrated by the calculation for the LB(LOCA) case (see Sub-section 16.2.2.4 - Figure 20), which shows two distinctly different phases. In the second phase, the ablation speed and the rate of release of concrete decomposition gas are significantly lower than in the preceding transient phase. The transient cooldown phase has ablation rates of the order of 1×10^{-4} m/s. After the end of the transient phase ablation has reached a depth of ~6 cm and further concrete erosion is controlled by decay heat alone and proceeds at rates of the order of 3×10^{-5} m/s. In the figure the time at which the bottom cooling structure is completely flooded is also marked.

The resulting temperatures in the melt are depicted in Sub-section 16.2.2.4 - Figure 21. This confirms that the initially superheated metallic melt quickly cools to its solidification temperature, where it remains for the remainder of the MCCI.

Whilst the metallic melt undergoes a rapid cooldown during MCCI, the temperature of the oxide only declines moderately. This is attributed to the fact that the liquidus temperature does not decline significantly with the incorporation of siliceous concrete. As a result, the oxidic melt temperature, which follows the evolution of the liquidus temperature, is still high at about 2050°C at the end of the MCCI phase.

This analysis does not consider the possible impact of the flooding process and the cooldown of the bulk melt by the incorporation of crust particles (bulk cooling). It thus yields bounding melt conditions, and therefore bounding thermal loads at the bottom of the cooling structure. The density difference between the oxidic and metallic melts at the end of the MCCI is predicted to be about 2000 kg/m³, which confirms the assumed stable layering.

2.4.1.5.3.2. Melt flooding and quenching

With the model assumption given above, the course of steam release into the containment has been calculated for a typical LB(LOCA) sequence. The initial conditions are taken from the COSACO analysis in sub-section 2.4.1.5.2.1.

The average pressure during quenching is assumed to be 3 bar, which corresponds to a saturation temperature of 134°C and a steam enthalpy of around 2.72 MJ/kg. The average decay heat power in the oxide at that time is assumed to be constant at 26 MW.

The temperature at which the volumetric solid fraction in the oxide reaches 50% is near 1400°C according to the relevant phase diagrams. This determines the minimum possible temperature of the oxidic melt after bulk cooling and thus the maximum corresponding energy release.

Characteristic times for the duration of the individual phases of the quenching process for an exemplary case with a sacrificial concrete layer of 10 cm thickness and flooding rates of 50 kg/s and 100 kg/s (one or two valves open) are given in Sub-section 16.2.2.4 - Table 9.

{CCI Removed}

e

SUB-SECTION 16.2.2.4 - TABLE 2

Total core melt inventory and melt initial temperatures [Ref-1]

Melt Composition										
Oxidation Level	**Oxidic Melt [kg]**			**Metallic Melt [kg]**				**RPV-bottom [kg]**		
40%	UO_2	ZrO_2	Zr	Fe	Cr	Ni	Zr	Fe	Cr	Ni
	141700	20920	20900	53985	7710	5100	2320	41215	5890	3900
Initial Temperatures										
Oxidic Melt*: 2500°C*			**Metallic Melt:** *1550°C*					**RPV-Bottom:** *800°C* *(failure temperature ~1300°C)*		

UK EPR

PRE-CONSTRUCTION SAFETY REPORT

CHAPTER 16: RISK REDUCTION AND SEVERE
ACCIDENT ANALYSES

SUB-CHAPTER : 16.2

PAGE   : 166 / 295

Document ID.No.
UKEPR-0002-162 Issue 05

SUB-SECTION 16.2.2.4 - TABLE 3

Matrix summarising the set of COSACO calculations performed [Ref-1].

The 1st number indicates the initial mass as a fraction of the total core melt inventory.
The 1st letter indicates the time of initial melt release (Early/Late).
The 2nd letter indicates the assumption made for the Layered/Mixed mode.

Case Nr.	Initial melt mass [% of the total mass of core melt obtained by MAAP]	Time of first melt release [sec after scram]	Layered Mode (L) Mixed Mode (M)
40%E-L	40	10000	L
40%L-L	40	86000	L
60%E-L	60	10000	L
60%L-L	60	86000	L
80%E-L	80	10000	L
80%L-L	80	86000	L
80%E-M	80	10000	M
80%L-M	80	86000	M

SUB-SECTION 16.2.2.4 - TABLE 4

Calculations for a first melt pour consisting solely of metallic melt

Case	Initial Zr-mass, kg	Initial Temperature, °C
Metal1160-1550	1160	1550
Metal1160-1700	1160	1700
Metal2320-1550	2320	1550
Metal2320-1700	2320	1700

SUB-SECTION 16.2.2.4 - TABLE 5

Calculated viscosity of the oxidic melts at the time of spreading for all analysed cases (determined using the viscosity model of Ramaciotti 1999 [Ref-1])

Case	Viscosity, Pa•s
40%E-L	0.029
40%L-L	0.034
60%E-L	0.027
60%L-L	0.03
80%E-L	0.026
80%L-L	0.029
80%E-M	0.03
80%L-M	0.034

{CCI Removed}

b

UK EPR

PRE-CONSTRUCTION SAFETY REPORT

CHAPTER 16: RISK REDUCTION AND SEVERE ACCIDENT ANALYSES

SUB-SECTION 16.2.2.4 – TABLE 7

Selected CORFLOW results regarding melt properties at t = 1 min after spreading for parametric study (cases 1-3) [Ref-1]

Variable	Unit	Case 1a	Case 1b	Case 2	Case 3
		Metal	Oxide+Slag	Oxide	Mixed (Ref.)
Maximum fluid temperature	K	2521	2489	2709	2567
Minimum fluid temperature	K	1723	2311	2368	2300
Maximum fluid liquid fraction	-	1	0.97	0.65	0.995
Minimum fluid liquid fraction	-	0.52	0.91	0	0.777
Decay heat produced	GJ	0.235	0.694	0.694	0.929
Heat removed by conduction	GJ	12.3	0.91	2.57	3.48
Heat removed by radiation	GJ	4.5	9.2	13	10.8

UK EPR

PRE-CONSTRUCTION SAFETY REPORT

CHAPTER 16: RISK REDUCTION AND SEVERE
ACCIDENT ANALYSES

SUB-CHAPTER : 16.2

PAGE   : 171 / 295

Document ID.No.
UKEPR-0002-162 Issue 05

SUB-SECTION 16.2.2.4 – TABLE 8

Selected CORFLOW results regarding melt propagation into the core catcher for standard case 3, as compared to parametric variations [Ref-1]

	Unit	Case 3	with low T_0	with low A_G
Gate area	m²	2.4	2.4	0.24
Initial fluid temperature	K	2600	2400	2600
Front propagation time to opposite wall	s	3.9	4.1	7.4
Time to cover entire spreading area	s	6.5	6.6	13
Maximum velocity in spreading direction	m/s	7.6	7.5	8.4

SUB-SECTION 16.2.2.4 – TABLE 9

Calculated steaming rate for the two flooding rates of 50 kg/s (top) and 100 kg/s (bottom)

The data in this table are principally applicable, but relate to the case of 10 cm sacrificial concrete. Data for 15 cm layer thickness are also available [Ref-1]

Period	Steaming rate
0-2246 s	**50 kg/s**
2246 – 8434 s	0
> 8434 s	11 kg/s

Period	Steaming rate
0-986 s	**100 kg/s**
986 – 7174 s	0
> 7174 s	11 kg/s

SUB-SECTION 16.2.2.4 – FIGURE 1

Main components of the EPR melt stabilisation system [Ref-1]
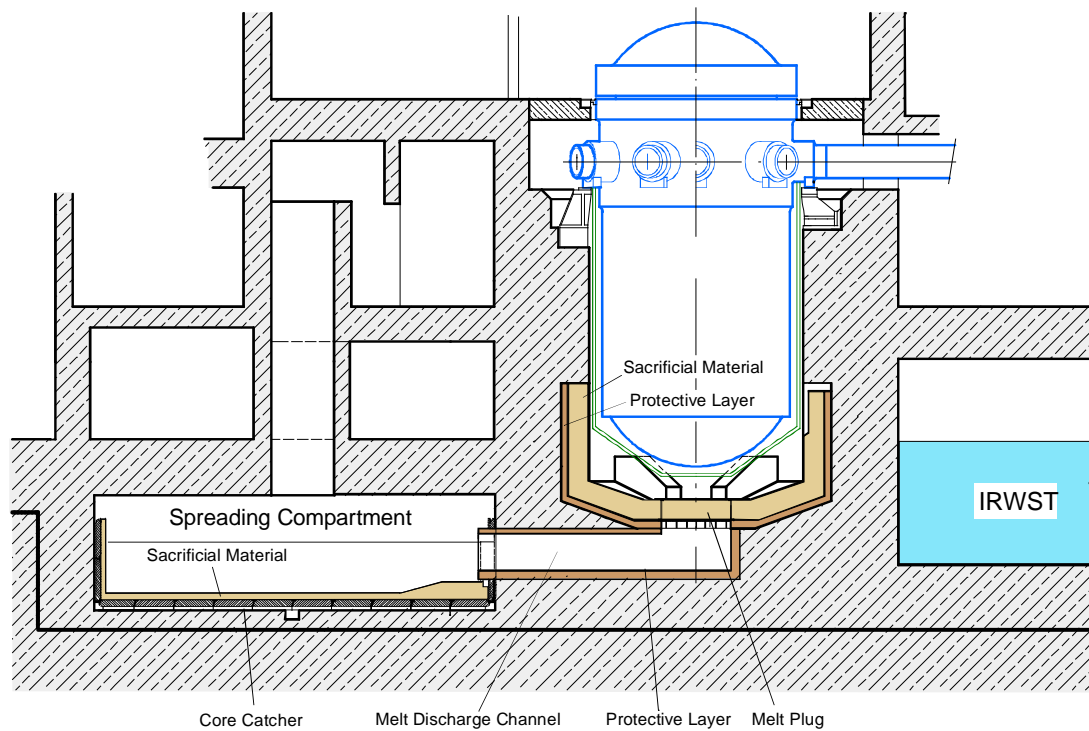
SUB-SECTION 16.2.2.4 – FIGURE 2

Modelling scheme applied for the generalised sequence of melt release from the reactor pressure vessel [Ref-1]. Note that, though the figure sketches only the layered configuration of the MCCI pool, the analysis also takes into account a mixed configuration.
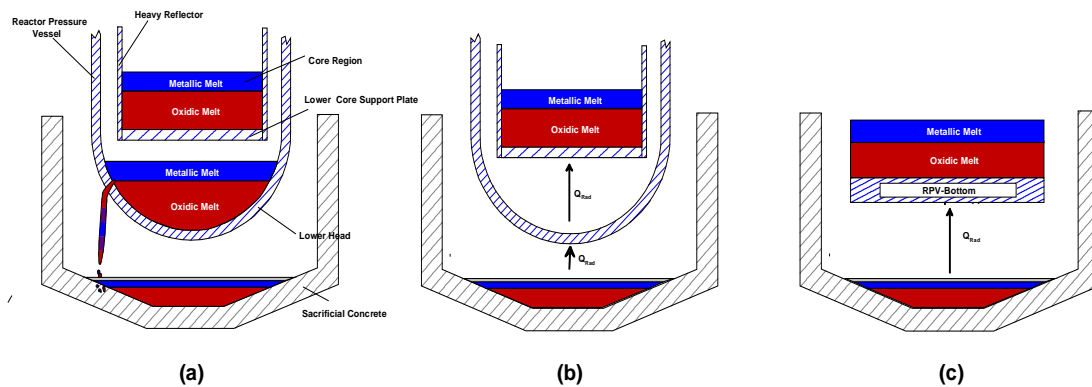
SUB-SECTION 16.2.2.4 – FIGURE 3

Histories of ablation front progression in the axial direction for the various cases analysed in the parametric study [Ref-1]
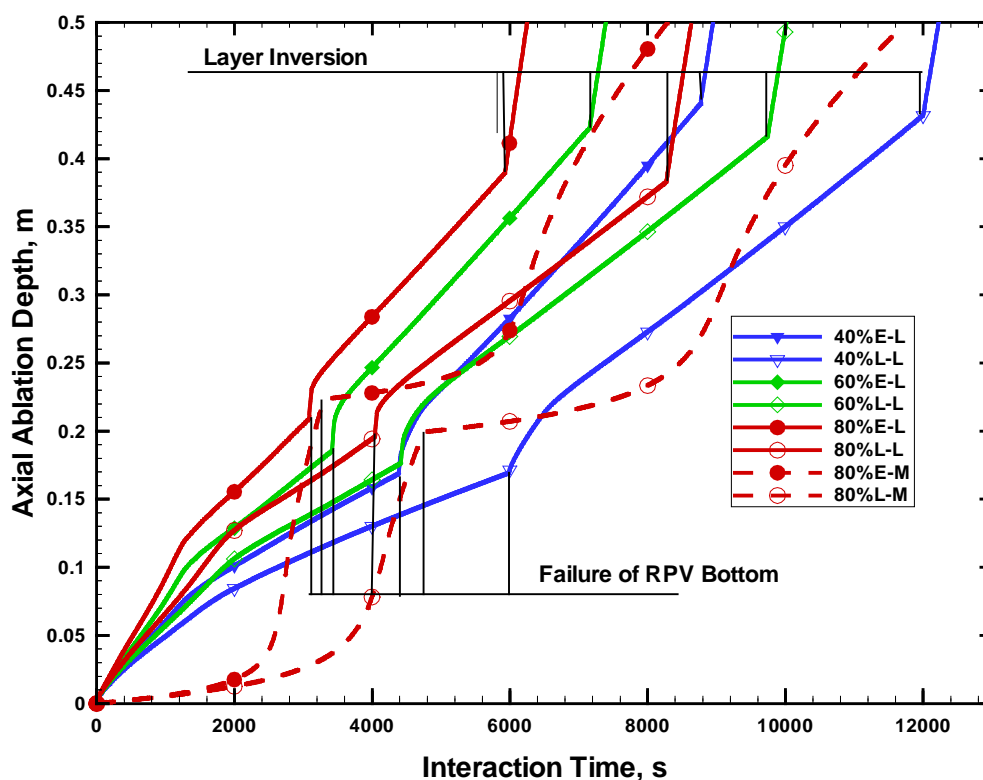
SUB-SECTION 16.2.2.4 – FIGURE 4

Temperature of the RPV-bottom as a function of ablation depth (a) and of decomposed concrete (b) for the various cases of the parametric study [Ref-1]
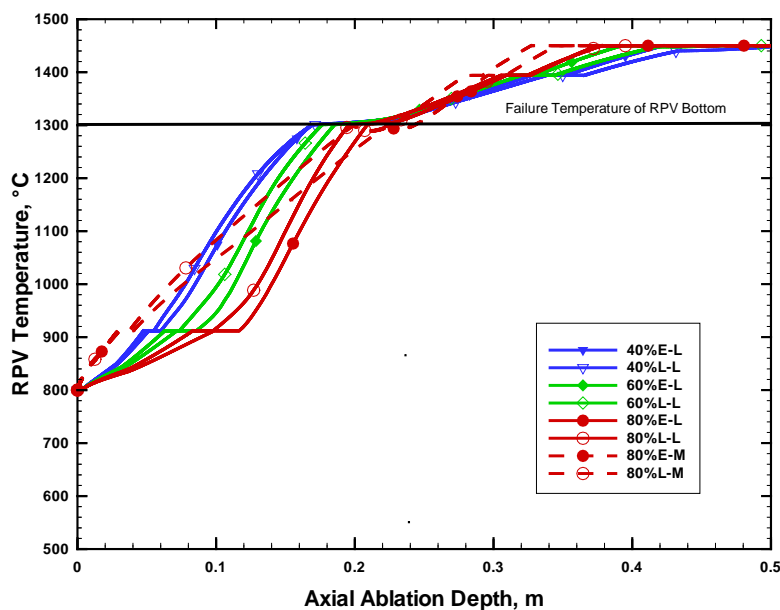
(a)
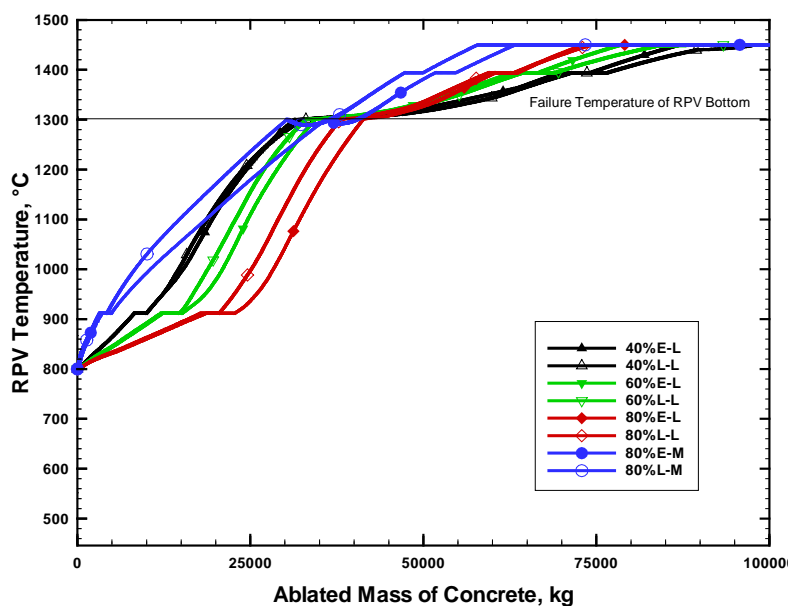
(b)

SUB-SECTION 16.2.2.4 – FIGURE 5

Comparison of the generalised melt release sequences used in the parametric study with scenario-specific sequences obtained by MAAP-4 [Ref-1] [Ref-2]
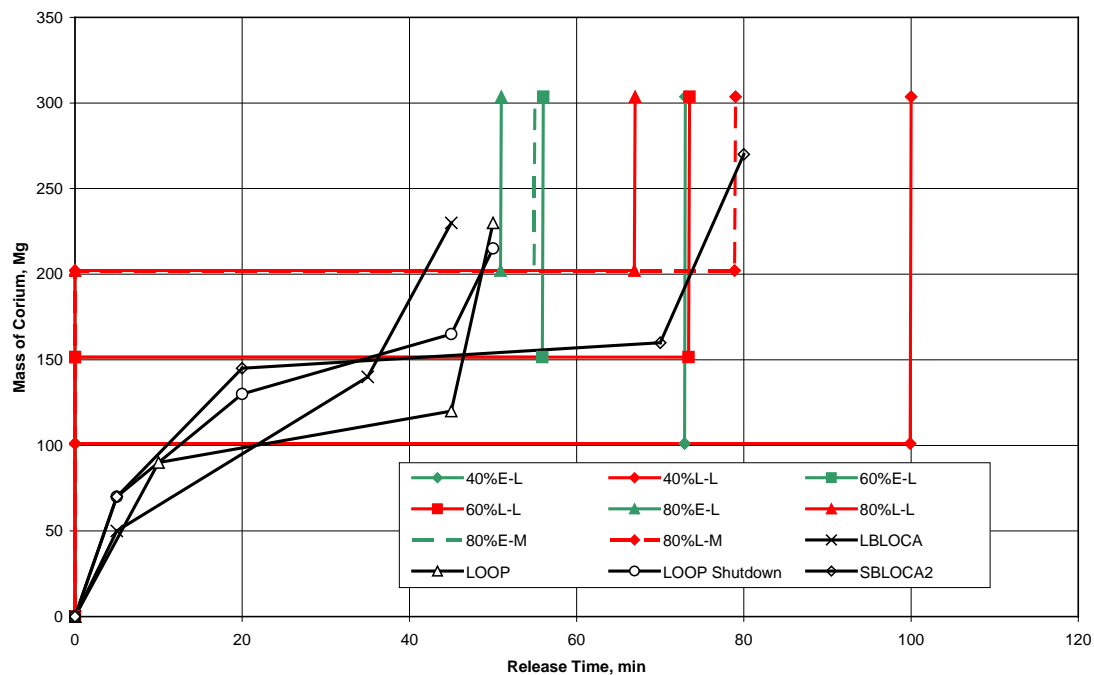
SUB-SECTION 16.2.2.4 – FIGURE 6

Temperature of the metallic melt as a function of time for the cases investigating the effect of a first pour consisting exclusively of metal
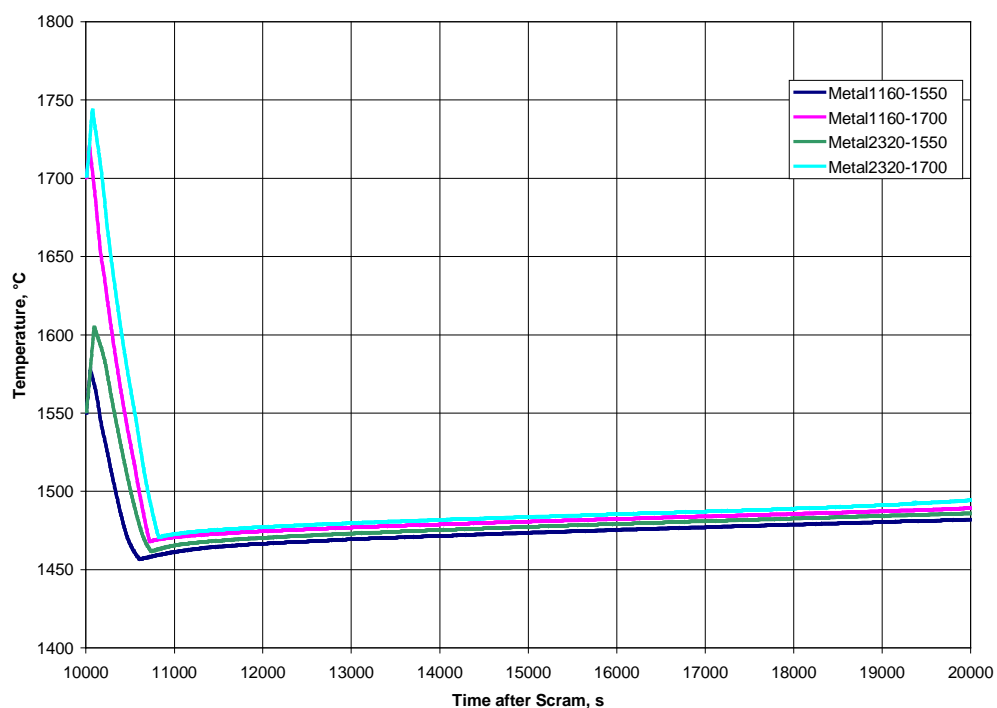
SUB-SECTION 16.2.2.4 – FIGURE 7

Axial ablation front progression for the cases, investigating the effect of a first pour consisting exclusively of metal
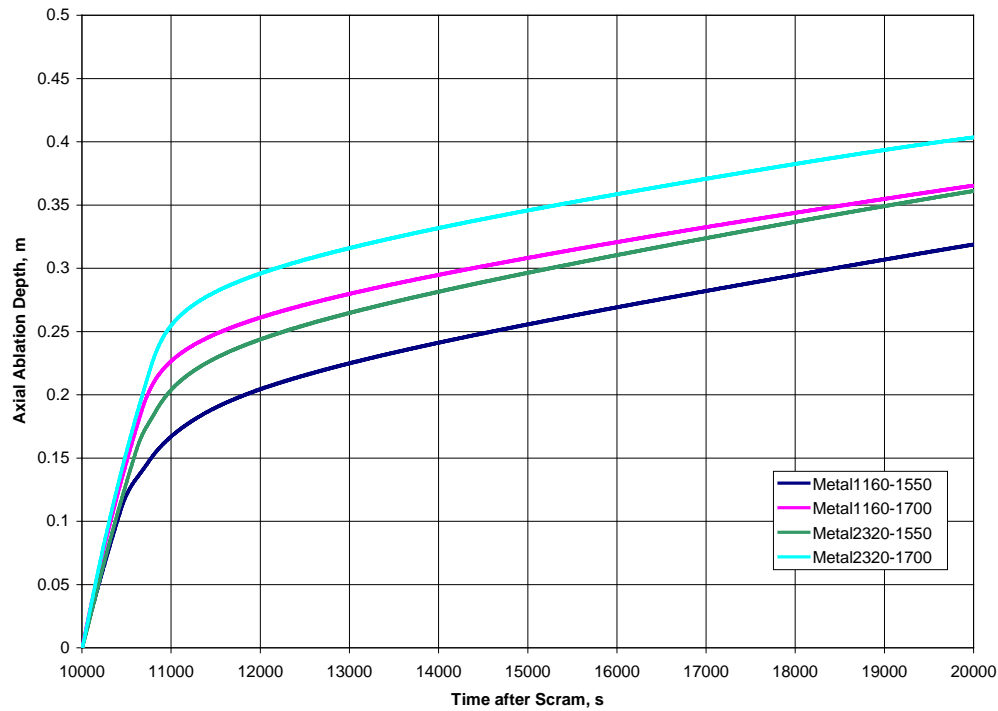
SUB-SECTION 16.2.2.4 – FIGURE 8

Composition of the oxidic melt at the end of the retention in the pit obtained for the various cases investigated in the parametric study (in % by weight - top, and molar fraction- bottom) [Ref-1].

Core Oxides: UO_2, ZrO_2 Concrete Oxides: Al_2O_3, CaO, MgO Iron Oxides: FeO, Fe_2O_3
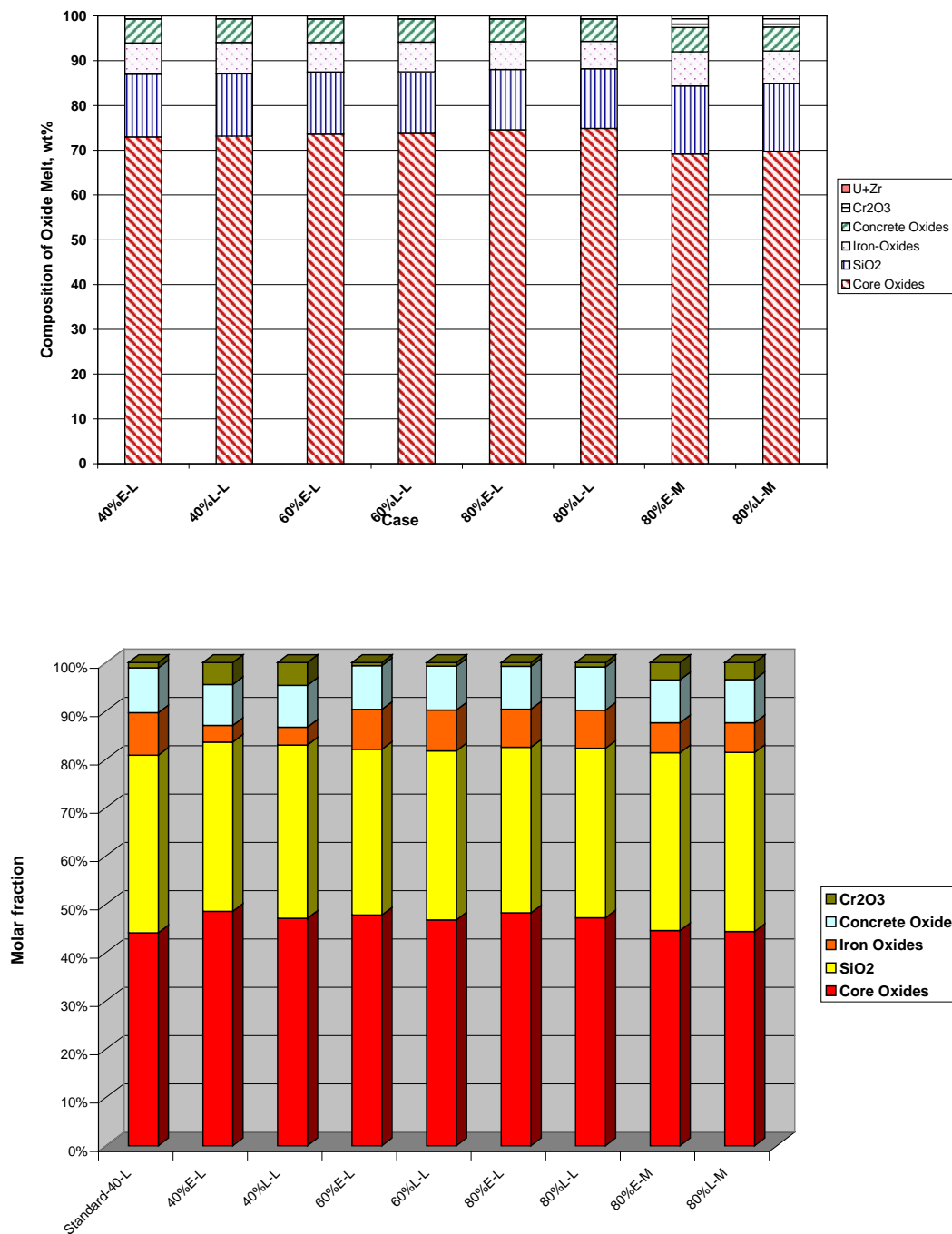
SUB-SECTION 16.2.2.4 – FIGURE 9

Calculated evolution of the liquidus temperature of the oxidic melt for various cases analysed in the parametric study [Ref-1]
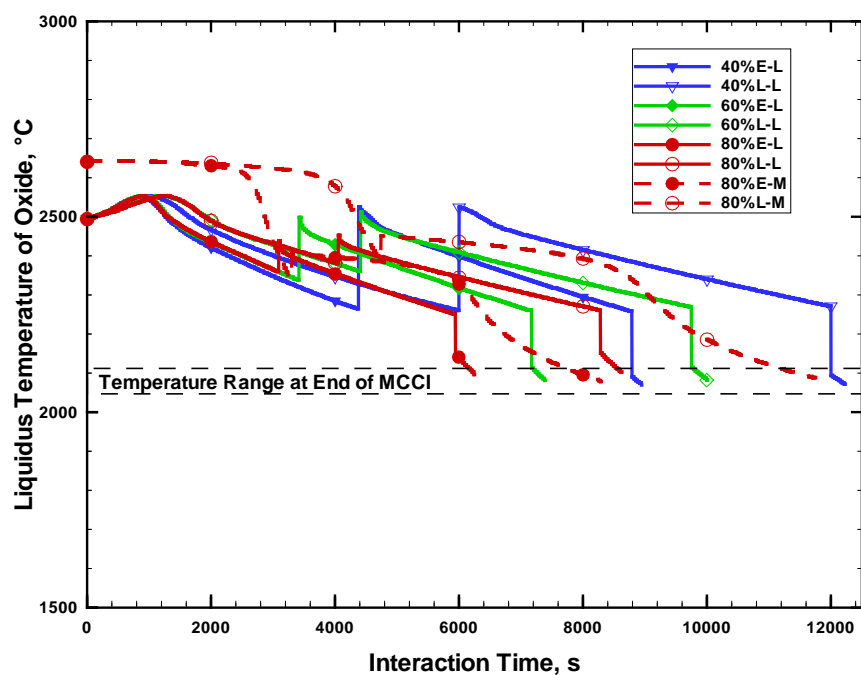
SUB-SECTION 16.2.2.4 – FIGURE 10

Evolution of the temperature of the oxidic melt for various cases analysed in the parametric study [Ref-1]
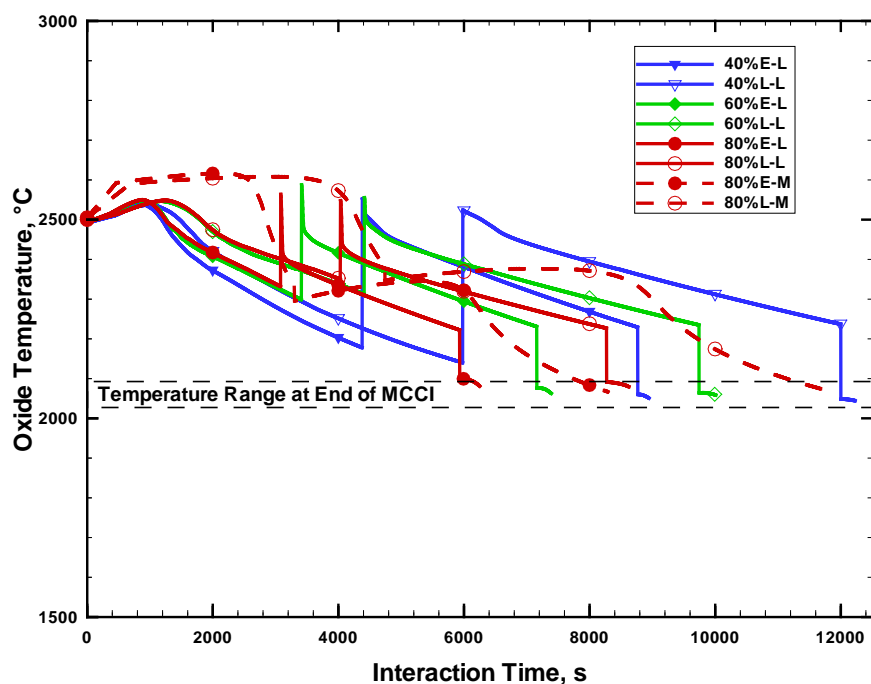
SUB-SECTION 16.2.2.4 – FIGURE 11

Evolution of the volumetric solid fraction in the oxidic melt for various cases analysed in the parametric study [Ref-1]
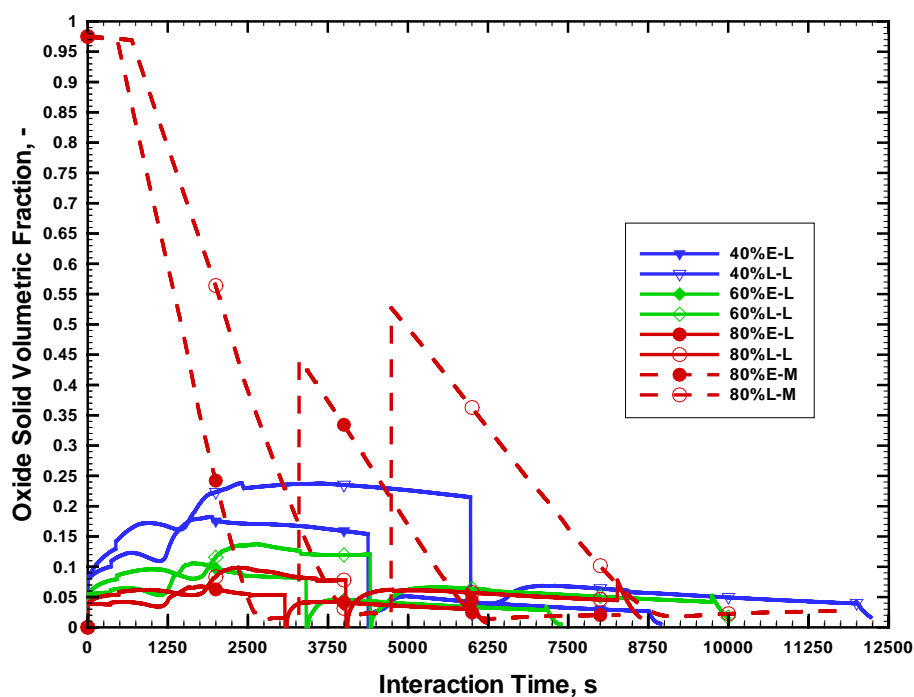
SUB-SECTION 16.2.2.4 – FIGURE 12

Mass of H_2O generated by the MCCI in the reactor pit [Ref-1]
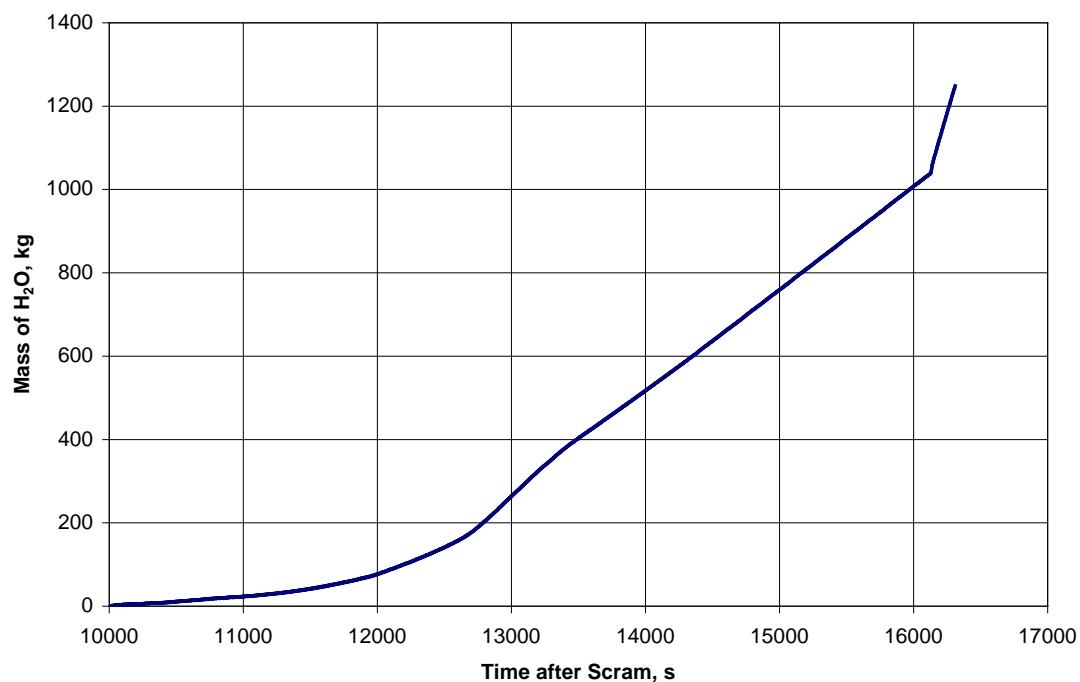
SUB-SECTION 16.2.2.4 – FIGURE 13

Mass of H_2 generated by the MCCI in the reactor pit [Ref-1]
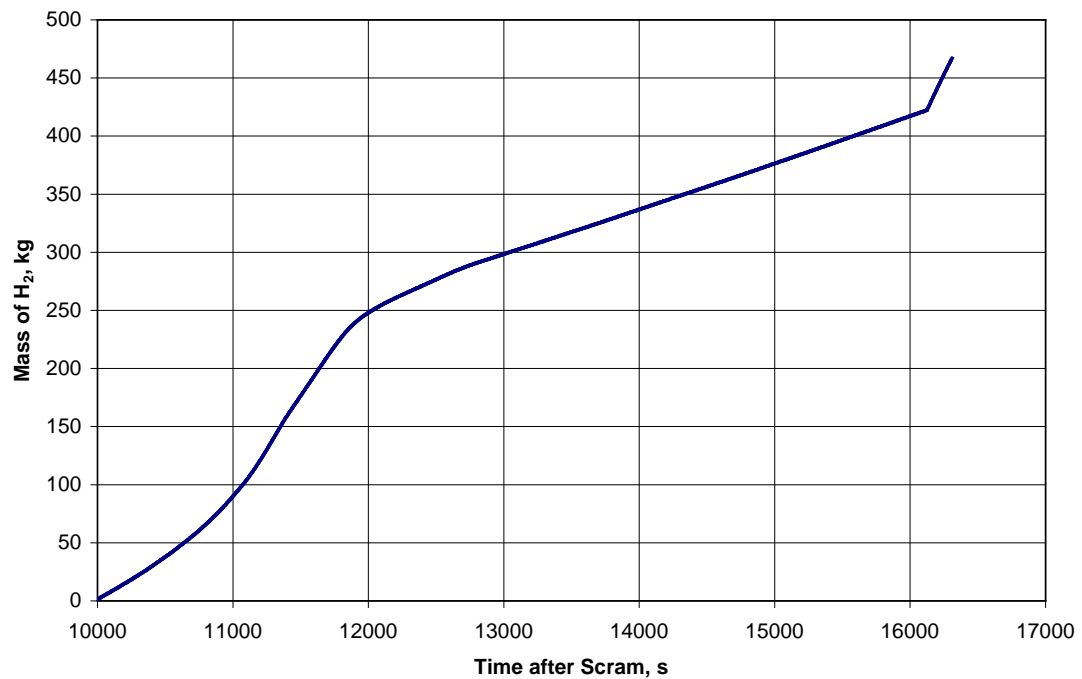
SUB-SECTION 16.2.2.4 – FIGURE 14

Mass of CO_2 generated by the MCCI in the reactor pit [Ref-1]
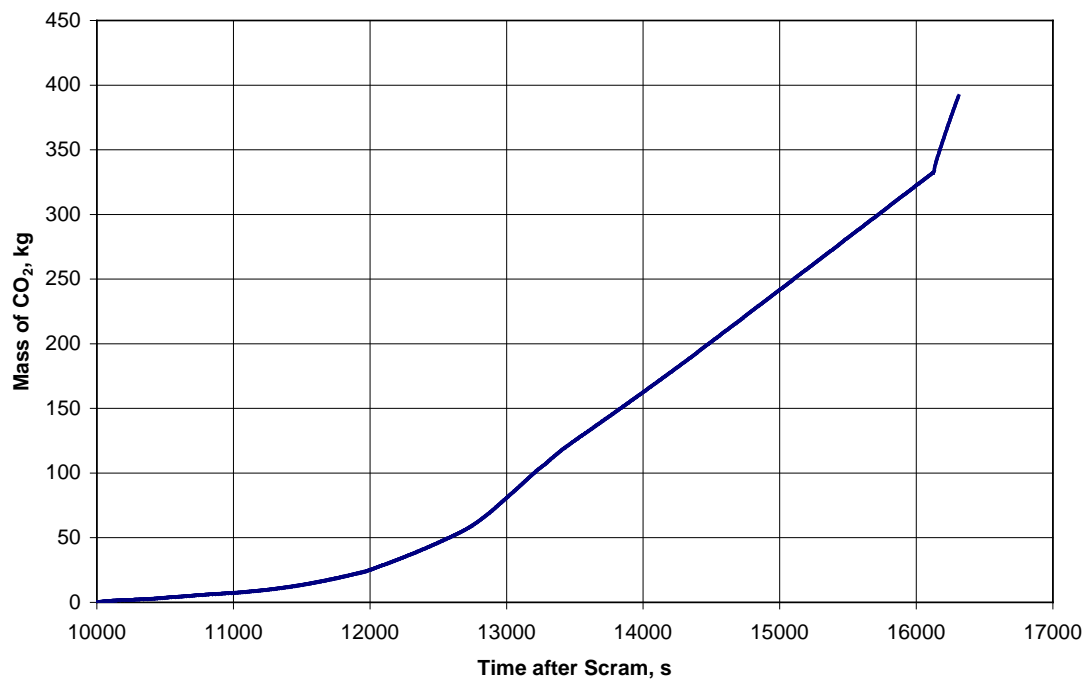
SUB-SECTION 16.2.2.4 – FIGURE 15

Mass of CO generated by the MCCI in the reactor pit [Ref-1]
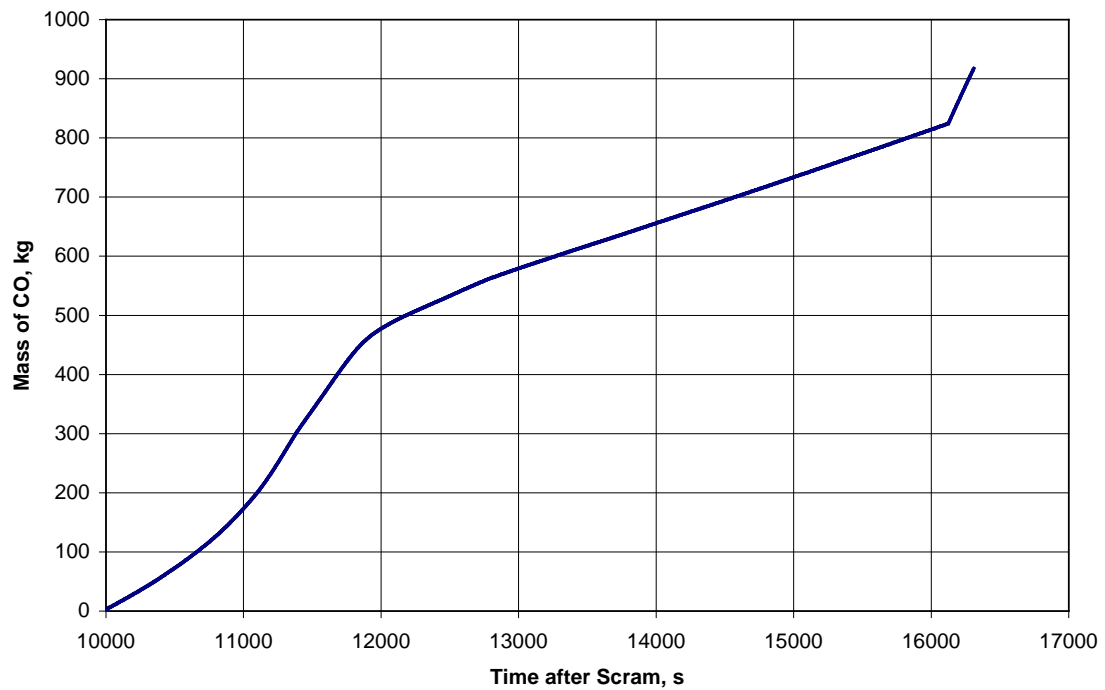
SUB-SECTION 16.2.2.4 – FIGURE 16

Release temperature of the gases generated by the MCCI in the reactor pit [Ref-1]
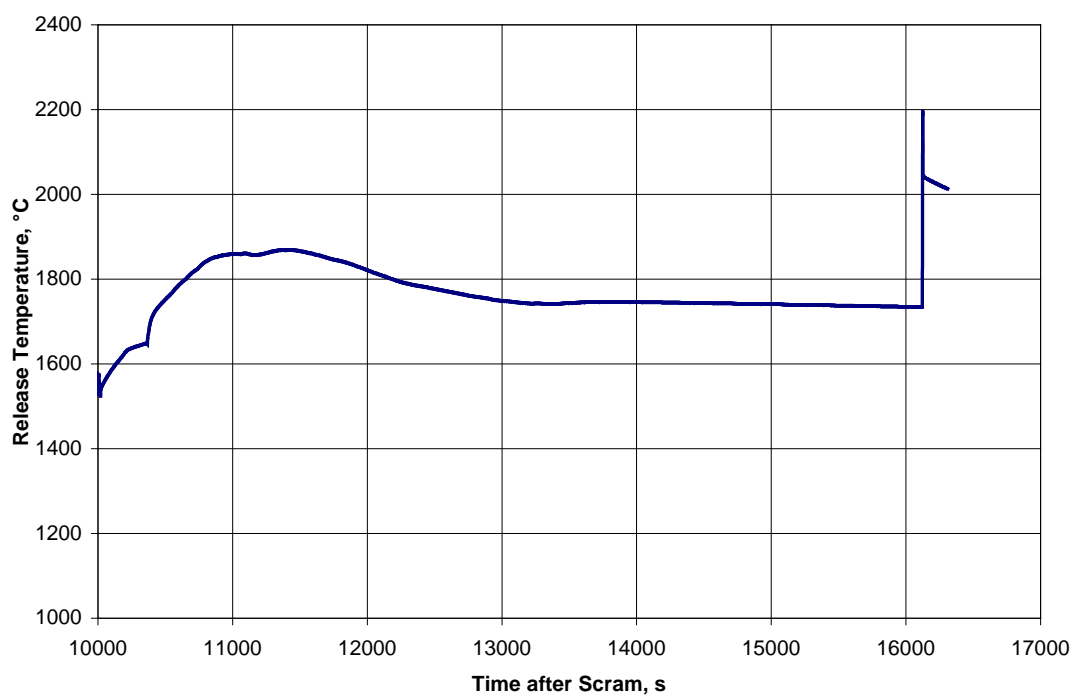
SUB-SECTION 16.2.2.4 – FIGURE 17

3D geometry model in Cartesian coordinates of the reactor pit, channel and core catcher (spreading compartment) [Ref-1]

UK EPR

PRE-CONSTRUCTION SAFETY REPORT

CHAPTER 16: RISK REDUCTION AND SEVERE ACCIDENT ANALYSES

SUB-CHAPTER : 16.2

PAGE   : 190 / 295

Document ID.No.
UKEPR-0002-162 Issue 05
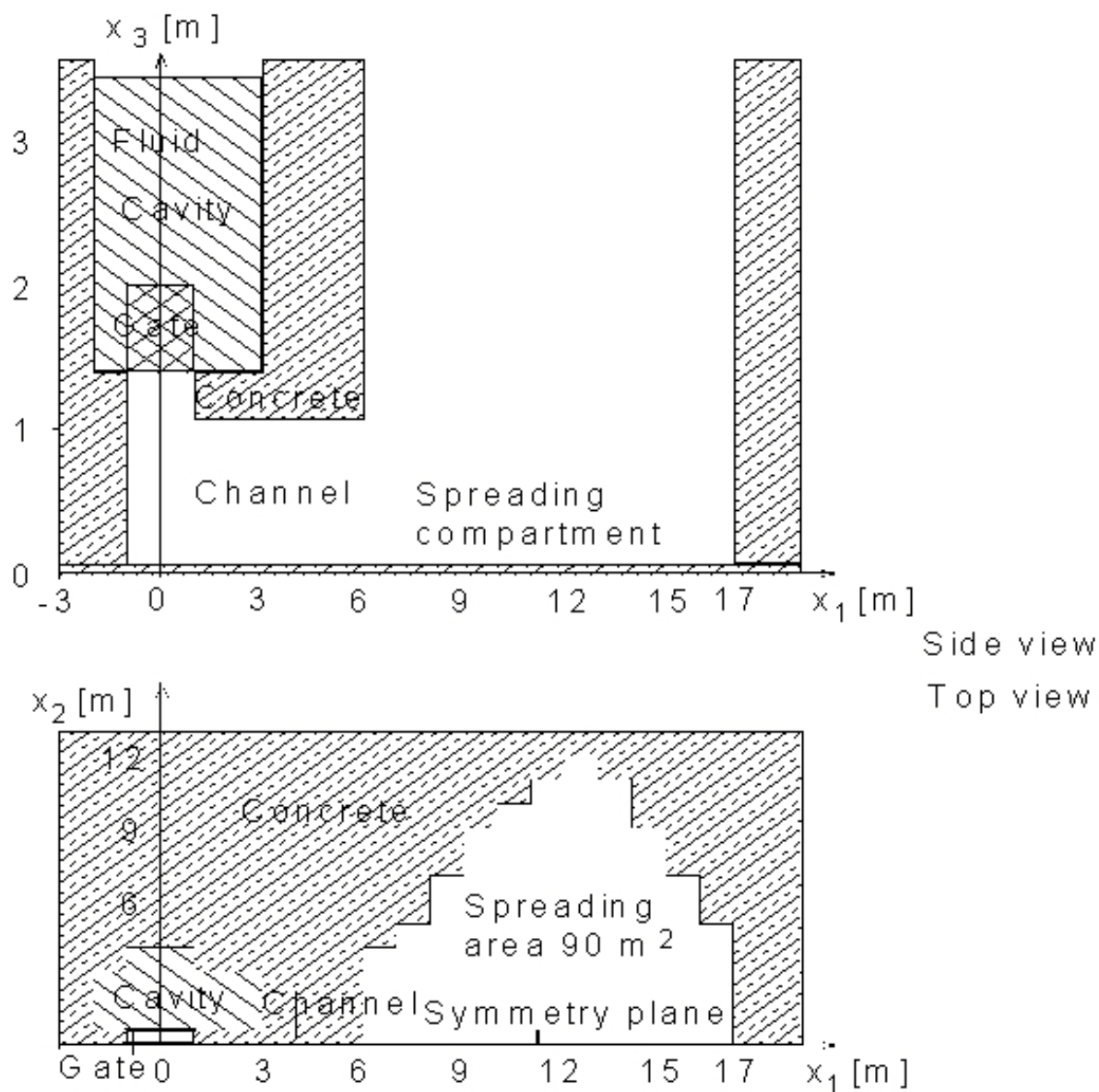
SUB-SECTION 16.2.2.4 – FIGURE 18

Schematic for the situation during passive melt cooling.

Equilibrium water levels in the pit and core catcher (spreading compartment) as a result of gravity-driven overflow from the IRWST [Ref-1][1]

---

[1] Previous revision

UK EPR

PRE-CONSTRUCTION SAFETY REPORT

CHAPTER 16: RISK REDUCTION AND SEVERE
ACCIDENT ANALYSES

SUB-CHAPTER : 16.2

PAGE   : 191 / 295

Document ID.No.
UKEPR-0002-162 Issue 05

SUB-SECTION 16.2.2.4 – FIGURE 19

Schematic for the situation during active melt cooling after injection of water by the CHRS [Ref-1] [Ref-2][2]
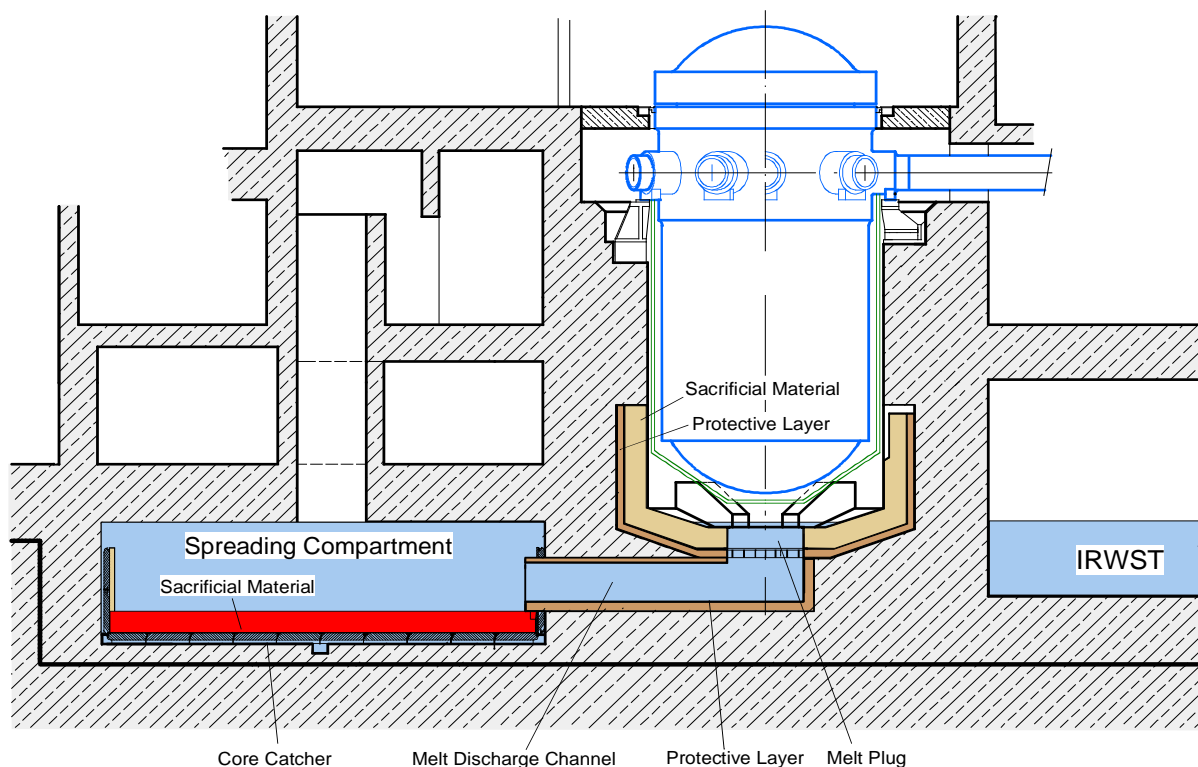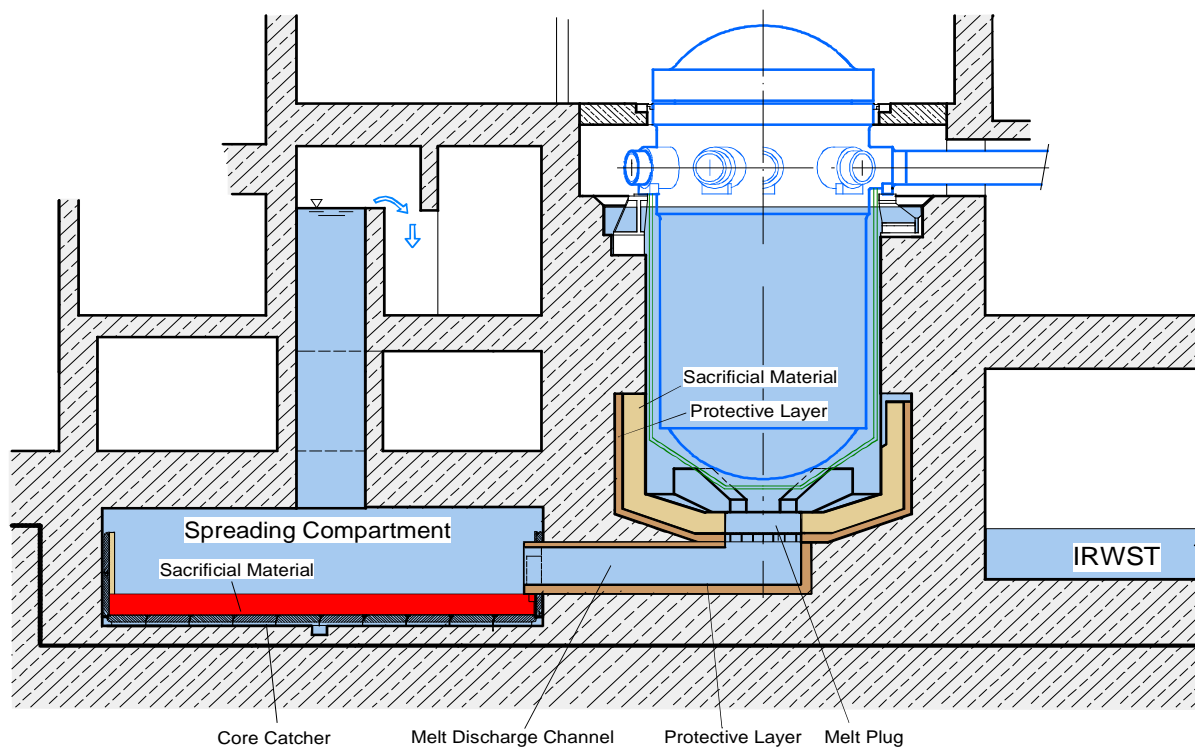
[2] Previous revision

SUB-SECTION 16.2.2.4 – FIGURE 20

Axial ablation front progression during MCCI in the core catcher (LB(LOCA) case) [Ref-1]
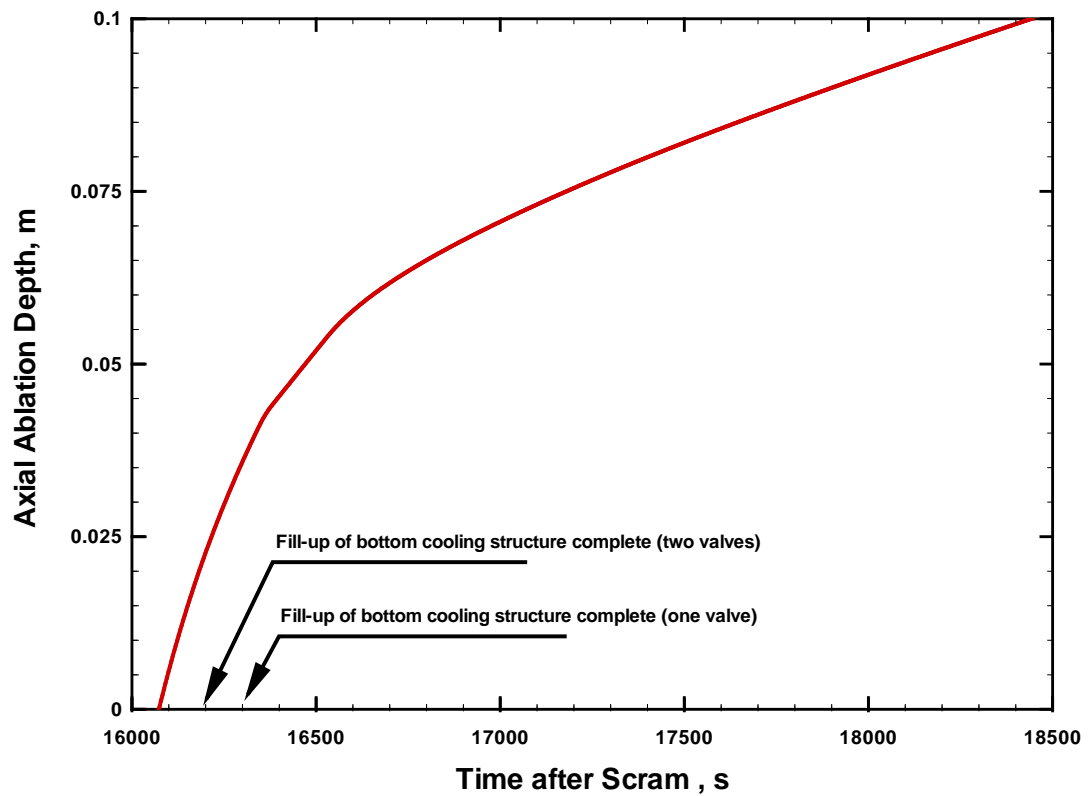
SUB-SECTION 16.2.2.4 – FIGURE 21

Time-dependent temperature evolution of the oxide and metal melt during MCCI in the core catcher [Ref-1]
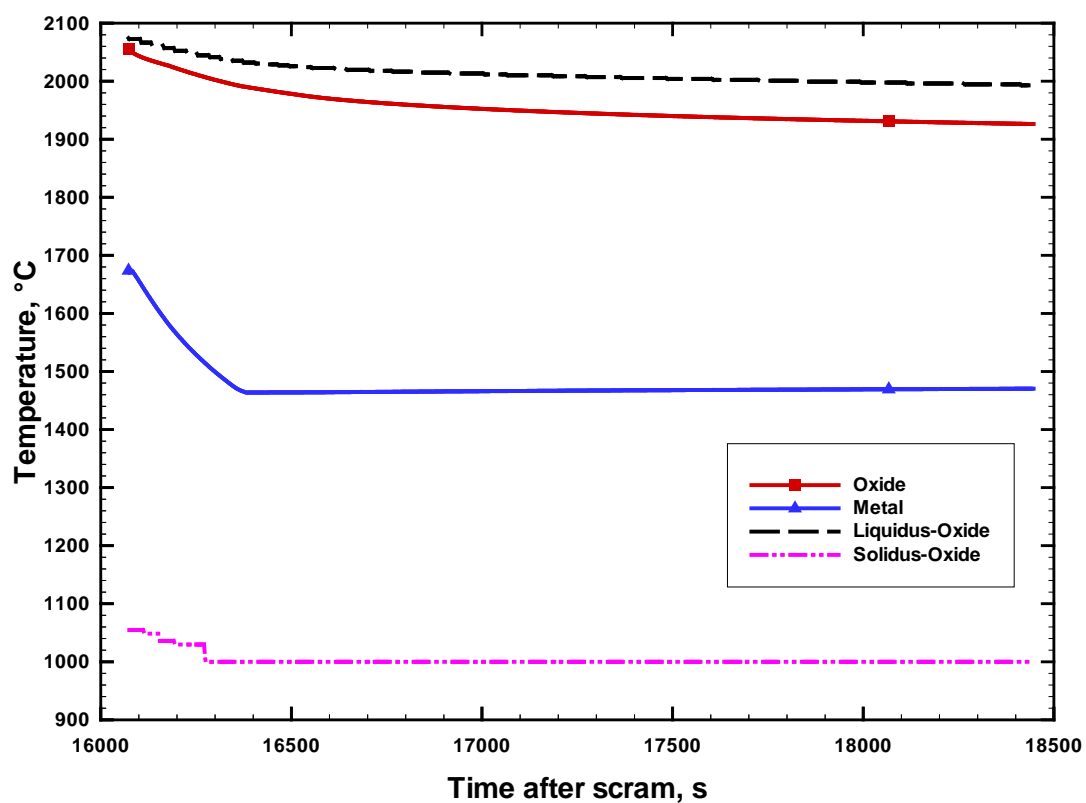
2.5. CONTAINMENT PRESSURE AND CONTAINMENT TEMPERATURE

Note: all pressures given in this section are absolute pressures.

2.5.1. Methods and basic assumptions for pressure and temperature calculations

2.5.1.1. Description of the scenarios

Three severe accident scenarios are studied:

- LB(LOCA) (double ended break of the surge line at the hot leg without safety injection).

- SB(LOCA) (5 cm diameter (20 cm²) leak at the cold leg with partial and fast secondary cooldown).

- LOOP (opening of the severe accident dedicated valves when core outlet gas temperature exceeds 650°C).

These scenarios were chosen as the reference cases for considering the temperature and pressure expected in the containment, particularly in the phase of corium spreading until operating the EVU [CHRS]. The analyses are based on representative initial and boundary conditions.

2.5.1.2. Pressure and temperature calculation code

The COCOSYS code (Appendix 16A) has been used for the pressure and temperature calculations in the containment. COCOSYS is based on mechanistic models for the comprehensive simulation of relevant processes and plant states during severe accidents. COCOSYS is a lumped parameter code that allows analysis of the local states (e.g. pressure, temperature, gas distribution) in the containment.

2.5.1.3. Determination of flow rates

The flow rate inputs for COCOSYS are generated with:

- MAAP-4 (Appendix 16A) for the in-vessel phase,

- COSACO (Appendix 16A) for MCCI in the reactor pit and core catcher.

20% core melt fragmentation is assumed during quenching in the core catcher [Ref-1]. This is important for the steam mass flow rate - see below for details.

For all scenarios a similar course of the ex-vessel phase is assumed:

- After vessel failure the core melt pours into the reactor pit and MCCI occurs. After consumption of the sacrificial concrete, the melt gate fails and the liquid core melt/concrete mixture flows down to the core catcher. Steam, hydrogen, CO_2 and CO are produced during MCCI in the reactor pit and released into the containment. Because of the high temperatures in the pit, an instantaneous combustion of the generated hydrogen and CO in a standing flame is assumed.

- Hydrogen, CO_2 and CO are produced during MCCI in the core catcher steam and released into the containment. Again, because of the high temperatures, an instantaneous combustion of the generated hydrogen and CO in a standing flame is assumed.

- Flooding of the core melt is triggered when the core melt arrives in the core catcher. After a time delay of 300 seconds, the quenching of the core melt starts using sub-cooled water from the IRWST. As a "best estimate" value a fragmentation of 20% of the over laying oxidic core melt layer is assumed. Because of the high heat fluxes in this phase, initially the whole water inflow of 100 kg/s is evaporated. This continues until the fragmented core melt has cooled down. Once this has happened, steam production ceases until the core catcher is filled with 450×10^3 kg of sub-cooled water which is heated up by the decay heat of the core melt. When this water reaches saturation, boiling starts and steam production occurs at a rate determined by the decay heat of the entire core melt. The water released as steam will be replaced by sub-cooled water from the IRWST.

In the long term, decay heat is used as an input for COCOSYS and the steaming rate is calculated by the code taking any time dependant properties into account, such as:

- IRWST water temperature,

- saturation temperature, (which is a function of the containment pressure),

- effective decay heat in the melt (accounting for fission product release from the melt).

The ex-vessel calculation is based on the assumption that MCCI and fragmentation in the spreading compartment occur simultaneously. Quenching proceeds from the sides of the core catcher to the centre. The rate of quenching is such that there is still no water on the surface of the melt in the centre at the end of MCCI.

The decay heat refers to a thermal power of 4500 MW(th) and is calculated using ORIGEN best-estimate values.

2.5.2. Containment data

2.5.2.1. Containment model for COCOSYS

The principle of the "lumped parameter" concept used in COCOSYS (Appendix 16A) consists of the subdividing a real building into a number of well defined zones connected by vent openings.

The basic assumptions are:

- Inside a zone there are no differences in the gas pressure, gas temperature and gas composition used for the determination of the thermodynamic state. Static pressure differences between zones are used to determine the mass flow through vent openings. All gases entering a zone become immediately homogeneously mixed.

- No counter-flow is possible through a vent opening.

- The governing flow paths must be modelled by a sufficient number of carefully arranged vent openings. Otherwise some flow paths existing in the real building could be suppressed, resulting in an artificial distortion of the flow field in the model.

- The boundaries of a zone are usually solid structures but may also be sub-divisions within the physical gas volume.

The "lumped parameter" concept allows the transient evolution of gas pressure, gas temperature and gas composition to be determined across the whole containment for different scenarios with reasonable accuracy in a reasonable time.

The key points related to the "lumped parameter" containment model are:

- use of best estimate data for volumes, structure surfaces, vent openings and material properties,

- limitation of the number of zones to that necessary to determine pressure and temperature in the important parts of the containment with the required accuracy,

- assignment of the zones to both the accessible and inaccessible parts of the containment ("two-room concept"),

- assignment of the zones of the SG and pump rooms such that each zone belongs to only one of the 4 loops to represent the effect of different break locations,

- where a physical volume is divided into several zones, the centre points of horizontally adjacent zones are at the same height level to avoid artificial gravity driven flows which can be an artefact of the lumped parameter model,

- important, well-defined rooms such as the reactor pit, cavity, IRWST and core catcher are explicitly modelled,

- modelling of the IRWST in two horizontal layers.

For the containment the "two-room concept" is used. The characteristic feature of this concept is that a large part of the containment is accessible to personnel during plant operation. This is an important advantage with respect to availability of the plant because maintenance measures inside the containment can be carried out at any time, without the need for a shutdown.

The accessible part of the containment includes zones Ac1 – Ac12 with a total volume of 63,800 m^3 (Sub-section 16.2.2.5 - Table 1) and marked in green in Sub-section 16.2.2.5 - Figure 1. The inaccessible part of the containment includes zones Eq1 – Eq18 (Sub-section 16.2.2.5 - Table 2) with a total volume of 16,200 m^3 and marked in orange in Figure 1.

The "two-room concept" imposes specific requirements on the ventilation system to maintain separation between accessible and inaccessible areas. These are realised by:

- permanent closure of the vents between SG compartments and annular compartments,

- closure of 4 vents between the accessible and inaccessible parts during normal plant operation by a system of rupture and convection foils and mixing dampers,

- provision of a combustible gas control system.

These vents open in the case of steam release from the leak or after quench tank disk rupture. The combustible gas control system and the opening conditions are described in section 5 of Sub-chapter 6.2. The rupture and convection foils are located between the upper SG rooms and the dome (Eq7-Ac7, Eq14-Ac7). The mixing dampers are located between IRWST and the lower annular rooms (Eq2-Ac1, Eq2-Ac2).

2.5.2.2. Boundary conditions

The total surface areas of the containment structures are taken to be [Ref-1]:

- Concrete structures: 43,300 m^2

- Steel structures: 24,600 m^2.

The steel liner covers the entire containment wall of 9,200 m^2. No gap between the liner and concrete is assumed. The results obtained remain valid even if a gap exists in a small part of the containment wall area (e.g. up to about 15%).

All structural surfaces, whether steel or concrete which are in contact with the containment atmosphere are protected by a paint layer of thickness 0.2 mm.

Typical material properties of the containment structures are listed in Sub-section 16.2.2.5 - Table 3.

The rupture and convection foils open completely in the case of a LB(LOCA) soon after the beginning of a steam release into the containment. In the case of SB(LOCA) and LOOP scenarios only the convection foils above the SG compartments open. The mixing dampers towards the IRWST open in all scenarios.

The arrangement of the recombiners in the containment is chosen in accordance with the hydrogen risk analyses performed using the CFD code GASFLOW, described in section 5 of Sub-chapter 6.2. The locations of the 41 large recombiners and 6 small recombiners are indicated in Sub-section 16.2.2.5 - Figure 1 by the symbol "Reco". The COCOSYS recombiner model takes into consideration hydrogen, CO and oxygen consumption and the connected heat, steam and CO_2 release to the containment. The recombination process starts automatically when the H_2 concentration rises above 2% by volume and stops when the H_2 concentration decreases below 0.5%.

After the start of cladding oxidation, the decay heat of volatiles is calculated according to the time dependent fission product distribution in the containment. Effects concerning settlement of aerosols on the walls, wash-down by condensate, transportation to the IRWST and aerosol re-suspension from the boiling sump in the spreading room are taken into account in this approach as they can influence pressure and temperature loads in the containment.

2.5.2.3. Initial conditions in the containment

The containment initial conditions are given in Sub-section 16.2.2.5 - Table 4. The initial structure temperatures are taken to be the same as the local gas temperature, and are taken as steady state.

2.5.3. LB(LOCA)

2.5.3.1. Time history and input data for the in-vessel phase

The LB(LOCA) scenario considered is defined as follows:

- double ended break of the surge line,

- partial secondary cooldown,

- no LHSI,

- no MHSI,

- accumulators available,

- opening of the severe accident dedicated valve when the maximum core outlet temperature exceeds 650°C.

The time history of key events for the in-vessel phase from MAAP-4.04 calculations is shown in Sub-section 16.2.2.5 - Table 5.

2.5.3.2. Time history and input data for the ex-vessel phase

The time history of key events for the ex-vessel phase is shown in Sub-section 16.2.2.5 - Table 6.

The RPV lower head fails at ~10,680 seconds and the core melt pours into the reactor pit. MCCI occurs and produces steam, hydrogen, CO_2 and CO which is released into the containment. The generation of these gases is modelled using COSACO. Because of the high temperatures in the pit, instantaneous combustion of the generated hydrogen and CO by in a standing flame is assumed.

At ~17,500 seconds, the melt gate fails and the liquid core melt/concrete mixture flows down into the core catcher. Further MCCI occurs there until all the sacrificial concrete is consumed at ~22,600 seconds. During the MCCI in the core catcher steam, hydrogen, CO_2 and CO are produced and released into the containment. As before, the generation of these gases is modelled using COSACO. Again, because of the high temperatures in the core catcher, instantaneous combustion of the generated hydrogen and CO in a standing flame is assumed.

UK EPR

PRE-CONSTRUCTION SAFETY REPORT

CHAPTER 16: RISK REDUCTION AND SEVERE
ACCIDENT ANALYSES

SUB-CHAPTER : 16.2

PAGE   : 199 / 295

Document ID.No.
UKEPR-0002-162 Issue 05

2.5.3.3. Results of the COCOSYS calculation

2.5.3.3.1. Containment pressure

The pressure time history for the LB(LOCA) case without EVU [CHRS] is shown in Sub-section 16.2.2.5 - Figure 2a and with activation of two EVU [CHRS] trains after 12.4 hours in Sub-section 16.2.2.5 - Figure 2b.

The relevant phases are:

- First pressure peak at the beginning of the event during blow-down and subsequent pressure decrease due to strongly decreasing steam and water release.

- Small pressure peak after core relocation (~7,400 seconds).

- Ex-vessel phase with MCCI in the reactor pit after initial vessel failure from ~10,680 seconds – 17,500 seconds.

- At ~17,300 seconds, a large hydrogen release due to the layer inversion in the core melt in the pit. The subsequent combustion leads to increase in containment pressure.

- The quenching of the core melt in the core catcher (starting at ~17,800 seconds) causes a significant pressure peak because of the (assumed) high steam production rate of 100 kg/s until ~19,300 seconds.

- Pressure decrease due to the cessation of steam production during the filling of the core catcher with sub-cooled water from the IRWST (from ~19,300 seconds – 25,000 seconds).

- Continuation of pressure decrease in the containment during the heat-up of the water inventory in the core catcher (without steam production) until saturation is reached at ~33,000 seconds.

- Long term pressure increase after commencement of boiling and subsequent steam production due to the decay heat of the core melt.

- In the case of activation of two trains of the EVU [CHRS] after 12.4 hours, the pressure decreases immediately.

The pressure development with and without activation of the EVU [CHRS] is summarised in Sub-section 16.2.2.5 - Table 7.

After blow down, the local pressure differences in the containment are very small in relation to the absolute pressure.

In the case of activation of two EVU [CHRS] trains after 12.4 hours, the containment pressure remains well below 5.5 bar. The long term pressure is below 2 bar and decreases steadily.

2.5.3.3.2. Containment temperature

The local gas temperature distribution in the containment is very inhomogeneous until ~30,000 seconds (Sub-section 16.2.2.5 - Figures 3a and 3b). During hydrogen combustion, the temperature peak is highest in the upper equipment compartments, i.e. zone Eq14. Later on, in the long term steaming phase, the temperature differences are reduced significantly.

In Sub-section 16.2.2.5 - Figure 3b, the temperature history is shown for the case with activation of 2 EVU [CHRS] trains after 12.4 hours (~44,700 seconds). After this, the temperature decreases in contrast to the behaviour without EVU [CHRS]. The temperatures in the inaccessible part of the containment eventually become higher than in the dome.

Sub-section 16.2.2.5 - Figures 4a, 4b show the liner surface temperature for the dome (zone Ac7) and a lower annular compartment (zone Ac4) with and without activation of 2 EVU [CHRS] trains with respect to the gas temperature. The liner temperature remains below 150°C. After activation of the EVU [CHRS], the temperature decreases continually, going below 100°C at ~57,000 seconds.

The liner temperature in the annular compartment Ac4 remains below the liner temperature in the dome in the case without activation of the EVU [CHRS]. After activation of the EVU [CHRS] the gas and liner temperatures equalise very quickly below 100°C (see Sub-section 16.2.2.5 - Table 8).

The IRWST water temperature and the saturation temperature (with respect to the containment pressure) are shown in Sub-section 16.2.2.5 - Figures 5a, 5b. The IRWST water, which is fed into the core catcher in the long term steaming phase, is significantly sub-cooled. The sub-cooling for the bottom water layer remains > 50°C without activation of the EVU [CHRS]. In the case with two EVU [CHRS] trains in operation, the sub-cooling is reduced to 20°C. This reduction in the sub-cooling margin results from both the higher IRWST water temperature and the lower saturation temperature (because of the lower containment pressure). The temperature of the surface water layer is closer to the saturation temperature when there is no activation of the EVU [CHRS].

2.5.3.3.3. Containment humidity

The local humidity distribution in the containment is very inhomogeneous (Sub-section 16.2.2.5 - Figures 6a and 6b). Later on, in the long term steaming phase, the humidity differences reduce with time. With the exception of the first phase of strong steam release after LOCA, the containment atmosphere remains in the superheated state everywhere in the containment without activation of the EVU [CHRS]. Even in the case with activation of the EVU [CHRS] (2 trains) after 12.4 hours, the lower equipment rooms remain superheated while the dome achieves a saturated state.

2.5.4. SB(LOCA)

2.5.4.1. Time history and input data for the in-vessel phase

The SB(LOCA) scenario considered is defined as follows:

- 5 cm diameter (20 cm²) SB(LOCA) in a cold leg,

- four steam generators fed by AFW,

- partial secondary cooldown with four SG initiated at RIS [SIS] signal for 20 minutes,

- fast secondary cooldown with four SG initiated 30 minutes after reactor scram,

- no opening by the normal PZR bleed valves,

- opening of the severe accident dedicated valve when maximum core outlet gas temperature exceeds 650°C,

- no LHSI,

- no MHSI,

- accumulators available.

The time history of key events for the in-vessel phase is shown in Sub-section 16.2.2.5 - Table 9 from MAAP-4.04 calculations.

2.5.4.2. Time history and input data for the ex-vessel phase

The time history of key events for the ex-vessel phase is given in Sub-section 16.2.2.5 – Table 10.

After vessel failure at ~168,700 seconds the core melt pours into the reactor pit and MCCI begins. Steam, hydrogen, CO_2 and CO are produced and released into the containment. The generation of these gases is modelled using COSACO. Because of the high temperatures in the pit, instantaneous combustion of the generated hydrogen and CO in a standing flame is assumed.

At ~180,200 seconds, the melt gate fails and the liquid core melt/concrete mixture flows down into the core catcher. During MCCI in the core catcher, steam, hydrogen, CO_2 and CO are produced and released into the containment. Again, the generation of these gases is modelled using COSACO. Because of the high temperatures in the core catcher, instantaneous combustion of the generated hydrogen and CO in a standing flame is assumed.

The activation of two EVU [CHRS] trains is considered at ~188,400 seconds (12 hours after the core outlet temperature reaches 650°C).

MCCI continues in the core catcher until all sacrificial concrete is consumed at ~188,600 seconds.

2.5.4.3. Results of the COCOSYS calculation

2.5.4.3.1. Containment pressure

The pressure time history for the SB(LOCA) case is shown in Sub-section 16.2.2.5 - Figure 7.

The relevant phases are:

- First pressure peak at the beginning of the event (1.45 bar at 1800 seconds). Subsequently, the pressure decreases due to strongly decreasing steam and water release.

- Second pressure increase due to the release from the leak after ~135,000 seconds.

- Occurrence of a short pressure peak of 1.6 bar after quench tank disk rupture (~167,000 seconds).

- Ex-vessel phase with MCCI in the reactor pit after initial vessel failure from ~168,700 seconds – ~180,200 seconds.

- Core melt quenching in the core catcher (starting at ~180,500 seconds) causes a significant pressure peak (3.6 bar at ~181,800 seconds) because of the (assumed) high steam production rate of 100 kg/s.

- Pressure decrease due to cessation of steam production during the filling of the core catcher (from ~181,800 seconds – 185,000 seconds).

- Continuation of pressure decrease in the containment during the heat-up of the water inventory in the core catcher (without steam production).

- Enhanced pressure decrease after start of two trains of the EVU [CHRS] at ~188,400 seconds.

- Beginning of steam production in the core catcher due to the decay heat of the core melt at ~202,000 seconds. Pressure rises to 1.4 bar.

- Long term rate of pressure decrease is 0.002 bar/hour.

At all times, the pressure remains well below the design pressure (5.5 bar), see Sub-section 16.2.2.5 - Table 11.

The local pressure differences in the containment are very small in relation to the absolute pressure.

2.5.4.3.2. Containment temperature

In the first ~135,000 seconds the local gas temperature distribution in the containment is fairly homogeneous (Sub-section 16.2.2.5 - Figure 8). During the second leak release, quench tank disk rupture and core melt quenching phases (i.e. ~140,000 seconds – 200,000 seconds), large local temperature differences arise in the containment. Later on, in the long term steaming phase, the temperature differences reduce to small values (< 15°C).

Sub-section 16.2.2.5 - Figure 9 shows the liner surface temperatures for the dome (zone Ac7) and a lower annular compartment (zone Ac4) with respect to the gas temperature. For most or the transient, the liner temperature remains below 80°C. During core melt quenching the temperature peaks briefly at 125°C.

The IRWST water temperature and the saturation temperature (with respect to the containment pressure) are shown in Sub-section 16.2.2.5 - Figure 10. The IRWST water, which is fed into the core catcher in the long term steaming phase, is significantly sub-cooled in both water layers. Sub-cooling decreases from 50°C in the in-vessel phase of 0 seconds – 168,700 seconds to 40°C in the long term (ex-vessel phase).

2.5.4.3.3. Containment humidity

In the first ~145,000 seconds, the local humidity distribution in the containment is fairly homogeneous at about 100% in the whole containment, see Sub-section 16.2.2.5 - Figure 11. During the second release, quench tank disk rupture and core melt quenching phases (i.e. ~140,000 seconds – 200,000 seconds), there are significant differences in local humidity. Later on, in the long-term steaming phase, the humidity differences reduce and eventually saturation is reached everywhere in the containment.

2.5.5. LOOP

2.5.5.1. Time history and input data for the in-vessel phase

The LOOP scenario with loss of all 6 diesels is defined as follows:

- loss of Main Feedwater System (ARE [MFWS]),

- closure of Main Steam Isolation Valves (VIV [MSIV]),

- loss of Startup and Shutdown System (AAD [SSS]),

- opening of the severe accident dedicated valves when maximum core outlet gas temperature exceeds 650°C,

- accumulators available,

- availability of power latest after 12 hours.

The time history of key events for the in-vessel phase is shown in Sub-section 16.2.2.5 – Table 12 from MAAP-4.04 calculations.

2.5.5.2. Time history and input data for the ex-vessel phase

The time history of key events for the ex-vessel phase is given in Sub-section 16.2.2.5 – Table 13.

After vessel failure at ~30,360 seconds the core melt pours into the reactor pit and MCCI occurs. Steam, hydrogen, CO_2 and CO are produced and released into the containment. The generation of these gases is modelled using COSACO. Because of the high temperatures in the pit, instantaneous combustion of the generated hydrogen and carbon monoxide in a standing flame is assumed.

At ~38,400 seconds the melt gate fails and the liquid core melt/concrete mixture flows down into the core catcher. MCCI occurs there in which steam, hydrogen, CO_2 and CO are produced and released into the containment. Again, the generation of these gases is modelled using COSACO. Because of the high temperatures in the core catcher, instantaneous combustion of the generated hydrogen and carbon monoxide in a standing flame is assumed. MCCI continues until all sacrificial concrete is consumed at ~44,300 seconds.

The activation of two EVU [CHRS] trains is considered at ~54,600 seconds (12 hours after the core outlet temperature reaches 650°C).

2.5.5.3. Results of COCOSYS calculation

2.5.5.3.1. Containment pressure

The pressure time history for the LOOP case is shown in Sub-section 16.2.2.5 - Figure 12.

The relevant phases are:

- First pressure increase due to release from the quench tank (2.6 bar at ~12,000 seconds). Subsequently the pressure decreases due to reduced steam release.

- Core melt quenching in the core catcher (starting at ~38,700 seconds) causes a significant pressure peak (4.7 bar at ~40,100 seconds) because of the (assumed) high steam production rate of 100 kg/s.

- Pressure decrease due to the cessation of steam production during the filling of the spreading room (from ~40,100 seconds – 45,000 seconds).

- Continuation of pressure decrease in the containment during the heat-up of the water inventory in the core catcher (without steam production) until saturation (with respect to the actual containment pressure) is reached at ~55,000 seconds.

- Enhanced pressure decrease after the start of two trains of the EVU [CHRS] at ~54,600 seconds.

- After the beginning of steam production in the core catcher, due to the decay heat of the core melt (at ~55,000 seconds), the rate of pressure decrease is reduced to 0.01 bar/hour at ~100,000 seconds.

The pressure remains well below 5.5 bar at all times. See Sub-section 16.2.2.5 - Table 14.

2.5.5.3.2. Containment temperature

Very significant local temperature differences arise in the containment (Sub-section 16.2.2.5 - Figure 13) during rapid steam releases. Later on, in the long term steaming phase, the temperature differences are reduced to small values (< 15°C).

Sub-section 16.2.2.5 - Figure 14 shows the liner surface temperature for the dome (zone Ac7) and a lower annular compartment (zone Ac4) with respect to the gas temperature. The liner temperatures remain below 150°C, with the exception of a short period after core melt quenching.

The IRWST water temperature of the surface layer, the bottom layer and the saturation temperature (with respect to the containment pressure) are shown in Sub-section 16.2.2.5 - Figure 15. The IRWST water coming from the bottom layer, which is fed into the core catcher in the long term steaming phase is significantly sub-cooled. The sub-cooling decreases from 80°C at ~20,000 seconds to 25°C at ~100,000 seconds.

2.5.5.3.3. Containment humidity

Large local humidity differences arise in the containment (see Sub-section 16.2.2.5 - Figure 16) until start of EVU [CHRS]. After this, the accessible rooms become saturated very quickly and the humidity in the equipment rooms increases. Later on, in the long term steaming phase, the equipment rooms are in a saturated state or close to saturation.

2.5.6. Conclusion

Three representative scenarios that may cause pressurisation of the containment after a severe accident have been analysed:

- A LB(LOCA) scenario that leads to early and fast pressurisation.

- A SB(LOCA) scenario with fast secondary cooldown, where heat is transferred to the SG for a long period of time, and pressurisation of the containment starts only after 40 hours.

- A LOOP scenario with steam release through the RPT (reactor pressure tank) and transient pressurisation between the above mentioned scenarios.

In all three severe accident scenarios analysed the containment pressure remains clearly below the containment design pressure of 5.5 bar.

High gas temperature occurs only for short time (during MCCI and during the quenching phase in the reactor pit and in the spreading room) in a few containment regions.

In all cases the water in the IRWST remains clearly below 150°C in the upper layer and below 100°C in the lower pool layer.

SUB-SECTION 16.2.2.5 - TABLE 1

Basic containment model - accessible zones [Ref-1]

Zone			Volume
Description	Name	No	[m³]
Lower annular rooms Loop 1&2	Ac1	19	650
Lower annular rooms Loop 3&4	Ac2	20	650
Middle annular rooms Loop 1&2	Ac3	21	5300
Middle annular rooms Loop 3&4	Ac4	22	5100
Upper annular rooms Loop 1&2	Ac5	23	2300
Upper annular rooms Loop 3&4	Ac6	24	1850
Dome	Ac7	25	45800
Access	Ac8	26	550
Staircase south	Ac9	27	400
Staircase north	Ac10	28	400
Elevator	Ac11	29	150
Hot piping	Ac12	30	650
Sum accessible zones	**Ac1-Ac12**		**63800**

SUB-SECTION 16.2.2.5 - TABLE 2

Basic containment model - inaccessible zones [Ref-1]

Zone			Volume
Description	Name	No	[m³]
Spreading room	Eq1	1	570
IRWST	Eq2	2	1660 (+1800 water)
Lower equipment rooms Loop 1 (pump & steam generator)	Eq3	3	740
Lower equipment rooms Loop 2 (pump & steam generator)	Eq4	4	700
Middle equipment rooms Loop 1	Eq5	5	1150
Middle equipment rooms Loop 2	Eq6	6	1120
Upper equipment rooms Loops 1&2	Eq7	7	1070
Reactor pit	Eq8	8	90
Reactor cavity	Eq9	9	1470
Lower equipment rooms Loop 3 (pump & steam generator)	Eq10	10	700
Lower equipment rooms Loop 4 (pump & steam generator)	Eq11	11	740
Middle equipment rooms Loop 3	Eq12	12	1020
Middle equipment rooms Loop 4	Eq13	13	1190
Upper equipment rooms Loops 1&2	Eq14	14	1070
Surge line	Eq15	15	1180
Pressuriser	Eq16	16	550
Components	Eq17	17	820
LCQ Heat exchanger etc.	Eq18	18	360
Sum inaccessible zones	**Eq1-Eq18**		**16200 (+1800 water)**

SUB-SECTION 16.2.2.5 - TABLE 3

Properties of containment materials [Ref-2]

Property		Steel, ferritic (containment structure)	Steel, austenitic (liner)	Concrete	Paint
Heat conductivity	W/mK	45	15	2	0.2
Density	kg/m^3	7850	7920	2400	1200
Specific heat c_p	J/kgK	500	512	960	1675

SUB-SECTION 16.2.2.5 - TABLE 4

Containment initial conditions [Ref-2]

State		Accessible part Zones Ac1 - Ac9	Inaccessible part Zones Eq1 – Eq18
Pressure P	bar	1.011	1.011
Gas temperature T	°C	30	42
Humidity	%	50	50

SUB-SECTION 16.2.2.5 - TABLE 5

LB(LOCA) sequence of events for in-vessel phase

(Data inferred from the information given in section 2.1)

KEY EVENTS	TIME	
Break in the hot leg	0 h 00 min	0 s
Reactor scram	0 h 00 min	< 60 s
Reactor coolant pump coast-down	0 h 00 min	< 60 s
Start of partial cooldown	0 h 00 min	< 60 s
Start of core uncovery	0 h 01 min	60 s
Accumulator water injection	0 h 02 min	120 s
Accumulator water depletion	0 h 03 min	180 s
SA dedicated valve opening	0 h 25 min	1500 s
Start of core oxidation	0 h 26 min	1560 s
Start of core melting	0 h 29 min	1740 s
Start of core relocation	2 h 03 min	7380 s
Initial vessel failure	2 h 58 min	10680 s

SUB-SECTION 16.2.2.5 - TABLE 6

LB(LOCA) sequence of events for ex-vessel phase [Ref-3]

LOCATION	KEY EVENTS	TIME	
Reactor pit	Start of MCCI in the reactor pit after initial vessel failure	2 h 58 min	10680 s
	End of MCCI in reactor pit	4 h 51 min 40 s	17500 s
Core catcher	Arrival of the melt in the core catcher		
	Initiation of flooding of bottom cooling system		
	Start of core melt quenching in the core catcher (time delay 300 s) with steam production of 100 kg/s	4 h 56 min 40 s	17800 s
	End of MCCI in core catcher (sacrificial concrete is consumed)	6 h 16 min 40 s	22600 s
	End of steam production due to core melt quenching	5 h 21 min 40 s	19300 s
	Start of filling of the core catcher with sub-cooled water from the IRWST		
	End of fill–up phase (water inventory of 450 x 10³ kg reached)	6 h 56 min 40 s	25000 s
	Start of boiling and steam production due to decay heat	8 h 53 min 20 s	33000 s

SUB-CHAPTER : 16.2

PRE-CONSTRUCTION SAFETY REPORT

PAGE : 212 / 295

UK EPR

CHAPTER 16: RISK REDUCTION AND SEVERE
ACCIDENT ANALYSES

Document ID.No.
UKEPR-0002-162 Issue 05

SUB-SECTION 16.2.2.5 - TABLE 7

LB(LOCA) pressure of selected times

(Data derived from the analysis results presented in
Sub-section 16.2.2.5 – Figures 2, 7 and 12)

	Time [s]	Pressure with EVU [CHRS] (2 trains) [bar]	Pressure without EVU [CHRS] [bar]
Blowdown pressure peak	100	3.5	3.5
Pressure at end of in-vessel phase	10680	2.2	2.2
Quench peak (flooding of core melt in core catcher)	19300	4.8	4.8
Pressure decrease until boiling starts in the core catcher	33000	2.6	2.6
Pressure at start of EVU [CHRS] operation	44700	3.4	3.4
Pressure after 22.2 hours	80000	2.0	4.7
Pressure increase rate at 22.2 hours	80000	-0.02 [bar/h]	0.12 [bar/h]

SUB-SECTION 16.2.2.5 - TABLE 8

Maximum liner surface temperature

MAXIMUM LINER SURFACE TEMPERATURE [°C]			
Quench Peak (19300 s)		Start of EVU [CHRS] (44700 s)	
Zone Ac4	Zone Ac7	Zone Ac4	Zone Ac7
130	140	120	130

SUB-SECTION 16.2.2.5 - TABLE 9

SB(LOCA) sequence of events for in-vessel phase

(Data inferred from the information given in section 2.1)

KEY EVENTS	TIME	
Reactor scram	0 h 00 min	120 s
Start of Partial Cooldown	0 h 04 min	240 s
Reactor Coolant Pump run down	0 h 09 min	540 s
Start of Fast Cooldown	0 h 31 min	1860 s
Accumulator injection start	0 h 32 min	1900 s
Accumulator water depletion	0 h 33 min	1980 s
Core uncovery	39 h 17 min	141420 s
Onset of oxidation	40 h 50 min	147000 s
SA dedicated PZR valve opening	40 h 20 min	145200 s
Start of core melting	40 h 56 min	147360 s
Start of core relocation to lower head	46 h 12 min	166320 s
RPV failure	46 h 52 min	168700 s

UK EPR

PRE-CONSTRUCTION SAFETY REPORT

CHAPTER 16: RISK REDUCTION AND SEVERE ACCIDENT ANALYSES

SUB-CHAPTER : 16.2

PAGE   : 215 / 295

Document ID.No.
UKEPR-0002-162 Issue 05

SUB-SECTION 16.2.2.5 - TABLE 10

SB(LOCA) sequence of events for ex-vessel phase [Ref-3]

LOCATION	KEY EVENTS	TIME	
Reactor pit	Start of MCCI in the reactor pit after initial vessel failure	46 h 51 min	168700 s
	End of MCCI in reactor pit		
Core catcher	Arrival of the melt in the core catcher	50 h 03 min	180200 s
	Initiation of flooding of bottom cooling system		
	Start of core melt quenching in the core catcher (time delay 300 s) with steam production of 100 kg/s	50 h 08 min	180500 s
	End of MCCI in core catcher (sacrificial concrete is consumed)	52 h 23 min	188600 s
	End of steam production due to core melt quenching	50 h 30 min	181800 s
	Start of filling of the core catcher with sub-cooled water from the IRWST		
	End of fill–up phase (water inventory of 450·x10^3 kg reached)	51 h 23 min	185000 s
	Start of boiling and steam production due to decay heat	56 h 06 min	202000 s

SUB-SECTION 16.2.2.5 - TABLE 11

SB(LOCA) pressure of selected times

(Data derived from the analysis results presented in
Sub-section 16.2.2.5 - Figures 2, 7 and 12)

	Time [s]	Pressure with EVU [CHRS] (2 trains) [bar]
Break pressure peak	1800	1.45
Maximum pressure until end of in-vessel phase	< 168700	1.5
Quench peak (flooding of core melt in core catcher)	181800	3.6
Pressure at start of EVU [CHRS] operation	188400	2.2
Pressure decrease until boiling starts in the core catcher	202000	1.1
Pressure after 3.5 days	300000	1.4
Pressure increase rate at 3.5 days	300000	-0.002 [bar/h]

SUB-SECTION 16.2.2.5 - TABLE 12

LOOP sequence of events for in-vessel phase

(Data inferred from the information given in section 2.1)

KEY EVENTS	TIME	
Reactor Coolant Pump run down	0 h 00 min	0 s
Reactor scram	0 h 00 min	0 s
Affected SG dry	2 h 06 min	7560 s
Quench tank disk rupture	2 h 12 min	7920 s
Core uncovery	2 h 55 min	10500 s
Accumulator injection start	3 h 19 min	11940 s
Accumulator depletion	3 h 31 min	12660 s
SA dedicated PZR valve opening	3 h 10 min	11400 s
Onset of oxidation	4 h 33 min	16380 s
Start of core melting	4 h 41 min	16860 s
Start of core relocation to lower head	7 h 23 min	26580 s
RPV failure	8 h 26 min	30360 s

SUB-SECTION 16.2.2.5 - TABLE 13

LOOP sequence of events for ex-vessel phase [Ref-3]

CONCERNED LOCATION	KEY EVENTS	TIME	
Reactor pit	Start of MCCI in the reactor pit after initial vessel failure	8 h 26 min	30360 s
	End of MCCI in reactor pit		
Core catcher	Arrival of the melt in the core catcher	10 h 40 min	38400 s
	Initiation of flooding of bottom cooling system		
	Start of core melt quenching in the core catcher (time delay 300 s) with steam production of 100 kg/s	10 h 45 min	38700 s
	End of MCCI in core catcher (sacrificial concrete is consumed)	12 h 18 min	44300 s
	End of steam production due to core melt quenching	11 h 08 min	40100 s
	Start of filling of the core catcher with sub-cooled water from the IRWST		
	End of fill–up phase (water inventory of 450×10^3 kg reached)	12 h 30 min	45000 s
	Start of boiling and steam production due to decay heat	15 h 16 min	55000 s

SUB-SECTION 16.2.2.5 - TABLE 14

LOOP pressure of selected times

(Data derived from the analysis results presented in
Sub-section 16.2.2.5 - Figures 2, 7 and 12)

	Time [s]	Pressure with EVU [CHRS] (2 trains) [bar]
Pressure peak due to release from quench tank	12000	2.6
Pressure at end of in-vessel phase	30360	2.2
Quench peak (flooding of core melt in core catcher)	40100	4.7
Pressure decrease until boiling starts in the core catcher	55000	2.3
Pressure at start of EVU [CHRS] operation	54600	2.6
Pressure after 1.2 days	100000	1.8
Pressure rate of increase at 1.2 days	100000	-0.01 [bar/h]

UK EPR

PRE-CONSTRUCTION SAFETY REPORT

CHAPTER 16: RISK REDUCTION AND SEVERE
ACCIDENT ANALYSES

SUB-CHAPTER : 16.2

PAGE   : 220 / 295

Document ID.No.
UKEPR-0002-162 Issue 05

SUB-SECTION 16.2.2.5 - FIGURE 1

EPR containment model [Ref-1]
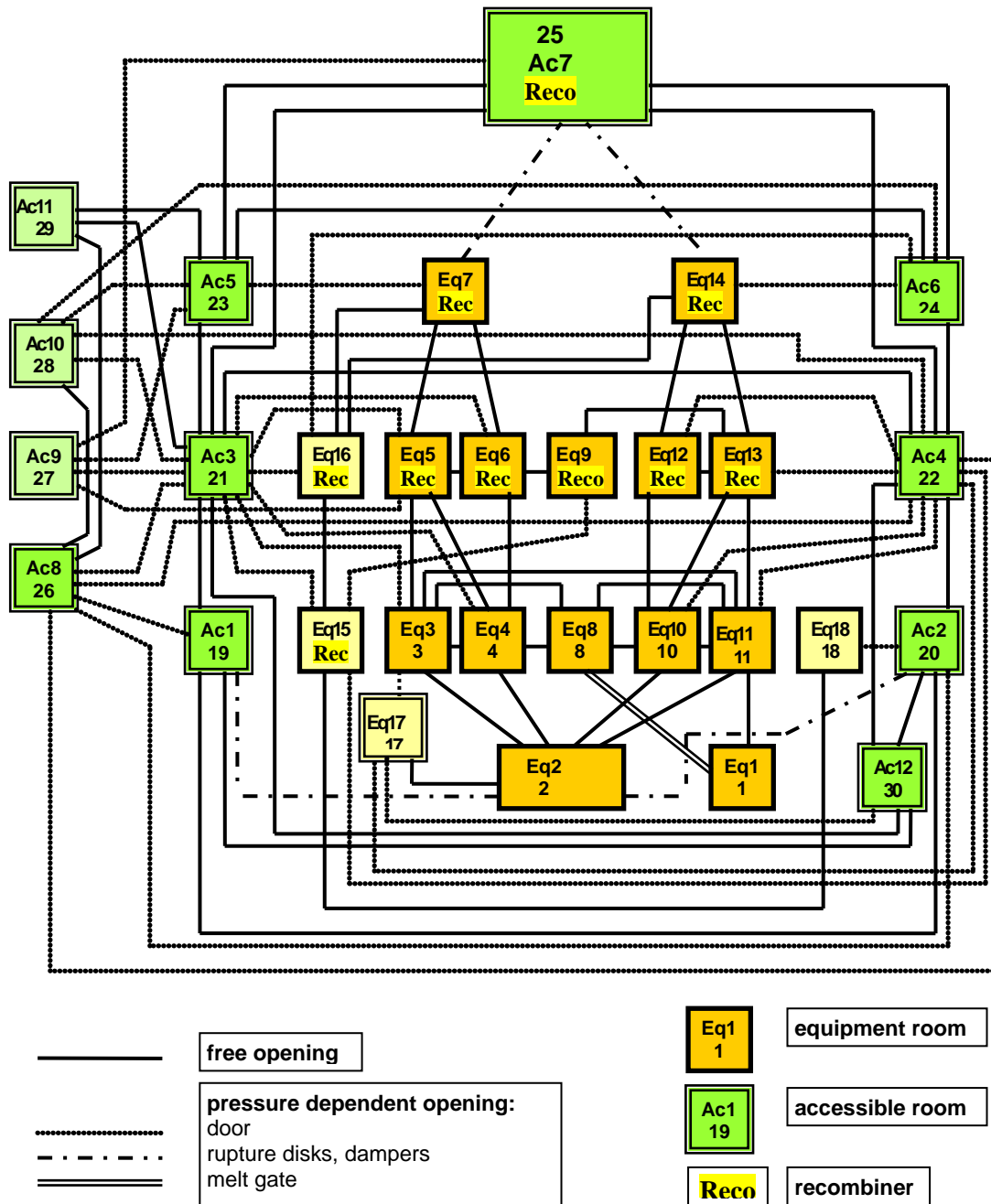
SUB-SECTION 16.2.2.5 - FIGURE 2

LB(LOCA) containment pressure [Ref-1]
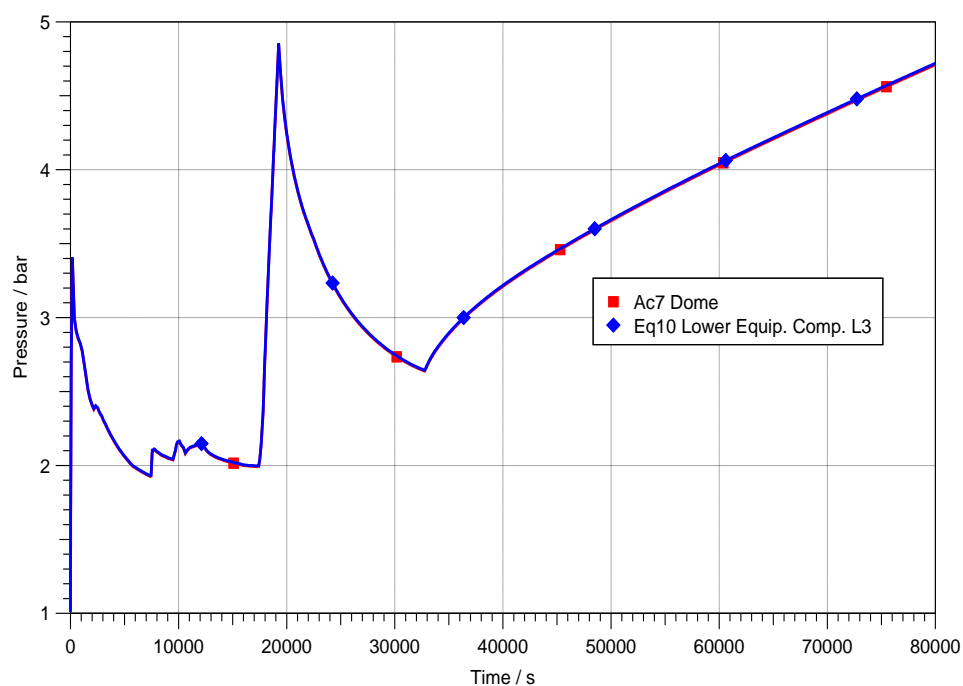
a) **Without EVU [CHRS]**
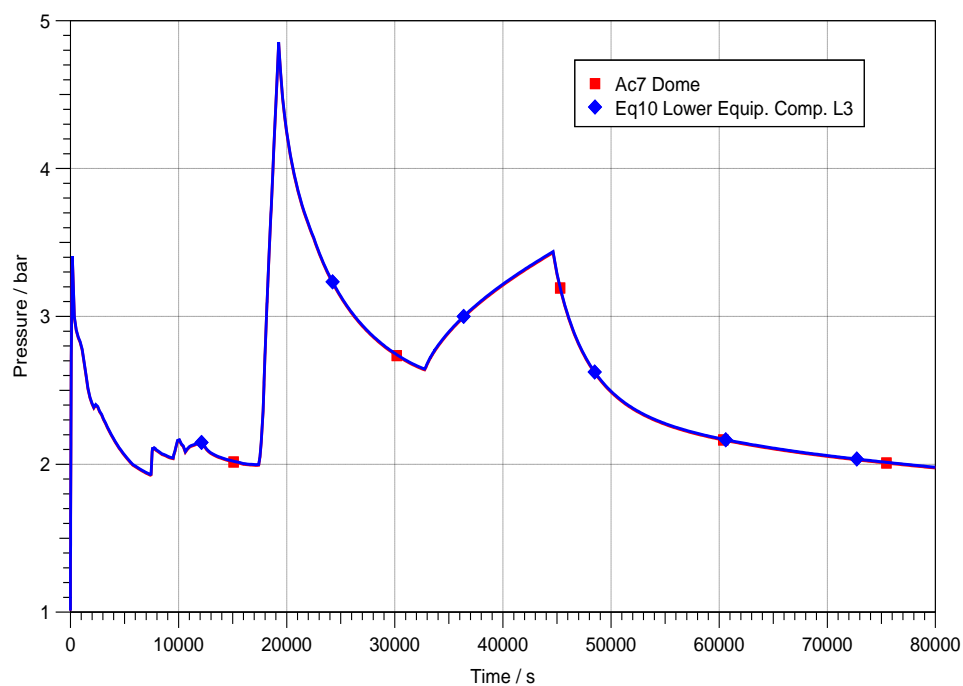
b)   With 2 EVU [CHRS] trains actuated for spraying after 12.4 h

SUB-SECTION 16.2.2.5 - FIGURE 3

LB(LOCA) containment gas temperature [Ref-1]
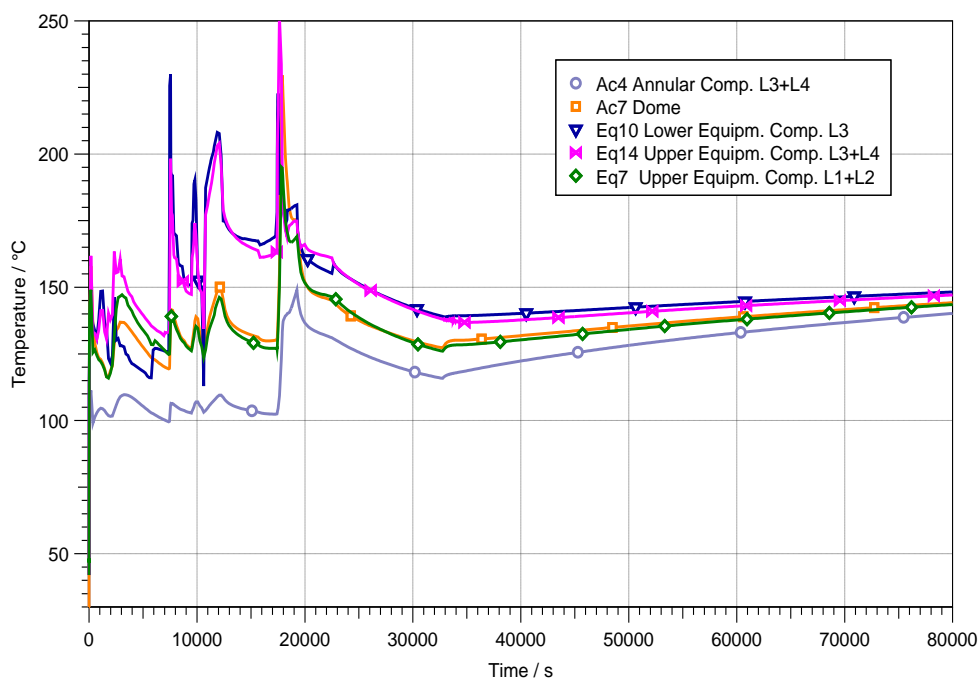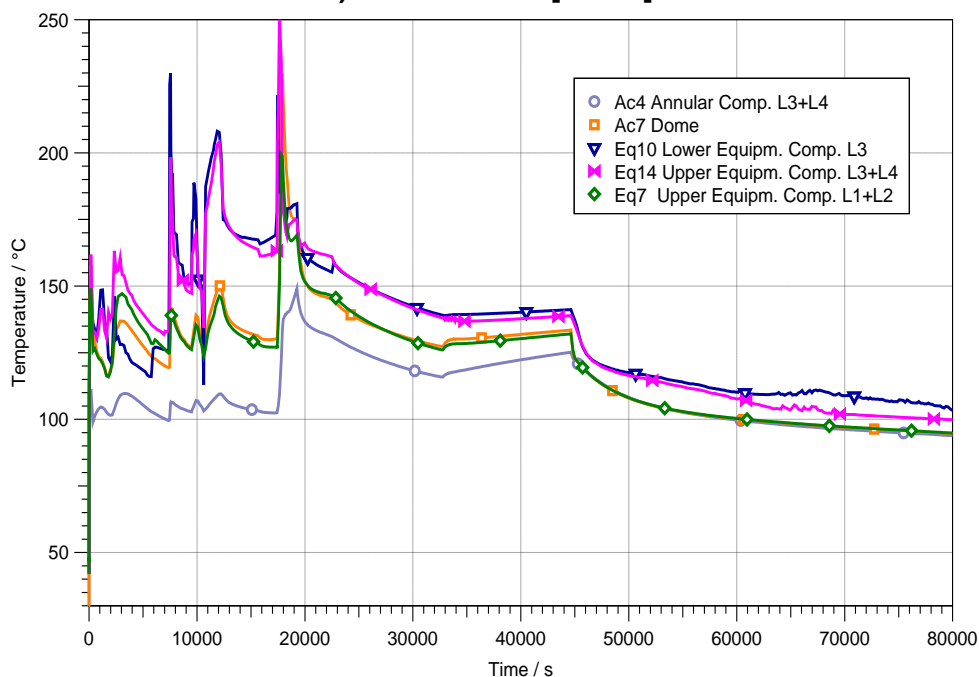
a) Without EVU [CHRS]

b) With 2 EVU [CHRS] trains actuated for spraying after 12.4 h

SUB-SECTION 16.2.2.5 - FIGURE 4

LB(LOCA) containment liner temperature [Ref-1]
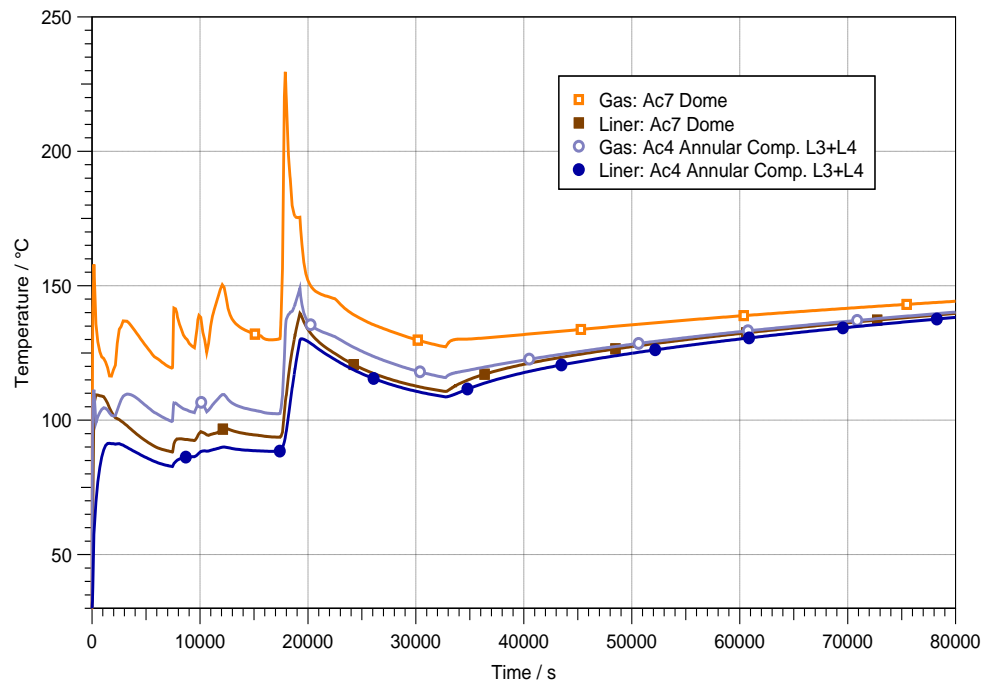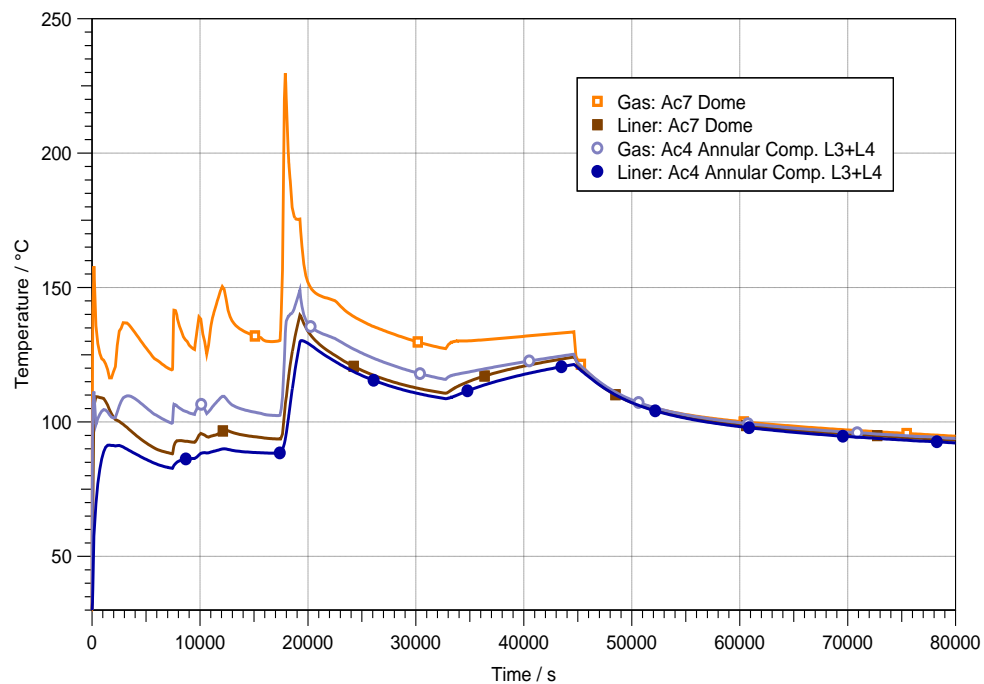
a) Without EVU [CHRS]

b) With 2 EVU [CHRS] trains actuated for spraying after 12.4 h

SUB-SECTION 16.2.2.5 - FIGURE 5

LB(LOCA) containment sump temperature and gas temperature in spreading compartment [Ref-1]
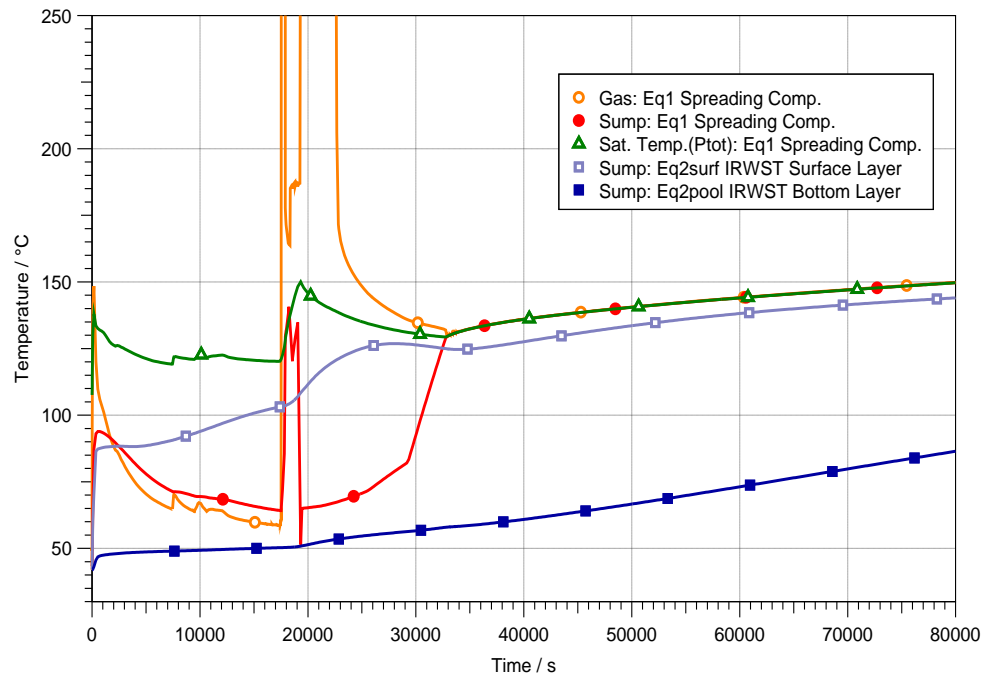
a) **Without EVU [CHRS]**
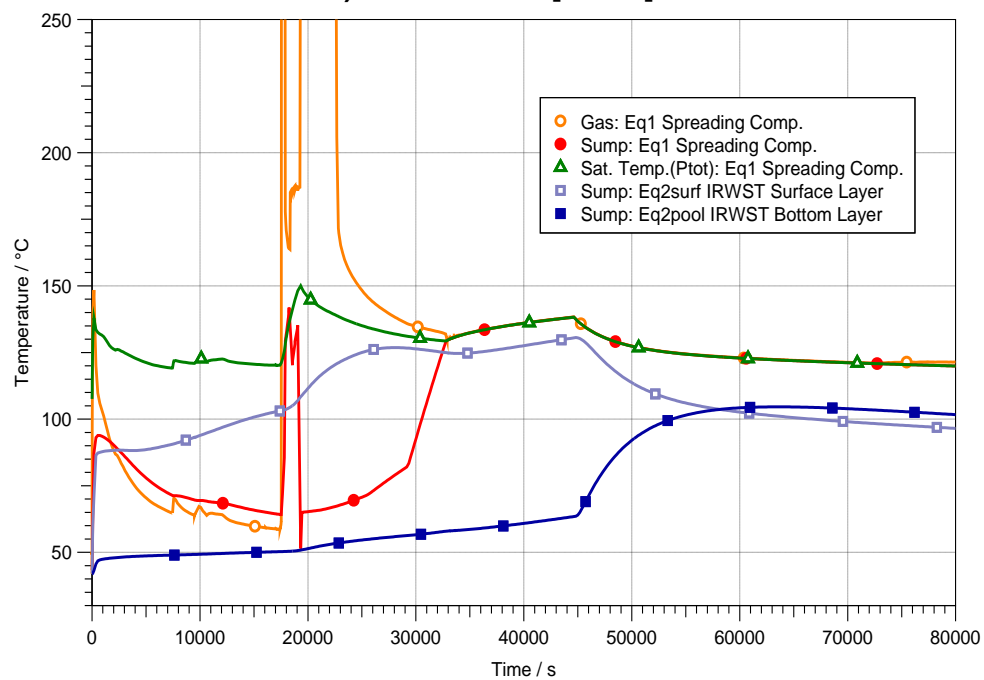
b) **With 2 EVU [CHRS] trains actuated for spraying after 12.4h**

SUB-SECTION 16.2.2.5 - FIGURE 6

LB(LOCA) containment humidity [Ref-1]
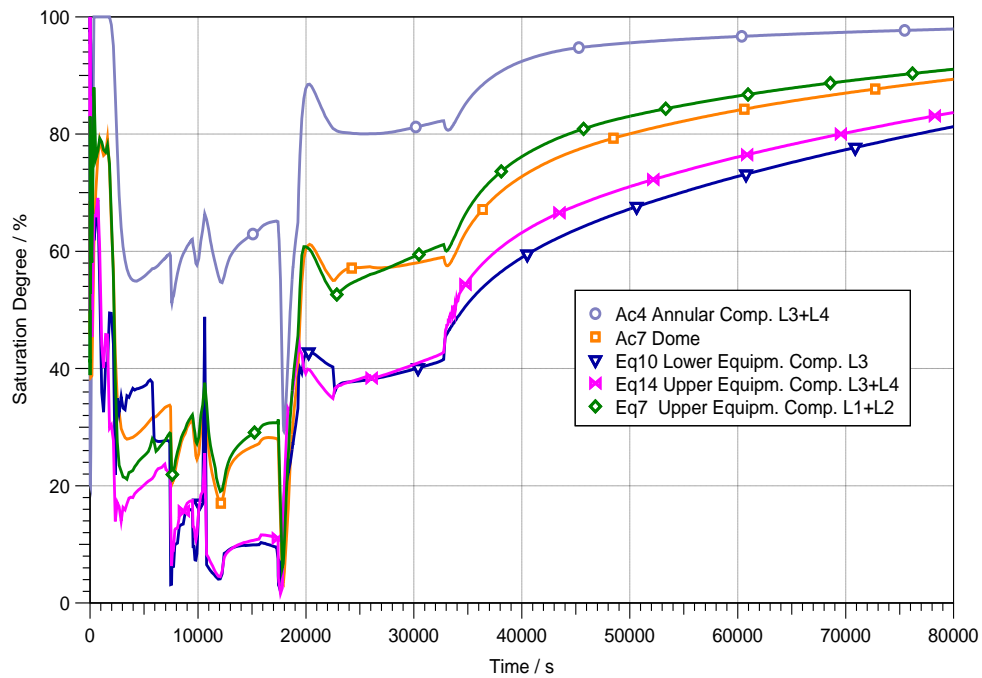
a) Without EVU [CHRS]

b) With 2 EVU [CHRS] trains actuated for spraying after 12.4 h

SUB-CHAPTER : 16.2

PAGE   : 226 / 295

PRE-CONSTRUCTION SAFETY REPORT

UK EPR

CHAPTER 16: RISK REDUCTION AND SEVERE
ACCIDENT ANALYSES

Document ID.No.
UKEPR-0002-162 Issue 05
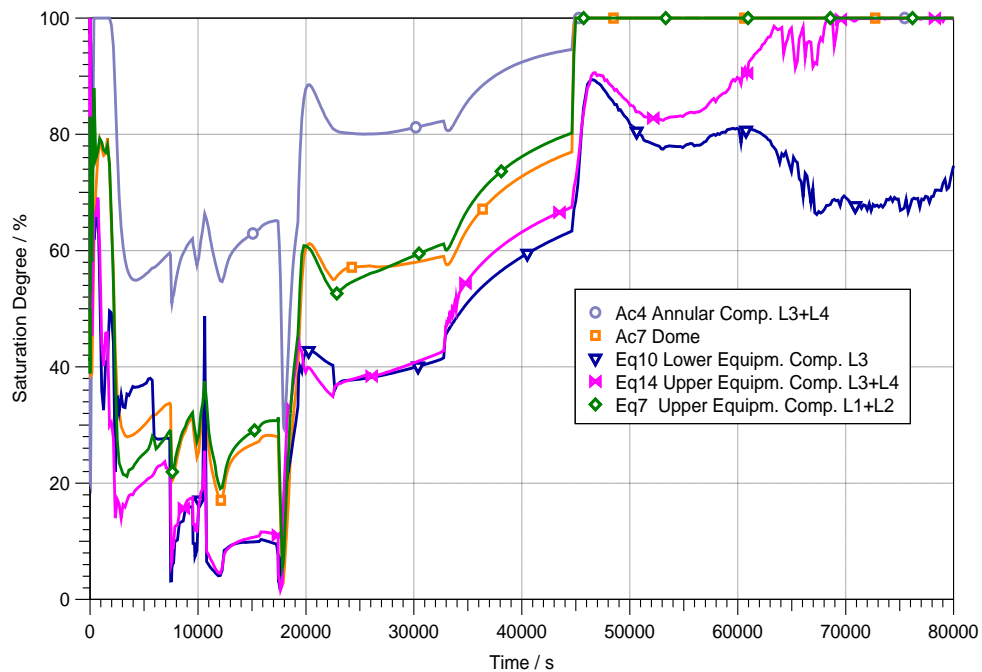
SUB-SECTION 16.2.2.5 - FIGURE 7

SB(LOCA) containment pressure [Ref-1]
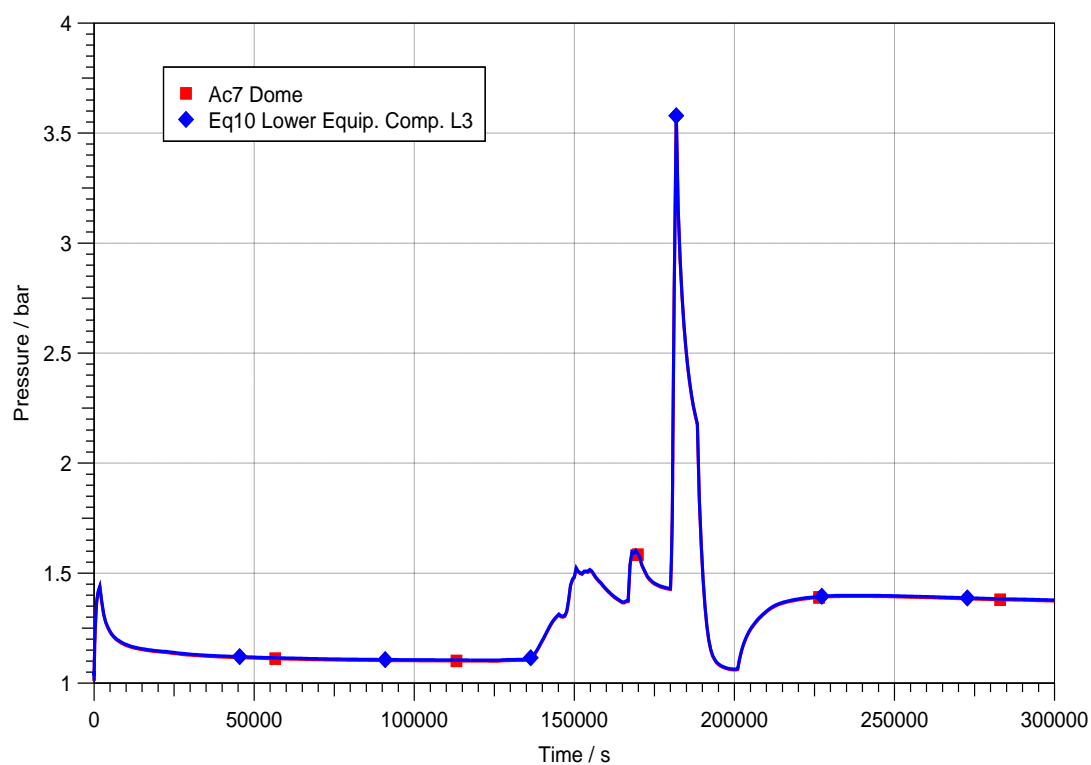
SUB-SECTION 16.2.2.5 - FIGURE 8

SB(LOCA) containment gas temperature [Ref-1]
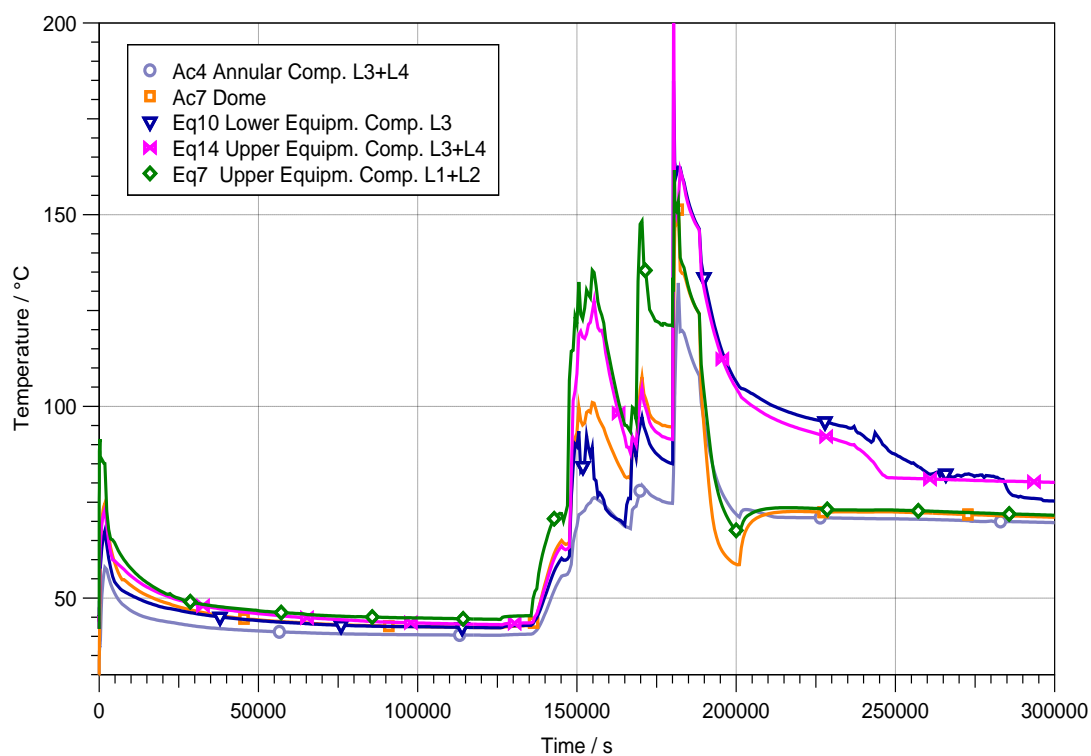
SUB-SECTION 16.2.2.5 - FIGURE 9

SB(LOCA) containment liner temperature [Ref-1]

SUB-CHAPTER : 16.2

PRE-CONSTRUCTION SAFETY REPORT

PAGE : 229 / 295

UK EPR

CHAPTER 16: RISK REDUCTION AND SEVERE
ACCIDENT ANALYSES

Document ID.No.
UKEPR-0002-162 Issue 05
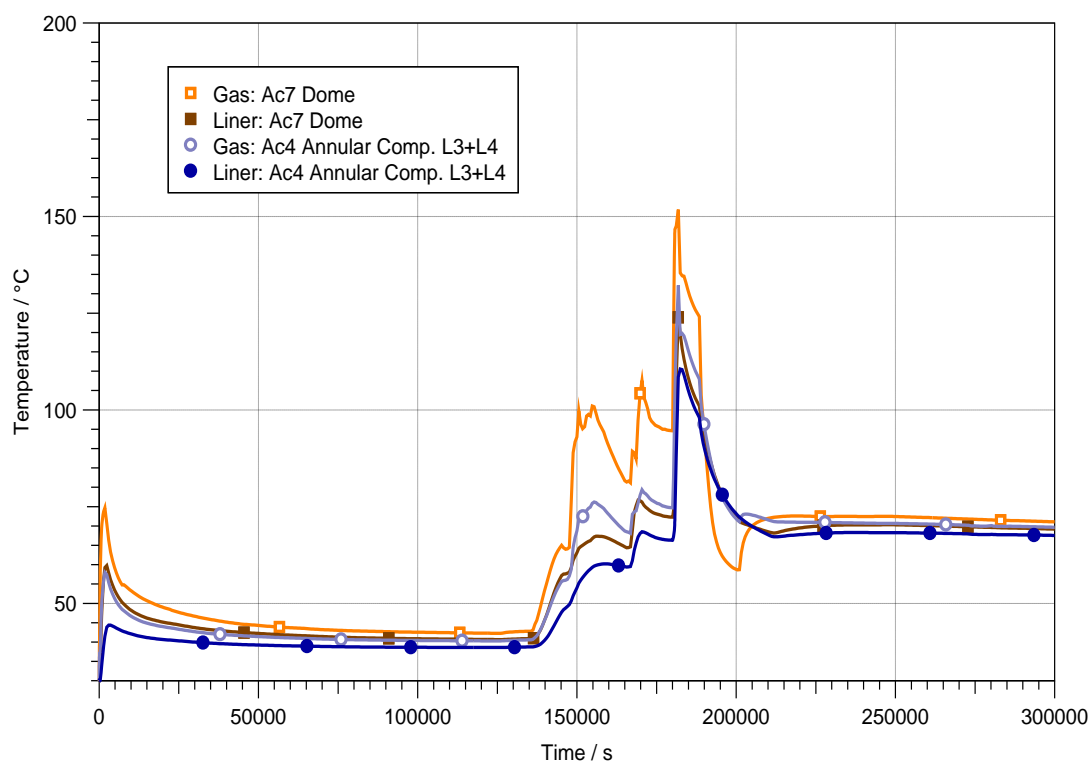
SUB-SECTION 16.2.2.5 - FIGURE 10

SB(LOCA) containment sump temperature and gas temperature in spreading compartment [Ref-1]
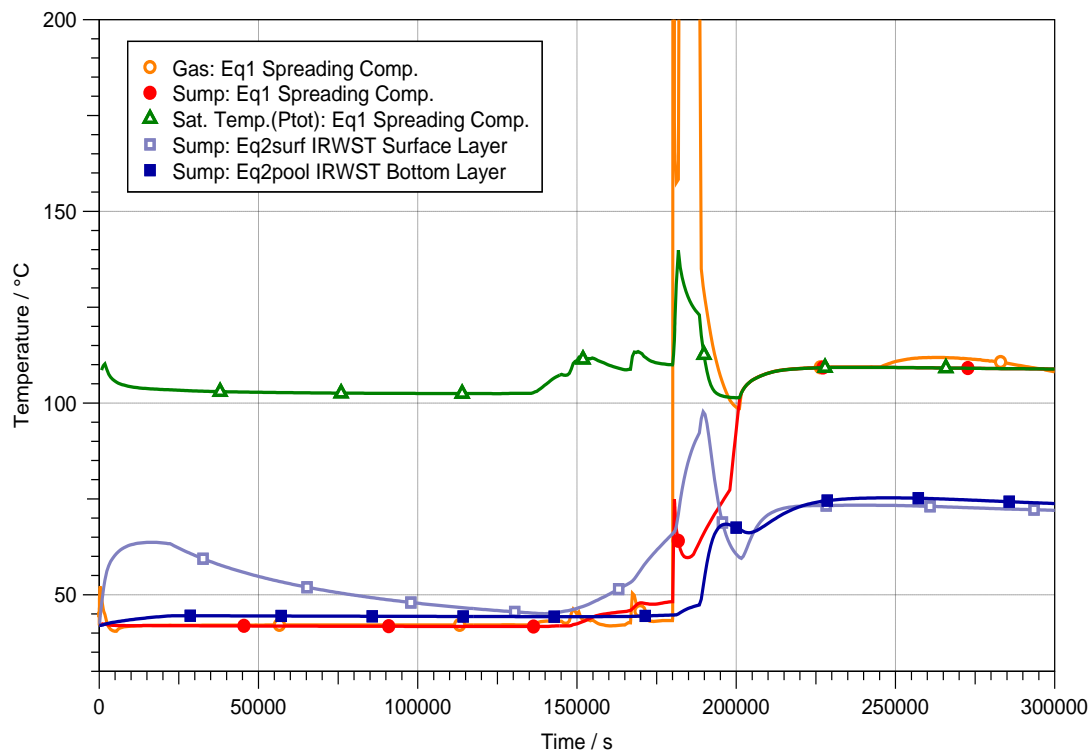
SUB-SECTION 16.2.2.5 - FIGURE 11

SB(LOCA) containment humidity [Ref-1]
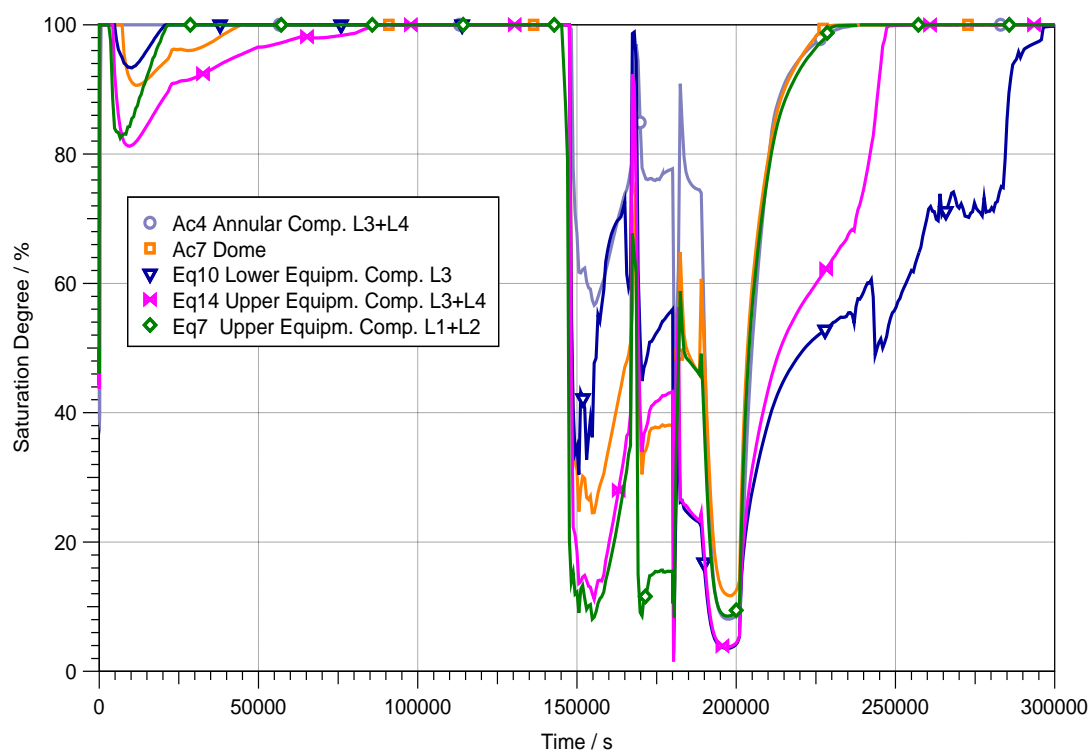
SUB-SECTION 16.2.2.5 - FIGURE 12

LOOP containment pressure [Ref-1]
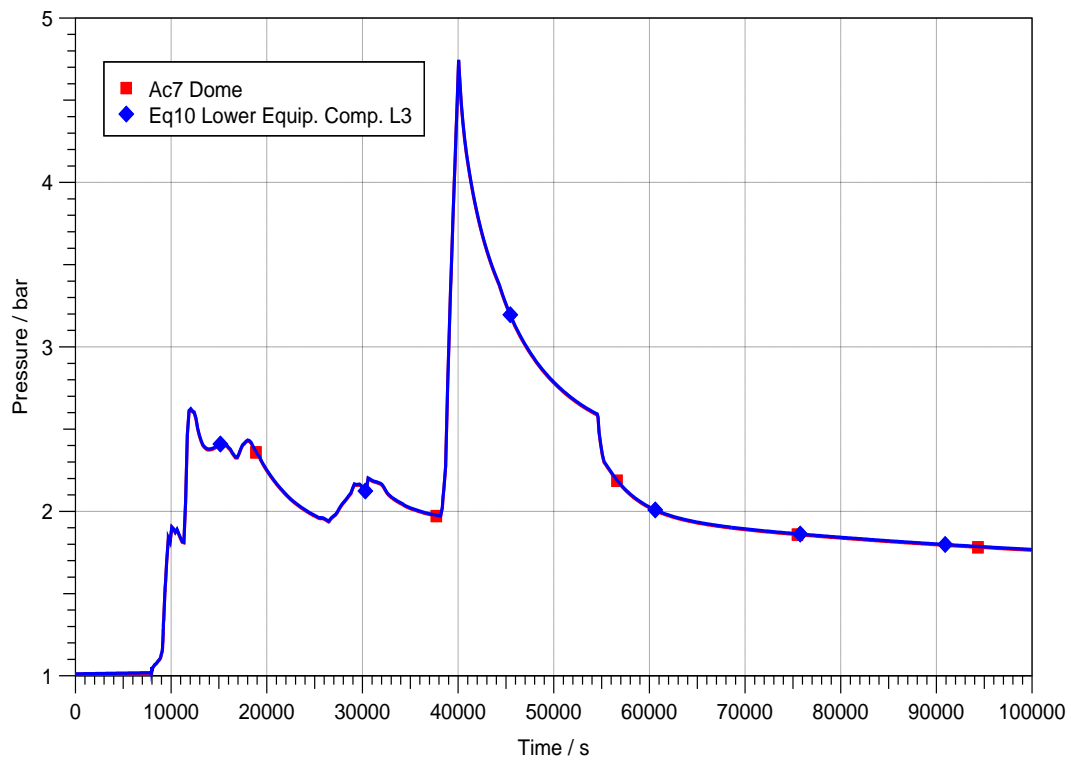
SUB-SECTION 16.2.2.5 - FIGURE 13

LOOP containment gas temperature [Ref-1]

UK EPR

PRE-CONSTRUCTION SAFETY REPORT

CHAPTER 16: RISK REDUCTION AND SEVERE
ACCIDENT ANALYSES

SUB-CHAPTER : 16.2

PAGE   : 233 / 295

Document ID.No.
UKEPR-0002-162 Issue 05
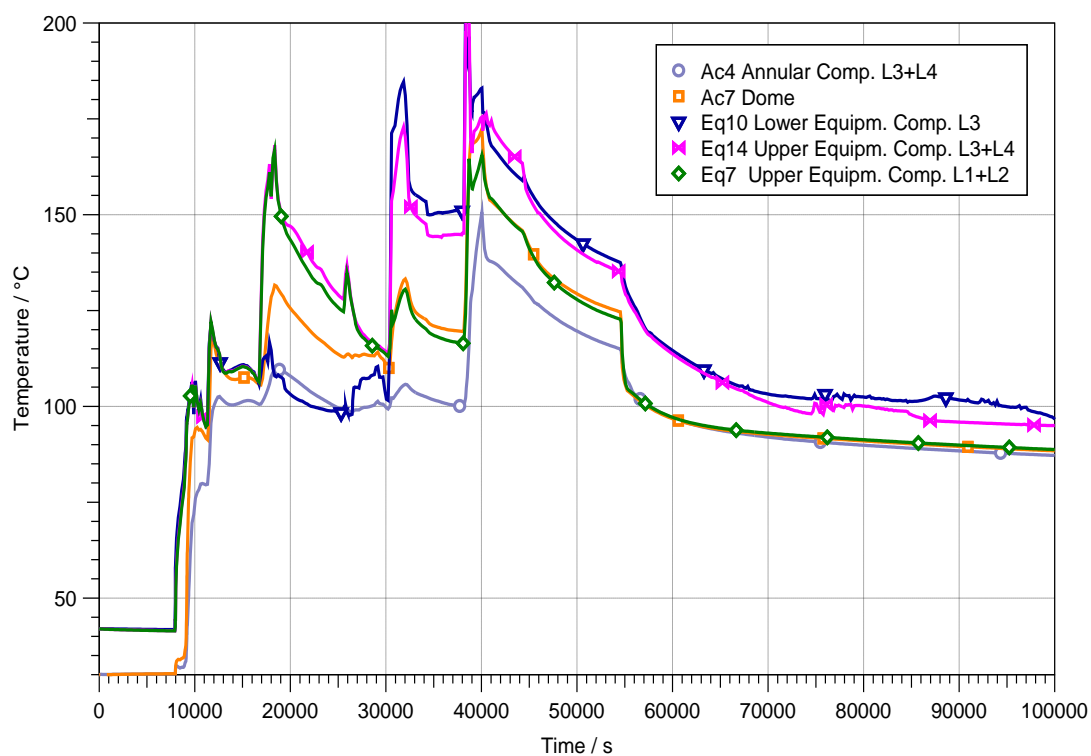
SUB-SECTION 16.2.2.5 - FIGURE 14

LOOP containment liner temperature [Ref-1]
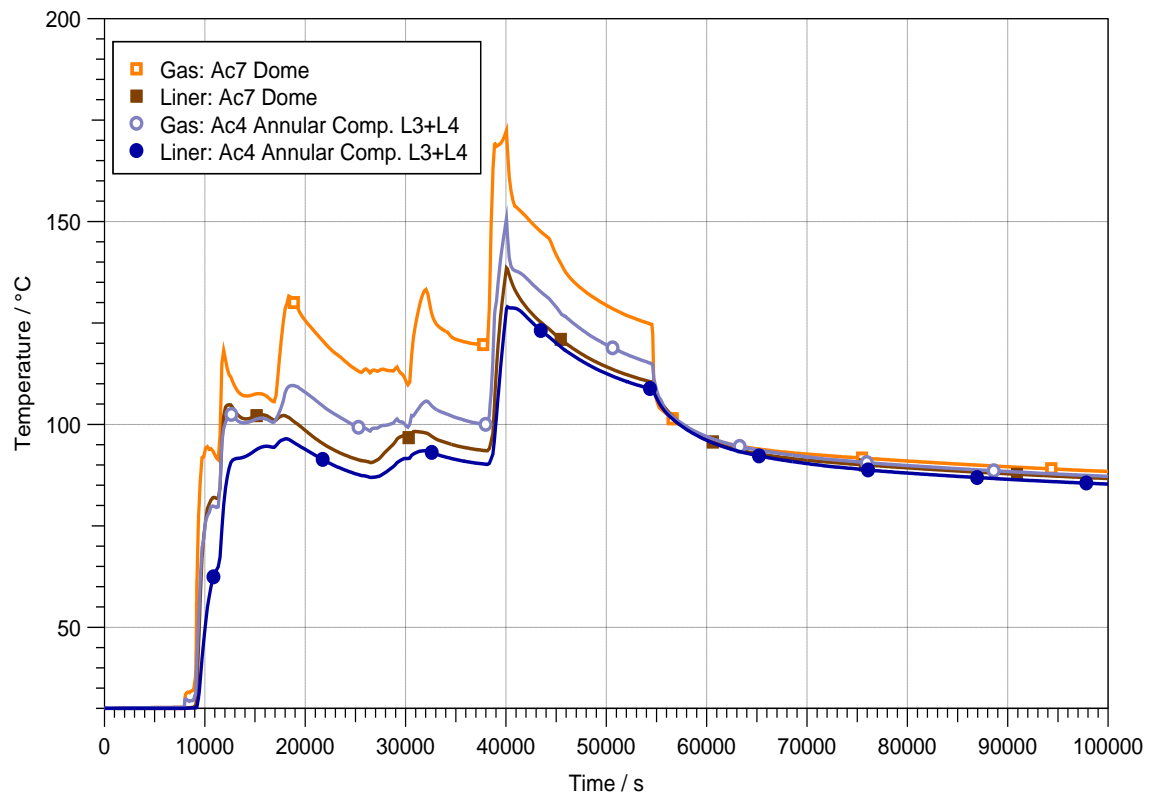
SUB-SECTION 16.2.2.5 - FIGURE 15

LOOP containment sump temperature gas temperature in spreading compartment [Ref-1]
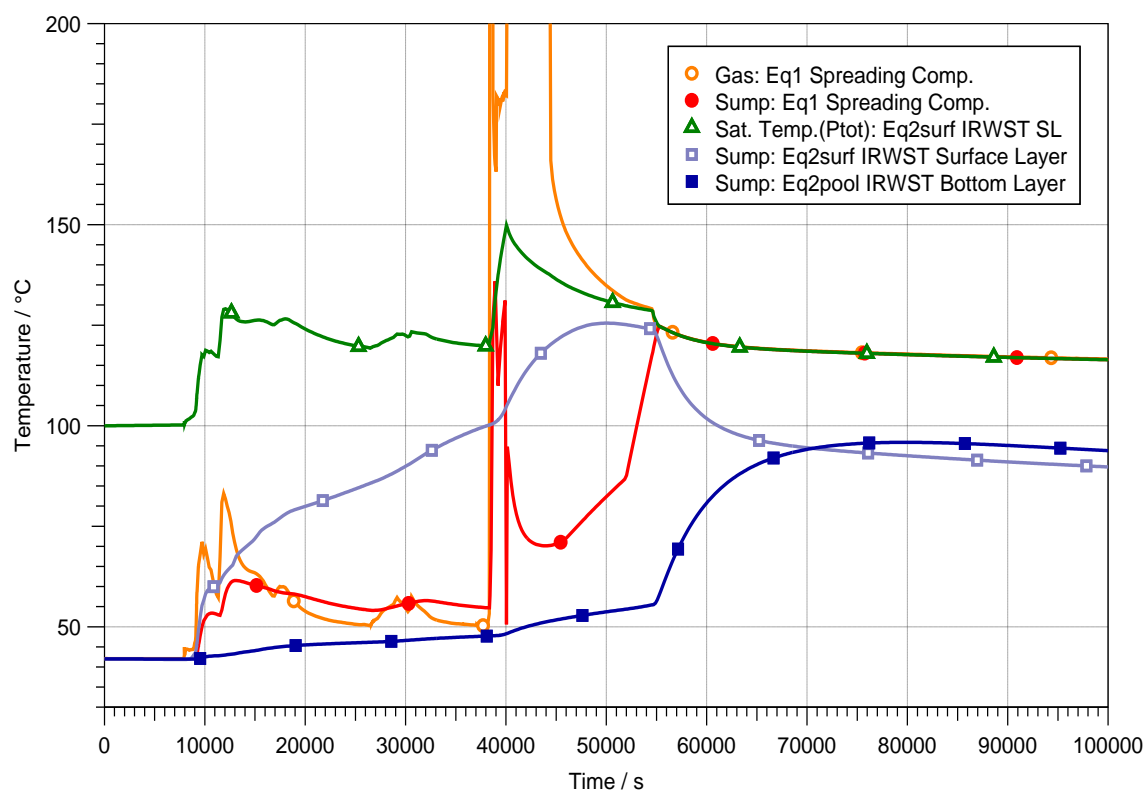
SUB-SECTION 16.2.2.5 - FIGURE 16

LOOP containment humidity [Ref-1]
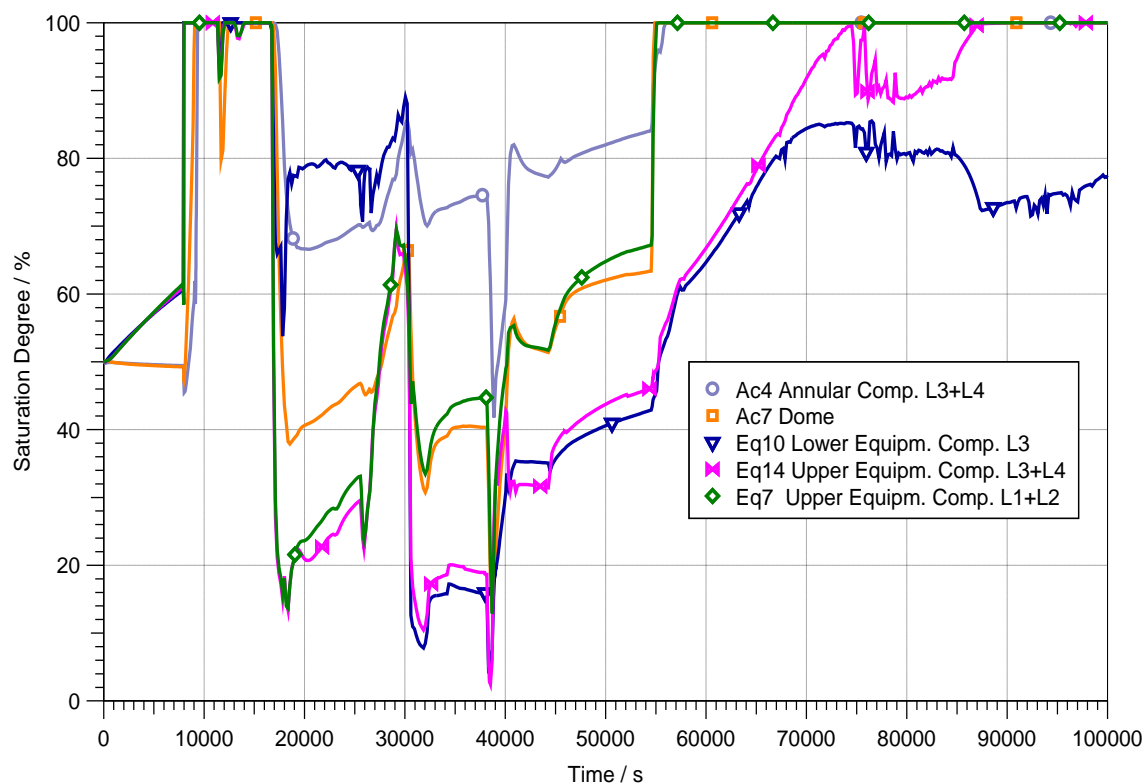
3. RADIOLOGICAL CONSEQUENCES OF CORE-MELT SEQUENCES

3.1. SAFETY REQUIREMENTS

3.1.1. Safety objectives

The safety approach for EPR reactors is deterministic, complemented by probabilistic analyses, based on the concept of defence in depth. Within this framework, a number of design provisions (depressurisation of the primary system, installation of re-combiner units, core catcher, EVU [CHRS]) are made to preserve the integrity of the containment in severe accidents and hence reduce the accident consequences.

The objective of the radiological consequence calculations for RRC-B core melt accidents is to show that, taking account of the above design provisions, the release of radioactive materials outside the plant remains within the limits set out below.

3.1.2. Radiological objectives

The radiological objectives associated with RRC-B accidents are that only very limited countermeasures, that is countermeasures limited in area and in time, should be necessary i.e.

- limited sheltering duration for the public,

- no need for emergency evacuation beyond the immediate vicinity of the plant,

- no permanent relocation,

- no long term restrictions on the consumption of foodstuffs.

These countermeasures, which are those laid down in ICRP 63 (see [Ref-1] and Section 16.2.3 - Table 3), relate to both the short term phase (sheltering and evacuation) and the medium and long term phases, (absence of permanent relocation). The ICRP associates dose bands or dose rates (averted doses or dose rates) with these protective measures, as follows:

- sheltering: 5 – 50 mSv (effective dose),

- evacuation; 50 – 500 mSv (effective dose),

- issue of iodine tablets: 50 – 500 mSv (thyroid dose),

- permanent relocation: 5 – 15 mSv/month for prolonged exposure (dose rate from contaminated ground). The value proposed by the ICRP is 10 mSv/month. The ICRP also recommends permanent relocation for an effective averted dose in excess of 1 Sv (i.e. if an effective committed dose of > 1 Sv can be averted thereby).

The thresholds of 10 and 50 mSv (calculated effective dose) have been adopted by the French General Health Directorate for, respectively, population sheltering and evacuation, and a threshold of 100 mSv in equivalent thyroid dose for issuing iodine tablets. The French General Health Directorate also recommends limiting any sheltering of more than 48 hours.

Possible restrictions of the consumption of foodstuffs from the vicinity of the power plant are in line with European regulations that establish limits for marketing these foodstuffs in the case of nuclear accident or other radiological emergency (see [Ref-2] and Section 16.2.3 - Table 4).

Taking these elements into account, the assumed thresholds associated with the different countermeasures for population protection are:

- short term measures:

    o imposition of sheltering: 10 mSv (effective dose),

    o evacuation; 50 mSv (effective dose),

    o issue of iodine tablets: 100 mSv (equivalent thyroid dose).

- medium and long term measures:

    o relocation: 10 mSv/month for prolonged exposure (irradiation dose rate by the ground) or 1 Sv (effective dose).

It must be noted that the previous approach is quite different from the one applied in the UK which is given here after.

In the UK, the National Radiological Protection Board (now part of the Health Protection Agency) defines intervention levels in terms of lower and upper Emergency Reference Levels (ERL) for emergency countermeasures: population sheltering, evacuation and the administration of stable iodine [Ref-3]. For averted doses greater than the upper ERL, implementation of the countermeasure would almost always be justified, whereas, for averted doses below the lower ERL, implementation of the countermeasure would be unlikely to be justified. For averted doses between these levels, ALARP considerations must be used. The recommended ERLs for emergency countermeasures are:

Countermeasure	Body/organ	Averted dose (mSv)	
		lower	**upper**
Sheltering	Whole body effective dose	3	30
Evacuation	Whole body effective dose	30	300
Stable iodine	Thyroid	30	300

Possible restrictions on the consumption of foodstuffs produced in the vicinity of the power plant are in line with European regulations that establish limits for consumption of contaminated foodstuffs in the case of a nuclear accident or other radiological emergency (see [Ref-4] and Section 16.2.3 - Table 4).

In the UK, these regulations are enacted under the Food and Environment Protection Act 1985 [Ref-5].

The assessment of effective dose takes account of the 4 exposure routes (exposure to direction radiation from the plume, inhalation, ingestion and exposure to radiation from deposits on the ground or other surfaces). The assessment also takes account of foodstuff restrictions, if appropriate (see above).

In general, dose calculation results are presented in a generic way for adults and for a 1-year-old infant at the site boundary (500 m) over 7 days, and for an adult at a distance of 2 km from the point of release over 50 years. The equivalent thyroid dose will also be assessed for these population groups. For a given nuclear site, the doses have to be calculated for the most exposed group (nearest habitation).

The presentation of dose results is supplemented with explanation in each case of how the radiological objectives are met (limited sheltering, evacuation only to the site boundary, absence of permanent relocation) with reference to the thresholds mentioned above.

The EPR reactor is a French-German design and the original method used to assess the radiological consequences of accidents was German. The method is presented in section 3.2 for the reference source term evaluation and in section 3.3 for the off-site consequences with the associated results.

Construction of the EPR in France made it necessary to apply the methodology used for other reactors operating in France to EPR. In terms of its functional principles the EPR reactor is similar to the reactors currently in operation in France – the main differences being design improvements such as design measures against severe accidents. Methods and assumptions adopted for operating French NPPs for evaluating fission product release into the environment during a severe accident can be applied, except where identified design differences require variations from the usual methods. A simplified implementation of this assessment method has been used for this safety report. The corresponding results are given in section 3.4. The approach will be reviewed to address UK specific requirements later in the licensing process.

3.2. REFERENCE SOURCE TERM

The assumed radiological consequences of RRC-B core melt sequences are based on a bounding reference source term, calculated with reasonably conservative and simplified bounding assumptions, independent of the accident scenario but which relate to the core melt sequence. These bounding assumptions relate to fission product behaviour and to the behaviour of the plant (containment leakage, filter efficiency, etc).

The reference source term, given in section 3.2.6., has been assessed with the original French-German design method. The corresponding assumptions are summarised in the following paragraphs, as well as the main differences between German and French NPP assumptions. The new features of the EPR are discussed when they might lead to different results.

3.2.1. Core Inventory

The reactor core activity inventory was determined assuming a reactor thermal output of 4900 MW(th), an equilibrium core with 5% U-235 enrichment and an average burn up of 43 MWd/kg; the precise boundary conditions for the calculation of the activity inventories are shown in Chapter 14 and the activity inventories of a series of nuclides are also listed in Chapter 14.

The calculations were performed using the computer program ORIGEN-S [Ref-1].

3.2.2. Release from the Molten Core

Release fractions from the molten core are given here for the most important radionuclides:

- noble gases, iodine and caesium 100%

- tellurium, selenium 25%

- strontium 3%

(Iodine is considered to be mainly in the form of aerosols, 2.5% in elemental form and 0.2% in organic form.)

A list of all relevant elements is given in Section 16.2.3 - Table 1 with corresponding release fractions.

The proportions of radiologically significant nuclides released from the molten core material generally correspond to the proportions usually seen in core melt accident analyses. The release fractions of noble gases, iodine and caesium isotopes are all equal to 1.

In addition to the in-vessel release an ex-vessel release also occurs, resulting essentially from melt-concrete interaction. This second fraction of the total release plays a particular role in terms of the release fractions for the less volatile fission products.

Because of the effective basemat cooling in EPR, melt-concrete interaction is ruled out; the release fractions for the alkaline earth-metals strontium and barium are at least one order of magnitude lower than for those cases in which melt-concrete interaction was considered during release. Furthermore, ruling out melt-concrete interaction means that, in the most unfavourable cases, the main portion of the release of all relevant radionuclides into the containment atmosphere would occur within the first few hours of the accident.

The release fractions from the molten core for the radionuclides most important for radiological consequences to an individual (noble gases, iodine and caesium) are quite similar to those taken into account for operating French plants. The French calculations presented in this report (see section 3.4.) have been carried out considering the highest release level from the French and German approaches (See Section 16.2.3 - Table 1).

3.2.3. In-containment aerosol behaviour

The quantity of airborne aerosols and (non-aerosol) elemental iodine decreases due to deposition in the containment.

{CCI Removed}

b

UK EPR

PRE-CONSTRUCTION SAFETY REPORT

CHAPTER 16: RISK REDUCTION AND SEVERE
ACCIDENT ANALYSES

SUB-CHAPTER : 16.2

PAGE   : 240 / 295

Document ID.No.
UKEPR-0002-162 Issue 05

3.2.4. Iodine behaviour in the containment

{CCI Removed}

b

After about 3 hours only 0.2% of the original total iodine still exists in elemental form and remains at that level. The long-term fraction of airborne iodine assumed to be in elemental form corresponds to a partition coefficient (mass of iodine per unit mass of liquid / mass of iodine per unit mass of gas) of 10^4 [Ref-1] and corresponds to values used for LOCAs inside containment.

A fraction of 0.2% of the iodine released from the core is in organic form and it is assumed that this iodine will not be deposited nor transformed [Ref-2]. This fraction of iodine assumed to be in organic form is about a factor of 2 higher than that measured long-term at Three Mile Island (TMI) [Ref-3].

The assumptions used for French operating NPPs concerning iodine behaviour are based on NUREG 1465 [Ref-4]: 95% of the iodine is assumed to be released as aerosols, 5% of the iodine being released in elemental form which partly interacts with the painted walls to form organic iodine. No further gaseous iodine is released into the containment from the IRWST since the pH is kept higher than 7 due to soda injection. Within a few hours 0.15% of the iodine release is assumed to be in organic form.

The potential impact of the additional volatile-iodine source term due to the conversion of metal-iodide aerosols (such as CsI) passing through the Passive Autocatalytic Recombiners (PARs) has been considered [Ref-5]. A sensitivity study [Ref-6] was performed where the recombiners were modelled by an additional source of gaseous iodine in the containment. The rate of iodine added was calculated based on a dissociation ratio applied to the CsI flow through the recombiners and a total gas flow into the PARs, estimated from hydrogen mass values produced and recombined. The in- and ex-vessel phases were considered. In order to cover the uncertainties, sensitivity studies were performed with four values of dissociation ratio: 1.4% (THAI experiment value [Ref-5]), 3%, 6% and 10%. The results of this sensitivity study are bounded by the assumptions used in the PCSR.

3.2.5. Activity release from the containment

A leakage of 0.3% volume per day from the containment to the annulus is assumed, **ignoring** the effects of measures taken to reduce the containment pressure.

The rate of aerosol depletion in the annulus is assumed to be identical to the rate for long term depletion in the containment.

Ventilation of the annulus: Pressure in the annulus is assumed to be held constantly below atmospheric pressure by the emergency ventilation system with an extraction rate of 200 m³/h (See Chapter 6).

Filters: Retention of all substances except noble gases (aerosols, elemental iodine and organic iodine) by filters reduces the release to the environment to 1% of its value upstream of the filter.

The assumption used for operating French NPPs for filter efficiency is that the release of molecular iodine and aerosols is ten times lower than this (i.e. 0.1% of the value upstream of the filter [Ref-1]). The sensitivity study presented in section 3.4 uses this latter value.

3.2.6. Release of Radioactive Substances to the Environment [Ref-1]

Radioactive releases to the environment have been calculated for a large number of nuclides using an established French-German assessment method for estimating environmental consequences.

The results for the nuclides Xe-133, I-131 and Cs-137 for a release period of 30 days are as follows:

Xe-133: $1.4 \cdot 10^5$ TBq
I-131:   7.5 TBq
Cs-137:   0.45 TBq

The chemical composition of the iodine 131 is as follows:

I-131   aerosol   3.0 TBq
I-131   elemental   2.3 TBq
I-131   organic   2.2 TBq

Only the dose factor corresponding to the elemental iodine is used for dose calculations but using conservative assumptions.

The cumulative release to the environment of the above three nuclides is given in Section 16.2.3 - Figure 3. The calculations were performed using the computer code ACARE[1].

A complete list of all relevant radionuclides, which are released to the environment, is given in Section 16.2.3 - Table 7 and Section 16.2.3 - Table 8.

---

[1] The computer code ACARE (Activity in interrelated compartments and release to the environment) was formerly used as a pre-program for PRODOS (Probabilistic Dose Calculation, section 3.3) to calculate the activity flow of nuclides in coupled compartments. Both programs were kind of complicated to handle and therefore taken out of use a couple of years ago and are not going to be reactivated.

Radioactive decay and production of daughter nuclides were taken into account. Deposition of aerosols and iodine in the single compartments could be considered in four different ways. The last compartment represented the atmosphere. The results were presented in a time dependent form for the activity inventory in every compartment, the release rates to the atmosphere and the total release.

The essential application was to sum over all nuclides the nuclide specific release multiplied with dose factors. These values were used in PRODOS to calculate probabilistic distributions of radiation doses in the vicinity of nuclear power plants after accidents. For the calculation of radiation doses the program chain ACARE-PRODOS was replaced by MACCS [Ref-1]

3.3. CALCULATION OF RADIOLOGICAL CONSEQUENCES

In the first instance, the radiological consequences of the reference source term (see section 3.2.6.) have been assessed using the German methodology [Ref-1].

With respect to environmental conditions, the following assumptions are made:

1) **Time of the accident:** The accident is postulated to occur in the growing season (spring to autumn).

2) **Weather conditions during the accident:** Although it is generally agreed that best estimate methods can be applied in demonstrating compliance with requirements for such extreme cases, a more conservative approach is chosen. As required for design basis accidents, it is assumed that the safety goals are met if they are not exceeded for 95% of the atmospheric dispersion conditions.

3) **Aerosol removal:** The dispersion, fallout, washout and ecological conditions (e.g. washout and deposition rates from the atmosphere, transfer rates of radionuclides from soil to plants, etc.) are selected in compliance with German rules for the evaluation of design basis accidents.

4) **Exposure of individuals:** It is assumed that an individual may be exposed during the whole accident at any location outside the plant boundary including the most unfavourable location.

5) **Biological data for exposed individuals:** The same biological data is used (e.g. breathing rates) as prescribed for the evaluation of design basis accidents; these values are based on basic data from recent ICRP Publications (see [Ref-2])

6) **Selection of Appropriate Weather Conditions:** The dispersion and deposition of the released radionuclides depend on the prevailing weather conditions, which are varied over a range determined by the conditions that have occurred in reality over a period of a year or longer. The variation of dispersion and deposition according to prevailing weather conditions means that the results of the evaluated radiation exposure are also influenced to a high degree by the postulated meteorological conditions.

Weather data (hourly measurements of wind speed, wind direction, diffusion class and precipitation rate) from a recent 4 year period from a seaside site in France was used. Radiological consequences were evaluated using the computer code PRODOS[2] using this data. The radiological consequences covering 95% of the possible maximum values have been chosen.

---

[2] The computer code PRODOS (Probabilistic Dose Calculation) was formerly used to make prediction of radiological impact in the environment resulting from accidental releases into air and for the assessment of emergency countermeasures after postulated severe accidents inside nuclear power plants, using input data from the computer code ACARE (Activity in interrelated compartments and release to the environment; cf. answer ch. 3.2.6). Both programs were kind of complicated to handle and therefore taken out of use a couple of years ago and are not going to be reactivated.

PRODOS calculated probability distributions of consequences to the environment of a plant due to a time depending release of radioactive substances out of this plant using a weather course of a larger time span. The release period was related to each possible weather sequences in the time span.

For the calculation of radiation doses the program chain ACARE-PRODOS was replaced by MACCS [Ref-3].

Two types of countermeasures were distinguished outside the area enclosed by the plant fence where specific protective measures are coordinated by the operator:

- Countermeasures to be performed before the accident is fully under control (evacuation):

  o In this initial stage, intervention will generally be performed over a circular area with radius r centred on the plant because it is difficult to predict changes in wind direction with sufficient confidence. In order to evaluate this kind of countermeasure, maximum dose values were calculated which will not be exceeded with a probability of 95% at any location beyond the distance r from the plant. The evaluation is performed for different values of r. Dose values are then plotted as a function of r.

- Countermeasures to be performed after termination of release of radioactive materials into the environment:

  o This second type of intervention (e.g. relocation and banning the sale of foodstuffs) will only be performed in those areas in which measurements show that an intervention level D is exceeded. D may be a dose, a dose rate or a contamination level for particular foodstuffs (measured in Bq/kg). For this type of intervention, the areas over which they may have to be applied are considered more important than the distance from the plant. The evaluation is therefore done for different types of area.

The potential radiological consequences depend on:

- Release height.

- Nuclide - specific activity of releases as a function of time.

- Meteorological conditions during a defined, representative time period.

The results of these calculations are given in the Section 16.2.3 - Figures 5 to 15.

Information about the potential dose originating from the passing radioactive cloud is given in Section 16.2.3 - Figure 5, which gives the effective dose to adults and to infants due to inhalation and direct radiation from the cloud as a function of distance, and Section 16.2.3 - Figure 6, which gives the thyroid dose for adults and for infants due to inhalation only as a function of distance. The portions of the dose values relating to inhalation account for radiation exposure due to inhaled radionuclides over a time period of 50 years for adults and 70 years for infants, respectively (committed dose).

For the area-related countermeasures, a corresponding calculation was performed. In this case, the main interest is related to the size of areas in which certain dose or contamination levels are exceeded. Twenty dose and contamination levels were evaluated simultaneously on the basis of the activity release pattern of the EPR Reference Source Term and a particular weather condition.

This calculation was performed for all weather conditions for the given representative time period. For each of the 20 dose and contamination levels, cumulative distribution functions of area sizes were calculated. It was then possible to select those area sizes for which the given dose and contamination levels are not exceeded in 95% of all evaluated cases.

Section 16.2.3 - Figures 7 to 15 show the size of these areas:

Section 16.2.3 - Figures 7 to 9 show the whole body dose a person would receive which are not exceeded in the cases 95% due to direct gamma radiation from ground contamination.

In addition to inhalation and direct radiation doses, it is necessary to evaluate ingestion doses. Therefore the direct contamination of leafy vegetables (salad - being representative of all plants used directly as foodstuffs) and the contamination of milk from animals grazing on contaminated pastures (representing plants used indirectly) are evaluated. Section 16.2.3 - Figures 10 to 15 show the calculated foodstuff contamination values immediately after the accident for leafy vegetables and milk, as a function of the size of the area, which is not exceeded in 95% of the cases.

For comparison with EU contamination limits for foodstuffs [Ref-4] only contamination with Cs-137, Cs-134, I-131 and Sr-90 is of concern. The curves labelled "all nuclides except Sr and I" are of minor importance since they include nuclides with relatively short half-lives.

All these results confirm that the radiological objectives stated in Sub-section 3.1 are met.

The next section presents the radiological consequence evaluation using EDF methodology. It must be noted that as yet no comparison with EU contamination limits for foodstuffs has been made.

3.4. EVALUATION OF THE POTENTIAL RADIOLOGICAL CONSEQUENCES USING FRENCH NPP ASSESSMENT METHOD

The principles involved in assessing the radiological consequences associated with severe accidents are listed below:

- the evaluation of the activity released is based on a reference source term, calculated with reasonably conservative bounding assumptions, independent of the accident scenario,

- the assumptions used in calculating radiological consequences (dose evaluation) are fixed realistically to give a reasonably conservative evaluation of the radiological consequences.

The calculation of the effective dose includes all potential exposure routes: external exposure to radiation plumes and deposits and internal exposure by inhalation and ingestion of contaminated foodstuffs. The dose is assessed over a period of up to 50 years.

The results are presented:

- At 7 days: The doses at 7 days correspond to the exposure of an individual located in the immediate vicinity of the site at the time of the release. The effective doses received via inhalation and external exposure to the plume and to deposits on the ground are calculated at 500 m from the reactor. In addition, the thyroid dose due to radio-iodine inhalation is evaluated for an adult and a 1-year-old infant at the same distance;

- At 50 years: The 50 year dose represents the effects integrated over the life of an individual. In addition to the doses received during the passage of a radioactive cloud, the doses received during this phase include those due to the persistency of the contamination deposited on the ground. Individuals living close to the power plant are subjected to external exposure to deposits on the ground and to internal exposure by ingesting contaminated foodstuffs, for a duration of 50 years. These doses are evaluated 2km from the point of release.

3.4.1. Dose calculation method

The atmospheric concentration integrated over the timescale of the passage of the plume is obtained using a differential equation representing atmospheric diffusion. The model used is a Gaussian plume model with a standard deviation evaluated using the 2 class Doury model [Ref-1].

The calculations were performed taking into account standard meteorological conditions which ensure a broad coverage of atmospheric dispersion effects. The conditions of weak diffusion with a wind speed of 2 m/sec were used. It can be seen that these cover around 90% of the conditions encountered whichever French NPP site is considered (even if the site is located on the sea shore such as Flamanville). Changes in meteorological conditions such as wind speed, wind direction and diffusion are taken into account depending on the release duration by suing a correction factor, ranging from 1 to 5, applied to the horizontal standard deviation.

The conversion factors for dose and respiratory flow rates are chosen in accordance with the International Commission on Radiological Protection (ICRP) and Euratom guidance and recommendations [Ref-2] [Ref-3].

Data concerning life habits, exposure conditions, integration time and transfer of radionuclides into the environment used in the EDF methodology is realistic in terms of all French sites [Ref-4].

The preliminary dose calculations obtained by applying the EDF methodology, and presented here, are considered to be generic in nature.

3.4.2. Reference source term

The design options available for the EPR are such that the risks of core melt are very low. As a result of the reinforced defence in depth concept, design provisions are adopted which make it possible to exclude severe accident phenomena which could lead to large early releases. Low pressure core melt sequences are dealt with in the design by specific provisions aimed at ensuring the integrity of the containment under such situations.

An examination of RRC-B conditions shows that, taking account of the design provisions adopted, the radiological objectives associated with these situations are met (see section 3.1.2. of this sub-chapter).

The main assumptions of the reference source term are as follows:

- 100% core melt,

- releases of the most significant radionuclides, from the point of view of radiological consequences (noble gases, iodine and caesium) have been maximised (100% release in the containment vessel),

UK EPR

PRE-CONSTRUCTION SAFETY REPORT

CHAPTER 16: RISK REDUCTION AND SEVERE
ACCIDENT ANALYSES

SUB-CHAPTER : 16.2

PAGE : 246 / 295

Document ID.No.
UKEPR-0002-162 Issue 05

- quantity of aerosols in suspension in the containment falls because of natural deposition only. The effectiveness of the containment spray system has not been taken into consideration.

During a severe accident in an EPR, the integrity of the containment vessel is ensured by specific provisions which justify the use of the PCC assumptions [Ref-1] to assess releases to the environment:

- an internal containment leak rate of 0.3% by volume/day (maximum internal containment leak rate at its absolute design pressure of 5.5 bar),

- filtration which allows 99.9% of the aerosols and molecular iodine and 99% of the organic iodine to be retained. Noble gases cannot be filtered.

Given the conservative assumptions taken, the reference source term bounds that from low pressure core melt accidents.

3.4.3. Radiological consequences calculations

Using the assumptions stated above into account, the preliminary reference source term is shown in the table below. It is expressed as percentages of the core activity released to the environment for selected radionuclides.

Radionuclides	^{133}Xe	^{131}I	^{137}Cs	^{132}Te	^{90}Sr	^{106}Ru	^{141}Ce	^{241}Pu
Source Term (% C.I.)[3]	$1.5 \times 10^{+0}$	6.1×10^{-5}	7.0×10^{-6}	5.1×10^{-6}	1.3×10^{-6}	2.6×10^{-7}	2.6×10^{-7}	4.6×10^{-8}

From the fractions released into the environment and the methods and assumptions described in section 3.2 of this sub-chapter, the short term and long term doses as a function of the distance around the reactor have been evaluated [Ref-1] and are shown below (see also Section 16.2.3 - Figures 16 to 19).

		Dose 500 m (7 days)		Dose 2 km (50 years)
	Dose (Sv)	Adult (Sv)	Infant 1y (Sv)	Adult (Sv)
Severe Accident RRC-B	Effective whole body Thyroid	$1.5 \ 10^{-2}$ $1.3 \ 10^{-2}$	$1.6 \ 10^{-2}$ $2.0 \ 10^{-2}$	$3.0 \ 10^{-3}$ $2.4 \ 10^{-3}$

These results confirm that the main radiological objectives are met:

- evacuation or relocation of the population is not necessary: only limited sheltering very close to the site boundary is envisaged;

---

[3] % C.I. : percentage of Core Inventory

- the dose rate due to radiation from radionuclides deposited on the ground and the effective whole body dose are much lower than the long term objectives.

SECTION 16.2.3 - TABLE 1

Release Fractions from the Molten Core

Element	Release Fraction (German assumptions)	Release Fraction (French NPPs assumptions)	Release Fraction considered in assessing the reference source term
Kr	1	1	1
Xe	1	1	1
Rb	1	1	1
Sr	0.03	0.065	0.065
Y	0.02	0.0065	0.02
Zr	0.03	0.0065	0.03
Nb	0.02	0.0065	0.02
Mo	0.02	0.39	0.39
Tc	0.02	0.0325	0.0325
Ru	0.02	0.0325	0.0325
Rh	0.02	0.0325	0.0325
Sb	0.25	1	1
Te	0.25	0.91	0.91
I	1	1	1
Cs	1	1	1
Ba	0.04	0.325	0.325
La	0.02	0.0065	0.02
Ce	0.02	0.0325	0.0325
Pr	0.02	0.0065	0.02
Nd	0.02	0.0065	0.02
Np	0.003	0.0325	0.0325
Pu	0.003	0.00325	0.00325
Cm	0.003	0.0065	0.0065

SECTION 16.2.3 - TABLE 2

Radiological Data and Assumptions Used for the Reference Core Melt Scenario

- Aerosol depletion in the containment : deposition only

Iodine behaviour:

- Starting point: ~ 97.5   % attached to aerosols,
                       2.5   % elemental iodine
                       0.2   % organic iodine

- Later on: Aerosol depletion : Deposition only.
                    Steady state for elemental iodine after 3 hours : 0.2%.
                    Constant level for organic iodine

- Containment leak rate:
  Inner Containment   0.3%   vol./day

- Leaks collected in Annulus are released to the environment filtered via the stack (aerosol depletion: identical to the long term depletion in the containment)

- Ventilation rate: 200 m^3/h

- Filter retention efficiency of 99% for aerosols and all gaseous iodine forms

- Emission height: 0 m.

- Weather conditions in respect of activity dispersion are assumed to have a conditional probability of 95%; i.e. probability that they will be exceeded is 5%.

- Dispersion parameters, gamma dose factors, deposition and washout factors as well as transfer factors from soil to plants are taken from German Accident Calculation Bases.

- Tissue weighting factors are taken from ICRP Publication 60. The committed doses were calculated for 50 years. Continuous occupancy at one location was assumed.

SECTION 16.2.3 - TABLE 3

Dose Criteria for Countermeasures, according to ICRP Publication 63

Action	... may be justified [mSv]	… almost always justified [mSv]	dose to:
Short-term			
sheltering	5 ... 50	50	whole body
iodine tablets	50 ... 500	500	thyroid
evacuation	50 ... 500	500	whole body
Long-term			
food-control		10 in 1 year	whole body
relocation	5 ... 15 per month	1000 in 50 years	whole body

SECTION 16.2.3 - TABLE 4

EC Contamination Limits for Foodstuffs

Nuclide Group	Baby Food Bq/kg	Beverages (milk) Bq/kg	Others Bq/kg
Strontium (particularly Sr 90)	75	125	750
Iodine (particularly I 131)	150	500	2000
Other nuclides (particularly Cs 134+137)	400	1000	1250

UK EPR

PRE-CONSTRUCTION SAFETY REPORT

CHAPTER 16: RISK REDUCTION AND SEVERE ACCIDENT ANALYSES

SUB-CHAPTER : 16.2

PAGE : 252 / 295

Document ID.No.
UKEPR-0002-162 Issue 05

SECTION 16.2.3 - TABLE 5

Activity concentration (Bq/m³) in the containment atmosphere

Time(h):	1.0E+00	4.0E+00	8.0E+00	1.6E+01	2.4E+01	4.8E+01	1.2E+02	2.4E+02	4.8E+02	7.2E+02
Kr83m	6.7E+12	2.9E+12	7.3E+11	4.0E+10	2.1E+09	3.3E+05	-	-	-	-
Kr85m	1.3E+13	8.4E+12	4.5E+12	1.3E+12	3.8E+11	9.2E+09	1.3E+05	-	-	-
Kr87	1.8E+13	3.5E+12	4.0E+11	5.1E+09	6.5E+07	1.4E+02	-	-	-	-
Kr88	3.4E+13	1.6E+13	6.1E+12	8.7E+11	1.2E+11	3.5E+08	8.0E+00	-	-	-
Rb88	3.1E+13	1.5E+13	6.2E+12	9.2E+11	1.3E+11	3.8E+08	8.8E+00	-	-	-
Rb89	2.3E+12	1.8E+08	1.0E+03	-	-	-	-	-	-	-
Sr89	1.1E+12	3.2E+11	1.0E+11	3.5E+10	1.6E+10	3.6E+09	1.4E+08	7.6E+05	2.1E+01	-
Sr90	1.1E+11	3.0E+10	1.0E+10	3.4E+09	1.6E+09	3.6E+08	1.5E+07	8.4E+04	2.7E+00	-
Y90	7.5E+10	2.1E+10	7.2E+09	2.5E+09	1.2E+09	2.9E+08	1.4E+07	8.2E+04	2.7E+00	-
Sr91	1.3E+12	2.9E+11	7.2E+10	1.4E+10	3.6E+09	1.4E+08	2.9E+04	-	-	-
Y91	9.6E+11	2.7E+11	8.9E+10	3.0E+10	1.4E+10	3.1E+09	1.3E+08	6.7E+05	1.9E+01	-
Sr92	1.1E+12	1.5E+11	1.8E+10	7.8E+08	4.8E+07	2.3E+04	-	-	-	-
Y92	1.0E+12	2.6E+11	5.5E+10	5.5E+09	6.4E+08	1.5E+06	-	-	-	-
Y93	7.0E+11	1.6E+11	4.0E+10	7.9E+09	2.2E+09	9.3E+07	2.8E+04	-	-	-
Y95	1.2E+10	1.8E+04	-	-	-	-	-	-	-	-
Zr95	1.9E+12	5.3E+11	1.8E+11	6.0E+10	2.8E+10	6.1E+09	2.5E+08	1.3E+06	3.8E+01	-
Nb95	1.3E+12	3.6E+11	1.2E+11	4.0E+10	1.9E+10	4.0E+09	1.6E+08	8.1E+05	2.1E+01	-
Zr97	1.7E+12	4.3E+11	1.2E+11	3.0E+10	1.0E+10	8.2E+08	1.8E+06	7.0E+01	-	-
Mo99	1.4E+12	3.8E+11	1.2E+11	3.7E+10	1.6E+10	2.8E+09	5.4E+07	8.7E+04	-	-
Tc99m	1.2E+12	3.4E+11	1.1E+11	3.5E+10	1.5E+10	2.7E+09	5.3E+07	8.4E+04	-	-
Ru103	1.1E+12	3.2E+11	1.0E+11	3.5E+10	1.6E+10	3.6E+09	1.4E+08	7.3E+05	2.0E+01	-
Rh103m	1.1E+12	3.2E+11	1.0E+11	3.5E+10	1.6E+10	3.6E+09	1.4E+08	7.4E+05	2.0E+01	-
Ru105	6.5E+11	1.1E+11	2.0E+10	2.0E+09	2.7E+08	1.4E+06	-	-	-	-
Rh105	7.1E+11	1.9E+11	6.2E+10	1.8E+10	7.5E+09	1.0E+09	1.1E+07	5.8E+03	-	-
Ru106	3.9E+11	1.1E+11	3.7E+10	1.2E+10	5.8E+09	1.3E+09	5.4E+07	3.0E+05	9.4E+00	-
Sb127	7.6E+11	2.1E+11	6.7E+10	2.1E+10	9.4E+09	1.7E+09	4.3E+07	9.8E+04	-	-
Te127	7.4E+11	2.0E+11	6.3E+10	2.0E+10	8.7E+09	1.6E+09	3.9E+07	9.2E+04	-	-
Sb129	2.5E+12	4.3E+11	7.7E+10	7.3E+09	9.8E+08	4.9E+06	2.4E+00	-	-	-
Te129m	5.5E+11	1.6E+11	5.1E+10	1.7E+10	8.1E+09	1.8E+09	6.9E+07	3.5E+05	9.1E+00	-
Te129	2.6E+12	5.4E+11	1.1E+11	1.9E+10	6.3E+09	1.2E+09	4.5E+07	2.3E+05	5.9E+00	-
Sb131	1.2E+12	1.5E+09	3.6E+05	-	-	-	-	-	-	-
Te131m	1.7E+12	4.5E+11	1.4E+11	3.9E+10	1.5E+10	1.9E+09	1.5E+07	5.4E+03	-	-
Te131	3.7E+12	1.2E+11	3.1E+10	8.6E+09	3.4E+09	4.3E+08	3.4E+06	1.2E+03	-	-
I131ae	3.6E+13	9.9E+12	3.2E+12	1.1E+12	4.9E+11	9.9E+10	3.2E+09	1.2E+07	1.6E+02	-
I131org	1.2E+11	1.2E+11	1.2E+11	1.1E+11	1.1E+11	1.0E+11	7.6E+10	4.9E+10	2.0E+10	8.2E+09
I131el	4.5E+11	1.2E+11	1.2E+11	1.1E+11	1.1E+11	1.0E+11	7.7E+10	4.9E+10	2.0E+10	8.2E+09
Te132	1.3E+13	3.6E+12	1.1E+12	3.6E+11	1.6E+11	2.8E+10	6.2E+08	1.2E+06	4.2E+00	-
I132ae	4.2E+13	7.0E+12	1.5E+12	3.8E+11	1.6E+11	2.9E+10	6.3E+08	1.2E+06	4.4E+00	1.6E-05
I132org	1.3E+11	5.3E+10	1.6E+10	1.4E+09	1.3E+08	9.2E+04	-	-	-	-
I132el	4.9E+11	5.5E+10	1.6E+10	1.4E+09	1.3E+08	9.2E+04	-	-	-	-
Te133m	4.1E+12	1.2E+11	2.0E+09	1.7E+06	1.9E+03	-	-	-	-	-
Te133	1.0E+12	2.0E+10	3.3E+08	2.8E+05	3.3E+02	-	-	-	-	-

SECTION 16.2.3 - TABLE 6

Activity concentration (Bq/m³) in the containment atmosphere (Part 2)

Time(h):	1.0E+00	4.0E+00	8.0E+00	1.6E+01	2.4E+01	4.8E+01	1.2E+02	2.4E+02	4.8E+02	7.2E+02
I133ae	7.2E+13	1.8E+13	5.3E+12	1.4E+12	5.0E+11	5.0E+10	1.9E+08	2.0E+04	-	-
I133org	2.4E+11	2.2E+11	1.9E+11	1.5E+11	1.1E+11	5.0E+10	4.5E+09	8.2E+07	2.7E+04	8.8E+00
I133el	9.1E+11	2.3E+11	1.9E+11	1.5E+11	1.1E+11	5.0E+10	4.5E+09	8.2E+07	2.7E+04	8.8E+00
Xe133m	3.9E+12	3.8E+12	3.6E+12	3.2E+12	2.9E+12	2.1E+12	8.1E+11	1.6E+11	6.7E+09	2.7E+08
Xe133	1.2E+14	1.2E+14	1.2E+14	1.1E+14	1.1E+14	9.4E+13	6.3E+13	3.2E+13	8.4E+12	2.2E+12
Te134	6.3E+12	8.9E+10	5.5E+08	6.5E+04	1.1E+01	-	-	-	-	-
I134ae	4.3E+13	1.4E+12	2.2E+10	1.3E+07	1.1E+04	-	-	-	-	-
I134org	1.2E+11	1.1E+10	4.7E+08	7.9E+05	1.3E+03	-	-	-	-	-
I134el	4.7E+11	1.2E+10	4.7E+08	7.9E+05	1.3E+03	-	-	-	-	-
Cs134	7.1E+12	2.0E+12	6.6E+11	2.2E+11	1.1E+11	2.3E+10	9.7E+08	5.5E+06	1.7E+02	-
I135ae	6.4E+13	1.3E+13	2.9E+12	4.2E+11	8.5E+10	1.5E+09	3.3E+04	-	-	-
I135org	2.1E+11	1.6E+11	1.0E+11	4.4E+10	1.9E+10	1.5E+09	7.9E+05	2.6E+00	-	-
I135el	8.1E+11	1.6E+11	1.0E+11	4.4E+10	1.9E+10	1.5E+09	7.9E+05	2.6E+00	-	-
Xe135m	1.3E+13	2.5E+12	5.0E+11	7.0E+10	1.4E+10	2.5E+08	5.4E+03	-	-	-
Xe135	4.1E+13	3.9E+13	3.0E+13	1.7E+13	9.3E+12	1.5E+12	6.2E+09	6.5E+05	-	-
Cs137	4.9E+12	1.4E+12	4.6E+11	1.5E+11	7.3E+10	1.6E+10	6.8E+08	3.8E+06	1.2E+02	-
Xe138	5.6E+12	8.0E+08	5.9E+03	-	-	-	-	-	-	-
Cs138	3.3E+13	2.3E+11	4.4E+08	4.9E+03	-	-	-	-	-	-
Ba140	2.7E+12	7.6E+11	2.5E+11	8.3E+10	3.8E+10	8.0E+09	2.9E+08	1.2E+06	2.3E+01	-
La140	1.5E+12	4.3E+11	1.5E+11	5.4E+10	2.7E+10	6.8E+09	3.0E+08	1.4E+06	2.6E+01	-
Ce141	1.2E+12	3.5E+11	1.2E+11	3.9E+10	1.8E+10	3.9E+09	1.5E+08	7.8E+05	2.0E+01	-
Ce143	1.1E+12	3.0E+11	9.2E+10	2.6E+10	1.0E+10	1.4E+09	1.3E+07	5.9E+03	-	-
Pr143	1.1E+12	3.2E+11	1.1E+11	3.6E+10	1.7E+10	3.6E+09	1.3E+08	5.9E+05	1.1E+01	-
Ce144	9.4E+11	2.6E+11	8.8E+10	3.0E+10	1.4E+10	3.1E+09	1.3E+08	7.1E+05	2.2E+01	-
Nd147	5.0E+11	1.4E+11	4.6E+10	1.5E+10	7.0E+09	1.5E+09	5.0E+07	2.1E+05	3.5E+00	-
Pu238	2.1E+08	5.8E+07	1.9E+07	6.5E+06	3.1E+06	6.8E+05	2.8E+04	1.6E+02	-	-
Np239	2.1E+12	5.6E+11	1.8E+11	5.5E+10	2.3E+10	3.9E+09	6.7E+07	8.7E+04	-	-
Pu241	1.8E+10	4.9E+09	1.6E+09	5.5E+08	2.6E+08	5.8E+07	2.4E+06	1.4E+04	-	-
Cm242	5.4E+09	1.5E+09	5.0E+08	1.7E+08	8.0E+07	1.8E+07	7.3E+05	4.0E+03	-	-
Cm244	3.8E+08	1.1E+08	3.6E+07	1.2E+07	5.7E+06	1.3E+06	5.2E+04	3.0E+02	-	-
Total	6.8E+14	2.8E+14	1.9E+14	1.4E+14	1.2E+14	9.8E+13	6.4E+13	3.2E+13	8.4E+12	2.2E+12

SECTION 16.2.3 - TABLE 7

Severe Accident - Cumulative activity release to the environment around the plant, Bq

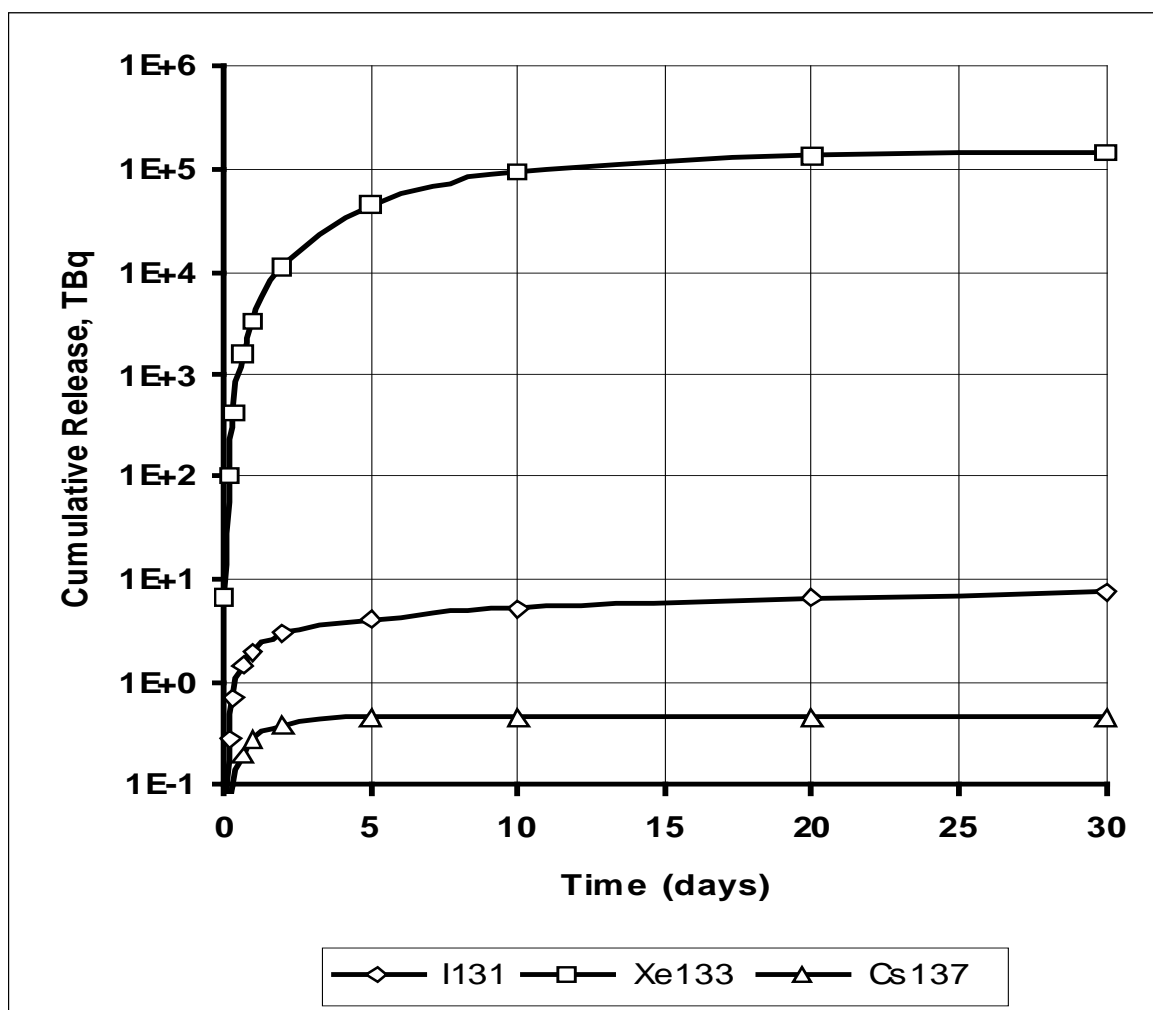| Time(h):	1.0E+00	4.0E+00	8.0E+00	1.6E+01	2.4E+01	4.8E+01	1.2E+02	2.4E+02	4.8E+02	7.2E+02
Kr83m	3.9E+11	4.2E+12	8.7E+12	1.1E+13	1.2E+13	1.2E+13	1.2E+13	1.2E+13	1.2E+13	1.2E+13
Kr85m	7.8E+11	9.2E+12	2.5E+13	4.9E+13	6.1E+13	6.7E+13	6.8E+13	6.8E+13	6.8E+13	6.8E+13
Kr87	1.2E+12	7.4E+12	1.1E+13	1.2E+13	1.2E+13	1.2E+13	1.2E+13	1.2E+13	1.2E+13	1.2E+13
Kr88	2.1E+12	2.0E+13	4.6E+13	7.0E+13	7.6E+13	7.8E+13	7.8E+13	7.8E+13	7.8E+13	7.8E+13
Rb88	2.1E+10	2.2E+11	4.9E+11	7.6E+11	8.2E+11	8.4E+11	8.4E+11	8.4E+11	8.4E+11	8.4E+11
Rb89	5.7E+09	7.2E+09	7.2E+09	7.2E+09	7.2E+09	7.2E+09	7.2E+09	7.2E+09	7.2E+09	7.2E+09
Sr89	8.5E+08	8.7E+09	2.2E+10	4.5E+10	6.3E+10	8.9E+10	1.0E+11	1.0E+11	1.0E+11	1.0E+11
Sr90	8.2E+07	8.4E+08	2.1E+09	4.4E+09	6.1E+09	8.6E+09	9.8E+09	9.9E+09	9.9E+09	9.9E+09
Y90	5.7E+07	5.9E+08	1.5E+09	3.1E+09	4.4E+09	6.4E+09	7.4E+09	7.5E+09	7.5E+09	7.5E+09
Sr91	1.0E+09	9.1E+09	2.0E+10	3.2E+10	3.7E+10	4.1E+10	4.1E+10	4.1E+10	4.1E+10	4.1E+10
Y91	7.3E+08	7.4E+09	1.9E+10	3.9E+10	5.4E+10	7.6E+10	8.7E+10	8.7E+10	8.7E+10	8.7E+10
Sr92	9.5E+08	6.3E+09	1.0E+10	1.2E+10	1.2E+10	1.2E+10	1.2E+10	1.2E+10	1.2E+10	1.2E+10
Y92	7.9E+08	7.8E+09	1.7E+10	2.4E+10	2.6E+10	2.6E+10	2.6E+10	2.6E+10	2.6E+10	2.6E+10
Y93	5.5E+08	4.9E+09	1.1E+10	1.8E+10	2.1E+10	2.3E+10	2.3E+10	2.3E+10	2.3E+10	2.3E+10
Y95	6.0E+07	6.5E+07	6.5E+07	6.5E+07	6.5E+07	6.5E+07	6.5E+07	6.5E+07	6.5E+07	6.5E+07
Zr95	1.5E+09	1.5E+10	3.7E+10	7.7E+10	1.1E+11	1.5E+11	1.7E+11	1.7E+11	1.7E+11	1.7E+11
Nb95	9.7E+08	9.9E+09	2.5E+10	5.1E+10	7.1E+10	1.0E+11	1.1E+11	1.1E+11	1.1E+11	1.1E+11
Zr97	1.3E+09	1.3E+10	3.0E+10	5.3E+10	6.6E+10	7.7E+10	7.8E+10	7.8E+10	7.8E+10	7.8E+10
Mo99	1.1E+09	1.1E+10	2.6E+10	5.2E+10	6.9E+10	9.3E+10	1.0E+11	1.0E+11	1.0E+11	1.0E+11
Tc99m	9.4E+08	9.5E+09	2.4E+10	4.8E+10	6.5E+10	8.7E+10	9.5E+10	9.5E+10	9.5E+10	9.5E+10
Ru103	8.6E+08	8.7E+09	2.2E+10	4.5E+10	6.3E+10	8.9E+10	1.0E+11	1.0E+11	1.0E+11	1.0E+11
Rh103m	8.6E+08	8.7E+09	2.2E+10	4.5E+10	6.3E+10	8.9E+10	1.0E+11	1.0E+11	1.0E+11	1.0E+11
Ru105	5.2E+08	4.1E+09	7.7E+09	1.0E+10	1.1E+10	1.1E+10	1.1E+10	1.1E+10	1.1E+10	1.1E+10
Rh105	5.4E+08	5.5E+09	1.4E+10	2.7E+10	3.5E+10	4.5E+10	4.8E+10	4.8E+10	4.8E+10	4.8E+10
Ru106	3.0E+08	3.1E+09	7.7E+09	1.6E+10	2.2E+10	3.1E+10	3.6E+10	3.6E+10	3.6E+10	3.6E+10
Ag110m	0.0E+00	0.0E+00	0.0E+00	0.0E+00	0.0E+00	0.0E+00	0.0E+00	0.0E+00	0.0E+00	0.0E+00
Sb127	5.8E+08	5.8E+09	1.4E+10	2.9E+10	3.9E+10	5.3E+10	5.8E+10	5.8E+10	5.8E+10	5.8E+10
Te127	5.6E+08	5.6E+09	1.4E+10	2.8E+10	3.7E+10	5.0E+10	5.5E+10	5.5E+10	5.5E+10	5.5E+10
Sb129	2.0E+09	1.6E+10	2.9E+10	3.9E+10	4.1E+10	4.2E+10	4.2E+10	4.2E+10	4.2E+10	4.2E+10
Te129m	4.2E+08	4.3E+09	1.1E+10	2.2E+10	3.1E+10	4.4E+10	5.0E+10	5.0E+10	5.0E+10	5.0E+10
Te129	2.0E+09	1.8E+10	3.6E+10	5.4E+10	6.2E+10	7.1E+10	7.5E+10	7.5E+10	7.5E+10	7.5E+10
Sb131	1.9E+09	3.1E+09	3.1E+09	3.1E+09	3.1E+09	3.1E+09	3.1E+09	3.1E+09	3.1E+09	3.1E+09
Te131m	1.3E+09	1.3E+10	3.1E+10	6.0E+10	7.7E+10	9.7E+10	1.0E+11	1.0E+11	1.0E+11	1.0E+11
Te131	4.0E+09	1.2E+10	1.6E+10	2.2E+10	2.6E+10	3.0E+10	3.1E+10	3.1E+10	3.1E+10	3.1E+10
I131ae	2.7E+10	2.7E+11	6.9E+11	1.4E+12	1.9E+12	2.7E+12	3.0E+12	3.0E+12	3.0E+12	3.0E+12
I131org	6.6E+07	1.0E+09	4.1E+09	1.5E+10	3.3E+10	1.2E+11	4.9E+11	1.1E+12	1.9E+12	2.2E+12
I131el	5.7E+08	4.5E+09	1.2E+10	3.0E+10	5.4E+01	1.5E+11	5.5E+11	1.2E+12	2.0E+12	2.3E+12
Te132	1.0E+10	1.0E+11	2.5E+11	5.0E+11	6.7E+11	9.0E+11	9.8E+11	9.9E+11	9.9E+11	9.9E+11
I132ae	3.5E+10	2.5E+11	4.9E+11	7.7E+11	9.5E+11	1.2E+12	1.3E+12	1.3E+12	1.3E+12	1.3E+12
I132org	8.0E+07	7.2E+08	1.5E+09	2.0E+09	2.1E+09	2.1E+09	2.1E+09	2.1E+09	2.1E+09	2.1E+09
I132el	6.9E+08	3.4E+09	5.2E+09	6.1E+09	6.2E+09	6.3E+09	6.3E+09	6.3E+09	6.3E+09	6.3E+09
Te133m	4.1E+09	1.4E+10	1.6E+10	1.6E+10	1.6E+10	1.6E+10	1.6E+10	1.6E+10	1.6E+10	1.6E+10
Te133	1.8E+09	3.6E+09	3.9E+09	3.9E+09	3.9E+09	3.9E+09	3.9E+09	3.9E+09	3.9E+09	3.9E+09

SECTION 16.2.3 - TABLE 8

Severe Accident - Cumulative activity release to the environment around the plant, Bq (Part 2)

Time(h):	1.0E+00	4.0E+00	8.0E+00	1.6E+01	2.4E+01	4.8E+01	1.2E+02	2.4E+02	4.8E+02	7.2E+02
I133ae	5.6E+10	5.4E+11	1.3E+12	2.3E+12	2.9E+12	3.5E+12	3.6E+12	3.6E+12	3.6E+12	3.6E+12
I133org	1.4E+08	2.0E+09	7.2E+09	2.4E+10	4.4E+10	1.0E+11	1.8E+11	1.9E+11	1.9E+11	1.9E+11
I133el	1.2E+09	8.8E+09	2.1E+10	4.8E+10	7.6E+10	1.5E+11	2.3E+11	2.4E+11	2.4E+11	2.4E+11
Xe133m	2.2E+11	3.4E+12	1.3E+13	4.7E+13	9.7E+13	2.9E+14	8.6E+14	1.3E+15	1.4E+15	1.4E+15
Xe133	6.7E+12	1.1E+14	4.1E+14	1.6E+15	3.3E+15	1.1E+16	4.4E+16	9.1E+16	1.3E+17	1.4E+17
Te134	7.0E+09	1.9E+10	2.0E+10	2.0E+10	2.0E+10	2.0E+10	2.0E+10	2.0E+10	2.0E+10	2.0E+10
I134ae	4.2E+10	1.5E+11	1.7E+11	1.7E+11	1.7E+11	1.7E+11	1.7E+11	1.7E+11	1.7E+11	1.7E+11
I134org	9.2E+07	4.0E+08	4.7E+08	4.8E+08	4.8E+08	4.8E+08	4.8E+08	4.8E+08	4.8E+08	4.8E+08
I134el	8.1E+08	2.3E+09	2.4E+09	2.5E+09	2.5E+09	2.5E+09	2.5E+09	2.5E+09	2.5E+09	2.5E+09
Cs134	5.4E+09	5.5E+10	1.4E+11	2.9E+11	4.0E+11	5.7E+11	6.4E+11	6.5E+11	6.5E+11	6.5E+11
I135ae	5.0E+10	4.3E+11	8.8E+11	1.3E+12	1.5E+12	1.5E+12	1.5E+12	1.5E+12	1.5E+12	1.5E+12
I135org	1.2E+08	1.6E+09	4.8E+09	1.2E+10	1.6E+10	2.1E+10	2.2E+10	2.2E+10	2.2E+10	2.2E+10
I135el	1.1E+09	7.1E+09	1.5E+10	2.6E+10	3.2E+10	3.8E+10	3.9E+10	3.9E+10	3.9E+10	3.9E+10
Xe135m	9.4E+11	7.3E+12	1.5E+13	2.2E+13	2.4E+13	2.5E+13	2.5E+13	2.5E+13	2.5E+13	2.5E+13
Xe135	2.2E+12	3.7E+13	1.3E+14	3.8E+14	6.0E+14	9.4E+14	1.0E+15	1.0E+15	1.0E+15	1.0E+15
Cs137	3.7E+09	3.8E+10	9.6E+10	2.0E+11	2.8E+11	3.9E+11	4.5E+11	4.5E+11	4.5E+11	4.5E+11
Xe138	1.1E+12	1.4E+12	1.4E+12	1.4E+12	1.4E+12	1.4E+12	1.4E+12	1.4E+12	1.4E+12	1.4E+12
Cs138	3.6E+10	8.7E+10	8.9E+10	8.9E+10	8.9E+10	8.9E+10	8.9E+10	8.9E+10	8.9E+10	8.9E+10
Ba140	2.1E+09	2.1E+10	5.3E+10	1.1E+11	1.5E+11	2.1E+11	2.3E+11	2.4E+11	2.4E+11	2.4E+11
La140	1.1E+09	1.2E+10	3.0E+10	6.5E+10	9.3E+10	1.4E+11	1.6E+11	1.6E+11	1.6E+11	1.6E+11
Ce141	9.5E+08	9.7E+09	2.4E+10	5.0E+10	6.9E+10	9.8E+10	1.1E+11	1.1E+11	1.1E+11	1.1E+11
Ce143	8.7E+08	8.6E+09	2.1E+10	4.0E+10	5.2E+10	6.6E+10	6.9E+10	6.9E+10	6.9E+10	6.9E+10
Pr143	8.6E+08	8.8E+09	2.2E+10	4.6E+10	6.3E+10	9.0E+10	1.0E+11	1.0E+11	1.0E+11	1.0E+11
Ce144	7.2E+08	7.3E+09	1.9E+10	3.8E+10	5.3E+10	7.5E+10	8.5E+10	8.6E+10	8.6E+10	8.6E+10
Nd147	3.8E+08	3.9E+09	9.7E+09	2.0E+10	2.7E+10	3.8E+10	4.3E+10	4.3E+10	4.3E+10	4.3E+10
Pu238	1.6E+05	1.6E+06	4.0E+06	8.4E+06	1.2E+07	1.6E+07	1.9E+07	1.9E+07	1.9E+07	1.9E+07
Np239	1.6E+09	1.6E+10	3.9E+10	7.8E+10	1.0E+11	1.4E+11	1.5E+11	1.5E+11	1.5E+11	1.5E+11
Pu241	1.3E+07	1.4E+08	3.4E+08	7.1E+08	9.8E+08	1.4E+09	1.6E+09	1.6E+09	1.6E+09	1.6E+09
Am241	1.6E+00	6.1E+01	2.9E+02	1.1E+03	2.1E+03	4.7E+03	7.0E+03	7.2E+03	7.2E+03	7.2E+03
Cm242	4.1E+06	4.2E+07	1.1E+08	2.2E+08	3.0E+08	4.3E+08	4.9E+08	4.9E+08	4.9E+08	4.9E+08
Cm244	2.9E+05	3.0E+06	7.5E+06	1.6E+07	2.1E+07	3.0E+07	3.5E+07	3.5E+07	3.5E+07	3.5E+07
Total	**1.6E+13**	**2.0E+14**	**6.7E+14**	**2.2E+15**	**4.2E+15**	**1.3E+16**	**4.6E+16**	**9.4E+16**	**1.4E+17**	**1.5E+17**

{CCI Removed}

UK EPR

PRE-CONSTRUCTION SAFETY REPORT

CHAPTER 16: RISK REDUCTION AND SEVERE ACCIDENT ANALYSES

SUB-CHAPTER : 16.2

PAGE   : 257 / 295

Document ID.No.
UKEPR-0002-162 Issue 05

{CCI Removed}

b

SECTION 16.2.3 - FIGURE 3

**Activity Release to the Environment Due to the Reference Core Melt Scenario**

SECTION 16.2.3 - FIGURE 4

Fission product release to the containment atmosphere

UK EPR

PRE-CONSTRUCTION SAFETY REPORT

CHAPTER 16: RISK REDUCTION AND SEVERE
ACCIDENT ANALYSES

SUB-CHAPTER : 16.2

PAGE   : 260 / 295

Document ID.No.
UKEPR-0002-162 Issue 05

.
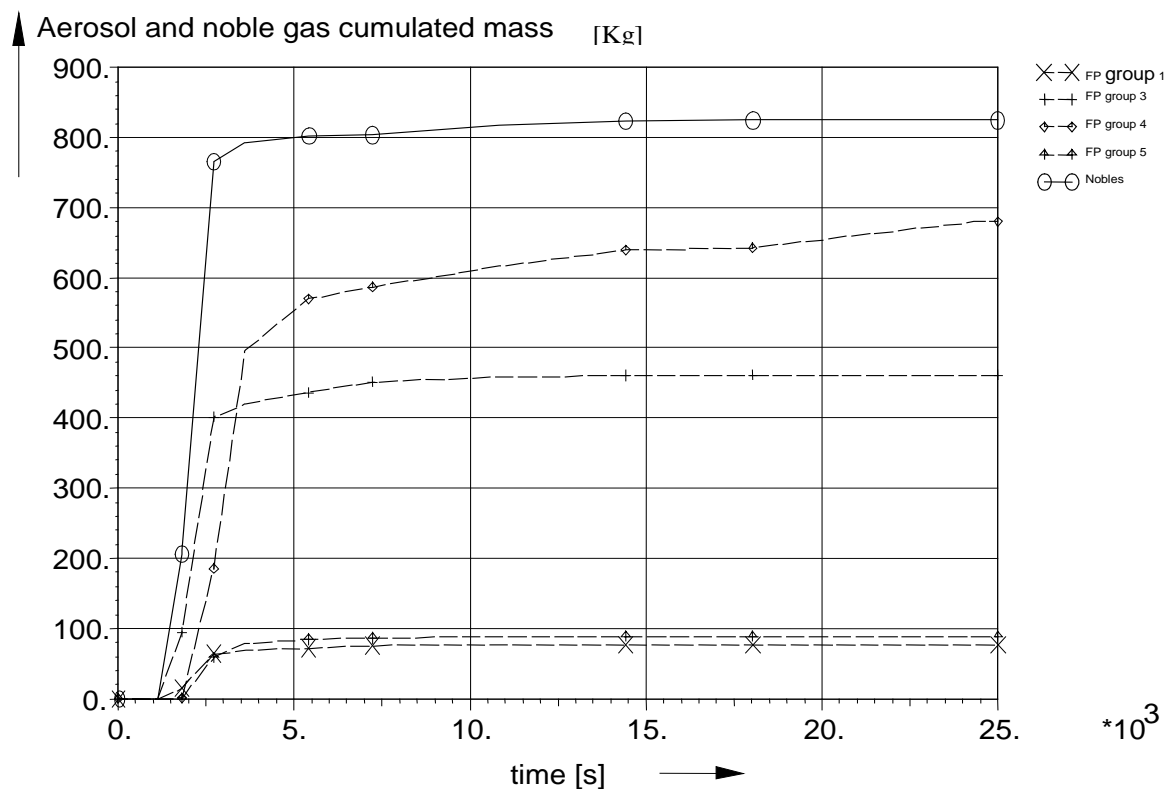
SECTION 16.2.3 - FIGURE 5

Effective dose to adults and infants by inhalation and direct radiation which is not exceeded beyond the given distance
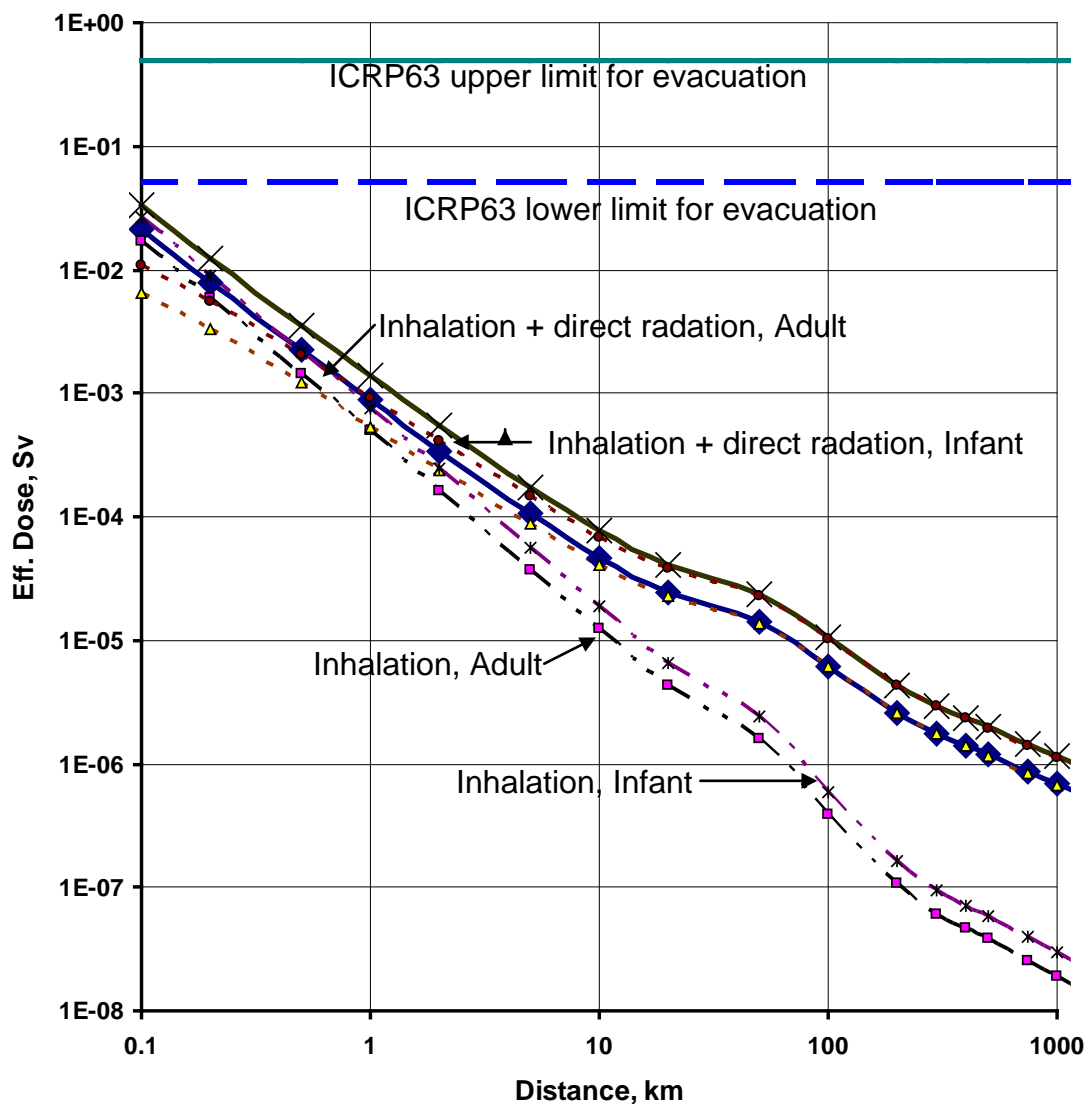
Remark: The dose by direct radiation is only a little bit smaller than the effective dose by direct radiation and inhalation. Therefore the dotted lines, which represent the doses by direct radiation only, have no legend.

SECTION 16.2.3 - FIGURE 6

Thyroid dose to adults and infants by inhalation which not exceeded beyond the given distance
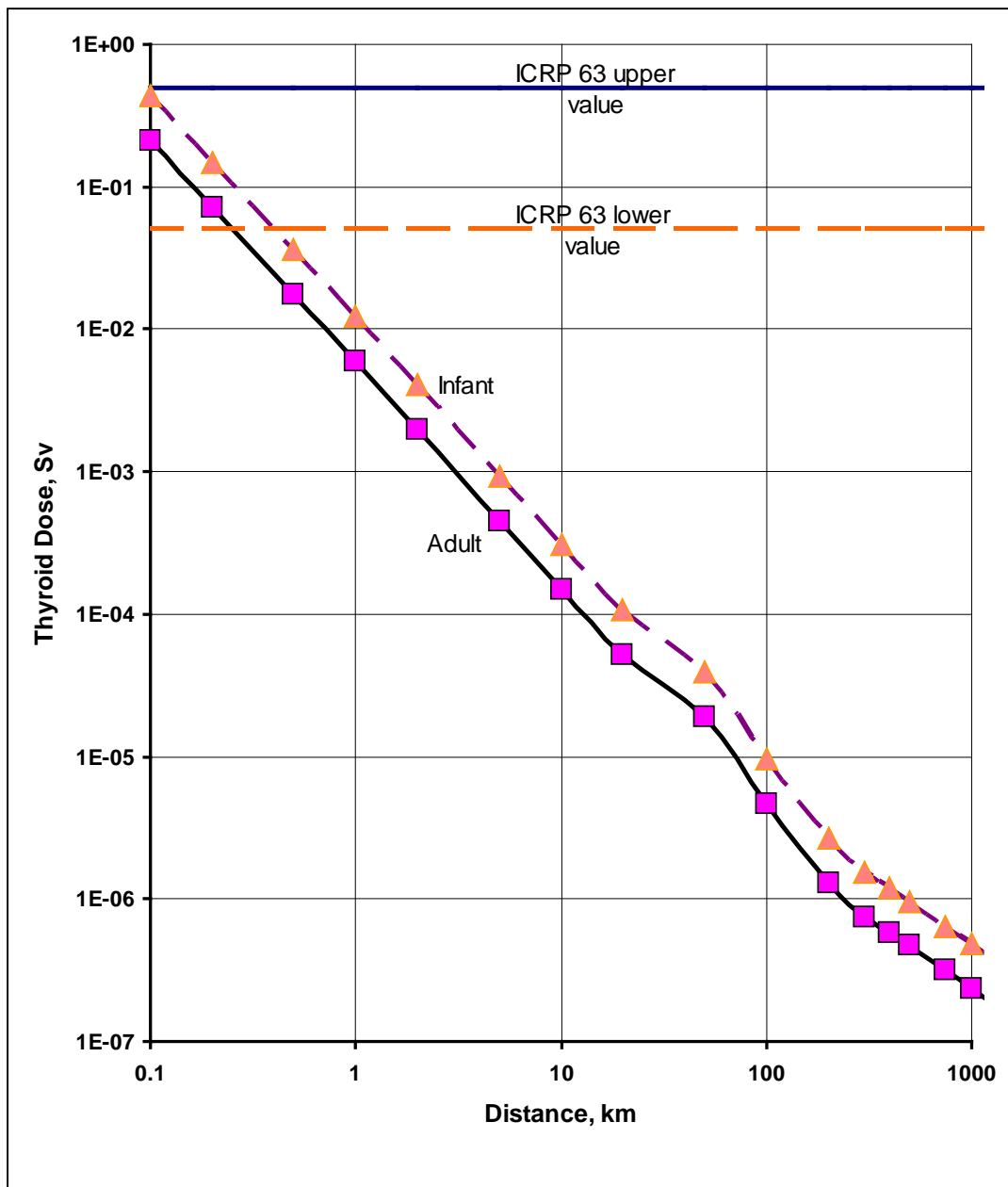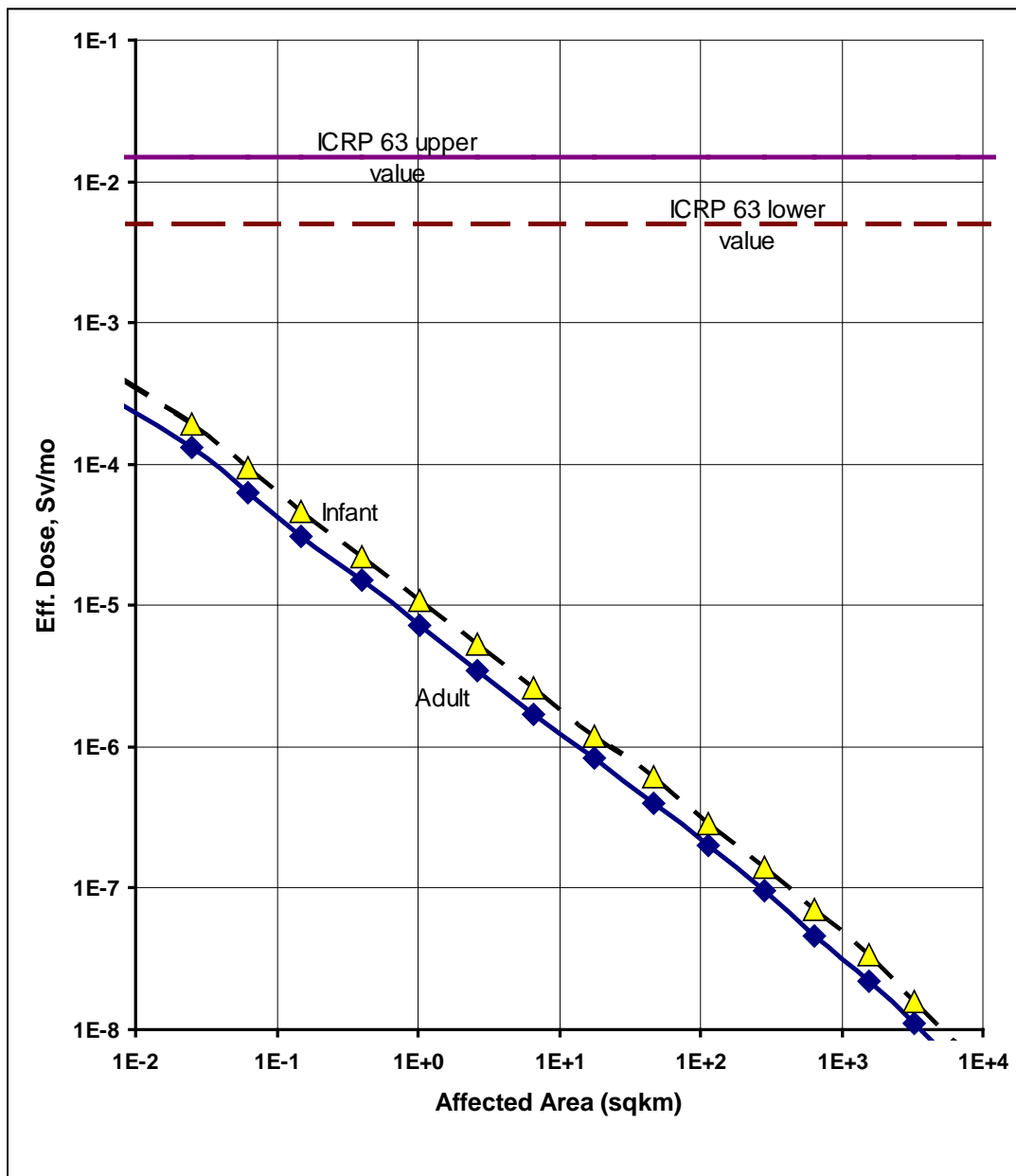
SECTION 16.2.3 - FIGURE 7

Effective dose to adults and infants due to ground radiation for the 1st month subsequent to the accident which is not exceeded beyond the given affected area
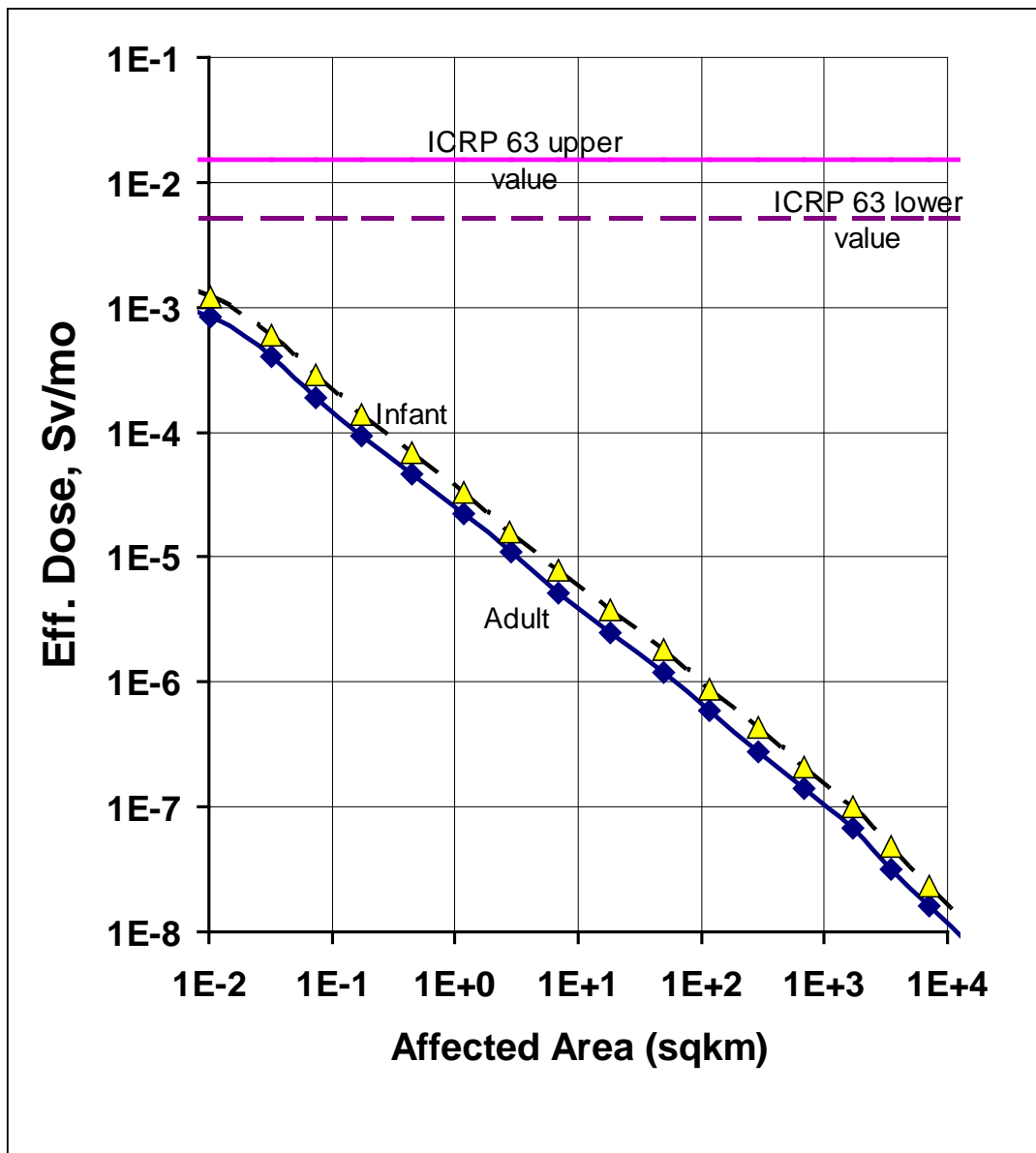
The ICRP 63 values are the limiting values for the need for relocation

SECTION 16.2.3 - FIGURE 8

Effective dose to adults and Infants due to ground radiation for the 12th month subsequent to the accident which is not exceeded beyond the given affected area
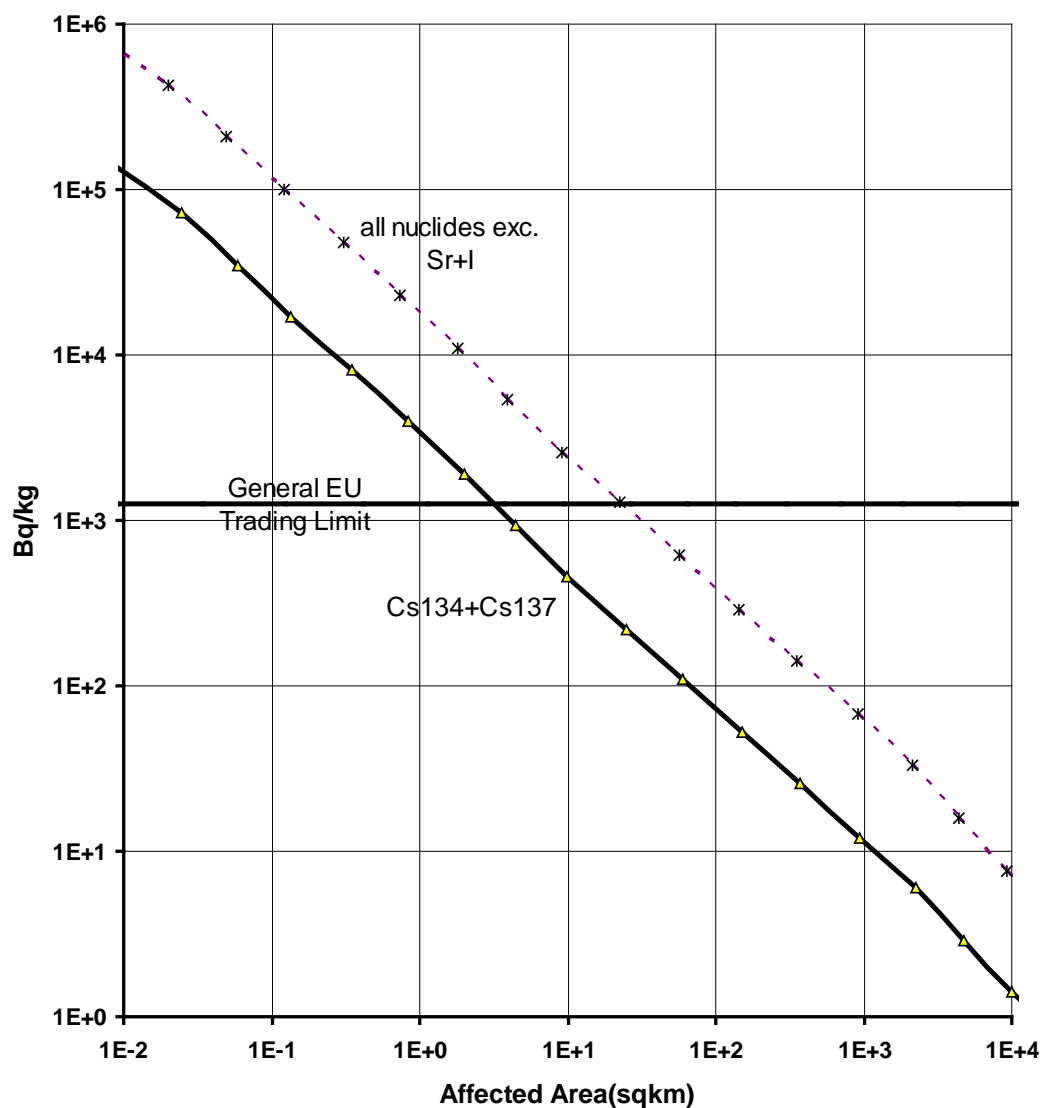
SECTION 16.2.3 - FIGURE 9

Effective dose to adults due to ground radiation for 50 years subsequent to the accident which is not exceeded beyond the given affected area
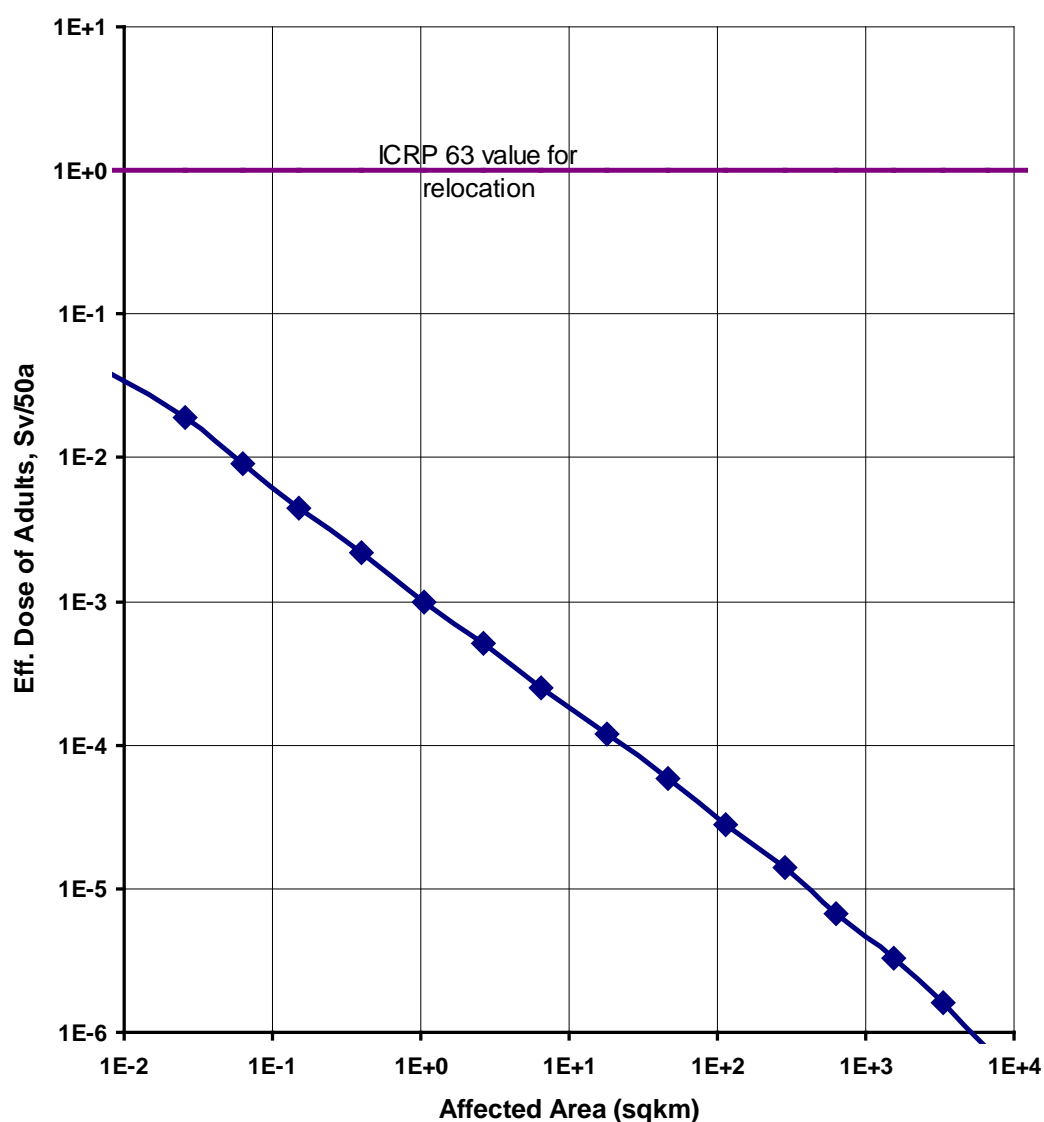
The effective dose rate from ground radiation for infants is multiplied by a factor of 1.5 compared to the dose rate for adults. Because infants grow this factor is much lower for the integrated dose over 50 years.
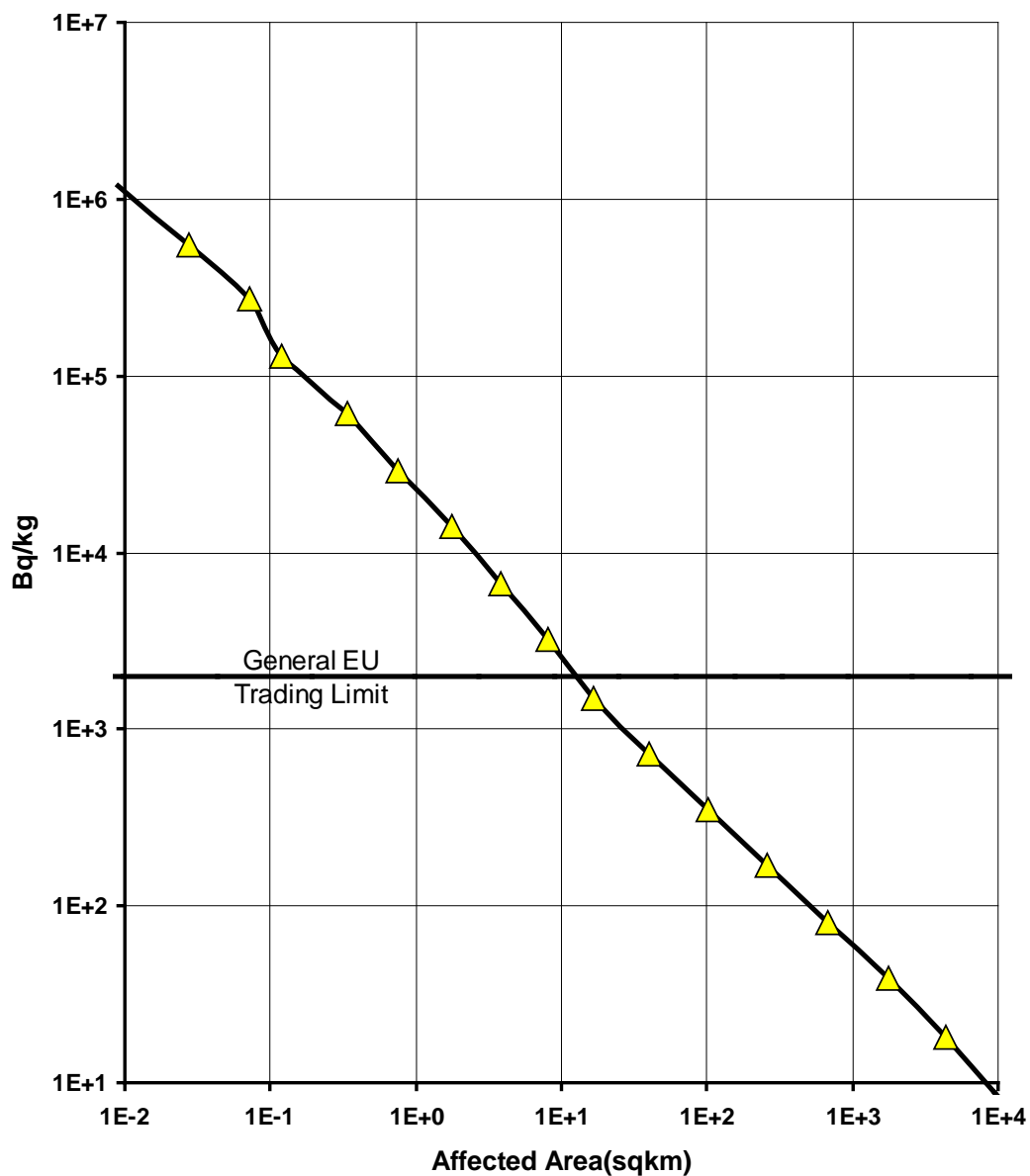
SECTION 16.2.3 - FIGURE 10

Direct contamination of leafy vegetables (Bq/kg) by Cs134+Cs137 and all nuclides except Sr+I which is not exceeded beyond the given affected area immediately after the accident
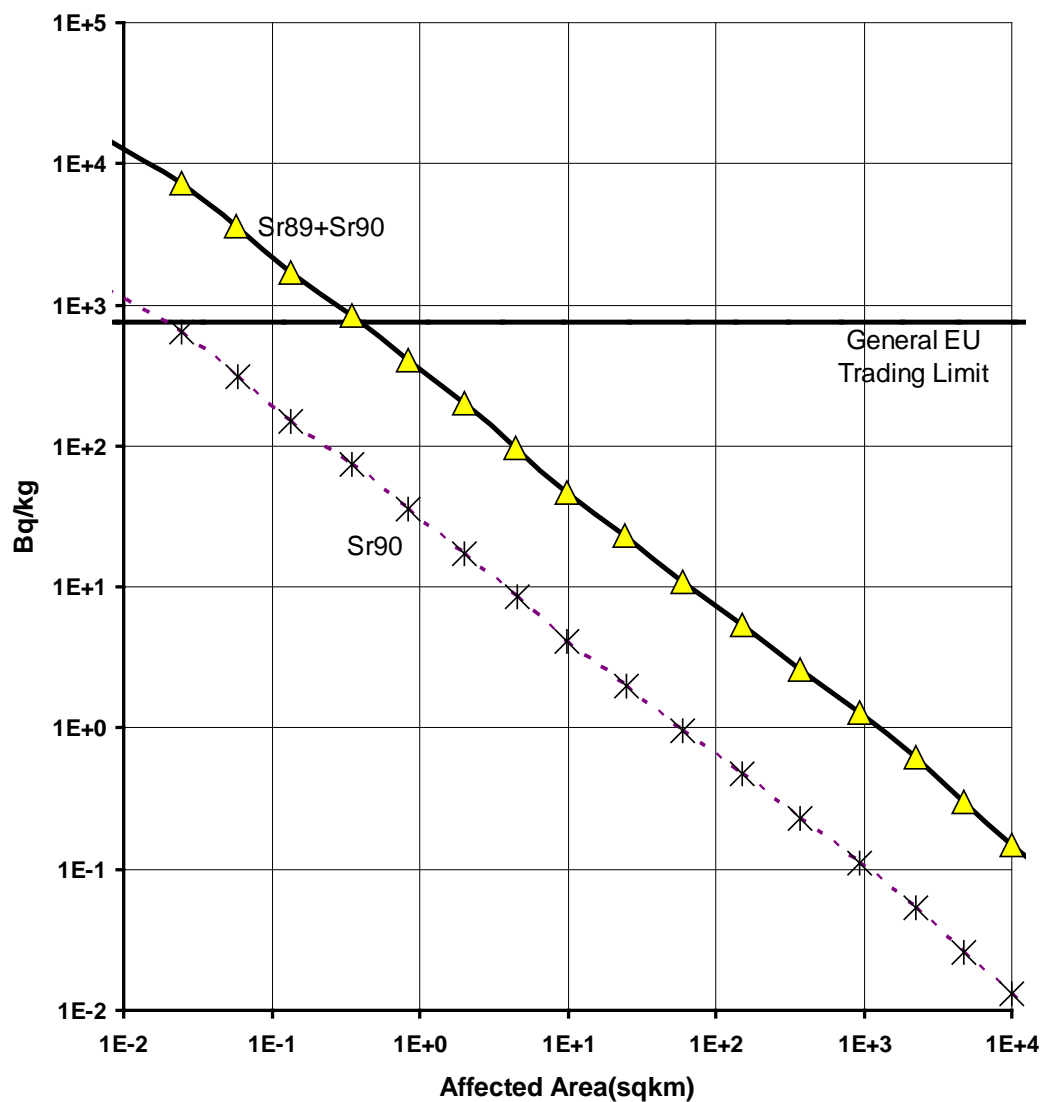
SECTION 16.2.3 - FIGURE 11

Direct contamination of leafy vegetables (Bq/kg) by Iodine-131 which is not exceeded beyond the given affected area immediately after the accident
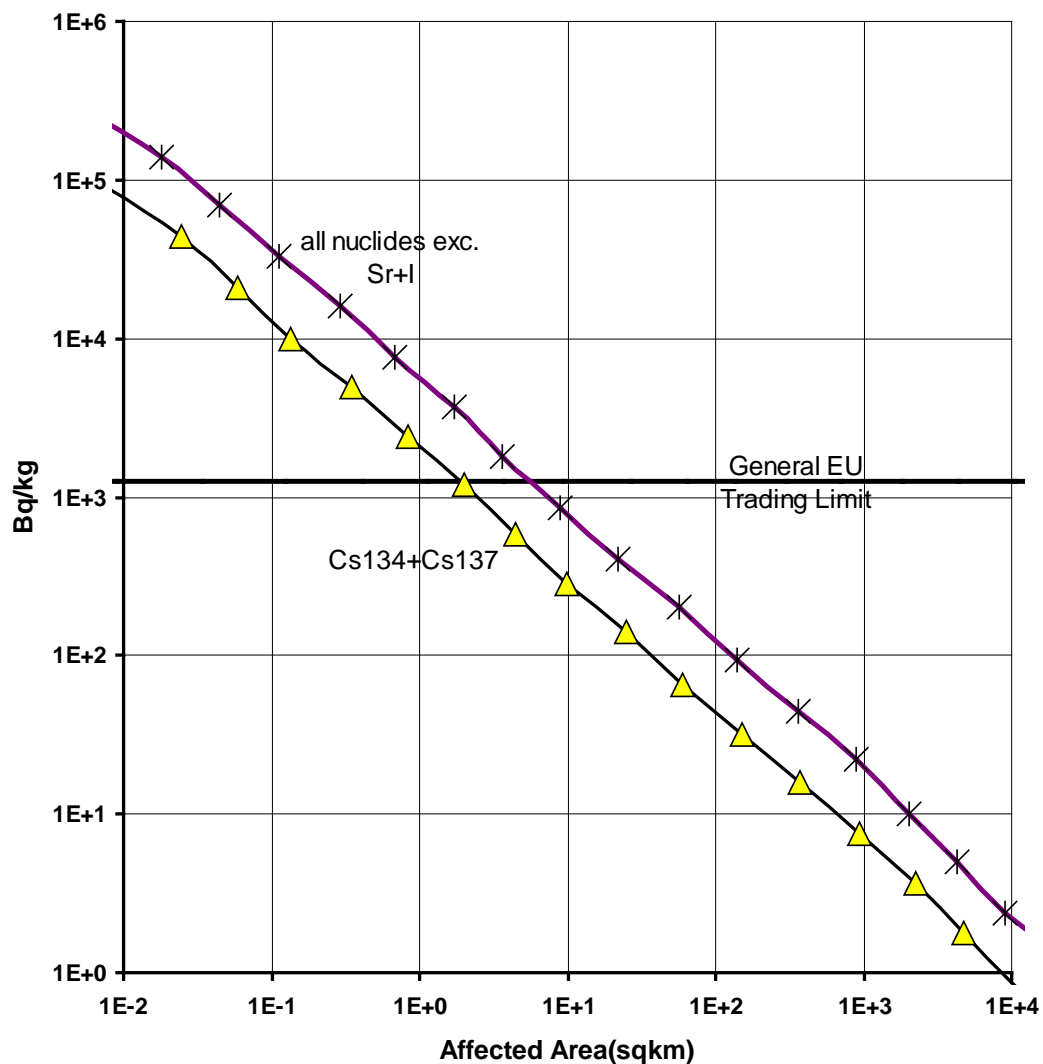
SECTION 16.2.3 - FIGURE 12

Direct contamination of leafy vegetables (Bq/kg) by Sr90 and Sr89+Sr90 which is not exceeded beyond the given affected area immediately after the accident
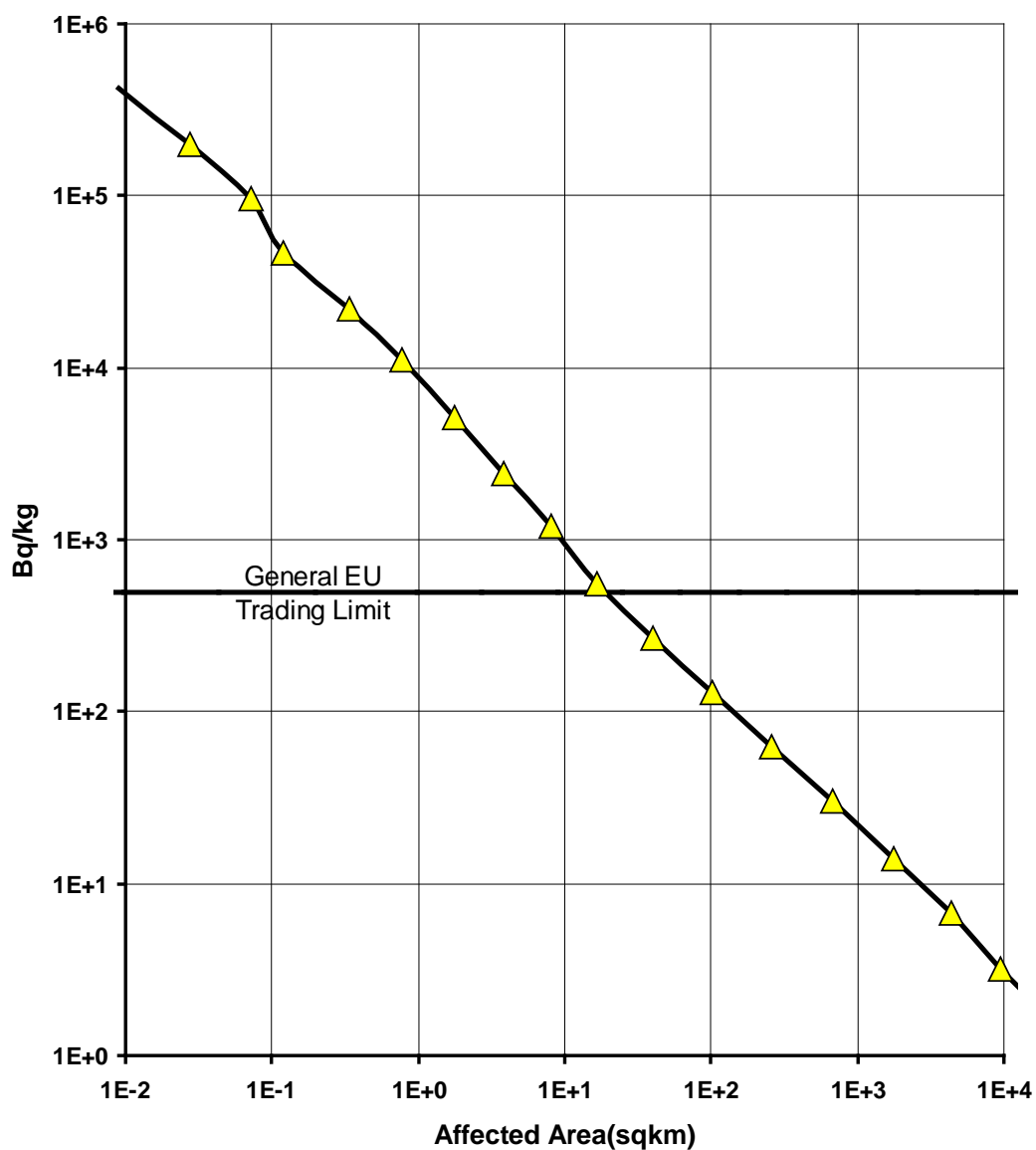
SECTION 16.2.3 - FIGURE 13

Contamination level in milk (Bq/kg) by Cs134+Cs137 and all nuclides except Sr+I immediately after the accident, which is not exceeded beyond the given affected area

UK EPR

PRE-CONSTRUCTION SAFETY REPORT

CHAPTER 16: RISK REDUCTION AND SEVERE
ACCIDENT ANALYSES

SUB-CHAPTER : 16.2

PAGE   : 269 / 295

Document ID.No.
UKEPR-0002-162 Issue 05

SECTION 16.2.3 - FIGURE 14

Contamination level in milk (Bq/kg) by Iodine-131 immediately after the accident, which is not exceeded beyond the given affected area

UK EPR

PRE-CONSTRUCTION SAFETY REPORT

CHAPTER 16: RISK REDUCTION AND SEVERE
ACCIDENT ANALYSES

SUB-CHAPTER : 16.2

PAGE   : 270 / 295

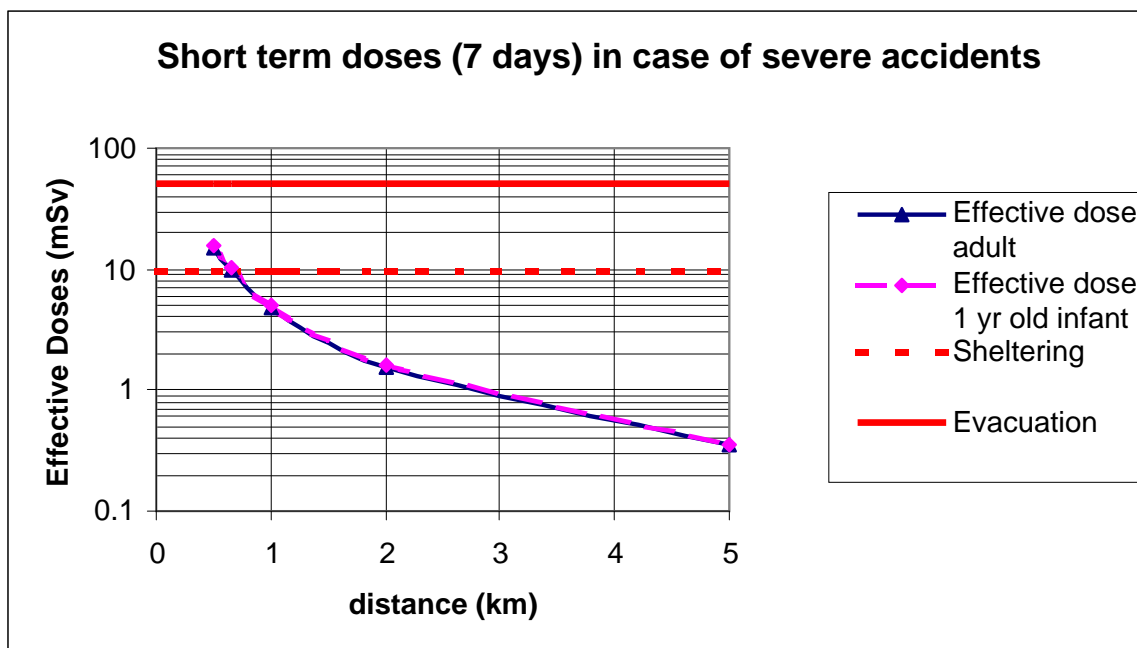Document ID.No.
UKEPR-0002-162 Issue 05

SECTION 16.2.3 - FIGURE 15

**Contamination level in milk (Bq/kg) by Sr90 and Sr89+Sr90 immediately after the
accident, which is not exceeded beyond the given affected area**
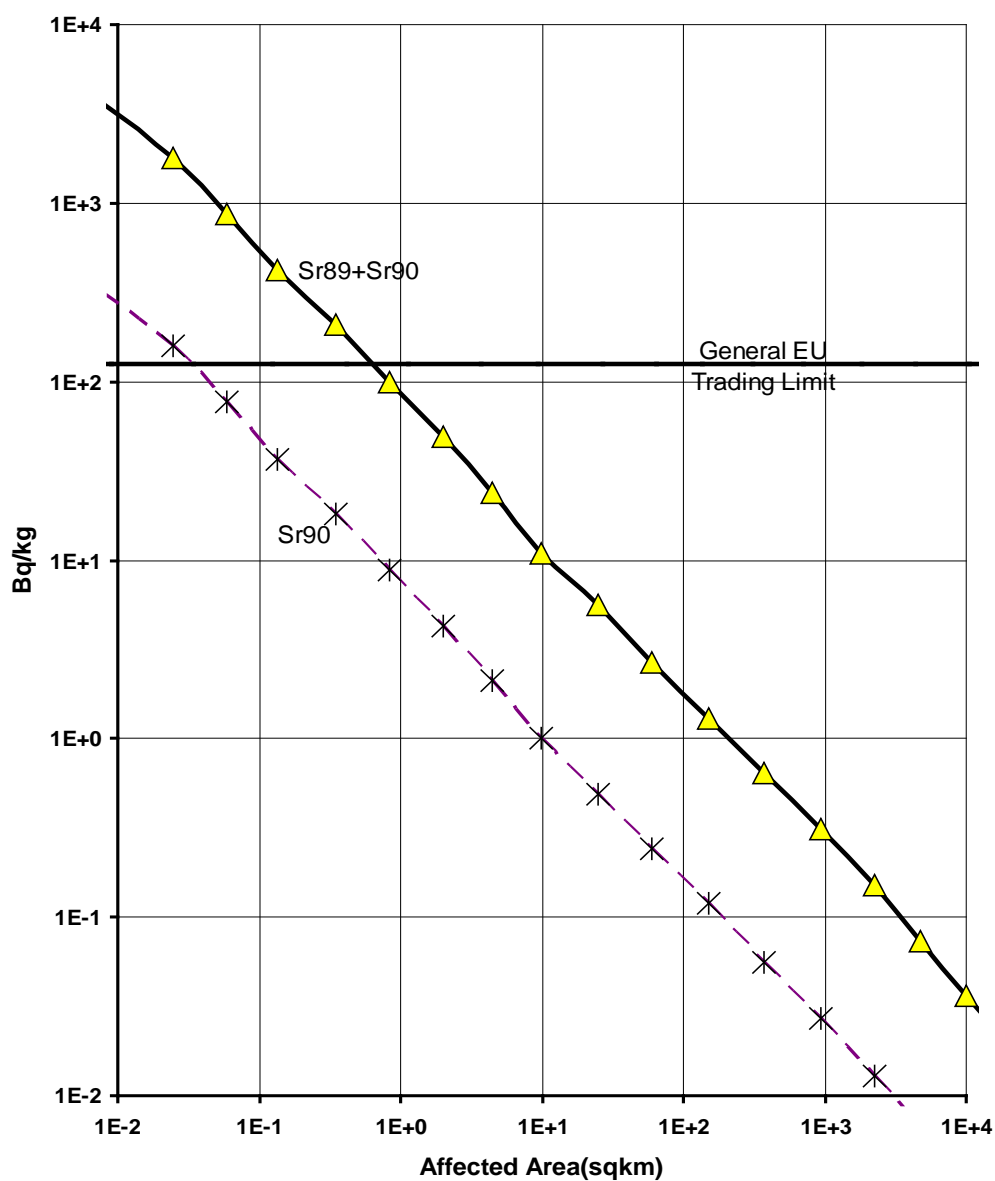
SECTION 16.2.3 - FIGURE 16

Effective Short Term Dose (7 Days) in the Case of a Severe Accident

Short term doses (7 days) in case of severe accidents

SECTION 16.2.3 - FIGURE 17

Short Term Thyroid Dose (7 Days) in the Case of a Severe Accident

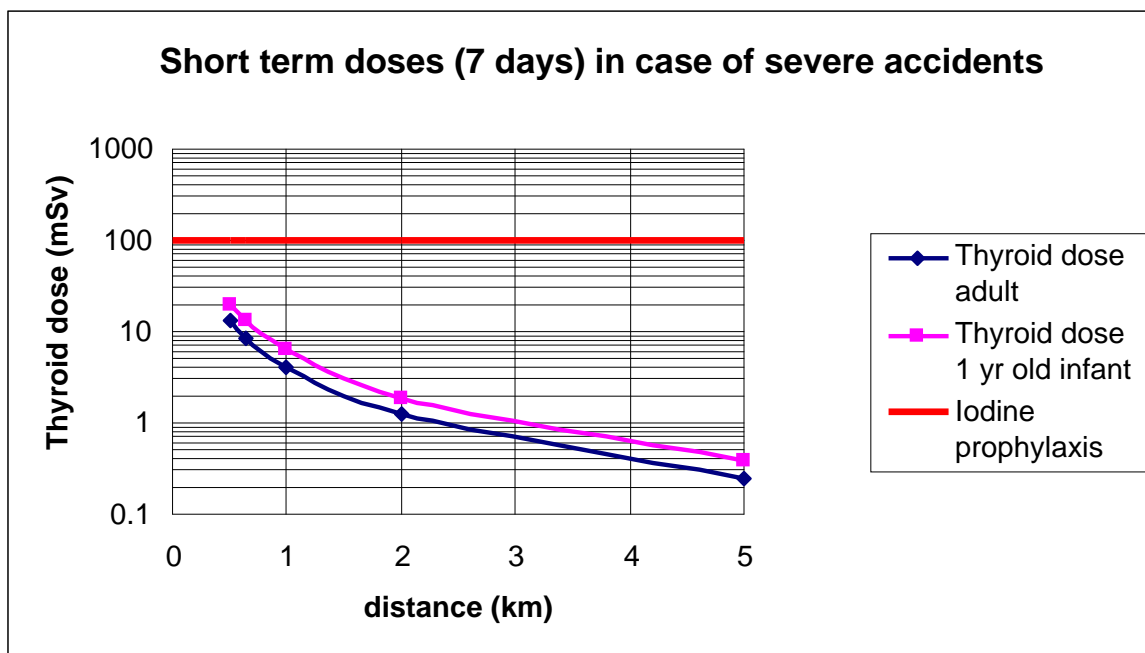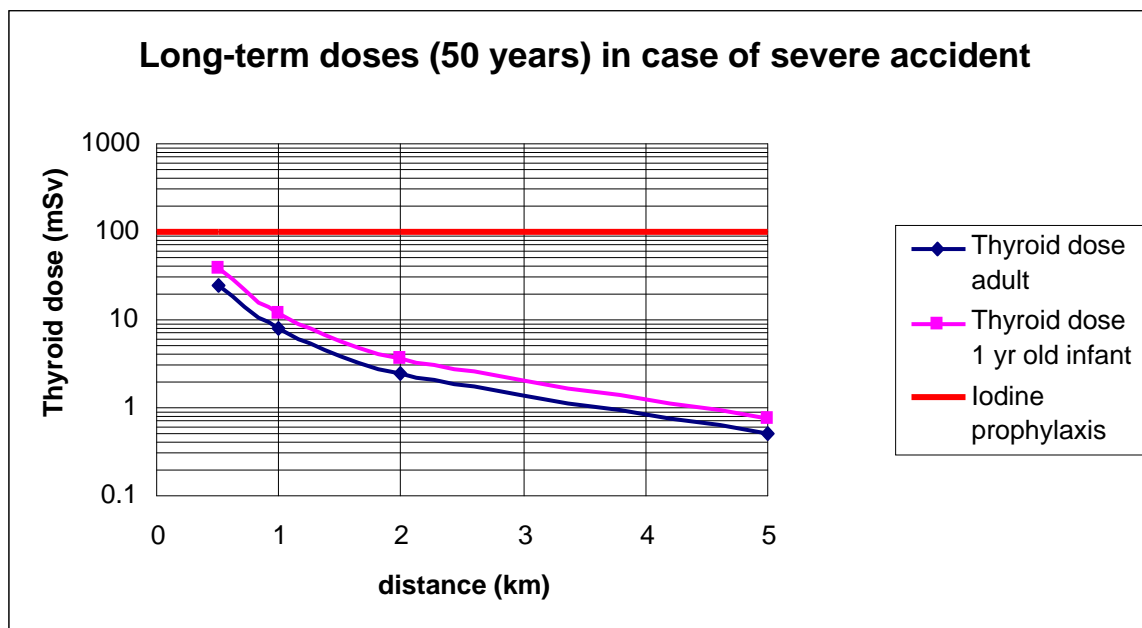Short term doses (7 days) in case of severe accidents

SECTION 16.2.3 - FIGURE 18

Effective Long Term Dose (50 Years) in the Case of a Severe Accident
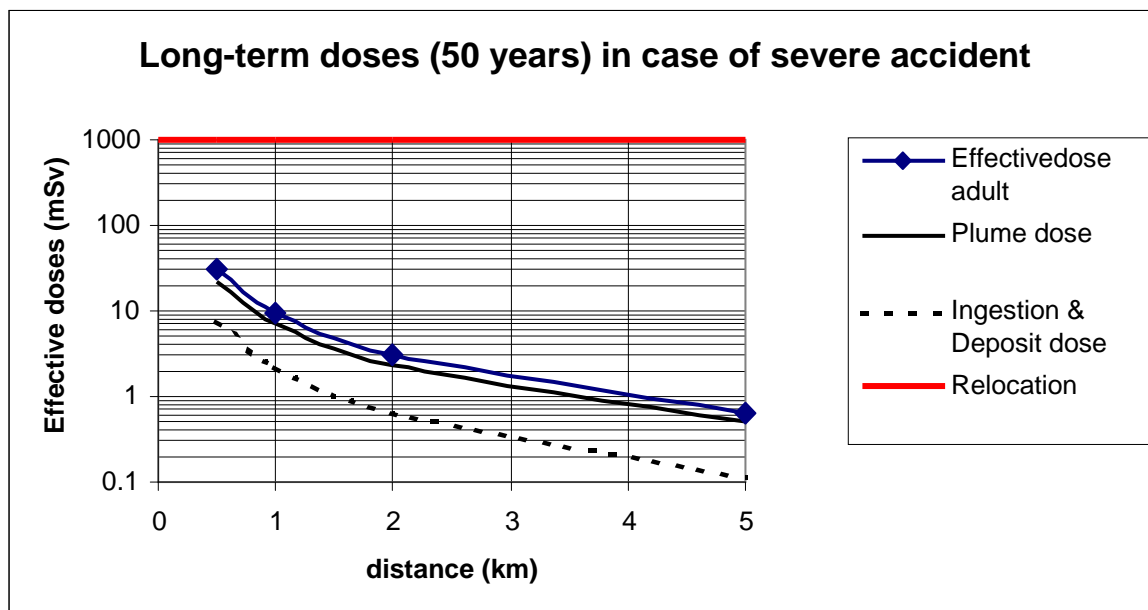
SECTION 16.2.3 - FIGURE 19

Long Term Thyroid Dose (50 Years) in the Case of a Severe Accident

Long-term doses (50 years) in case of severe accident

SUB-CHAPTER 16.2 – REFERENCES

External references are identified within this sub-chapter by the text [Ref-1], [Ref-2], etc at the appropriate point within the sub-chapter. These references are listed here under the heading of the section or sub-section in which they are quoted.

0. SAFETY OBJECTIVES

0.1. GENERAL

[Ref-1] Technical Guidelines for the design and construction of the next generation of nuclear power plants with pressurized water reactors. Adopted during the GPR/German experts plenary meetings. October 19th and 26th 2000. (E)

[Ref-2] Principles for Intervention for Protection of the Public in a Radiological Emergency, A report by a task group of Committee 4 of ICRP, adopted by the ICRP in November 1992, Oxford, New York, Seoul, Tokyo. ICRP Publication 63. ICRP. 1993. (E)

1. APPROACH TO SEVERE ACCIDENT CONTROL

1.1. BASIC STRATEGY

[Ref-1] D Struwe et al. Consequence evaluation of In-vessel Fuel Coolant Interaction in the European Pressurized Water Reactor. FZK Final Report No. 6316. 1999. (E)

1.3. SPECIAL ISSUES

1.3.1. Steam explosion

1.3.1.1. In-vessel steam explosion

[Ref-1] B De Boeck. Introduction to Severe Accidents. O/Ref. 97-2589.DOC, Class. XP.00.NS AVN-97/013. 1997.

1.3.1.1.1.   Involved Physical Phenomena

[Ref-1] Technical Opinion Paper on Fuel-Coolant Interaction. NEA/CSNI/R(99)24. OECD. 1999. (E)

1.3.1.1.1.4. Expansion Phase

[Ref-1] Leon Cizelj et al. Vulnerability of partially flooded PWR reactor cavity to a steam explosion. Nuclear Engineering and Design, Volume 236 (August 2006), pp. 1617-1627. "Jozef Stefan" Institute. 2005. (E)

1.3.1.1.2.   Insights from Previous Studies

[Ref-1] N Rasmussen. Reactor Safety Study. WASH-1400 (NRC). 1975. (E)

1.3.1.1.2.1. Pressure Influence

[Ref-1] R E Henry. Overview: Uncertainties Remaining in Severe Accident Phenomenology. MSC\N19. Fauske & Associates Inc. 1995. (E)

1.3.1.1.2.2. Mixing Behaviour

[Ref-1] R E Henry and H K Fauske. A different approach to Fragmentation in Steam Explosions. Fauske & Associates Inc. MSC\N14. 1996. (E)

1.3.1.1.2.3. Influence of Particulate Debris and Steam Generation

[Ref-1] T Morii et al. Benchmark Analysis of Premixing Phase of FCI Experiment by the VESUVIUS Code. The 10th International Topical Meeting on Nuclear Reactor Thermal Hydraulics. NURETH-10. 2003. (E)

[Ref-2] US-NRC. TMI-2 Vessel Investigation Project. SECY-93-119. 1993. (E)

1.3.1.1.3.   US-NRC Studies

[Ref-1] R E Henry. Overview: Uncertainties Remaining in Severe Accident Phenomenology. Fauske & Associates Inc. MSC\N19. 1995. (E)

[Ref-2] B R Sehgal et al. Pre-Project on Development and Validation of Melt Behaviour in Severe Accidents. NKS-99. ISBN 87-7893-158-4. 2004. (E)

[Ref-3] T G Theofanous, W W Yuen and S Angilini. The verification basis of the PM-ALPHA code. Nuclear Engineering and Design Volume 189, 59-102. 1999. (E)

[Ref-4] N Rasmussen. Reactor Safety Study. WASH-1400 (NRC). 1975. (E)

1.3.1.1.4.   Recent European Studies

[Ref-1] B R Sehgal et al. Pre-Project on Development and Validation of Melt Behaviour in Severe Accidents. NKS-99. ISBN 87-7893-158-4. 2004. (E)

[Ref-2] B R Sehgal. Accomplishments and challenges of the severe accident research. Nuclear Engineering and Design, Volume 210, 79-94. Elsevier. 2001. (E)

[Ref-3] A simplified approach to estimating reference source terms for LWR designs. TECDOC-1127. IAEA. 1999. (E)

[Ref-4] Current Severe Accident Research Facilities and Projects. NEA/CSNI/R(2004)6. OECD. 2004. (E)

[Ref-5] J M Bonnet et al. KROTOS FCI Experimental Programme at CEA Cadarache: New Features and Status. Popes' Palace Conference Centre, Avignon, France. October 2-6, 2005.

[Ref-6] N I Kolev. Verification of IVA5 Computer Code for Melt-Water Interaction Analysis. 7th International Conference on Nuclear Engineering, ICONE-7359, Tokyo, Japan. 1999. (E)

[Ref-7] T G Theofanous, W W Yuen, K Freeman and X Chen. The verification basis of the ESPROSE.m code. Nuclear Engineering and Design Volume 189, 103-138. Elsevier. 1999. (E)

[Ref-8] T G Theofanous, W W Yuen and S Angilini. The verification basis of the PM-ALPHA code. Nuclear Engineering and Design Volume 189, 59-102. Elsevier. 1999. (E)

[Ref-9] Identification of Relevant Conditions and Experiments for Fuel-Coolant Interactions in Nuclear Power Plants. NEA/CSNI/R(2004)7. OECD NEA. 2004. (E)

1.3.1.2. Ex-vessel steam explosion

[Ref-1] M T Farmer, et al. MACE Test M3b, Data Report. MACE-TR-D13, Volume. 1/2. Argonne Nat. Lab. November 1997. (E)

[Ref-2] M T Farmer, et al. MACE Test M4, Data Report. MACE-TR-D16. Argonne Nat. Lab. August 1999. (E)

[Ref-3] M T Farmer, S Basu. A Summary of Findings from the Melt Coolability and Concrete Interactions (MCCI) Program. Proceedings of ICAPP 2007, Nice, France, paper 7544. May 2007. (E)

1.3.2   Recriticality

1.3.2.1 In-Vessel Recriticality

[Ref-1] J.F. Briefmeister. MCNP – A General Monte Carlo N-Particle Transport Code. V. 4C, LANL-13709-M. (E)

[Ref-2] G. Ducros. "An overview of the VERCORS experimental programme". International VERCORS Seminar, Greoux les bains, France. October 2007. (E)

1.3.2.1.2   Assessment of the Potential for Recriticality during Phase 2

[Ref-1] Staff Reports to the President's Commission on the Accident at Three Mile Island. NRC. (E)

2. ANALYSIS OF CORE MELT SEQUENCES

2.1. IN-VESSEL ACCIDENT PROGRESSION AND SELECTION OF RELEVANT SCENARIOS

2.1.1. Analysis of Core Melt Scenarios

2.1.1.2. Analyses of Core Melt Scenarios

2.1.1.2.3. *Identification of Main Scenarios for Representative Cases*

2.1.1.2.3.1. *Full Power Conditions*

Family 1: SB(LOCA) and SGTR with partial and fast secondary cooldown (Table 7).

[Ref-1] A Caillaux. EPR RF002. Severe Accident. 5.5.2 In-vessel analysis. Hydrogen Source Term. NFEPD DC 59 Revision B. Framatome ANP. January 2004. (E)

SGTR: core melt scenario

[Ref-2] P Gandrille. EPR RF002. Severe Accident. In-vessel MAAP 4 study for containment by-pass radiological releases. NFEPD DC 53 Revision B. Framatome ANP. January 2004. (E)

Family 2: LB(LOCA) and SB(LOCA) with partial secondary cooldown only (Section 16.2.2.1 - Table 8

[Ref-3] A Caillaux. EPR RF002. Severe Accident. 5.5.2 In-vessel analysis. Hydrogen Source Term. NFEPD DC 59 Revision B. Framatome ANP. January 2004. (E)

Family 3: Scenarios without RCS break and with SG dryout (Section 16.2.2.1 - Table 9)

[Ref-4] P Gandrille. EPR RF002. Severe Accidents. Dedicated Reactor Coolant System Depressurisation. Functional requirements. NFEPD DC 91 Revision C. Framatome ANP. August 2004. (E)

2.1.2. Selection of Relevant Scenarios to Design Mitigation Features

2.1.2.1. Prevention of High Pressure Core Melt Scenarios

2.1.2.1.2. *Reference Scenarios*

[Ref-1] P Gandrille. EPR RF002. Severe Accidents. Dedicated Reactor Coolant System Depressurisation. Functional requirements. NFEPD DC 91 Revision C. Framatome ANP. August 2004. (E)

2.1.2.2. Hydrogen Risk

2.1.2.2.2.   Hydrogen Production

2.1.2.2.2.1. Representative Scenarios

[Ref-1] A Caillaux. EPR RF002. Severe Accident. 5.5.2 In-vessel analysis. Hydrogen Source Term. NFEPD DC 59 Revision B. Framatome ANP. January 2004. (E)

2.1.2.2.3.   Hydrogen Release Mode

[Ref-1] A Caillaux. EPR RF002. Severe Accident. 5.5.2 In-vessel analysis. Hydrogen Source Term. NFEPD DC 59 Revision B. Framatome ANP. January 2004. (E)

2.1.2.2.4.   Selection of Hydrogen Releases into the Containment

[Ref-1] A Caillaux. EPR RF002. Severe Accident. 5.5.2 In-vessel analysis. Hydrogen Source Term. NFEPD DC 59 Revision B. Framatome ANP. January 2004. (E)

2.1.2.3. Risk of Basemat and Reactor Pit Ablation

2.1.2.3.1.   Parameters of Interest to select Reference Scenarios

Modes of reactor vessel failure:

[Ref-1] A Caillaux, G Azarian. EPR RF002. Severe Accident. 5.5.2 In-vessel analysis. Melt release conditions from the vessel. EPSL DC 851. Framatome ANP. October 2002. (E).

Amount of corium:

[Ref-2] A Caillaux, G Azarian. EPR RF002. Severe Accident. 5.5.2 In-vessel analysis. Melt release conditions from the vessel. EPSL DC 851. Framatome ANP. October 2002. (E).

2.1.2.3.2.   Selection of Corium Releases into the Reactor Pit

[Ref-1] A Caillaux, G Azarian. EPR RF002. Severe Accident. 5.5.2 In-vessel analysis. Melt release conditions from the vessel. EPSL DC 851. Framatome ANP. October 2002. (E).

SECTION 16.2.2.1 – TABLES 1 TO 14

[Ref-1] M Nie, K-G Petzold. Main data for severe accident analyses. AREVA Report FANP NGES2/2002/en/0006 Revision D. Erlangen. January 2004. (E)

[Ref-2] A Caillaux. EPR RF002. Severe Accident. 5.5.2 In-vessel analysis. Hydrogen Source Term. NFEPD DC 59 Revision B. Framatome ANP. January 2004 (E)

[Ref-3] P Gandrille. EPR RF002. Severe Accidents. Dedicated Reactor Coolant System Depressurisation. Functional requirements. NFEPD DC 91 Revision C. Framatome ANP. August 2004. (E).

[Ref-4] A Caillaux, G Azarian. EPR RF002. Severe Accident. 5.5.2 In-vessel analysis. Melt release conditions from the vessel. EPSL DC 851. Framatome ANP. October 2002. (E)

SECTION 16.2.2.1 - FIGURES 1 TO 14

[Ref-1] A Caillaux. EPR RF002. Severe Accident. 5.5.2 In-vessel analysis. Hydrogen Source Term. NFEPD DC 59 Revision B. Framatome ANP. January 2004. (E)

[Ref-2] A Caillaux, G Azarian. EPR RF002. Severe Accident. 5.5.2 In-vessel analysis. Melt release conditions from the vessel. EPSL DC 851. Framatome ANP. October 2002. (E)

[Ref-3] M Nie, K-G Petzold. Main data for severe accident analyses. FANP NGES2/2002/en/0006 Revision D. AREVA Erlangen. January 2004. (E)

[Ref-4] P Gandrille. EPR RF002. Severe Accident. In-vessel MAAP 4 study for containment by-pass radiological releases. NFEPD DC 53 Revision B. Framatome ANP. January 2004. (E)

[Ref-5] P Gandrille. EPR RF002. Severe Accident. In-vessel analysis. MAAP 4 study in case of LB LOCA. Fission products into the containment. NF EPD DC 56 Revision B. Framatome ANP. January 2004. (E).

2.2. ASSESSMENT OF PRIMARY SYSTEM DEPRESSURISATION

2.2.2. Characteristics of the Considered Scenarios

2.2.2.1. Station Blackout Sequence

[Ref-1] P Gandrille. EPR RF002. Severe Accidents. Dedicated Reactor Coolant System Depressurisation. Functional requirements. NFEPD DC 91 Revision C. Framatome ANP. August 2004. (E)

2.2.2.2. Total Loss of Feed Water Sequence

[Ref-1] P Gandrille. EPR RF002. Severe Accidents. Dedicated Reactor Coolant System Depressurisation. Functional requirements. NFEPD DC 91 Revision C. Framatome ANP. August 2004. (E)

2.2.3. Criteria for RCP [RCS] depressurisation and identification of available Time Periods

2.2.3.3. Identification of margins for a delayed depressurisation

[Ref-1] P Gandrille. EPR RF002. Severe Accidents. Dedicated Reactor Coolant System Depressurisation. Functional requirements. NFEPD DC 91 Revision C. Framatome ANP. August 2004. (E)

2.2.3.4. Temperatures in the Primary System

2.2.3.4.2. Risk of Creep Rupture in RCS Pipes in case of Delayed Depressurisation

[Ref-1] P Gandrille. EPR RF002. Severe Accidents. Dedicated Reactor Coolant System Depressurisation. Functional requirements. NFEPD DC 91 Revision C. Framatome ANP. August 2004. (E)

[Ref-2] J Heliot, G Azarian. EPR BD. Severe Accidents. Assessment of steam generator tube rupture risk induced by a core melt scenario. ETSS DC 782 Revision A. Framatome ANP. February 1999. (E)

SECTION 16.2.2.2 - TABLES 1 TO 2

[Ref-1] J Heliot, G Azarian. EPR BD. Severe Accidents. Assessment of steam generator tube rupture risk induced by a core melt scenario. ETSS DC 782. Framatome ANP. December 1994.

SECTION 16.2.2.2 - FIGURES 2 TO 15

[Ref-1] J Heliot, G Azarian. EPR BD. Severe Accidents. Assessment of steam generator tube rupture risk induced by a core melt scenario. ETSS DC 782 Revision A. Framatome ANP. February 1999. (E)

SECTION 16.2.2.2 – FIGURE 16

[Ref-1] Dolleans. FA3. Severe accident. Thermo-hydraulic loads on vessel support and reactor pit in case of lower head failure at 20 bar. FRA1 Contract A. AREVA Report NEPDF DC 22. February 2008. (E)

2.3. ASSESSMENT OF HYDROGEN CONTROL

2.3.1. Approach to the verification of the efficiency of the Combustible Gas Control System

[Ref-1] A Caillaux. EPR RF002. Severe Accident. 5.5.2 In-vessel analysis. Hydrogen Source Term. NFEPD DC 59 Revision B. Framatome ANP. January 2004. (E)

[Ref-2] W Hering, Ch Homann, J-S Lamy. ISP 45-OECD Comparison Report on the Blind Phase of the OECD International Standard Problem n° 45 exercise (QUENCH06). Report FZKA-6677. March 2002. (E)

[Ref-3] M Bauer, M A Movahed, J Eyink. Prevention and mitigation of hydrogen risk impact of the two room concept and metallic liner, interface with civil work and layout. NGPS4/2006/en/1014 Revision D. Framatome ANP. June 2007. (E)

[Ref-4] U Schwarz. PAR Qualification Report. General Description. PESB-G/2011/en/1001 Revision A. AREVA NP. January 2011. (E)

UK EPR

PRE-CONSTRUCTION SAFETY REPORT

CHAPTER 16: RISK REDUCTION AND SEVERE
ACCIDENT ANALYSES

SUB-CHAPTER : 16.2

PAGE : 282 / 295

Document ID.No.
UKEPR-0002-162 Issue 05

[Ref-5] M Hupp. Description of validation of AREVA recombiner modeling in computational programs based on extensive, international, qualificational testing. PEPA-G/2011/en/1001 Revision B. AREVA NP. January 2011. (E)

[Ref-6] M.Hupp, H.Dimmelmeier, Sensitivity analysis of a postulated reduced recombiner performance during severe accidents. PEPA-G/2011/en/1021 Revision A. AREVA NP. September 2011. (E)

2.3.2. Potential Pressure Loads

2.3.2.2. Hydrogen Distribution

[Ref-1] M Bauer, M A Movahed, J Eyink. Prevention and mitigation of hydrogen risk impact of the two room concept and metallic liner, interface with civil work and layout. NGPS4/2006/en/1014 Revision D. Framatome ANP. June 2007. (E)

2.3.2.3. AICC and Expected Combustion Pressure

[Ref-1] J Eyink. Pressure and Temperature Loads for EPR with Steel Liner resulting from Hydrogen Combustion. NGPS4/2003/en/0020 Revision D. Framatome ANP. February 2004. (E)

[Ref-2] J Eyink, M Movahed, K-G Petzold. Justification of the H2 mitigation concept: Direct hydrogen release into the containment. Siemens Report KWU NA-T/1999/E/042 Revision B. September 1999. (E)

2.3.3. Assessment of the Combustion Mode

2.3.3.3. Influence of the Activation of the Spray System

[Ref-1] J Eyink, M Movahed. Effect of Spray Activation on the Reactivity of the Hydrogen-Air-Steam Mixture. NGES2/2002/en/0018 Revision B. Framatome ANP. (E)

2.3.3.4. Dynamic Pressure Loads

2.3.3.4.1. 5 cm (20 cm²) SB(LOCA) in the Cold Leg with Fast Secondary Cool-down

[Ref-1] J Eyink. Pressure and Temperature Loads for EPR with Steel Liner resulting from Hydrogen Combustion. NGPS4/2003/en/0020. Framatome ANP. (E)

2.3.3.4.2. 7.5 cm (46 cm²) SB(LOCA) in the Pressuriser with Fast Secondary Cool-down

[Ref-1] J Eyink. Pressure and Temperature Loads for EPR with Steel Liner resulting from Hydrogen Combustion. NGPS4/2003/en/0020. Framatome ANP. (E)

2.3.3.4.3. 5 cm (20 cm²) SB(LOCA) with Partial Cool-down and Delayed Depressurisation

[Ref-1] J Eyink. Pressure and Temperature Loads for EPR with Steel Liner resulting from Hydrogen Combustion. NGPS4/2003/en/0020. Framatome ANP. (E)

UK EPR

PRE-CONSTRUCTION SAFETY REPORT

CHAPTER 16: RISK REDUCTION AND SEVERE
ACCIDENT ANALYSES

SUB-CHAPTER : 16.2

PAGE : 283 / 295

Document ID.No.
UKEPR-0002-162 Issue 05

2.3.3.4.4.   5 cm (20 cm²) SB(LOCA) in the Cold Leg with Re-flood

[Ref-1] J Eyink. Pressure and Temperature Loads for EPR with Steel Liner resulting from
Hydrogen Combustion. NGPS4/2003/en/0020. Framatome ANP. (E)

2.3.3.5. Temperature Loads

2.3.3.5.1.   Temperature Loads Due to Recombination

[Ref-1] J Eyink, M Movahed, K-G Petzold. Thermal loads on the EPR containment wall due to
hydrogen removal. KWU NA-T/2000/E018 Revision A. Siemens. (E)

2.3.3.5.2.   Temperature Loads Due to Combustion

2.3.3.5.2.1. 5 cm (20 cm²) SB(LOCA) in the Cold Leg and Fast Secondary Cool-down

[Ref-1] J Eyink, M Movahed. Thermal loads due to accidental ignition (SBLOCA).
KWU NA-T/2000/E010 Revision A. Siemens. (E)

2.3.3.5.2.2. 5 cm (20 cm²) SB(LOCA) in the Cold Leg with Partial Cool-down (Ex-Vessel Hydrogen)

[Ref-1] J Eyink, M Movahed. Hydrogen risk from ex-vessel release. SNP NA T/2000/E035
Revision A. Siemens. (E)

2.3.3.5.2.3. 5 cm (20 cm²) SB(LOCA) in the Cold Leg with Partial Cool-down and Delayed Depressurisation

[Ref-1] J Eyink, K-G Petzold. Thermal loads due to accidental ignition (SBLOCA/D).
KWU NA-T/2000/E017 Revision A. Siemens. (E)

2.3.4. Conclusions from the Verification Process

[Ref-1] M Fischer, J Eyink. R&D for severe accidents. NGES2/2002/en/0007 Revision E
(TR03/131). Framatome ANP. (E)

SECTION 16.2.2.3 - TABLE 2

[Ref-1] J Eyink. The EPR Hydrogen Mitigation Concept. NGPS4/2003/en/0192 (Table 4.7.1.1,
page 66). Framatome ANP. (E)

SECTION 16.2.2.3 – FIGURE 1

[Ref-1] J Eyink. Pressure and Temperature Loads for EPR with Steel Liner resulting from
Hydrogen Combustion. NGPS4/2003/en/0020. Framatome ANP. (E)

SECTION 16.2.2.3 - FIGURES 2 TO 7

[Ref-1] J Eyink. The EPR Hydrogen Mitigation Concept. NGPS4/2003/en/0192. Framatome ANP. (E)

SECTION 16.2.2.3 - FIGURES 8 AND 9

[Ref-1] J Eyink, M Movahed. Effect of Spray Activation on the Reactivity of the Hydrogen-Air-Steam Mixture. NEGS2/2002/en/0018 Revision B. Framatome ANP. (E)

SECTION 16.2.2.3 – FIGURE 10

[Ref-1] J Eyink. Pressure and Temperature Loads for EPR with Steel Liner resulting from Hydrogen Combustion. NGPS4/2003/en/0020 Revision D. Framatome ANP. February 2004. (E)

SECTION 16.2.2.3 – FIGURE 11

[Ref-1] J Eyink. Hydrogen Control: Status of the Justification of Tools and Methods with regard to GPR and IRSN Concerns. NGPS4/2003/en/0132. Framatome ANP. (E)

SECTION 16.2.2.3 – FIGURE 12

[Ref-1] J Eyink. The EPR Hydrogen Mitigation Concept. NGPS4/2003/en/0192. Framatome ANP. (E)

SECTION 16.2.2.3 - FIGURE 13

[Ref-1] J Eyink. Pressure and Temperature Loads for EPR with Steel Liner resulting from Hydrogen Combustion. NGPS4/2003/en/0020 Revision D. Framatome ANP. February 2004. (E)

2.4. ASSESSMENT OF MELT STABILISATION

2.4.1. Basic strategy

[Ref-1] M Fischer, M Klicheva. Functional principle of the core melt stabilization system of the EPR including a description of the relevant phenomena, the related experimental background, and the impact of remaining uncertainties. NEPA-G/2010/en/1022 Revision C. AREVA NP. June 2010. (E)

2.4.1.1. Assessment of the general robustness of the concept

2.4.1.1.1. Tolerance to melt release conditions from the RPV

[Ref-1] M Nie, M Fischer. Analysis of the melt retention in the reactor pit for various release sequences. NGPS4/2003/en/0003. AREVA NP. July 2003. (E)

2.4.1.1.2. Tolerance to loads during RPV failure

Mechanical impact of the detaching lower head

[Ref-1] B R Sehgal et al. Final Report for the "Melt-Vessel Interactions (MVI)" Project. SKI Report 00:53. December 2000. (E)

Erosive effect of the out-flowing melt

[Ref-2] H. Alsmeyer, et al. "The COMET concept for Cooling of Ex-Vessel Corium Melts". 6th International Conference on Nuclear Engineering ICONE-6, San Diego CA, May 10-15 1998. (E)

Melt dispersal

[Ref-3] L Meyer, M Gargallo. Low pressure Corium Dispersion Experiments with Simulant Fluids in a Scaled Annular Cavity. Nuclear Technology, 141, pp. 257-274, 2003. (E)

[Ref-4] T Y Chu, M Pilch, J Bentz et al. Lower Head Failure Experiments and Analyses. NUREG/CR-5582, SAND98-2047. 1999. (E)

[Ref-5] B R Sehgal, R R Nourgaliev and T N Dinh. Characterization of Heat Transfer Processes in a Melt Pool, Convection and Vessel-Creep. Nuclear Engineering and Design. Volume.211, 2002, pp. 172-187. February 2002. (E)

[Ref-6] A Theerthan, A Karbojian and B R Sehgal. FOREVER Experiments on Thermal and Mechanical Behaviour of Reactor Pressure Vessel during a Severe Accident. The EC-FOREVER-1 Test. Proceedings of the 16th International Conference on Structural Mechanics in Reactor Technology (SMIRT-16), Washington DC. August 2002. (E)

2.4.1.1.3. Tolerance to a postulated late re-flood

Water injection after initial RPV failure

[Ref-1] M T Farmer, et al. MACE Test M3b, Data Report. MACE-TR-D13, Volume 1/2. Argonne Nat. Lab. November 1997. (E)

[Ref-2] M T Farmer, et al. MACE Test M1B, Data Report. MACE-TR-D6. Argonne Nat. Lab. September 1992. (E)

[Ref-3] M T Farmer, et al. MACE Test M4, Data Report. MACE-TR-D16. Argonne Nat. Lab. August 1999. (E)

2.4.1.2. Assessment of melt retention in the pit

[Ref-1] M Fischer. System CMSS: Justification of the type of protective layer used in the reactor pit and melt discharge channel. AREVA NP. NEPS-G/2008/en/1157 Revision B. November 2010. (E)

2.4.1.2.2. Modelling approach

Generalised release cases

[Ref-1] M Nie, M Fischer. "Use of Molten Core Concrete Interactions in the Melt Stabilization Strategy of the EPR", Proceedings of ICAPP'06, paper 6330. Reno NV USA. June 4-8, 2006. (E)

[Ref-2] M Nie, M Fischer. "Analysis of the melt retention in the reactor pit for various release sequences". NGPS4/2003/en/0003. AREVA NP. (E)

[Ref-3] V G Asmolov et al., "Partitioning of fission products between the corium melt metallic and oxidic phases resulting from the STFM-FP tests". OECD MASCA Project, Report MP-TR-10, Kurtschatov Institute Moscow, June 2003. (E)

2.4.1.2.3. Results

2.4.1.2.3.2. Melt conditioning

[Ref-1] M Nie. Temporary Melt Retention in the Reactor Pit of the European Pressurised Water Reactor (EPR). Stuttgart University. February 2005. (E)

2.4.1.2.4. Conclusion on temporary melt retention in the pit

[Ref-1] M T Farmer, et al. MACE Test M4, Data Report. MACE-TR-D16. Argonne Nat. Lab. August 1999. (E)

2.4.1.3. Assessment of gate failure

2.4.1.3.1. Validation strategy

[Ref-1] M T Farmer, et al. MACE Test M3b, Data Report. MACE-TR-D13, Volume 1/2. Argonne Nat. Lab. November 1997. (E)

[Ref-2] M T Farmer, et al. MACE Test M1B, Data Report. MACE-TR-D6. Argonne Nat. Lab. September 1992. (E)

[Ref-3] M T Farmer, et al. MACE Test M4, Data Report. MACE-TR-D16. Argonne Nat. Lab. August 1999. (E)

[Ref-4] M T Farmer, S. Basu, et al. "A Summary of Findings from the Melt Coolability and Concrete Interaction (MCCI) Program". Proceedings of ICAPP 2007 paper 7544. May 2007. (E)

2.4.1.3.3. Results

[Ref-1] M Fischer. Description and validation of the improved gate design. NGPS4/2005/en/1026 Revision A (TR 05/219). AREVA NP. July 2005. (E)

2.4.1.4. Assessment of melt spreading

2.4.1.4.1. Validation strategy

[Ref-1] B R Sehgal, T N Dinh, R R Nourgaliev, M J Konovalikhin, V A Bui. "Assessment of Core Melt Spreading in EPR Melt Retention Device". Sehgal Associates Inc., October 15, 1998. (E)

[Ref-2] M Eddy, G Bandini. Preliminary analysis on corium spreading in reactor core-catcher with THEMA code. EU Community Research. SAM-ECOSTAR-P07-17/01. February 2002. (E)

[Ref-3] J-M Seiler, et al. European Group for Analysis of Corium Recovery Concepts – EUROCORE. Synthesis report, presented at FISA 2001, Luxembourg, Nov 12-14, 2001. (E)

2.4.1.4.2. Modelling approach

2.4.1.4.2.1. CORFLOW code

[Ref-1] W Koller, W Steinwarz. 2D-spreading test COMAS EU-4. EU Community Research. EXV-COMAS(97)-D10. December 1997. (E)

[Ref-2] R Wittmaack. Post calculation of the COMAS EU-4 test with the CORFLOW computer code. EU Community Research. EXV-COMAS(98)-D25. March 1998. (E)

[Ref-3] R Wittmaack. EPR corium spreading analysis with the CORFLOW computer code. KWU NA-T/1998/E077 Revision A. AREVA NP Erlangen. August 1998. (E)

2.4.1.4.2.2. RIT model

[Ref-1] B R Sehgal, T N Dinh, R R Nourgaliev, M J Konovalikhin, V A Bui. "Assessment of Core Melt Spreading in EPR Melt Retention Device". Sehgal Associates Inc. October 15, 1998. (E)

[Ref-2] W Steinwarz, et al. "Investigations on the Phenomenology of Ex-vessel Core Melt Behaviour". Final report, EU 4th FWP. EXV-COMAS(99)-D27. (E)

2.4.1.4.3. Results

2.4.1.4.3.1. CORFLOW code

[Ref-1] R Wittmaack. EPR corium spreading analysis with the CORFLOW computer code. KWU NA-T/1998/E077 Revision A. AREVA NP Erlangen. August 1998. (E)

UK EPR

PRE-CONSTRUCTION SAFETY REPORT

CHAPTER 16: RISK REDUCTION AND SEVERE
ACCIDENT ANALYSES

SUB-CHAPTER : 16.2

PAGE   : 288 / 295

Document ID.No.
UKEPR-0002-162 Issue 05

2.4.1.4.3.2. RIT model

[Ref-1] B R Sehgal, T N Dinh, R R Nourgaliev, M J Konovalikhin, V A Bui. "Assessment of Core
Melt Spreading in EPR Melt Retention Device". Sehgal Associates Inc., October 15,
1998. (E)

2.4.1.5. Assessment of melt flooding and quenching

[Ref-1] M Fischer. System CMSS: CMSS System Description. NEPS-G/2008/en/1116.
AREVA NP. (E)

[Ref-2] M T Farmer, et al, S. Basu. "A Summary of Findings from the Melt Coolability and
Concrete Interaction (MCCI) Program". Proceedings of ICAPP 2007 paper 7544. Nice,
France, May 13-18, 2007. (E)

[Ref-3] D H Thompson, et al. "Compilation, Analysis, and Interpretation of ACE Phase C and
MACE Experimental Data: Volume I – MCCI Thermohydraulic results", ACEX TR-C-14,
Argonne Nat. Lab. November 1997. (E)

[Ref-4] H Alsmeyer, et al. The COMET-L1 experiment on long-term Melt Concrete Interaction
and Cooling by top flooding. Forschungszentrum Karlsruhe, Report FZKA 7213.
June 2006. (E)

[Ref-5] M Fischer, O Herbst, H Schmidt. Demonstration of the heat removing capabilities of the
EPR core catcher. 3rd International symposium on two-phase flow modelling and
experimentation, Pisa, Italy, September 22-24, 2004. (E)

[Ref-6] M Nie, M Fischer. Parametric examination of the sacrificial concrete layer thickness in
the spreading compartment. NGPS4/2004/en/0185 Revision A. TR04/166. AREVA NP.
(E)

[Ref-7] M Fischer, M Klicheva. Functional principle of the core melt stabilization system of the
EPR including a description of the relevant phenomena, the related experimental
background, and the impact of remaining uncertainties.
NEPA-G/2010/en/1022 Revision C. AREVA NP. June 2010. (E)

2.4.1.5.1.   Validation strategy

[Ref-1] M T Farmer, et al. MACE Test M3b, Data Report. MACE-TR-D13, Vol. 1/2. Argonne
Nat. Lab. November 1997. (E)

[Ref-2] M T Farmer, et al. MACE Test M1B, Data Report. MACE-TR-D6. Argonne Nat. Lab.
September 1992. (E)

[Ref-3] M T Farmer, et al. MACE Test M4, Data Report. MACE-TR-D16. Argonne Nat. Lab.
August 1999. (E)

[Ref-4] B R Sehgal, T N Dinh, R R Nourgaliev, M J Konovalikhin, V A Bui. "Assessment of Core
Melt Spreading in EPR Melt Retention Device". Sehgal Associates Inc., October 15,
1998. (E)

[Ref-5] H Alsmeyer et al. "ECOKATS-2: A large scale experiment on melt spreading and
subsequent cooling by top flooding". Proc. ICAPP 2004, paper 4134. Pittsburgh, PA
USA, June 13-17, 2004. (E)

2.4.1.5.2. Modelling approach

2.4.1.5.2.2. Melt flooding and quenching

[Ref-1] M T Farmer, et al. MACE Test M3b, Data Report. MACE-TR-D13, Vol. 1/2. Argonne Nat. Lab. November 1997. (E)

[Ref-2] M T Farmer, et al. MACE Test M1B, Data Report. MACE-TR-D6. Argonne Nat. Lab. September 1992. (E)

[Ref-3] M T Farmer, et al. MACE Test M4, Data Report. MACE-TR-D16. Argonne Nat. Lab. August 1999. (E)

[Ref-4] B R Sehgal, T N Dinh, R R Nourgaliev, M J Konovalikhin, V A Bui. "Assessment of Core Melt Spreading in EPR Melt Retention Device". Sehgal Associates Inc., October 15, 1998. (E)

[Ref-5] W Schmidt. "Mass and Energy Release into the Containment due to Ex-Vessel Melt Stabilization". NGPS4/2005/en/1061 Revision B. AREVA NP. June 2007. (E)

SECTION 16.2.2.4 - TABLE 1

[Ref-1] M Nie, M Fischer. Parametric examination of the sacrificial concrete layer thickness in the spreading compartment. NGPS4/2004/en/0185 Revision A. TR04/166. AREVA NP. (E)

SECTION 16.2.2.4 – TABLE 2

[Ref-1] W Schmidt. Mass- and Energy Release into the Containment due to Ex-Vessel Melt Stabilization. NGPS4/2005/en/1061 Revision B. AREVA NP. June 2007. (E)

SECTION 16.2.2.4 – TABLE 3

[Ref-1] M Nie, M Fischer. Analysis of the melt retention in the reactor pit for various release sequences. NGPS4/2003/en/0003. AREVA NP. July 2003. (E)

SECTION 16.2.2.4 – TABLE 5

[Ref-1] M Nie, M Fischer. "Analysis of the melt retention in the reactor pit for various release sequences". NGPS4/2003/en/0003. AREVA NP. July 2003. (E)

SECTION 16.2.2.4 - TABLES 6 TO 8

[Ref-1] R Wittmaack. EPR corium spreading analysis with the CORFLOW computer code. KWU NA-T/1998/E077 Revision A. AREVA NP Erlangen. August 1998. (E)

UK EPR

PRE-CONSTRUCTION SAFETY REPORT

CHAPTER 16: RISK REDUCTION AND SEVERE ACCIDENT ANALYSES

SUB-CHAPTER : 16.2

PAGE : 290 / 295

Document ID.No.
UKEPR-0002-162 Issue 05

SECTION 16.2.2.4 - TABLE 9

[Ref-1] W Schmidt. Mass- and Energy Release into the Containment due to Ex-Vessel Melt Stabilization. NGPS4/2005/en/1061 Revision B. AREVA NP. June 2007. (E)

SECTION 16.2.2.4 - FIGURE 1

[Ref-1] M Fischer. System CMSS: CMSS System Description. NEPS-G/2008/en/1116. AREVA NP. (E)

SECTION 16.2.2.4 - FIGURES 2 TO 4

[Ref-1] M Nie, M Fischer. Analysis of the melt retention in the reactor pit for various release sequences. NGPS4/2003/en/0003. AREVA NP. July 2003. (E)

SECTION 16.2.2.4 - FIGURE 5

[Ref-1] P Gandrille. EPR RF002. Severe Accidents. Dedicated Reactor Coolant System Depressurisation. Functional requirements. NFEPD DC 0091. Framatome ANP. January 2003. (E)

[Ref-2] M Nie, M Fischer. Analysis of the melt retention in the reactor pit for various release sequences. NGPS4/2003/en/0003. AREVA NP. July 2003. (E)

SECTION 16.2.2.4 – FIGURES 8 TO 11

[Ref-1] M Nie, M Fischer. Analysis of the melt retention in the reactor pit for various release sequences. NGPS4/2003/en/0003. AREVA NP. July 2003. (E)

SECTION 16.2.2.4 - FIGURES 12 TO 16

[Ref-1] W Schmidt. Mass and Energy Release into the Containment due to Ex-Vessel Melt Stabilization. NGPS4/2005/en/1061 Revision B. AREVA NP. June 2007. (E)

SECTION 16.2.2.4 – FIGURE 17

[Ref-1] R Wittmaack. EPR corium spreading analysis with the CORFLOW computer code. KWU NA-T/1998/E077 Revision A. AREVA NP Erlangen. August 1998. (E)

SECTION 16.2.2.4 - FIGURE 18

[Ref-1] M Fischer. Long-term Melt Stabilization as Part of the Severe Accident Mitigation Strategy of the European Pressurized Water Reactor. ICAPP05-5001, Seoul, Korea, 15-19 May 2005. (E)

SECTION 16.2.2.4 – FIGURE 19

[Ref-1] M Fischer. Long-term Melt Stabilization as Part of the Severe Accident Mitigation Strategy of the European Pressurized Water Reactor. ICAPP05-5001, Seoul, Korea, 15-19 May 2005. (E)

[Ref-2] M Fischer. The Core Melt Stabilization Concept of the EPR and its Experimental Validation. ICONE 14-89088, Miami FL, USA, 19-23 July 2006. (E)

SECTION 16.2.2.4 - FIGURES 20 AND 21

[Ref-1] M Nie, M Fischer. "Analysis of the melt retention in the reactor pit for various release sequences". NGPS4/2003/en/0003. AREVA NP. (E)

2.5. CONTAINMENT PRESSURE AND CONTAINMENT TEMPERATURE

2.5.1. Methods and basic assumptions for pressure and temperature calculations

2.5.1.3. Determination of flow rates

[Ref-1] M Fischer, M Nie. Updating of mass and energy release into the containment based on the latest R&D results. NGPS4/2003/en/0059 Revision B. AREVA NP. January 2004. (E)

2.5.2. Containment data

2.5.2.2. Boundary conditions

[Ref-1] K-G Petzold. EPR Basic Containment Model for the "Lumped Parameter" code COCOSYS including the Combustible Gas Control System. NEPS-G/2007/en/0035. AREVA NP. December 2007. (E)

SECTION 16.2.2.5 - TABLES

[Ref-1] K-G Petzold. EPR Basic Containment Model for the "Lumped Parameter" code COCOSYS including the Combustible Gas Control System. NEPS-G/2007/en/0035. AREVA NP. December 2007. (E)

[Ref-2] M Nie, K-G Petzold. Main data for severe accident analyses. FANP NGES2/2002/en/0006 Revision D. AREVA Erlangen. January 2004. (E)

[Ref-3] W Schmidt. Mass- and Energy Release into the Containment due to Ex-Vessel Melt Stabilization. NGPS4/2005/en/1061 Revision B. AREVA NP. June 2007. (E)

SECTION 16.2.2.5 - FIGURES

[Ref-1] M Nie, et al. Loads on Containment Civil Structures resulting from Severe Accidents. NGPS4/2005/en/1067 Revision E. AREVA NP. June 2008. (E)

3. RADIOLOGICAL CONSEQUENCES OF CORE-MELT SEQUENCES

3.1. SAFETY REQUIREMENTS

3.1.2. Radiological objectives

[Ref-1] Principles for Intervention for Protection of the Public in a Radiological Emergency, A report by a task group of Committee 4 of ICRP, adopted by the ICRP in November 1992, Oxford, New York, Seoul, Tokyo. ICRP Publication 63. ICRP. 1993. (E)

[Ref-2] European Council. Council Regulation (Euratom) 3954/87 Specifying Maximum Values for Radioactivity in Foodstuffs and Animal Feeds in the Event of a Nuclear Accident or Other Radiological Emergency. Official Journal of the European Community No. L371/11, 1987, amended by Council Regulation 2218/89. Official Journal of the European Community No. L211/1. 1989. (E)

[Ref-3] National Radiological Protection Board. Emergency reference levels of dose for early countermeasures to protect the public. Doc NRPB 1(4). 1990. (E)

[Ref-4] European Council. Council Regulation (Euratom) 3954/87 Specifying Maximum Values for Radioactivity in Foodstuffs and Animal Feeds in the Event of a Nuclear Accident or Other Radiological Emergency. Official Journal of the European Community No. L371/11, 1987, amended by Council Regulation 2218/89. Official Journal of the European Community No. L211/1, 1989. (E)

[Ref-5] Food and Environment Protection Act 1985. HMSO. 1985. (E)

3.2. REFERENCE SOURCE TERM

3.2.1. Core Inventory

[Ref-1] C Gauld, O W Hermann, R M Westfall. ORIGEN-S: Scale System Module to calculate fuel depletion, actinide transmutation, fission product build-up and decay, and associated radiation source terms.
NUREG/CR-200, ORNL/TM-2005/39 Version 6 Volume. II, Section. F7.
Oak Ridge National Laboratory. 2002. (E)

3.2.3. In-containment aerosol behaviour

[Ref-1] J L Droulas. Physical assumptions for calculating the source term under severe accident conditions. ENTTH/0000277 Revision B1. EDF. December 2010. (E)

ENTTH/0000277 Revision B1 is the English translation of ENTTH/0000277 Revision B.

3.2.4. Iodine behaviour in the containment

[Ref-1] Störfallberechnungsgrundlagen für die Leitlinien des BMI zur Berurteilung der Auslegung von Kernkraftwerken mit DWR gemäß §28 Abs. 3. StrlSchV, Veröffentlichung der Strahlenschutzkommision, Band 1, 1989.
[Incident Calculation Bases for the Guidelines Issued by the Federal Minister of the Interior (BMI) for the assessment of the design of PWR Nuclear Power Plants pursuant to Sec. 28, para. (3) of the Radiological Protection Ordinance (StrlSchV)] 1989 (E)

[Ref-2] K H Neeb. The Radiochemistry of Nuclear Power Plants with Light Water Reactors. Walter de Gruyter, Berlin, New York. 1997. (E)

[Ref-3] Iodine Chemical forms in LWR Severe Accidents. NUREG/CR-5732. 1992. (E)

[Ref-4] L Soffer, et al. Accident Source Terms for Light-Water Nuclear Power Plants. NUREG-1465. 1992. (E)

[Ref-5] F Payot, F Cousin, N Meynet, Dissociation of iodide aerosols into gaseous iodine in hydrogen recombiners – impact on the iodine source term. DPAM-SEMIC-2011-353. IRSN. January 2012. (E)

[Ref-6] C Seitan, Sensitivity study of the potential impact of recombiners on volatile iodine release during a severe accident. 002161-100-DE003-A BPE. Bertin Technologies. September 2012. (E)

3.2.5. Activity release from the containment

[Ref-1] C Cherbonnel. Hypothesis to be used for evaluating the radiological consequences of design basis accident – Analysis of the ability of the different ventilation systems to reduce the fission products releases. ENFPIN/0100177 Revision A1. EDF. September 2009. (E)

ENFPIN/0100177 Revision A1 is the English translation of ENFPIN/0100177 Revision A

3.2.6. Release of Radioactive Substances to the Environment

[Ref-1] D Chanin, M L Young. Code Manual for MACCS2: Volume 1, User's Guide. NUREG/CR-6613. SAND97-0594, Volume. 1, Sandia National Laboratories, Albuquerque, NM, USA. 1998. (E)

3.3. CALCULATION OF RADIOLOGICAL CONSEQUENCES

[Ref-1] Störfallberechnungsgrundlagen für die Leitlinien des BMI zur Berurteilung der Auslegung von Kernkraftwerken mit DWR gemäß §28 Abs. 3. StrlSchV, Veröffentlichung der Strahlenschutzkommision, Band 1, 1989.
[Incident Calculation Bases for the Guidelines Issued by the Federal Minister of the Interior (BMI) for the assessment of the design of PWR Nuclear Power Plants pursuant to Sec. 28, para. (3) of the Radiological Protection Ordinance (StrlSchV)]. 1989. (E)

[Ref-2] International Commission on Radiological Protection: ICRP Publication 56. Age-Dependent Doses to the Public from Intake of Radionuclides; Part 1; 1990. (E)

1990 Recommendations of the International Commission on Radiological Protection. ICRP Publication 60. Ann. ICRP 21 (1-3). 1991. (E)

ICRP Publication 67. Age-Dependent Doses to Members of the Public from Intake of Radionuclides; Part 2; Ingestion Dose Coefficients 1990. 1994. (E)

ICRP Publication 69. Age-Dependent Doses to Members of the Public from Intake of Radionuclides; Part 3; Ingestion Dose Coefficients.1995. (E)

ICRP Publication 71. Age-Dependent Doses to Members of the Public from Intake of Radionuclides; Part 4; Ingestion Dose Coefficients. 1996. (E)

ICRP Publication 72. Age-Dependent Doses to Members of the Public from Intake of Radionuclides; Part 5; Compilation of Ingestion and Inhalation Dose Coefficients.1996. (E)

[Ref-3] D Chanin, M L Young. Code Manual for MACCS2: Volume 1, User's Guide. NUREG/CR-6613. SAND97-0594, Volume. 1, Sandia National Laboratories, Albuquerque, NM, USA. 1998. (E)

[Ref-4] European Council. Council Regulation (Euratom) 3954/87 Specifying Maximum Values for Radioactivity in Foodstuffs and Animal Feeds in the Event of a Nuclear Accident or Other Radiological Emergency. Official Journal of the European Community No. L371/11, 1987, amended by Council Regulation 2218/89. Official Journal of the European Community No. L211/1, 1989. (E)

3.4. EVALUATION OF THE POTENTIAL RADIOLOGICAL CONSEQUENCES USING FRENCH NPP ASSESSMENT METHOD

3.4.1. Dose calculation method

[Ref-1] Doury. Le vadémécum des transferts atmosphériques [Atmospheric Transfer Handbook] Report DSN n° 440. February 1992.

[Ref-2] International Commission on Radiological Protection:
ICRP Publication 56. Age-Dependent Doses to the Public from Intake of Radionuclides; Part 1; 1990. (E)

1990 Recommendations of the International Commission on Radiological Protection. ICRP Publication 60. Ann. ICRP 21 (1-3). 1991. (E)

ICRP Publication 67. Age-Dependent Doses to Members of the Public from Intake of Radionuclides; Part 2; Ingestion Dose Coefficients 1990. 1994. (E)

ICRP Publication 69. Age-Dependent Doses to Members of the Public from Intake of Radionuclides; Part 3; Ingestion Dose Coefficients.1995. (E)

ICRP Publication 71. Age-Dependent Doses to Members of the Public from Intake of Radionuclides; Part 4; Ingestion Dose Coefficients. 1996. (E)

ICRP Publication 72. Age-Dependent Doses to Members of the Public from Intake of Radionuclides; Part 5; Compilation of Ingestion and Inhalation Dose Coefficients.1996. (E)

[Ref-3] Council Directive 96/29/Euratom which sets out the basic standards for the protection of the health of workers and the general public against the dangers arising from ionising radiation. Official Journal of the European Communities, L159; Volume. 39; European Council. June 1996. (E)

[Ref-4] G Fleury. Methodology for evaluating the radiological consequences of an accidental atmospheric release. ENTEAG090116 Revision A. EDF. April 2009. (E)

ENTEAG090116 Revision A is the English translation of ENTEAG030152 Revision B.

3.4.2. Reference source term

[Ref-1] M H Boschiero. EPR-fleet convergence of methodologies for assessment of the radiological consequences of accidents. ENSN090080 Revision A. EDF. (E)

ENSN090080 Revision A is the English translation of ENSNEA040124 Revision A.

3.4.3. Radiological consequences calculations

[Ref-1] P Jan. PSAR EPR - Sensitivity analysis about radiological consequences in fault situations. ENTEAG090113 Revision A. EDF. April 2009. (E)

ENTEAG090113 Revision A is the English translation of ENTEAG050091 Revision B.